UNIVERSITY
OF TASMANIA

Resistive heating for multidimensional gas chromatography

By Matthew Ronald Jacobs

B.Med Sci, B.Sc (Hons)

School of Physical Sciences

Submitted in fulfilment of the requirements for the degree Doctor of Philosophy

University of Tasmania, March 23rd 2016

Declaration

This thesis contains no material which has been accepted for a degree or diploma by the University or any other institution, except by way of background information and duly acknowledged in the thesis, and to the best of my knowledge and belief no material previously published or written by another person except where due acknowledgement is made in the text of the thesis, nor does the thesis contain any material that infringes copyright.

The publishers of the papers in this thesis hold the copyright for that content, and access to the material should be sought from the respective journals. The remaining non-published content of the thesis may be made available for loan and limited copying and communication in accordance with the Copyright Act 1968.

Matthew Ronald Jacobs

List of publications

Forming part of this thesis

- M. R. Jacobs, E. F. Hilder, R. A. Shellie, Applications of resistive heating in gas chromatography: A review, Analytica Chimica Acta 803 (2013) 2-14.
- M. R. Jacobs, R. Gras, P. N. Nesterenko, J. Luong, R. A. Shellie, Back-flushing and heart cut capillary gas chromatography using planar microfluidic Deans' switching for the separation of benzene and alkyl benzenes in industrial samples, Journal of Chromatography A 1421 (2015) 123-128
- M. R. Jacobs, M. Edwards, T. Góreckci, P. N. Nesterenko, R. A. Shellie, Evaluation of a miniaturised single-stage modulator for comprehensive two-dimensional gas chromatography of petroleum contaminated soils, (submitted, 2016).

Not forming part of this thesis

- B. Savareear, M.R. Jacobs, R.A. Shellie, Multiplexed dual first-dimension comprehensive two-dimensional gas chromatography–mass spectrometry with contra-directional thermal modulation, Journal of Chromatography A 1365 (2014) 183-190.

Conference presentations

Oral presentations:

- M. R. Jacobs, M. Edwards, T. Górecki, R. A. Shellie, Evaluation of a miniaturised single-stage resistively heated modulator for comprehensive two-dimensional GC, 8th Conference on Analytical Sciences Ireland (CASI), Dublin, Ireland, 2016.

- M. R. Jacobs, M. Edwards, T. Górecki, R. A. Shellie, GC × GC, GC × GC-MS and Miniaturised GC × GC with single stage thermal modulation, 38th International Symposium on Capillary Chromatography and 11th GC × GC Symposium, Riva del Garda, Italy, 2014.
- B. Savareear, M. R. Jacobs, R. A. Shellie, R.A. Shellie, Multi-multidimensional gas chromatography, 38th International Symposium on Capillary Chromatography and 11th GC × GC Symposium, Riva del Garda, Italy, 2014.
- M. R. Jacobs, E. F. Hilder, R. A. Shellie, Analysis of Sub-Antarctic petroleum spill sites by resistively heated gas chromatography, 20th Annual Research and Development Topics, Royal Australian Chemical Society (RACI), Deakin University, Geelong, Victoria, Australia, 2012.

Poster presentations:

- M. R. Jacobs, M. Edwards, T. Górecki, R. A. Shellie, Comprehensive multidimensional GC for environmental analysis. Strategic Science in Antarctica Conference, 37th International Symposium on Capillary Chromatography (ISCC) and 10th GC×GC Symposium, Palm Springs, California, USA, 2013.
- M.R. Jacobs, T. Górecki, R.A. Shellie, Strategic Science in Antarctica, University of Tasmania, Hobart, Tasmania, Australia, 2013.

Awards:

- Australian Postgraduate Award (2012), University of Tasmania.
- CASSS travel grant to attend Riva del Garda, Italy (2014).
- University of Tasmania Graduate Research Travel Award (2014).

Abstract

Gas chromatography is a critical technique used for the separation of volatile and semi-volatile samples prior to analyte detection for qualitative identification and quantitation. The separation of samples prior to detection provides useful information on the physical properties of analytes based on their retention within the chromatographic system, and separating sample components prior to their detection vastly simplifies the identification and quantitation of each component due to the reduction in sample complexity at the point of signal transduction.

The optimisation of GC methods is crucial for ensuring high quality, timely and repeatable separations. Often a goal of method optimisation is to minimise the time required for an analysis while ensuring that adequate separation of target analytes is obtained. Such optimisations are achieved through the selection of column dimensions, stationary phase coating, carrier gas flow rate, and column temperature. While changing the column dimensions and stationary phase properties are very effective methods for adjusting separations, they are not programmable and require changes in hardware configuration. The carrier gas flow rate can be manipulated *via* pressure control of the carrier gas; unfortunately high carrier gas flow rates are detrimental to separation efficiency, without offering proportional gains in the speed for analysis. Another control parameter that is potentially very useful for high speed GC is the temperature of analysis. Changing the temperature of analysis can vastly increase the speed of analysis while maintaining separation efficiency.

Temperature control of GC columns has been achieved using convection ovens for over 50 years. Convection ovens are simple to operate, safe and provide accurate control of column temperature during moderate temperature programming rates compared to classical alternatives such as liquid bath heating. Convection ovens simplified the

installation of injectors, GC columns and detectors due to the connectivity provided by the heated oven cavity, which minimised solute condensation in the analyte flow path. The main limitation of convection ovens is their large thermal mass, which can cause thermal hysteresis during fast temperature programming. Secondly large amounts of electrical power are required to facilitate fast temperature programming, which can be detrimental in applications such as portable analysis. The separation column is normally the only component that needs to be temperature-programmed during GC analysis, while the injector and detector components are held at high isothermal temperatures to prevent solute condensation; therefore convection ovens present a source of instrument inefficiency.

The resistive heating of capillary columns is an alternative to convection oven based heating that is significantly faster since only the mass of the capillary columns and associated heating elements need be heated. There are a number of commercially available GC instruments that offer the option of resistively heated capillary columns however these instruments still maintain the legacy convection oven for column to injector and detector connectivity. Commercial GC instrumentation is almost entirely limited to bench-top laboratory analysis, with few options for portable GC analysis systems. Portable analysis offers significant benefits over laboratory-based analysis. Performing an analysis at the point of sampling abolishes the need for transporting samples back to a laboratory-based facility, eliminating the time delay between sampling and analysis. Removing the sample transport step also minimises the risk of sample degradation or cross contamination arising from the analyte storage procedure, time, or sample preparation steps back at the laboratory. This allows portable analysis to provide greater confidence in the quality of measurements made compared to laboratory analysis. Portable analysers must be robust, repeatable, simple to use, and relatively low in cost to facilitate their deployment in the field.

The Falcon Calidus™ GC was selected as the analytical platform in this research due to its use of resistive column heating for fast GC analysis, excellent power efficiency, small form factor and low cost that would make it ideal for deployment in the field for portable GC analysis.

Since the separation of complex mixtures using one-dimensional GC is generally unfeasible due to instrument and time constraints, multi-dimensional (MD) separation techniques were investigated as a strategy for maximising the separation capabilities of the Calidus™ GC instrument. Specifically comprehensive two-dimensional gas chromatography (GC × GC) was investigated due to its potential to separate a large numbers of components without substantially increasing the time of analysis. Resistively heated thermal modulation and flow modulation strategies using PMDs were explored as a means to incorporate MD GC analysis techniques into the Calidus™ GC.

The Calidus™ GC instrument was evaluated and found to be capable of providing comprehensive two-dimensional GC × GC analyses for the characterisation of a range of complex samples, while maintaining the capability of portable analysis unlike conventional bench top GC instruments. Additionally a novel single-stage thermal modulator was characterised, optimised and applied for GC × GC and found to be very effective at modulating a range of solutes without the need for the cryogenic focusing common in commercial GC × GC modulators. PMDs were also investigated as a low cost means of controlling injection bandwidths and providing effluent modulation in the Calidus™ system and were found to be similarly effective compared to thermal focusing strategies.

Acknowledgements

I would like to acknowledge the large number of people at the University of Tasmania and Australian Centre for Research on Separation Science (ACROSS) who have supported me and contributed towards my PhD studies.

Firstly I would like to thank Dr Robert Shellie and Professor Emily Hilder for providing me with the opportunity to study at the University of Tasmania, and for their guidance during my studies. Thank you to Professor Pavel Nesterenko for your assistance and advice on the preparation of my PhD thesis and research manuscripts, your assistance was invaluable and greatly appreciated.

Next I would like to acknowledge the talented researchers that I have had the pleasure of working with including: Professor Tadeusz Gorecki (University of Waterloo), Dr Jim Luong (Dow Chemical Company), Professor Michael Breadmore (University of Tasmania), Mr Matthew Edwards (University of Waterloo), Ms Ronda Gras (Dow Chemical Company), Mr Paul Walker (University of Tasmania) Mr John Davis (University of Tasmania), Dr Lauren Wise (Australian Antarctic Division) and Mr Greg Hince (Australian Antarctic Division). In particular I would like to acknowledge Professor Gorecki and Dr Luong for their invaluable discussions and mentoring in the techniques of GC, MDGC and comprehensive GC × GC, I learned an immeasurable amount from you both during my PhD. Additionally I would like to acknowledge Professor Breadmore for all of his advice and thoughtful discussions throughout my PhD studies.

Thank you to my friends and colleagues: Mari Egeness, Laura Tedone and Esme Candish, who I have studied with throughout my PhD. In particular I would like to thank Dr Emer Duffy who has encouraged me throughout my PhD and assisted greatly in proofreading this thesis. Finally, I want to acknowledge my family (Anthony, Wendy, Kelly, Emma and John) who encouraged me to undertake these studies, thank you.

Table of contents

List of Figures

List of Tables

List of Abbreviations and Symbols

^{1}D	First-dimension separation column
^1t_R	First-dimension retention time
^{2}D	Second-dimension separation column
^2t_R	Second-dimension retention time
BTEX	Benzene, toluene, ethylbenzene, and *m/p/o*-xylene
CFT	Capillary flow technology
C_m	Resistance to mass transfer in the mobile phase
C_s	Resistance to mass transfer in the stationary phase
d_f	Stationary phase film thickness
EDS	Energy dispersive X-ray electron spectroscopy
EPC	Electronic pressure control
FFF	Forward fill flush (GC × GC modulation type)
FID	Flame ionisation detector
FWHM	Full width at half maximum
GC	Gas chromatography *or* gas chromatograph instrument
GC × GC	Comprehensive two-dimensional gas chromatography
GC-FID	Gas chromatography with flame ionisation detection
GC-MS	Gas chromatography with mass spectrometry detection
HETP	Height equivalent to a theoretical plate
ID	Internal diameter
LOD	Limit of detection
LOQ	Limit of quantification
LMCS	Longitudinally Modulating Cryogenic System
LTM	Low thermal mass
MD	Multidimensional

MDGC	Multidimensional gas chromatography
MS	Mass Spectrometry *or* Mass Spectrometer
n	Giddings peak capacity
N	Theoretical plate count
N_{max}	Estimated maximum number of theoretical plates
PAH	Poly aromatic hydrocarbon
PCA	Principal component analysis
PDMS	dimethylpolysiloxane (polydimethylsiloxane)
PEG	Polyethylene glycol
P_i	Injection period
p_i	Column inlet pressure
PLOT	Porous layer open tubular
P_m	Modulation period
p_o	Column outlet pressure
PMD	Planar microfluidic device
Q	Plate duration
RFF	Reverse fill flush (GC × GC modulation type)
RTD	Resistance temperature detector
SAB	Special Antarctic blend diesel
SEM	Scanning electron microscopy
SIM	Selective ion monitoring
SS	Stainless steel
S/SL	Split-splitless injector
TCD	Thermal conductivity detector
T_m	Column void time
t_R	Retention time
ū	Average carrier gas linear velocity

µGC	Micro gas chromatograph instrument
VOC	Volatile organic compound
$w_{0.5}$	Peak width at 50% of peak maximum
w_b	Peak width at peak base
WCOT	Wall coated open tubular capillary
XPS	X-ray photoelectron spectroscopy

Chapter 1: Introduction

1.1 General Introduction

One of the most pressing needs of modern science is the ability to identify and measure the amounts of known and unknown compounds in naturally and synthetically derived samples. Analytical chemistry is the scientific discipline responsible for the analysis of these samples, which are often highly complex. Due to the diversity of compounds present in most samples, a combination of separation or selective detection is required for adequate characterisation. For example, in the case of petroleum there are many compounds that can interfere with the quantitation of particular targets of interest such as the carcinogen benzene, which is a very small component of the overall sample matrix. While selective detection of target analytes is a rapid and effective means of obtaining essential quantitative analytical data the selectivity required to eliminate interferences from target analytes is often unfeasible. In these situations, it is essential that complex samples are simplified using sample preparation and separation techniques to reduce the demands made upon detection systems.

There are a number of techniques available to separate complex samples, however the most prevalent method is that of chromatography, whereby compounds are separated in the time dimension based on partitioning between two phases [1]. A typical setup involves passing a narrow plug of a sample through a separation device known as a column, using a controlled flow of gas or liquid eluent. This liquid or gas serves as the mobile phase of the separation system. The column is generally a long, narrow tube that contains a liquid phase that is immobilised *via* chemical bonding to solid particles or the walls of the column. Solid adsorbent phases are also possible, however they typically utilise an adsorption mechanism of chromatography rather than a partition based

separation mechanism. This solid or immobilised liquid phase serves as the stationary phase of the column. As the sample plug flows through the column, analytes partition between the stationary and mobile phases based on the physical properties of each respective analyte. Analytes are physically separated in the time-dimension based on the degree of retention each analyte has for the stationary phase. Retention time provides characteristic information about the chemical properties of each solute that can be used to support compound identification. A detection system is installed after the column to characterise the column eluent and generate a time dependent response output known as a chromatogram.

Perhaps one of the most well-known and successful chromatographic techniques utilised in analytical chemistry is gas chromatography (GC), which is broadly used for the separation of volatile and semi-volatile compounds [2,3]. In GC volatile and semi-volatiles analytes are vaporised in a hot inlet (200 to 350 °C), or injector. The injector transfers the vaporised sample into a separation column using a flow of inert gas such as hydrogen, helium, or nitrogen. This gas flow, serves as the mobile phase, which is used to transport the sample through the column. GC columns are typically long (10 to 100 m) narrow (0.1 - 0.53 mm internal diameter) capillary tubes that are constructed from fused glass silica or stainless steel (SS). A range of different stationary phases can be chemically bonded to the walls of narrow capillaries in a thin layer (0.1 to 10 μm), which are referred to as wall coated open tubular columns (WCOT) [4,5]. Alternatively, solid adsorbent stationary phases are immobilised in the porous layer open tubular (PLOT) format, where a thin coating of solid adsorbent is similarly attached to the walls of a capillary enabling adsorption based retention rather than partition chromatography [5,6]. Separation is achieved by the partitioning of components between the inert mobile gaseous phase and immobilised stationary phase on the basis of two general physical parameters, the vapour pressure of each respective analyte, and the selectivity each analyte possesses for the stationary phase.

There are a number of considerations that are important to GC analysis that determine the quality of results obtained using the technique including the:

1. Injection procedure;
2. Carrier gas;
3. Separation column;
4. Detector;
5. Temperature of analysis;
6. Sample.

Optimal sample injection is achieved when a representative portion of a sample is introduced to the separation column in a narrow injection bandwidth [7-9]. Wide injection bandwidths critically limit the performance of GC separations, particularly in the case of fast GC separations where the timescale taken to complete an injection approaches the time scale over which a separation is to be completed [9]. Injection bandwidths can be minimised by careful optimisation of injection conditions and the selection of high-speed valve-based injection or thermal focusing strategies as will be discussed in Chapter 2 and Chapter 3.

Inert carrier gases including hydrogen, helium, nitrogen and argon are preferred in GC to ensure that chemical transformation of analytes does not occur during high temperature analysis. Out of these gases, hydrogen and helium are preferred due to the high molecular diffusivities of solutes in these two mobile phases, compared to nitrogen and argon [10,11]. Hydrogen has 20 % greater diffusivity compared to helium, which corresponds to a 20 % faster speed of analysis, however this speed gain comes at the safety risk of flammable hydrogen gas [12]. Modern instrumentation has come a long way towards mitigating the safety hazards associated with hydrogen carrier gas use; furthermore helium is a non-renewable resource which provides additional incentive to move towards hydrogen carrier gas.

Separations columns are the critical component of GC instruments, and as a result a wide range of separation columns have been developed to suit different applications. Columns are available with a range of physical dimensions and stationary phase coatings that vary in polarity and selectivity [5,13]. The separation performance obtainable with a GC column can be related to the dimensions and properties of the stationary phase coating and the conditions at the outlet of the column with plate height theory [14,15] and the van Deemter equation [16]. The effect of the outlet pressure is pronounced; since decompression of the carrier gas vastly enhances mass transfer within the mobile phase. Most commonly the outlet pressure is either at atmospheric pressure such as with a Flame Ionisation Detector (FID), or at vacuum conditions like with a Mass Spectrometer detector (MS). In situations where a column is operating with a low-pressure drop between the inlet (p_i) and outlet (p_o), ($p_i / p_o \approx 1$), the height equivalent to a theoretical plate (*HETP*) is defined as follows (Eq. 1).

$$HETP = (B / \bar{u}) + C_1\bar{u} + C_2\bar{u} \qquad \text{(Eq.1)}$$

Where B corresponds to the diffusion coefficient of solutes in the longitudinal axis of the column, $\bar{u}$ corresponds to the average linear velocity of the carrier gas, and C_1 anC_2 correspond to a solute's resistance to mass transfer in the mobile phase and stationary phase respectively. This relation between plate height and peak broadening was later reconciled for high-pressure drop conditions, which yielded (Eq. 2) [10,17,18].

$$HETP = (B / \bar{u}^2) + C_1\bar{u}^2 + C_2\bar{u} \qquad \text{(Eq.2)}$$

Optimal selection of column dimensions and experimental conditions has been the topic of intense research; however theoretical modelling of GC conditions has yielded some rigorously supported starting points for obtaining quality GC separations [10,11,19-21]. In particular, carrier gas flow rate has been demonstrated as a convenient control parameter compared to average linear carrier gas velocity that has classically been used for column performance optimisation [20]. Furthermore GC analyses can be

rapidly optimised to achieve either high speed or high efficiency separations for any capillary column by considering the internal diameter of a given column [20].

The analysis temperature is also critical to the separation performance of GC due to its impact on solute retention factors and the speed of analysis. Blumberg and Klee have shown that an acceptable compromise between speed and resolution is achieved when the heating rate is set at a rate of 10 °C per void time, where the void time (T_m) corresponds to the time taken to elute one column volume of carrier gas at a given flow rate [22]. Combining optimal flow rates with optimal heating rates provides a robust starting point from which methods can be developed to achieve a target separation. Typically analysts have the analytical goal of separating components of a sample in the minimum possible analysis time to increase the throughput of analysis, so that replicate analysis can be achieved and false positive and false negative measurements can be avoided. As a result research has been focused on developing strategies capable of modifying existing GC methods to operate in the fast GC mode while still maintaining robust analysis systems. The general parameters that can be varied to increase the speed of analysis include:

1. Reduction of column length;
2. Reduction of column internal diameter;
3. Reduction of the stationary phase film thickness;
4. Increasing the carrier gas flow rate;
5. Increasing analysis temperature or temperature programming rate.

While shortening a column's length is an effective means for decreasing the time of analysis, this comes at the cost of a loss of separation efficiency that is detrimental in many separations. Alternatively a column's inner diameter can be reduced to enhance the speed of analysis and enhance separation efficiency. Scaling the internal diameter and length of GC columns often provides a robust means of decreasing the time of

analysis while maintaining a high separation efficiency, however implementing this strategy can lead to the overloading of stationary phases and poor peak symmetry [9,12,23]. Reducing the stationary phase film thickness provides a small enhancement to the rate of mass transfer between the stationary and the mobile phase of GC, however this comes with the cost of diminishing the solute loading capabilities of the stationary phase, which leads to the overloading of peaks and a reduction in column efficiency while offering little in the way of separation speed enhancement [21].

Changing column properties to enhance the speed of an analysis requires hardware to be changed which is an inconvenient requirement. Modification of the carrier gas flow rate and the temperature of analysis can be achieved using software control without the need for changing column hardware. Of these two control parameters temperature programming is the more robust choice for modifying the speed of analysis since this directly impacts the retention factors of solutes, and can be readily varied throughout an experiment. Changing the carrier gas flow rate can be used to increase the speed of analysis, however the gain in analysis speed causes a significant loss in column efficiency at very high flow rates, while temperature programming does not cause a similar reduction in column efficiency [20]. For this reason temperature programming is perhaps the most flexible control parameter for affecting the separation of a GC system. Modern GC instruments are limited by the speed at which they can be temperature programmed, due to the large thermal mass of the convection ovens used for connectivity and column heating. Generally these ovens can not be heated at rates exceeding 50 °C min^{-1} as a result of their large mass, and there are significant losses in temperature repeatability caused by such fast programming rates. A potential means of overcoming this instrument limitation is to adopt alternative heating strategies such as resistive heating of GC columns, rather than convection oven heating.

1.2 Resistive heating for gas chromatography (modified from reference Jacobs et al. [24].

The technical challenges of resistively heating a capillary column are significant compared to convection oven heating. As a result, a single best technology for resistive heating in GC is yet to be determined, despite a large amount of research having been performed to optimise such technologies. There are a myriad of approaches available for the construction of resistively heated capillary columns of which there are three broad classes, as identified in by Wang *et al.* [25]:

1. Direct resistive heating, where the column itself is either constructed from a conductor (*e.g.* SS) or coated in a conductive material, which enables electrical current flow for resistive heating;
2. The coaxial design, where the column is placed inside a conductive tube through which a current is passed to provide heating;
3. The collinear method where the column is heated by contact with a resistive heater threaded around and parallel to the GC column.

Before adopting a different column heating strategy it is important to ascertain whether the performance of resistive heating is competitive with convection oven heating. Furthermore it must provide the desired benefits of fast analysis, high throughput, reduced power consumption and portability to justify a paradigm shift in heating strategies. Issues relevant to temperature programming in GC include speed, reproducibility, accuracy and precision of the column heating process. Reproducibility is an essential performance criterion for chromatographic analysis as retention time is the primary means of peak identification, especially where non-selective detection is used.

The simplest means by which the reproducibility can be determined is by calculating the retention time reproducibility of peaks eluting from replicate runs. Analysis of a homologous series, such as a mixture of *n*-alkanes, is typical as this allows a holistic

analysis of retention time variability across a given temperature programming range. Analysis of the reproducibility of single peaks of interest is also commonly accepted depending on the application. Comparative studies of the reproducibility of different embodiments of resistively heated and convection oven GC are summarised in Table 1. In order to perform comparisons between the effectiveness different resistive heating strategies, it is important to note that column dimensions, injector and detector conditions must be standardised to obtain useful comparisons. In general, more rapid temperature ramps will show greater retention time variance, impacting reproducibility.

Table 1 Summary table comparing retention time and peak area relative standard deviations, as well as power efficiencies of various column heating embodiments.

Ref	GC Embodiment	Maximum ramping rate used	Relative Standard Deviation		Power efficiency
		°C s^{-1}	Retention time (t_R %)	Peak Area (%)	W m^{-1}
[26]	Direct	2.4	0.9	3.5	11.7
[27]		10	0.46	1.8-6.9	20-35
[28]	Convection Oven	-	0.010-0.128	-	n/a
	Collinear	0.5	0.016-0.117	-	2.6
[29]		6.7	0.04	2.9	5
[30]		3.33	0.055	2-5	-
[31]		1.25	0.00-0.80	2.03-4.85	-
[32]		10	0.98	-	15.8
	Convection Oven	-	0.27	-	n/a
[33]		-	2.5		n/a
	Collinear/ Coaxial	0.25	0.01	-	20-35
[34]	Coaxial	5	0.2	3.4	-
[35]		20	-	4-9	-
[36]		16	0.75	-	-

Hail and Yost [26] used a resistively heated aluminium clad capillary column that was capable of being heated at a rate of up to 40 °C s^{-1}. It was apparent that application

of a constant electric current and voltage does not yield a linear heating ramp (Figure 1). The resistance of the aluminium clad column varied as a function of temperature necessitating calibration *via* a compensation algorithm. A retention time relative standard deviation (RSD) of 0.9 % with a respective peak area RSD of 3.5 % for *n*-tetradecane was observed during a heating ramp of 2.4 °C s^{-1}. This heating rate is more than twice as fast as is possible using modern convection oven based instruments.

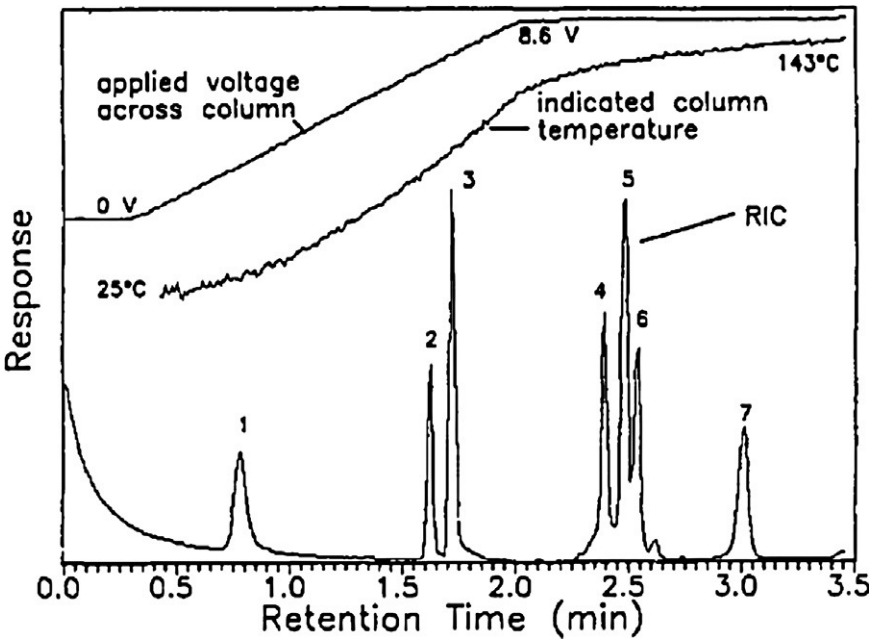

Figure 1 Chromatogram obtained with an aluminium-clad resistively heated GC column (BP1, 3.19 m × 530 µm ID × 1.0 µm d_f). Peak identifications: (1) 2-chlorophenol, (2) 2,4-dimethylaniline, (3) *n*-undecane, (4) 1-undecanol, (5) acenaphthylene, (6) *n*-tetradecane and (7) *n*-pentadecane. Reproduced from reference [26] with permission from ACS Publications.

Ehrmann *et al.* utilised a coaxial and collinear resistive heating setup, comparing the two methods to one another followed by benchmarking against convection oven GC [32]. The collinear heating method was superior in terms of design ruggedness compared to coaxial heating, which suffered from poor mechanical stability due to the differing thermal expansion coefficients of its components. The collinear setup was compared with convection oven GC at a temperature programming rate of 1 °C s^{-1}. The

retention time RSD of *n*-decane was 0.98 % for the resistively heated setup compared to 0.27 % for the convection oven setup indicating that the reproducibility of the resistively heated GC instrument had some way to go before truly competing with convection oven GC.

Coaxial resistively heated GC technologies were further investigated by van Deursen and co-workers who tested the effectiveness of the EZ flash resistively heated GC module which allows the user to thread a capillary column through the core of a resistively heated SS tube [34]. The RSD of the retention time and peak areas for *n*-dodecane was 0.2 % and 3.4 % respectively when a temperature programming rate of 5 °C s^{-1} was applied. These performance metrics are comparable to convection oven GC. Dalluge *et al.* compared three GC column-heating configurations to determine the performance of each setup including; fast temperature programming with a convection oven (50 °C held for 60 s and then ramped at 0.66 °C s^{-1} to 200 °C and then ramped at 0.33 °C s^{-1} to 280 °C), a ballistic convection oven heating (50 °C held for 60 s and then ramped at 1.16 °C s^{-1} to 280 °C), and coaxial heating via resistive techniques (50 °C held for 15 s and then ramped at 3.33 °C s^{-1} to 280 °C) [35]. Analysis of a series of *n*-alkanes revealed that fast and ballistic temperature programmed convection oven approaches led to significantly higher peak widths and retention time variance compared to coaxial resistive heating.

Collinear resistively heated GC columns (often referred to as Low Thermal Mass or LTM columns) have been investigated extensively in the literature. Sloan *et al.* performed an analysis of retention time reproducibility with RVM Scientific's (now Agilent Technologies) collinear resistively heated column module [28]. In this study the reproducibility of collinear resistively heated GC for a mixture of *n*-alkanes was maximally 0.117 % RSD (heptane) compared to convection oven GC 0.096 % RSD (heptane) at a temperature programming rate of 0.5 °C s^{-1}, indicating that the technology is equally as precise as existing convection oven systems when operating

within the confines of a convection oven's maximum temperature programming rate. Sasamoto *et al.* calculated retention time reproducibility for 82 pesticides of interest and found RSD values between 0.00 to 0.80 % and peak area RSD values of 2.03 to 4.85 % following separation with collinear resistive GC heating temperature programming at a rate of 1.25 °C min^{-1} [31]. Luong *et al.* tested collinear columns operated at rapid temperature programming rates of up to 6.7 °C s^{-1}, far beyond the maximum rate of any convection oven [29]. Promising retention time and area count RSD was obtained for methanol of 0.04 % and 2.9 %, respectively. No direct comparison between resistively heated and convection oven GC was possible in this study. The speed and precision of collinear resistive heating represents an important step forward in the development of GC.

Another promising variant of collinear resistive heating is that of nickel wired capillary columns, which do not require a thermocouple or platinum resistance sensor like their LTM counterparts [33]. The resistance of nickel has a high temperature coefficient making it possible to directly measure the temperature of the column based upon a simple resistance measurement. This reduces the thermal mass of the column and simplifies column module construction. Ramping rates of up to 13.33 °C s^{-1} have been reported using nickel wired GC columns with good programmable linearity as shown in Figure 2. Reported retention time RSD for *n*-dodecane was on the order of 0.010 %, which was superior to convection oven GC that yielded a retention RSD of 0.025 % using a temperature programming rate of only 0.25 °C s^{-1}.

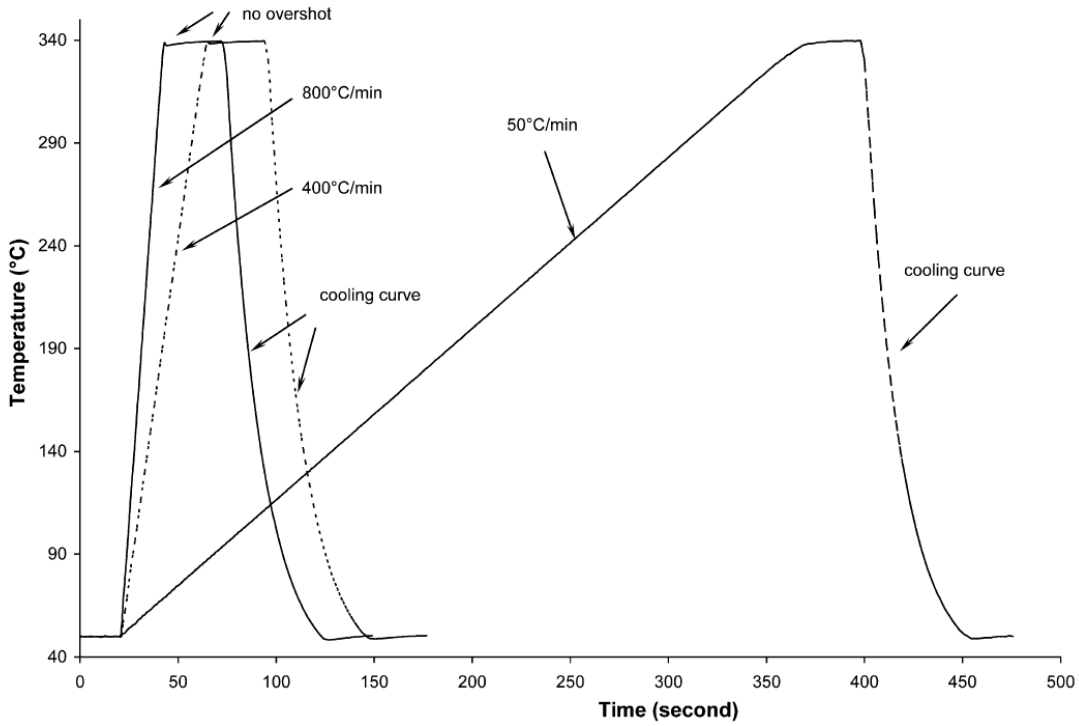

Figure 2 Temperature programming linearity of a nickel-wired collinear resistively heated GC column at two fast temperature-programming rates (13.33 °C s^{-1}, 6.66 °C s^{-1}) compared to a convection oven GC (0.83 °C s^{-1}) temperature program. Reproduced from reference [33] with permission from Elsevier.

Comparison of nickel wired columns to nickel electroplated columns revealed that nickel electroplated columns have slightly improved temperature programmability (3 %) compared their wired counterparts [33]. Despite the relatively minimal gain in performance, nickel electroplated columns also boast increased mechanical ruggedness, and potentially faster temperature equilibration times due to reduced thermal mass. Xu *et al.* performed a study on direct resistive heating with SS GC columns [27]. A retention time RSD of 0.46 % for *n*-undecane using a rapid 10 °C s^{-1} temperature program was obtained, along with a peak area reproducibility of 1.8 to 6.9 % (0.5 µL, splitless) and 2.8 to 4.5 % (10:1 split ratio), which is excellent considering the speed of the temperature program used.

There has been continuous improvement in the technology used for resistive heating in GC and many engineering challenges of resistively heating a capillary column have been overcome. The above mentioned studies indicate that resistively heated column construction for collinear column modules, directly heated SS columns, nickel-wired and electroplated columns have reached the stage where they are capable of providing fast temperature programming accompanied by reproducible retention times that can not be achieved with a convection oven GC. At this point it should be noted that while retention time reproducibility is very important for any GC experiment, there is a wide range of software and literature available concerning the topic of retention time correction [37-40]. Retention time correction allows users to align chromatograms to correlate the retention times of various peaks between different GC experiments, enhancing peak identification capabilities of GC systems.

1.2.1 Advantages and challenges of resistive heating in GC

The possibility of rapid temperature ramping *via* direct or indirect resistive heating of a capillary column has a demonstrable impact on the practice, speed and cost of GC analysis. Resistively heating capillary columns has a number of benefits including: reduced power consumption, fast analysis, high throughput analysis, and improved portability.

Three factors determine the speed and power consumption of a temperature programmed GC system: the thermal mass and design of the column heating assembly, the voltage provided by the GC power supply, and the efficiency of the heat extraction mechanism. The thermal mass of a resistively heated GC column is made up of the heating element, column and any insulation, meanwhile a convection oven instrument's thermal mass includes all of these components in addition to the materials from which the oven itself is constructed. This means that resistively GC has substantially lower thermal mass than a convection oven which accounts for the rapid programmability and

low power consumption of such systems. Both resistive and convection based instruments use similar resistance temperature detectors (RTDs), however the fan throughput to surface area/thermal mass ratios favour resistive heating in terms of cool down and equilibration speed. In one study it was found that a modern GC requires 11 min to cool down from 300 °C and equilibrate at 30 °C with an ambient room temperature of 22 °C, while a resistively heated collinear column (18 m) requires only 4 min to perform the same equilibration [29]. Any reduction in cool down time can lead to substantial sample throughput increases, as this time is essentially wasted time between analyses. High throughput analysis reduces the need for multiple instruments in analytical laboratories, prevents sample backlog, and minimises instrument operation costs in terms of power consumption.

When comparing between different resistive heating iterations it is common for power consumption to be reported in Watts of power required for analysis divided by the length of the column since column length is proportional to thermal mass. While this is quite a good means of standardising the power efficiencies of different resistive heating embodiments, it is important to remember that the temperature programming rate, range and ambient instrument temperature also affect power usage. This makes direct comparison between different resistively heated GC experiments difficult. Hail *et al.* identified the potential power consumption benefits for resistively heated GC. A mere 25 W of power over 25 s was sufficient to heat a 2.2 m (11.7 W m^{-1}) aluminium clad column from 50 to 150 °C at a rate of 4 °C s^{-1} [26]. Aluminium clad columns are no longer commercially produced; however a number of studies have since been performed to benchmark the power consumption of current day GC technology. Ehrmann *et al*. reported power efficiency of 15.8 W m^{-1} for a collinear resistively heated GC using a nickel alloy heating wire insulated within a Teflon tube threaded through a SS tube [32]. Sloan *et al.* measured the power consumption of a conventional GC oven during the analysis of an alkane mixture at a rate of 0.17 °C s^{-1} and found that 681 W of

power was required to power the oven, after subtracting the baseline power required for heating the instruments injector (250 °C) and MS heated transfer line (280 °C) [28]. In comparison to this, a resistively heated collinear column required 42 W of power (2.6 W m^{-1}), after subtracting the injector and heated MS transfer line power requirements as before. Here resistive heating represents a reduction in power requirements by 94 %. In another study the average peak power consumption for a collinear resistively heated column (1 m × 250 µm ID × 0.25 µm d_f) was found to require a respective 5 W (5 W m^{-1}) while a convection oven GC operating with similar instrument conditions required 1.09 kW for a single analysis; a 99 % reduction in power consumption [29]. SS columns are an alternative to the collinear column technologies and have been found to operate with power requirements of 20-35 W m^{-1} in order to temperature program through a range of 50 to 250 °C at rapid rates of up to 10 °C s^{-1} [27]. Nickel wired and nickel electroplated columns have demonstrated power efficiencies on the order of 3.6 W m^{-1} for a ramp rate of 3.33 °C s^{-1} [33]. The power requirements for various resistively heated GC technologies have been summarised in Table 1. All of these embodiments are amenable towards incorporation into portable GC instruments as well as having a reduced environmental impact in terms of power consumption.

Technological developments in resistive column heating can potentially reduce analysis times by a factor of ten, without sacrificing substantial amounts of column efficiency [41]. Jain and Phillips constructed a resistively heated GC column by coating a capillary (SE-30, 0.85 m × 250 µm ID × 0.25 µm d_f) with a thin film of an electrically conductive paint that was able to enable a separation of an *n*-alkane mixture in 2 s [42]. This setup provided high throughput, as a chromatogram could be generated every 5 s, however the resolving power of this system was low. No comments were made about the linearity of the resistive heating procedure or reproducibility of this separation, however the study demonstrated some interesting applications of resistively heated GC for continuous monitoring or process analysis. In another work, Jain and Phillips

investigated the effect of temperature gradients across narrow bore capillary columns [43] to enable the separations of 13 volatile and semi-volatile components in just 3.5 s. Such rapid separations could be valuable in process monitoring or sensor-based GC applications. Painted capillary columns have since been abandoned due to poor mechanical ruggedness arising from differing thermal expansion coefficients between the coating and the capillary column itself.

van Lieshout *et al.* evaluated the effectiveness of fast temperature programming using resistive heating and convection ovens with narrow bore columns as a means to rapid analysis [41]. In this study a petrochemical sample was analysed and the resolution of critical peak pairs was measured to determine the efficiency of each chromatographic setup. The authors concluded that resistive heating did not provide adequate resolution to separate the petrochemical sample of interest compared to the narrow bore GC columns. However the conclusion was biased since the peak capacities of each analytical system considered were not normalised. The narrow bore column used in the convection oven (10 m × 50 μm ID × 0.1 μm d_f; $N_{max} \sim 200{,}000$) is superior in terms of its ability to separate a mixture compared to the EZ flash resistively heated column module used in this experiment (6 m × 250 μm ID × 0.25 μm d_f; $N_{max,} \sim 24{,}000$) by almost an order of magnitude. This means that the lack of resolution demonstrated by the resistively heated system was not necessarily a reflection of the mode of column heating but rather a reflection of different column dimensions. van Deursen *et al*. showed considerable scope for speed increase by applying resistive heating with fast temperature programs to petroleum and mineral oil samples in comparison to speed increases gained *via* the use of short capillary columns [34]. The authors reported that rapid temperature programming is superior to shortening capillary length when a faster analytical cycle is desired, since the loss of resolution resulting from using shorter capillaries is much more significant than efficiency lost due to fast temperature programming.

Grall *et al.* evaluated the effect of flow rates, column lengths, and fast temperature programs using a coaxial resistively heated column, and evaluated the impact of each of these parameters upon peak capacity [44]. The analysis of a series of *n*-alkanes at different temperature programming rates afforded some interesting insights towards fast GC analysis as shown in Figure 3.

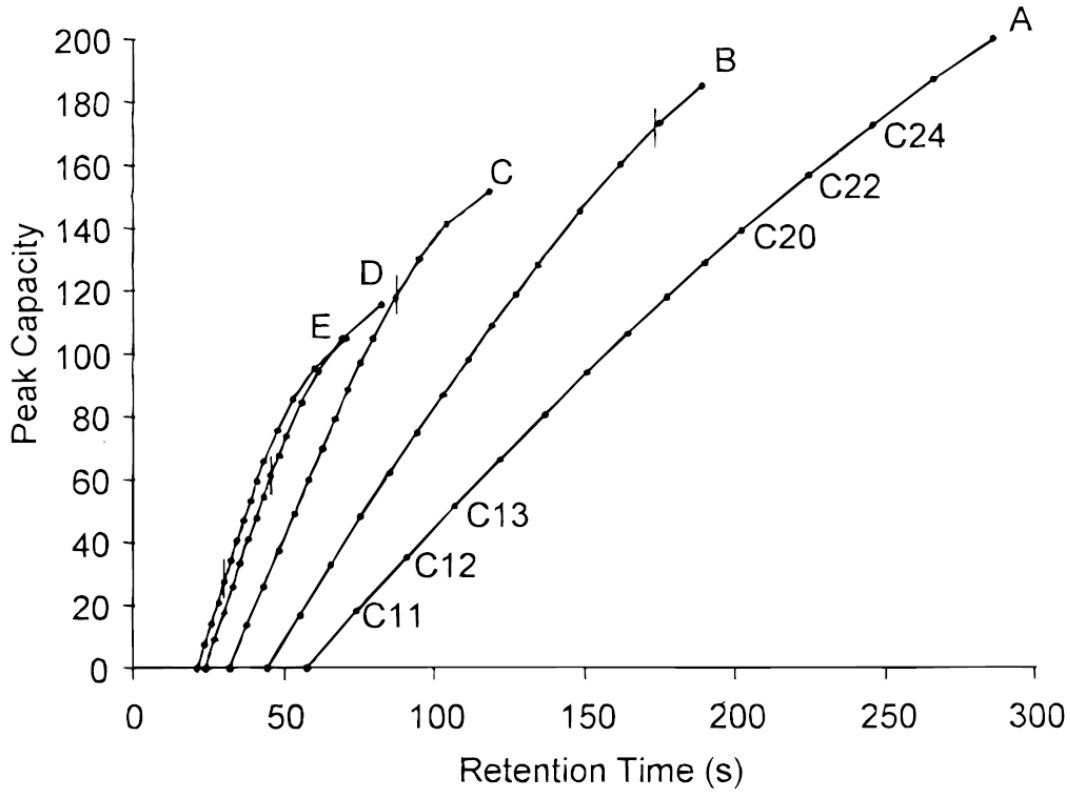

Figure 3 Cumulative peak capacity *vs.* retention time plots for a column (DB-1, 18 m × 250 µm ID × 0.25 µm d_f) with different temperature programming rates: 1 (A), 1.67 (B), 3.33 (C), 6.66 (D) and 10 (E) °C s^{-1}. Vertical tick marks on the plot indicate the end of the temperature program. Reproduced from reference [44] with permission from ACS publications.

Specifically the speed gains possible with rapid temperature programming are much greater than the corresponding loss in peak capacity, providing the reproducibility and precision of the resistive heating process is maintained. For example, increasing the temperature programming rate from 1 °C s^{-1} to 1.66 °C s^{-1}, a ramping rate inaccessible

with convection oven GC, led to a reduction in analysis time of 35% with a corresponding peak capacity loss of only 5%. The use of very high flow rates or shorter columns on the other hand considerably reduced peak capacity. This means that if adequate peak capacity is available to perform the desired separation, faster temperature programming can be used to reduce overall analysis time without adversely affecting the quality of a separation.

This potential for speed gain in GC was reiterated by Bicchi and co-workers who performed a comprehensive study on the performance of a restively heated GC compared to convection oven GC, for separating and characterising bergamot essential oils and various pesticides of interest in food matrices [45]. In this article Blumberg's separation measure (S) [46] was compared to Giddings' peak capacity (n) to evaluate the separation capabilities of different chromatographic systems [47-49]. This article effectively highlighted how optimisation of flow rate and temperature programming are necessary for minimising the separation time of critical pairs. Faster GC experiments have the added benefit of reducing on-column peak broadening. As chromatographic analysis takes place, peaks experience longitudinal band broadening as a result of analyte concentration differentials at peak boundaries [16]. Minimisation of longitudinal band broadening further maximises the ability of a chromatographic system to resolve components, increases the signal-to-noise ratio and sensitivity of any GC method.

1.2.2 Portable gas chromatography

Resistively heated columns permit instrument miniaturisation by several orders of magnitude compared to convection oven GC instruments, since an oven cavity is no longer required. This simplifies the application of GC towards transportable and portable instruments and should lead to a reduction in the cost of instruments, as fewer materials are required for their construction. The scale of portable GC instruments varies greatly as this is an active area of research and development, with high

commercial demand. Instrument sizes range from kilogram scale transportable instruments, through to gram scale chip-based GC devices. Smith [50] has recently reviewed the development and capabilities of portable GC-MS instruments.

On-site GC analyses minimise the potential for sample integrity losses during storage and transportation. This reduces analysis time and provides the analyst with increased sampling flexibility. For example the analyst is free to resample areas on site that appear to warrant further investigation. Although resistively heated column technology lends itself well towards the development of portable GC instruments, the ability to provide rapid, reproducible, and power efficient GC separations in a small instrument footprint is a significant hurdle which needs to be addressed for such instruments to be realised. A number of small form factor and portable GC instruments are available from commercial vendors, however these units generally use small convection ovens that operate in the isothermal mode rather than offering temperature programming as an option. These units are normally optimised by the vendor for a specific analytical application at the point of sale, which simplifies the deployment of these instruments at the expense of analytical flexibility.

Beyond the portable GC instruments is the development of chip based, micro-fabricated GC (μGC) platforms that combines the benefits of fast analysis, low power consumption and portability into a single cohesive unit that is potentially hand portable. The development of μGC systems had its genesis thirty years ago when Terry *et al.* constructed a μGC upon a silicon wafer *via* chemical etching to form the necessary column channels [51,52]. To date there have been a number of reports of μGC systems, however the vast majority of these systems operate in the isothermal analysis mode, which seriously limits the range of analytes that can be resolved within a given period.

Resistively heated μGC instruments with temperature programming could alleviate this limitation in μGC and facilitate the analysis of a wide variety of samples in a timely

fashion. μGC instruments are particularly useful when applied in sensor applications for monitoring environmental contamination, industrial processes, or in forensic investigations. However the challenges associated with the construction of such micro-fabricated instruments are non-trivial [53]. Manginell and Frye-Mason obtained the first patent for a resistively heated μGC instrument in 2003 [54]. In their design a column (0.86 m × 100 μm ID × 400 μm d_f) was etched into a silicon wafer that was heated by the application of current to a resistive element in contact with the wafer. This wafer could be heated at a rate of up to 20.1 °C s^{-1} requiring 10.4 W (12.1 W m^{-1}) of power using a thin deposition of a resistive material on the back of the wafer. Temperatures between ambient and 150 °C were accessible with this instrument limiting its ability to analyse higher boiling point semi-volatile compounds.

Lu *et al.* constructed a μGC from a silicon-etched chip for the purposes of analysing volatile organic compounds (VOCs) [55]. This μGC was able to sample and pre-concentrate VOCs from air using an on-board adsorbent trap, and then thermally release and refocus the trapped VOCs prior to separation with a resistively heated GC column. In this study a resistively heated pad was affixed to the base of the chip to provide heating and temperature was monitored by an attached thermocouple. This allowed the programming of the μGC from ambient to 100 °C at a rate of 1°C s^{-1}. Column effluent was detected with a sensor array of four different chemical resistors. This setup allowed the separation, identification and quantification of 11 different VOCs present in a sample by measuring the differential response of each column eluent with respect to four chemical resistors. No studies upon the linearity of the heating process of the chip were carried out however the retention time RSD was reported to be approximately 1.8 % across the boiling point range of interest. This μGC system required further mounting and miniaturisation of key components including valves and pumps at the time of publication to make it truly portable.

Tienpont *et al.* developed a resistively heated μGC for analysis of air samples with a sample enrichment trap. The system showed selectivity for sulfur, phosphorus and chlorine containing analytes utilising a novel miniaturised plasma emission detector [56]. Agah *et al.* developed a μGC platform, on the scale of a coin in size, with resistive column heating for the analysis of an 11-component *n*-alkane mixture in less than 20 s [57]. Since the entire instrument was so small, the authors identified the potential of constructing a GC matrix where a group of μGC platforms could be combined to generate data using an array of different GC conditions. For example, each component of the GC matric could use a different stationary phase, temperature program or flow rate to generate complementary data that can be analysed to identify and quantify components of complex mixtures, while maintaining the potential for portability. Agah and Wise extended this work by producing micro-fabricated separation columns of low thermal mass and high thermal isolation to overcome the large thermal mass of silicon micro-fabricated chips [58]. This new device was again able to separate a multicomponent mixture of *n*-alkanes, with temperature programing requiring a mere 60 mW of power to heat to 150 °C at a rate of 20 °C s^{-1}.

Potkay *et al.* developed a low power resistively heated μGC system including a VOC pre-concentrator unit to perform analyses of 10 VOCs, as well as another analysis of 4 chemical warfare agent simulants and an explosive simulant using a 60 s GC method [59]. Stadermann *et al.* employed a single walled carbon nanotube stationary phase grown within a μGC channel *via* chemical vapour deposition [60]. This μGC was integrated with a resistive heater offering a temperature programming rate of 60 °C s^{-1} between a range of 90 to 150 °C. Ultra-fast chromatographic separation of two, four component mixtures: a series of *n*-alkanes and a mixture of different functional groups (methanol, 2-pentanone, anisole and decane) was achieved in less than 1 s reiterating the massive speed gains possible with μGC systems. Reid *et al.* followed up this work with an improved carbon nanotube stationary phase [61]. A separation of 5 *n*-alkanes

was achieved in 2.5 s with the application of a temperature program (50 °C then ramped at 26 °C s^{-1} to 115 °) affording a peak capacity of 8 in a 1.5 s timeframe. Both systems used a commercial instrument's liquid injector combined with high-speed diaphragm valves to provide minimised injection bandwidths to deliver these high-speed separations [60,61].

Zampolli *et al.* developed a complete portable μGC instrument for the monitoring of volatile aromatics present in urban air [62]. Luong *et al.* utilised a silicon micro-fabricated GC chip with resistive heating coupled to a micro-machined differential ion mobility spectrometer for the direct analysis of ethylene oxide [63]. An on board pump was used to inject air samples collected with Tedlar bags. A rapid (60 s) and sensitive (LOD 5 ppb) of ethylene oxide was demonstrated without the need for sample derivatisation. Application of a similar instrument platform has recently been demonstrated for the rapid analysis of non-sulfur odorants in natural gas [64].

As an aside to resistive heating, thermoelectric heaters, or Peltier devices are often used for small heating and cooling applications and deserve some mention. Peltier devices heat or cool materials based on the transfer of current and heat between the junctions of two dissimilar conductors. The origin of the heating ability of these systems is not resistive in nature, however Peltier usage is sometimes used in combination with μGC and warrants brief mention. The power efficiency of Peltier devices is substantially lower than resistive heating, however Peltier devices have the added utility of being capable of cooling to sub-ambient temperatures that can be advantageous for some applications. High temperatures required to analyse semi-volatile compounds are seldom accessible without stacking Peltier devices or the addition of other means of heating or cooling [65]. Lewis *et al.* constructed a μGC from glass wafers that combined a Peltier and a resistive heating element with an inbuilt micro-fabricated photoionization detector, which was used for the analysis of benzene, toluene, ethyl benzene and xylenes (BTEX) [66]. This μGC demonstrated very low power consumption (25 W maximum)

with an accessible temperature range of 0 to 200 °C. The micro-fabricated PID required only 100 mW to operate and demonstrated excellent sensitivity towards aromatic and terpenoid compounds.

An important and overlooked issue in portable GC instruments is that of carrier gas supply. The transportation of large pressurised cylinders of carrier gas is undesirable in field applications although sometimes unavoidable. Some routes to overcome this include the usage of filtered air as the carrier gas which is viable up to a temperature limit of 210 °C without causing damage to commercial phases [67]. Snyder *et al.* developed a portable GC instrument, using air as the carrier gas and was coupled to an ion mobility spectrometer for detection [68]. Grall *et al.* similarly used air as carrier gas for high-speed separations of VOCs, and also modified a GC system to be driven using a vacuum pump rather than a pressurised gas source to obtain the system's flow [69]. A GC system using resistive heating, and vacuum outlet conditions has been demonstrated by Sanchez *et al.* however this approach has not been pursued further due to the limited separation efficiency available while using air as the carrier gas [70].

While resistively heated GC is capable of increasing the speed of GC analysis and facilitating portable analysis, the separation capabilities of such systems are limited by the short analysis times required for viable field analysis. Furthermore it is often the case that one-dimensional GC separations lack the required peak capacity to resolve all components of highly complex samples, which means that the utility of such systems is limited in many applications. The flame ionisation detectors (FID) and thermal conductivity detectors (TCD) that are commonly used in portable GC instruments due to their low cost and universal response to chemical species, can not discern whether a given peak is pure in composition, which can lead to false positive measurements [71,72]. Selective detectors and mass spectrometry (MS) can be used to overcome the limitations of incomplete chromatographic separation, since these detectors provide additional, compound specific information about the peak eluting from a

chromatographic column. Selective detectors are useful in targeted analysis applications where an analyte has a chemical feature that is unique compared to other matrix components, however this is not always the case. MS detection provides fragmentation information for each compound at the point of elution, which provides an additional dimension of unique information about the content of each chromatographic peak. Compounds that elute from a chromatographic system at the same retention time will yield a mass spectrum that is a combination of all the fragmentation patterns of each individual solute. Deconvolution procedures can be used to determine the individual components of a multi-component peak [73]. Unfortunately MS detection is not readily amenable towards portable analysis, and the options that are available are relatively expensive [50]. A promising strategy that is capable of enhancing the peak capacity of portable GC analysis systems while maintaining the capacity for fast GC analysis is multidimensional (MD) GC, in which multiple separation steps are used to achieve total separation of complex samples [48,74].

1.3 Multidimensional separations with gas chromatography

Due to the aforementioned complexity of most samples, it has become increasingly necessary to utilise multiple separation steps to ensure that adequate characterisation is possible. Multiple step or MD separations leverage different molecular properties to provide the selectivity necessary to resolve complex samples. Molecular properties such as polarity, vapour pressure, electronegativity, aromaticity and more, can be targeted using chromatographic techniques to provide separation. Each sample has a unique range of compounds with corresponding molecular properties which gives rise to sample dimensionality, whereby multiple separation mechanisms can be utilised to obtain a separation. For example, petroleum based samples are comprised of a range of linear and branched chain aliphatic hydrocarbon compounds, aromatic and polyaromatic hydrocarbon compounds, as well as low levels of sulfated, nitrogenated, metallic and oxygenated species. Meanwhile a sample like coffee aroma contains a range of different polar molecules such as furans, aldehydes, ketones, pyridines, pyrazines and more [75]. Knowledge of the dimensionality of a sample can be utilised to construct a MD separation capable of resolving target compounds or holistically separating a sample [76]. There are a massive number of chromatographic combinations that can be utilised for MD analysis of complex samples depending on the goals and time constraints imposed [76-80].

Analyses are said to be MD when the separation mechanism of each analytical dimension is independent of one and other [48,49,81], in this way each separation dimension provides the maximum amount of information [82]. Correlation between separation mechanisms reduces chromatographic performance, and reduces the amount of information obtained during MD analysis [79,83]. Ideally the separation obtained during the first separation step should also be maintained in subsequent separation steps to maximise chromatographic resolution [81], however it has been

demonstrated that sacrificing some performance from the first-dimension separation can often yield benefits during MD analyses [82,84]. MDGC can operate in one of two analysis modes, either the heart-cut or the comprehensive two-dimensional (GC × GC) modes. During heart-cut MDGC analysis a sample is first separated using a primary column as is normal for single-dimensional GC. The first-separation column is then connected to a switching valve or Deans' switch, which is used to redirect a small portion of effluent from the first-dimension column to either a second separation column or a detector module. Only a small portion of first-dimension column effluent is transferred to the second-dimension column, so that the retention time of the analytes separated on the first dimension column is well defined and further so that the separation obtained on this first column is maintained in the latter separation. Heart cut MDGC has been demonstrated to be a very useful technique for targeted analysis of compounds in complex mixtures [85]. Utilising a combination of selective stationary phase combinations provides the opportunity to resolve individual target analytes rapidly and at low cost. The main weakness of the heart-cut analysis method is that only a small portion of the sample can be separated with both columns, since cutting long durations of solutes reduces the information obtained from the first-dimension separation, and there is an additional risk of recombining peaks that were previously separated during the first-dimension separation.

Comprehensive two-dimensional GC (GC × GC) was developed to enable the complete separation of samples in two separation dimensions [86]. GC × GC has been the topic of significant research focus due to the ability of this technique to separate large numbers of compounds in a fast and efficient manner [19,87-92]. In GC × GC, solutes are initially separated on a long first-dimension column (^{1}D), similar to one-dimensional GC. The outlet of the ^{1}D GC column is then connected to an interfacing device known as a modulator, which serves to sample a precise duration of first-dimension column effluent, and then inject that effluent into a second-dimension

column (^{2}D) for further separation. The ^{2}D separation is then completed quickly before another injection of effluent from the ^{1}D column effluent is carried out. This column configuration leads to the production of a series of short ^{2}D separations that can be placed in a two-dimensional array for visualisation and reconstruction of the ^{1}D retention times. The construction and optimisation of GC × GC systems is complicated by the interdependence of the two dimensions and the physical conditions of the GC analysis, however significant progress has been made in the optimisation of such systems [19,87,88,93].

1.4 Hardware for GC × GC modulation and MDGC

The critical component of GC × GC analyses is the modulator interface, which serves to trap and focus effluent from the first-dimension column. Narrow ^{2}D injection bandwidths are critical for maximising the separation performance of the ^{2}D column. As a result there has been a large amount of research carried out on the development of modulator technology [94-96]. Conventional modulators are based on some form of solute trapping or valve-controlled modulation. Solute trapping modulators generally utilise cryogenic jets that are used to cool a segment of capillary to trap solutes *via* condensation. Solutes are then released by deactivating the cold jet and applying heat, usually using heated air. Such cryogenic modulation strategies, while effective, are quite costly to operate, making alternative modulation techniques based on resistive heating very attractive. Valve based modulation is another effective means for delivering GC × GC separations, as the hardware required for this technique is low cost and simple to implement with modern electronic pressure control and the commercial availability of PMDs for GC × GC.

The connectivity and flexibility provided by PMDs has been exceptionally useful for the development and implementation of heart cut MDGC and GC × GC in modern GC systems, however the applications of these devices within portable GC systems has thus far been lacking [85,97]. Classical column connectivity was built to fulfill the needs of packed column technology that operates at high flow rates to ensure that system dead volumes are sufficiently purged to prevent undesirable peak broadening. Deactivated glass “press-fit” connectors were developed to address the connectivity issues of modern capillary column technologies, however these connectors still introduce void volumes to capillary GC systems and they are prone to leakage after multiple thermal cycles, precluding them from long term implementation [98,99].

PMDs are an exciting development for modern GC connectivity as they were designed with capillary column use in mind, and provide highly robust inert connections between instrument components [100]. PMDs are constructed from a series of thin micro-aligned metal plates, each of which can be laser milled to construct the desired flow architecture. Diffusion bonding is used to combine these plates into a single unified wafer, and metal injection molding and milling are then used to attach unions for column connectivity. These wafers have low thermal masses and minimal void volumes, so that they rapidly equilibrate to the temperatures and pressures applied. Metallic surfaces within the wafer are also chemically deactivated to ensure inert surface chemistry. Planar microfluidic wafers have been developed in a number of formats to enable Deans' switching, MDGC and GC × GC, makeup flow addition and flow splitting [101-108]. Investigation of PMDs with portable GC systems with MDGC and GC × GC capabilities could be very beneficial towards enhancing the separation power of GC systems for portable and high throughput analysis.

1.5 Scope of thesis

The aim of this thesis was to investigate the effectiveness of resistive heating for fast and portable GC analysis using the Falcon Calidus™ GC platform. The Calidus™ weighs 11.4 kg, and is 43 x 22 x 28 cm in size, which offers the possibility for portable analysis once provided with power and gases. The modular format of the instrument was expected to be rugged for portable analysis as well as providing flexibility to satisfy a wide range of GC applications. This instrument has not previously been evaluated for academic research, and is generally distributed as a process monitoring GC with high throughput analysis capabilities. The Calidus™ uses short, SS GC columns, which are directly heated by the application of electric current that resistively heats the column. The ability to rapidly and precisely control column temperatures using resistive heating was expected to provide substantial enhancements, in terms of the speed of analysis and the power efficiency of the instrument. The combination of fast separations, a compact instrument and low power requirements made this GC instrument very amenable towards portable GC analysis.

Since complex samples are very challenging to separate using standard one-dimensional GC techniques, heart cut MDGC analysis and comprehensive GC ×, GC were investigated. PMD devices for MDGC and GC × GC were integrated into the Calidus™ for the purposes of enhancing its separation capabilities, and the performance of these modifications were evaluated and compared with bench top MDGC and GC × GC instruments. Additionally a novel single-stage resistively heated focusing device was evaluated for injection bandwidth focusing, and comprehensive GC × GC analysis. The ability of this modulator to trap and release solutes was compared to commercial modulation strategies such as cryogenic and valve based modulation and found to be very effective. The single-stage thermal modulator was similarly integrated into the Calidus™ GC instrument and tested for effectiveness. The capabilities of the Calidus™

and a range of MDGC and GC × GC applications were demonstrated using complex samples derived from the natural environment.

1.6 References

[1] C.F. Poole, The essence of chromatography, Amsterdam; Boston : Elsevier, 2003. 1st ed., 2003.

[2] F.L. Dorman, E.B. Overton, J.J. Whiting, J.W. Cochran, J. Gardea-Torresdey, Gas Chromatography, Anal. Chem. 80 (2008) 4487-4497.

[3] F.L. Dorman, J.J. Whiting, J.W. Cochran, J. Gardea-Torresdey, Gas Chromatography, Anal. Chem. 82 (2010) 4775-4785.

[4] J. de Zeeuw, J. Luong, Developments in stationary phase technology for gas chromatography, Trends Anal. Chem. 21 (2002) 594-607.

[5] C.F. Poole, S.K. Poole, Separation characteristics of wall-coated open-tubular columns for gas chromatography, J. Chromatogr. A 1184 (2008) 254-280.

[6] J. de Zeeuw, The Development and Applications of PLOT Columns in Gas-Solid Chromatography, LC-GC Europe 24 (2011) 38-45.

[7] K. Grob, Injection techniques in capillary GC, Anal. Chem. 66 (1994) 1009A-1019A.

[8] R. Bailey, Injectors for capillary gas chromatography and their application to environmental analysis, J. Environ. Monit. 7 (2005) 1054-1058.

[9] V.R. Reid, R.E. Synovec, High-speed gas chromatography: The importance of instrumentation optimization and the elimination of extra-column band broadening, Talanta 76 (2008) 703-717.

[10] L.M. Blumberg, Theory of fast capillary gas chromatography. Part 1. Column efficiency, J. High Resolut. Chromatogr. 20 (1997) 597-604.

[11] L.M. Blumberg, Theory of fast capillary gas chromatography. Part 2. Speed of analysis, J. High Resolut. Chromatogr. 20 (1997) 679-687.

[12] M.S. Klee, L.M. Blumberg, Theoretical and practical aspects of fast gas chromatography and method translation, J. Chromatogr. Sci. 40 (2002) 234-247.

[13] C.F. Poole, N. Lenca, Gas chromatography on wall-coated open-tubular columns with ionic liquid stationary phases, J. Chromatogr. A 1357 (2014) 87-109.

[14] G.H. Stewart, S.L. Seager, J.C. Giddings, Influence of pressure gradients on resolution in gas chromatography, Anal. Chem. 31 (1959) 1738.

[15] J.C. Giddings, S.L. Seager, L.R. Stucki, G.H. Stewart, Plate height in gas chromatography, Anal. Chem. 32 (1960) 867-870.

[16] J.J. van Deemter, F.J. Zuiderweg, A. Klinkenberg, Longitudinal diffusion and resistance to mass transfer as causes of nonideality in chromatography, Chem. Eng. Sci. 5 (1956) 271-289.

[17] P.A. Leclercq, C.A. Cramers, Optimum performance of capillary GC columns as a function of tube diameter and film thickness under various operating conditions. Computer program for calculation of H-u curves and minimum analysis times, HRC CC, J. High Resolut. Chromatogr. Chromatogr. Commun. 8 (1985) 764-771.

[18] L.M. Blumberg, Plate height formula widely accepted in GC is not correct, J. Chromatogr. A 1218 (2011) 8722-8723.

[19] L.M. Blumberg, Temperature-Programmed Gas Chromatography, John Wiley & Sons, 2011.

[20] L.M. Blumberg, Theory of fast capillary gas chromatography. Part 3. Column performance vs. gas flow rate, J. High Resolut. Chromatogr. 22 (1999) 403-413.

[21] L.M. Blumberg, Theory of fast capillary gas chromatography. Part 4. Column performance vs. liquid film thickness, J. High Resolut. Chromatogr. 22 (1999) 501-508.

[22] L.M. Blumberg, M.S. Klee, Optimal heating rate in gas chromatography, J. Microcolumn Sep. 12 (2000) 508-514.

[23] P.Q. Tranchida, L. Mondello, Current-day employment of the micro-bore open-tubular capillary column in the gas chromatography field, J. Chromatogr. A 1261 (2012) 23-36.

[24] M.R. Jacobs, E.F. Hilder, R.A. Shellie, Applications of resistive heating in gas chromatography: A review, Anal. Chim. Acta 803 (2013) 2-14.

[25] A. Wang, H.D. Tolley, M.L. Lee, Gas chromatography using resistive heating technology, J. Chromatogr. A 1261 (2012) 46-57.

[26] M.E. Hail, R.A. Yost, Compact gas chromatograph probe for gas chromatography/mass spectrometry utilizing resistively heated aluminum-clad capillary columns, Anal. Chem. 61 (1989) 2410-2416.

[27] F. Xu, W. Guan, G. Yao, Y. Guan, Fast temperature programming on a stainless-steel narrow-bore capillary column by direct resistive heating for fast gas chromatography, J. Chromatogr. A 1186 (2008) 183-188.

[28] K.M. Sloan, R.V. Mustacich, B.A. Eckenrode, Development and evaluation of a low thermal mass gas chromatograph for rapid forensic GC-MS analyses, Field Anal. Chem. Technol. 5 (2001) 288-301.

[29] J. Luong, R. Gras, R. Mustacich, H. Cortes, Low thermal mass gas chromatography: Principle and applications, J. Chromatogr. Sci. 44 (2006) 253-261.

[30] F. David, R. Szucs, J. Makwana, P. Sandra, Fast capillary GC using a low thermal mass column oven for the determination of residual solvents in pharmaceuticals, J. Sep. Sci. 29 (2006) 695-698.

[31] K. Sasamoto, N. Ochiai, H. Kanda, Dual low thermal mass gas chromatography-mass spectrometry for fast dual-column separation of pesticides in complex sample, Talanta 72 (2007) 1637-1643.

[32] E.U. Ehrmann, H.P. Dharmasena, K. Carney, E.B. Overton, Novel column heater for fast capillary gas chromatography, J. Chromatogr. Sci. 34 (1996) 533-539.

[33] S.D. Stearns, H. Cai, J.A. Koehn, M. Brisbin, C. Cowles, C. Bishop, S. Puente, D. Ashworth, A direct resistively heated gas chromatography column with heating and sensing on the same nickel element, J. Chromatogr. A 1217 (2010) 4629-4638.

[34] M. van Deursen, J. Beens, C.A. Cramers, H. Janssen, Possibilities and limitations of fast temperature programming as a route towards fast GC, J. High Resolut. Chromatogr. 22 (1999) 509-513.

[35] J. Dalluge, R. Ou-Aissa, J.J. Vreuls, U.A.T. Brinkman, Fast temperature programming in gas chromatography using resistive heating, J. High Resolut. Chromatogr. 22 (1999) 459-464.

[36] T.A. Williams, M. Riddle, S.L. Morgan, W.E. Brewer, Rapid gas chromatographic analysis of drugs of forensic interest, J. Chromatogr. Sci. 37 (1999) 210-214.

[37] T.I. Dearing, J.S. Nadeau, B.G. Rohrback, L.S. Ramos, R.E. Synovec, Real-time target selection optimization to enhance alignment of gas chromatograms, Talanta 83 (2011) 738-743.

[38] J.S. Nadeau, B.W. Wright, R.E. Synovec, Chemometric analysis of gas chromatography-mass spectrometry data using fast retention time alignment via a total ion current shift function, Talanta 81 (2010) 120-128.

[39] T. Skov, d.B.F. van, G. Tomasi, R. Bro, Automated alignment of chromatographic data, J. Chemom. 20 (2007) 484-497.

[40] K.M. Pierce, B. Kehimkar, L.C. Marney, J.C. Hoggard, R.E. Synovec, Review of chemometric analysis techniques for comprehensive two dimensional separations data, J. Chromatogr. A 1255 (2012) 3-11.

[41] M. van Lieshout, R. Derks, H. Janssen, C.A. Cramers, Fast capillary gas chromatography. Comparison of different approaches, J. High Resolut. Chromatogr. 21 (1998) 583-586.

[42] V. Jain, J.B. Phillips, Fast temperature programming on fused-silica open-tubular capillary columns by direct resistive heating, J. Chromatogr. Sci. 33 (1995) 55-59.

[43] V. Jain, J.B. Phillips, High-speed gas chromatography using simultaneous temperature gradients in both time and distance along narrow-bore capillary columns, J. Chromatogr. Sci. 33 (1995) 601-605.

[44] A. Grall, C. Leonard, R. Sacks, Peak capacity, peak-capacity production rate, and boiling point resolution for temperature-programmed GC with very high programming rates, Anal. Chem. 72 (2000) 591-598.

[45] C. Bicchi, C. Brunelli, C. Cordero, P. Rubiolo, M. Galli, A. Sironi, High-speed gas chromatography with direct resistively-heated column (ultra fast module-GC)-separation measure (S) and other chromatographic parameters under different analysis conditions for samples of different complexities and volatilities, J. Chromatogr. A 1071 (2005) 3-12.

[46] L.M. Blumberg, M.S. Klee, Metrics of separation in chromatography, J. Chromatogr. A 933 (2001) 1-11.

[47] J.M. Davis, J.C. Giddings, Statistical method for estimation of number of components from single complex chromatograms: application to experimental chromatograms, Anal. Chem. 57 (1985) 2178-2182.

[48] J.C. Giddings, Two-dimensional separations: concept and promise, Anal. Chem. 56 (1984) 1258A-1260A, 1262A, 1264A, 1266A, 1268A, 1270A.

[49] J.C. Giddings, Concepts and comparisons in multidimensional separation, HRC CC, J. High Resolut. Chromatogr. Chromatogr. Commun. 10 (1987) 319-323.

[50] P.A. Smith, Person-portable gas chromatography: Rapid temperature program operation through resistive heating of columns with inherently low thermal mass properties, J. Chromatogr. A 1261 (2012) 37-45.

[51] S.C. Terry, J.B. Angell, A column gas chromatography system on a single wafer of silicon, Theory, Des., Biomed. Appl. Solid State Chem. Sens. (1978) 207-218.

[52] S.C. Terry, J.H. Jerman, J.B. Angell, A gas chromatographic air analyzer fabricated on a silicon wafer, IEEE Trans. Electron Devices ED-26 (1979) 1880-1886.

[53] J. Luong, H. Cai, R. Gras, J. Curvers, Developments in Ultra-Fast Temperature Programming with Silicon Micromachined Gas Chromatography: Performance and Limitations, J. Chromatogr. Sci. 50 (2012) 245-252.

[54] R.P. Manginell, G.C. Frye-Mason, Temperature programmable microfabricated gas chromatography column, US6666907B1 (2003) Sandia Corporation, USA.

[55] C.-J. Lu, W.H. Steinecker, W.-C. Tian, M.C. Oborny, J.M. Nichols, M. Agah, J.A. Potkay, H.K.L. Chan, J. Driscoll, R.D. Sacks, K.D. Wise, S.W. Pang, E.T. Zellers, First-generation hybrid MEMS gas chromatograph, Lab Chip 5 (2005) 1123-1131.

[56] B. Tienpont, F. David, W. Witdouck, D. Vermeersch, H. Stoeri, P. Sandra, Features of a micro-gas chromatograph equipped with enrichment device and microchip plasma emission detection (μPED) for air monitoring, Lab Chip 8 (2008) 1819-1828.

[57] M. Agah, G.R. Lambertus, R. Sacks, K. Wise, High-speed MEMS-based gas chromatography, J. Microelectromech. Syst. 15 (2006) 1371-1378.

[58] M. Agah, K.D. Wise, Low-mass PECVD oxynitride gas chromatographic columns, J. Microelectromech. Syst. 16 (2007) 853-860.

[59] J.A. Potkay, G.R. Lambertus, R.D. Sacks, K.D. Wise, A low-power pressure- and temperature-programmable micro gas chromatography column, J. Microelectromech. Syst. 16 (2007) 1071-1079.

[60] M. Stadermann, A.D. McBrady, B. Dick, V.R. Reid, A. Noy, R.E. Synovec, O. Bakajin, Ultrafast Gas Chromatography on Single-Wall Carbon Nanotube Stationary Phases in Microfabricated Channels, Anal. Chem. 78 (2006) 5639-5644.

[61] V.R. Reid, M. Stadermann, O. Bakajin, R.E. Synovec, High-speed, temperature programmable gas chromatography utilizing a microfabricated chip with an improved carbon nanotube stationary phase, Talanta 77 (2009) 1420-1425.

[62] S. Zampolli, I. Elmi, F. Mancarella, P. Betti, E. Dalcanale, G.C. Cardinali, M. Severi, Real-time monitoring of sub-ppb concentrations of aromatic volatiles with a MEMS-enabled miniaturized gas-chromatograph, Sens. Actuators, B B141 (2009) 322-328.

[63] J. Luong, R. Gras, H.J. Cortes, R.A. Shellie, Temperature-programmable low thermal mass silicon micromachined gas chromatography and differential mobility detection for

the fast analysis of trace level of ethylene oxide in medical work place atmospheres, J. Chromatogr. A 1261 (2012) 136-141.

[64] J. Luong, R. Gras, H.J. Cortes, R.A. Shellie, Temperature-Programmable Resistively Heated Micromachined Gas Chromatography and Differential Mobility Spectrometry Detection for the Determination of Non-Sulfur Odorants in Natural Gas, Anal. Chem. 85 (2013) 3369-3373.

[65] A.L. Robinson, L.F. Anderson, Sub- to super-ambient temperature programmable microfabricated gas chromatography column, US6706091B1 (2004) Sandia Corporation, USA.

[66] A.C. Lewis, J.F. Hamilton, C.N. Rhodes, J. Halliday, K.D. Bartle, P. Homewood, R.J.P. Grenfell, B. Goody, A.M. Harling, P. Brewer, G. Vargha, M.J.T. Milton, Microfabricated planar glass gas chromatography with photoionization detection, J. Chromatogr. A 1217 (2010) 768-774.

[67] A.J. Grall, R.D. Sacks, Column performance and stability for high-speed vacuum-outlet GC of volatile organic compounds using atmospheric pressure air as carrier gas, Anal. Chem. 71 (1999) 5199-5205.

[68] A.P. Snyder, C.S. Harden, A.H. Brittain, M.G. Kim, N.S. Arnold, H.L.C. Meuzelaar, Portable hand-held gas chromatography/ion mobility spectrometry device, Anal. Chem. 65 (1993) 299-306.

[69] A.J. Grall, E.T. Zellers, R.D. Sacks, High-Speed Analysis of Complex Indoor VOC Mixtures by Vacuum-Outlet GC with Air Carrier Gas and Programmable Retention, Environ. Sci. Technol. 35 (2001) 163-169.

[70] J.M. Sanchez, R.D. Sacks, Performance characteristics of a new prototype for a portable GC using ambient air as carrier gas for on-site analysis, J. Sep. Sci. 30 (2007) 1052-1060.

[71] L.S. Ettre, The invention, development, and triumph of the flame ionization detector, LCGC North America 20 (2002) 48-60.

[72] C.F. Poole, Ionization-based detectors for gas chromatography, J. Chromatogr. A 1421 (2015) 137-153.

[73] T. Veriotti, R. Sacks, Characterization and Quantitative Analysis with GC/TOFMS Comparing Enhanced Separation with Tandem-Column Stop-Flow GC and Spectral Deconvolution of Overlapping Peaks, Anal. Chem. 75 (2003) 4211-4216.

[74] L.M. Blumberg, Comprehensive two-dimensional gas chromatography: metrics, potentials, limits, J. Chromatogr., A 985 (2003) 29-38.

[75] M.R. Ruosi, C. Cordero, C. Cagliero, P. Rubiolo, C. Bicchi, B. Sgorbini, E. Liberto, A Further Tool To Monitor the Coffee Roasting Process: Aroma Composition and Chemical Indices, J. Agric. Food Chem. 60 (2012) 11283-11291.

[76] J.C. Giddings, Sample dimensionality: a predictor of order-disorder in component peak distribution in multidimensional separation, J. Chromatogr. A 703 (1995) 3-15.

[77] J.M. Davis, C. Samuel, The need for two-dimensional gas chromatography: extent of overlap in one-dimensional gas chromatograms, J. High Resolut. Chromatogr. 23 (2000) 235-244.

[78] J. Harynuk, B. Vlaeminck, P. Zaher, P.J. Marriott, Projection of multidimensional GC data into alternative dimensions-exploiting sample dimensionality and structured retention patterns, Anal. Bioanal. Chem. 386 (2006) 602-613.

[79] S.K. Poole, C.F. Poole, The orthogonal character of stationary phases for gas chromatography, J. Sep. Sci. 31 (2008) 1118-1123.

[80] J.V. Seeley, C.T. Bates, J.D. McCurry, S.K. Seeley, Stationary phase selection and comprehensive two-dimensional gas chromatographic analysis of trace biodiesel in petroleum-based fuel, J. Chromatogr. A 1226 (2012) 103-109.

[81] J.C. Giddings, H.J. in: Cortes, Multidimensional chromatography : techniques and applications, M. Dekker, New York, 1990.

[82] L. Blumberg, M.S. Klee, A critical look at the definition of multidimensional separations, J. Chromatogr. A 1217 (2010) 99-103.

[83] N.E. Watson, J.M. Davis, R.E. Synovec, Observations on "orthogonality" in comprehensive two-dimensional separations, Anal. Chem. 79 (2007) 7924-7927.

[84] M.S. Klee, J. Cochran, M. Merrick, L.M. Blumberg, Evaluation of conditions of comprehensive two-dimensional gas chromatography that yield a near-theoretical maximum in peak capacity gain, Journal of Chromatography A 1383 (2015) 151-159.

[85] P.Q. Tranchida, D. Sciarrone, P. Dugo, L. Mondello, Heart-cutting multidimensional gas chromatography: A review of recent evolution, applications, and future prospects, Anal. Chim. Acta 716 (2012) 66-75.

[86] Z. Liu, J.B. Phillips, Comprehensive two-dimensional gas chromatography using an on-column thermal modulator interface, J. Chromatogr. Sci. 29 (1991) 227-231.

[87] W. Bertsch, Two-dimensional gas chromatography. Concepts, instrumentation, and applications - part 1: fundamentals, conventional two-dimensional gas chromatography, selected applications, J. High Resolut. Chromatogr. 22 (1999) 647-665.

[88] W. Bertsch, Two-dimensional gas chromatography. Concepts, instrumentation, and applications - part 2: comprehensive two-dimensional gas chromatography, J. High Resolut. Chromatogr. 23 (2000) 167-181.

[89] M. Adahchour, J. Beens, U.A.T. Brinkman, Recent developments in the application of comprehensive two-dimensional gas chromatography, J. Chromatogr. A 1186 (2008) 67-108.

[90] L.M. Blumberg, Multidimensional gas chromatography: theoretical considerations, Comprehensive Chromatography in Combination with Mass Spectrometry, John Wiley & Sons, Inc., 2011, p. 13-63.

[91] J.V. Seeley, S.K. Seeley, Multidimensional Gas Chromatography: Fundamental Advances and New Applications, Anal. Chem. 85 (2013) 557-578.

[92] M. Edwards, H. Boswell, T. Górecki, Comprehensive Multidimensional Chromatography, Curr. Chromatogr. 2 (2015) 80-109.

[93] A. Mostafa, M. Edwards, T. Górecki, Optimization aspects of comprehensive two-dimensional gas chromatography, J. Chromatogr. A 1255 (2012) 38-55.

[94] A.L. Lee, A.C. Lewis, K.D. Bartle, J.B. McQuaid, P.J. Marriott, A comparison of modulating interface technologies in comprehensive two-dimensional gas chromatography (GC × GC), J. Microcolumn Sep. 12 (2000) 187-193.

[95] P.Q. Tranchida, G. Purcaro, P. Dugo, L. Mondello, G. Purcaro, Modulators for comprehensive two-dimensional gas chromatography, Trends Anal. Chem. 30 (2011) 1437-1461.

[96] M. Edwards, A. Mostafa, T. Górecki, Modulation in comprehensive two-dimensional gas chromatography: 20 years of innovation, Anal. Bioanal. Chem. 401 (2011) 2335-2349.

[97] J.V. Seeley, Recent advances in flow-controlled multidimensional gas chromatography, J. Chromatogr. A 1255 (2012) 24-37.

[98] C. Ibanez, Construction of an all-glass/fused silica, zero dead volume multidimensional gas chromatographic system using press-fit connectors: Preliminary results, J. High Resolut. Chromatogr. 16 (1993) 552-554.

[99] K. Grob, M. Biedermann, K. Bernath, H.P. Neukom, M. Galli, Call for fused silica tubing furnishing tight press-fit connections, J. High Resolut. Chromatogr. 15 (1992) 613-614.

[100] J. Luong, Planar microfluidic devices and selective detection in gas chromatography : techniques and applications, 2013., 2013.

[101] J.V. Seeley, N.J. Micyus, J.D. McCurry, S.K. Seeley, Comprehensive two-dimensional gas chromatography with a simple fluidic modulator, Am. Lab. 38 (2006) 24-26.

[102] J.V. Seeley, N.J. Primeau, S.V. Bandurski, S.K. Seeley, J.D. McCurry, Microfluidic Deans Switch for Comprehensive Two-Dimensional Gas Chromatography, Anal. Chem. 79 (2007) 1840-1847.

[103] B. Quimby, J. McCurry, W. Norman, Capillary Flow Technique for Gas Chromatography: Reinvigorating a Mature Analytical Discipline, LC-GC The Peak (2007) 7-10.

[104] J. Luong, R. Gras, G. Yang, L. Sieben, H. Cortes, Capillary flow technology with multi-dimensional gas chromatography for trace analysis of oxygenated compounds in complex hydrocarbon matrices, J. Chromatogr. Sci. 45 (2007) 664-670.

[105] P.Q. Tranchida, G. Purcaro, A. Visco, L. Conte, P. Dugo, P. Dawes, L. Mondello, A flexible loop-type flow modulator for comprehensive two-dimensional gas chromatography, J. Chromatogr. A 1218 (2011) 3140-3145.

[106] J. Luong, R. Gras, H. Cortes, R.A. Shellie, Multi-dimensional gas chromatography with a planar microfluidic device for the characterization of volatile oxygenated organic compounds, J. Chromatogr. A 1255 (2012) 216-220.

[107] J. Luong, R. Gras, R.A. Shellie, H.J. Cortes, Applications of planar microfluidic devices and gas chromatography for complex problem solving, J. Sep. Sci. 36 (2013) 182-191.

[108] R.A. Shellie, H.J. Cortes, R. Gras, J. Luong, Planar microfluidic devices in flow modulated comprehensive two dimensional gas chromatography for challenging petrochemical applications, Anal. Methods 5 (2013) 6598-6604.

Chapter 2: Planar microfluidics and resistively heated GC

Summary

While resistive heating enables GC users to achieve rapid separations, such analyses have a number of additional requirements to ensure sufficient quality. As run times are reduced, the effects of off-column peak broadening are exacerbated since the time that an analyte spends in the column decreases along with associated peak broadening. Dead volumes, cold spots, and active surfaces are all potential sources of off-column band broadening, however the initial injection volume is usually the performance-limiting component of GC instrumentation. The initial injection volume impacts the amount of displacement that is required to separate two adjacent compounds on a chromatogram, therefore the narrower the initial injection band the less displacement is required to separate two compounds.

Injection bandwidths can be minimised using one of three strategies. The simplest method is to use a split injector with a high split ratio to reduce the time required to complete a sample injection. Most modern GC instruments include a split/splitless (S/SL) injector that is capable of providing high split ratios, however this injection technique reduces analytical sensitivity since only a small fraction of a sample injection is transferred to the GC column. The second method involves using thermal focusing to spatially confine analytes in a narrow injection volume before transferring the sample to the column and this strategy was evaluated in Chapter 3. Finally electrically or pneumatically actuated valves can be used to physically control the width of the injections that are transferred to GC a column during the injection procedure. In this chapter PMDs were evaluated for the manipulation of injection bandwidths and this technique was compared to S/SL injection for the purpose of enabling fast GC and multidimensional GC (MDGC) analysis.

2.1 Introduction

Traditional temperature programmed GC requires between 20 min and 2 hours for a complete analysis depending on the column used and the sample to be separated. While an hour-long analysis time is acceptable for a small number of samples, a long separation time can quickly become a bottleneck when a large number of samples require analysis. To overcome this bottleneck, it is common for analytical laboratories to operate multiple GC instruments to maintain an acceptable level of sample throughput. This need for high throughput GC analysis has led to the development of fast GC techniques, which can reduce analysis times by one and two orders of magnitude, and minimise the need for the operation of multiple GC instruments. Fast GC uses short capillary columns with a narrow internal diameter to vastly increase the speed of analysis, with little compromise in separation performance [1,2]. The main drawback of fast GC is that narrow bore columns typically have reduced solute loading capacity compared to wide bore columns [3-5]. While GC theory and method translation can be used to considerably accelerate the speed of GC separations, this procedure is not without its challenges. Fast GC separations place stringent demands on all components of GC instruments including the sample injection procedure, separation column, column heating method, instrument connectivity and peak detection modules.

The capillary column and strategy used to heat it during temperature-programmed analysis have a significant impact on the performance of fast GC separations. Convection oven column heating is affected by thermal hysteresis due to the relatively large thermal mass of the convection oven that is present in modern GC instruments [6,7]. Resistive column heating has been developed as an alternative means of providing rapid, accurate and precise temperature programming for fast GC, while using minimal electrical power [8-10]. As the time of analysis is reduced, the initial injection bandwidth and off-column sources of peak broadening have a proportionally greater impact upon the final performance of a GC separation. As a result of this, instrument vendors have gone a long

way towards minimising off-column peak broadening by reducing system dead volumes and eliminating thermal cold spots in carrier gas flow path [11,12]. Furthermore chemical passivation has been critical to improving peak shape, since tailing peaks often cause peak co-elutions and a reduction in analyte detectability [13-17].

Fast GC also requires detectors with correspondingly fast data sampling rates to ensure that peaks are adequately sampled during elution to enable integration. The FID is a staple detector for fast GC due to its universal and sensitive response towards organic compounds, and its flexible data sampling rate that is well suited to fast analysis. TCD and photoionisation detectors are some other detectors that are also capable of providing rapid data sampling rates with universal responses for a wide variety of organic compounds. In cases where mass spectral data is desired, time of flight mass spectrometers (TOF-MS) detectors are preferred due to their ability to acquire full mass range spectra while maintaining adequate data sampling rates [18]. Quadrupole MD detectors, despite their prevalence in GC laboratories, are generally unsuitable in fast analysis due to the negative affect that fast mass scanning has on the sensitivity and spectra obtained using such instruments [19].

Perhaps the most overlooked component of GC instruments is the injection technique. Often the S/SL injector that is incorporated in conventional GC instruments limits the performance of fast GC separations due to the limited ability of S/SL injectors to provide narrow injection bandwidths [20-23]. S/SL became the dominant injection method in GC, due its convenient ability to introduce liquid-based samples to capillary GC columns in a controlled and repeatable manner [24-26]. In the split mode, the S/SL injector provides a convenient means of diluting concentrated samples prior to analysis. In situations where dilution of a sample at the point of injection limits the detection of trace level analytes the SL injection mode can be used to prevent sample dilution. Unfortunately neither of these injection modes provides any pre-column peak focusing, with injection bandwidths being determined by the physical construction and flow rates

within the injector [27,28]. SL injections take place on the minute time scale and rely on post-injection solute focusing, while split injections reduce injection bandwidths at a rate proportional to the split ratio; however injection bandwidths narrower than 200 ms are rarely achieved using S/SL injection due to the high split ratios required for achieving such narrow injection bandwidths.

Alternative methods for injection bandwidth minimisation are based on valve switching and solute focusing approaches. Valves can be used to physically control the injection bandwidth by manipulating the duration of time over which a sample is transferred to a separation column. It is essential that switching valves have a fast actuation time and minimal internal dead volume so that they are capable of providing narrow injection bandwidths. Valves must also be physically robust, chemically inert and capable of operating at high temperature. Valves can be actuated in one of two ways, either by electrically energising an electromagnetic solenoid, or using a pneumatically controlled switch.

The first type of valve utilised for GC injection was the rotary valve, which is constructed from a pair of engraved plates that can be rotated between two states to change the direction of flow within the valve. Rotary valves have been used for process stream sampling, heart cutting, and column effluent modulation to achieve GC × GC separations [29-31]. Despite the relatively large inertia and high amount of friction between rotary valve components, injection durations of just 2 ms have been obtained while using pneumatic switching [32]. Injection using mechanical actuation is much slower (Table 2) due to the limited force generated by electric solenoids. Unfortunately, rotary valves are not well suited to operation at temperatures exceeding 200 °C, due to their limited thermal stability, and long-term maintenance requirements.

An attempt to minimise the inertia within a mechanical injector design was realised by Tijssen *et al.*, who prepared an injector based on a mechanically actuated sliding tube

with a small pinhole [33]. The low mass of the sliding tube could be rapidly shifted with the use of an electric solenoid eliminating the need for pneumatic actuation. A vaporised sample was passed through the tube, and the sample was injected to the inlet of a capillary column during the actuation of the sliding tube, whereby the entrance of the capillary column and pin hole in the sliding tube were aligned to allow analyte transfer from the injector to the column. Injection bandwidths as narrow as 6 ms were obtained with this design (Table 2), however the alignment of the sliding pin hole with the GC capillary column inlet proved to be a problem causing poor peak area repeatability (> 10 % RSD) [34,35].

Diaphragm valves are a promising alternative to classical rotary valve designs that were limited by inertia, friction and internal dead volumes. Diaphragm valves have been used to control injection bandwidths in heart cut MDGC and comprehensive two-dimensional GC × GC. Diaphragm valves operate by shifting the position of a small flexible polymer membrane that can constrict a narrow channel within the device. The position of the valve can be electrically or pneumatically actuated, similar to rotary valves. The low mass of the diaphragm and the small inertia of the carrier gas displaced during actuation leads to diaphragm valves having exceptionally fast actuation times of less than 10 ms (Table 2). Additionally these valves exhibit excellent peak area repeatability ± 1 % RSD, which is ideal for quantitative analysis [46]. Unfortunately, the polymers used for membrane construction impose a temperature limitation of 200 to 250 °C after which they begin to decompose. Furthermore, these devices typically have limited lifespan before the flexible polymer must be serviced.

Table 2 Summary table of valve based injection bandwidths achieved using different injection techniques.

Injection method	Peak width (ms)	Test compound	Actuation mode	Reference
Deans' switch GC × GC	40	*n*-heptane	Electrical solenoid	[36]
		n-pentane		[37]
Diaphragm valve	7.1	Methane		[38]
	56	1,3,5-trimethylbenzene	Pneumatic actuation	[39]
	35	Ethanol		[40]
	23.5	*n*-octane		[41]
	54	*n*-pentane		[42]
	250	Methanol		[43]
	10	Not reported		[44]
Dual diaphragm valves	30	*n*-alkanes		[45]
	4	Methanol		[46]
Fluidic logic gate	9.5	Methane		[47]
	4			[20]
	48			[48]
	5	*n*-pentane		[49]
Pulsed flow GC × GC	20	*n*-pentane	Electrical solenoid	[50]
	155	*n*-hexane		[51]
Rotary valve	4.6	*n*-pentane	Pneumatic actuation	[38]
	2	N/A		[32]
	80	Methane	Electrical solenoid	[52]
Sliding needle injection	6			[33]
	14.1			[35]

Switching devices based on pneumatically controlling the flow of gases using the Deans' switching principle eliminate the problem of moving parts and high temperature operation [53]. Initially injection bandwidth minimisation using the Deans' switching principle was explored using fluidic logic gates technologies [20,47]. These devices that are based on classical GC unions are able to achieve switching times of just 1 ms when provided with sufficient controlling gas flows. Fluidic logic gates require high auxiliary

gas flow rates between 2 and 5 L min^{-1} to ensure that turbulent gas flow conditions are obtained to enable switching. This led to a large expenditure of gas that has limited the uptake of fluidic logic gates in GC. Deans' switching without turbulent flow based switching has been used in heart cut MDGC and GC × GC applications however these devices have not been applied for injection bandwidth minimisation [54,55].

Based on the principles of Deans' switching and fluidic logic gates, modern PMDs have been designed for a range of applications including: MDGC, GC × GC, column effluent flow splitting and make up gas addition [11,36,56-58]. PMDs have a number of exciting properties that could be beneficial towards GC injection procedures. Firstly, unlike classical column unions and fluidic logic gates, PMDs are designed to incorporate minimal internal dead volumes, which minimises valve actuation time and the potential of peak broadening. PMDs contain no moving parts, and as a result they can be maintained at high temperatures without impacting their integrity. In particular, PMDs have been combined with high-speed solenoid valves for use in comprehensive two-dimensional GC × GC and heart cut MDGC analysis to great effect [36,37,50,51,54]. Electrically controlled solenoid valves are installed outside any heated compartments and connected using short SS capillaries. This prevents the thermal degradation of solenoid valves which rotary and diaphragm valves experience. An alternative to valve controlled injection is thermal focusing, which was considered in Chapter 3.

Currently S/SL injection procedures deliver relatively wide injection bandwidths to GC columns, which affects the separation performance of fast GC methods [24]. The use of PMDs for pneumatically controlled injection has been neglected in favour of heart-cut MDGC, GC × GC applications [18]. The aim of this research chapter was to investigate the possibility of using PMDs to control and minimise injection bandwidths in capillary GC columns to improve separation performance. Since PMDs have minimal internal dead volumes, and do not have any physical moving parts or temperature limitations affecting their operation, they should be ideal for controlling the GC injection procedure

to facilitate fast separations. Unlike the fluidic logic gates pioneered by Wade and Cram [47], these devices are expected to operate at lower carrier gas flow rates, which prevents the excessive consumption of inert carrier gases that was required for the operation of fluidic logic gates.

2.2 Materials and Methods

2.2.1 Carrier and fuel gases

Hydrogen gas was generated in-house using a Parker-Balston laboratory gas generator (Parker-Hannafin, Cleveland, USA). All hydrogen was purified using a hydrocarbon (Agilent Technologies, Wilmington, Delaware, USA, #17972), moisture (Agilent #17971) and oxygen filter (Agilent #17970). Compressed air was purified using a Parker-Balston zero air generator (Parker-Hannafin) that was then connected in series with a filter designed to remove and remaining moisture and hydrocarbon species (Restek, Bellefonte, Pennsylvania, USA, #22022). Compressed nitrogen was purified using a triple filter designed to remove moisture, oxygen and hydrocarbon species (Restek, #22020) prior to use.

2.2.2 Instrument 1: Agilent 6850 GC

A small form-factor Agilent 6850 GC (Agilent Technologies, Wilmington, Delaware, USA) was used for GC, MDGC and GC × GC experiments. The 6850 GC is equipped with a split/splitless (S/SL) inlet, FID module, small convection oven, and a three-channel auxiliary EPC.

A laptop computer (Dell Latitude, Model: D630) with Microsoft Windows XP (Service Pack 3), a dual core Intel processor (T7500, 2.2 GHz) and 4.00 GB of RAM was used for instrument control, data collection and processing with Agilent ChemStation software (Rev B.04.03[16]).

2.2.3 Instrument 2: Falcon Calidus™ GC

A Calidus™ GC (Falcon Analytical, Lewisburg, West Virginia, USA) was used as the platform for resistively heated GC. The Calidus™ GC is a modular instrument with a number of interchangeable components. The core component of the Calidus™ GC system

is the central oven, which is a small cavity (172 mm × 98 mm × 38 mm), which is used to provide connectivity between each GC module. The oven can be set to an isothermal temperature between room temperature and 400 °C. A S/SL inlet was incorporated into the central oven to facilitate liquid, headspace or SPME sample introduction. A pair of manual needle valves were used for controlling the septum purge and split flow rates, the outlet of each of these vents was monitored using a hand held flow meter (Restek).

The Calidus™ GC has capacity for two resistively heated column modules. A column module contains a SS capillary column with a length of up to 3 m, with internal diameters ranging from 180 µm to 530 µm. There are a wide range of SS GC columns available from Restek (Bellefonte, Pennsylvania, USA), which can be mounted in a column module by Falcon Analytical. The columns employed in the present studies are summarised in Table 3.

Table 3 Resistively heated column modules available for Calidus™ GC research.

Column type	Stationary phase coating	Column Length (m)	Internal diameter (µm)	Film thickness µm
MXT-5	5 % diphenyl- 95 % dimethylpolysiloxane	3	180	0.18
MXT-1	100 % dimethylpolysiloxane	3	180	1.0
MXT-1701	14 % cyanopropylphenyl- 76 % dimethylpolysiloxane	3	250	0.1
MXT-50	50% diphenyl- 50 % dimethylpolysiloxane	1	180	0.18

Falcon Analytical provides two detector options for the Calidus™ GC, either a micro machined FID or TCD. Presently the FID was selected due to its excellent sensitivity (compared to the TCD) and its universal response to organic compounds. The Calidus™ instrument was shipped with a series of VICI Valco column and inlet unions, which incorporated graphite vespel ferrules that are prone to gas leaks after repeated

temperature cycles, as well as potentially being active towards certain analytes. All unions were therefore replaced with SilTite µ-union fixtures and deactivated metallic ferrules. These unions minimise dead volumes and active sites in the flow path of the GC system [59].

A laptop computer (ASUS, Model UL30V) with Windows 7 Enterprise OS, an Intel U7300 1.3 GHz CPU and 4.00 GB of RAM was used for instrument control *via* an Ethernet connection. Chrom Perfect Chromatography Data System software (Version 6.0.4, Justice Laboratory Software, Danville, New Jersey, USA) was used for instrument control, data collection and processing.

2.2.4 Pressure and flow calculation procedure

For single column GC systems, a commercially available flow calculator was used to calculate the inlet pressure required to deliver a target carrier gas flow rate through a column [60,61]. These calculators consider the column length, internal diameter, film thickness, column temperature, type of carrier gas, and the outlet pressure to determine the inlet pressure required to deliver a desired carrier gas flow or linear velocity.

In systems where there are multiple segments of capillaries that have different physical dimensions, compartment temperatures, flow rates and outlet pressures, it is important to consider each piece of the system individually to ensure that the correct inlet pressure is set to maintain a target carrier gas flow rate. For example, to determine the inlet pressure required to deliver a desired flow rate in a system comprised of two capillaries, with different dimensions, which are connected in series to a detector operating at atmospheric pressure the pressure required to deliver a flow through that segment can be calculated once its outlet pressure is known. Since the outlet pressure for the final capillary segment of system is the same as the operating pressure for the detector, this is used to determine the pressure required to drive flow through that segment. This pressure can then be added to the outlet pressure of the detector, to

determine the outlet pressure of the next segment. This new outlet pressure can be inputted into the flow calculator along with the capillary dimensions and temperature to determine the pressure required to drive a selected flow through that capillary and the previous capillary.

This procedure of considering each instrument segment sequentially can be extended through as many segments as necessary. A Microsoft Excel spread sheet was prepared based on the equations summarised by Stafford *et al.* [62]. This simplified the programming of flow rates for the 6850 and Calidus™ GC instruments, since they both operated using EPC units that could not be configured to consider multiple capillary dimensions with different temperatures and flow rates. Generally, column flow rates and temperature programing rates were selected based on the recommendations provided by Blumberg and co-workers [1,5,63].

2.2.5 Calidus™ methane injection bandwidth measurements

A Calidus™ GC (Falcon) equipped with a S/SL inlet, a resistively heated column and FID module was used for methane injection bandwidth studies. A piece of deactivated fused silica (DFS) (0.65 m × 75 µm ID, Trajan Scientific and Medical, Ringwood, Australia) was connected to the S/SL inlet of the GC. The outlet of this DFS piece was connected to a MXT-5 column (3 m × 180 µm ID × 0.18 µm d_f, Restek) using a SilTite SilFlow union (Trajan). The outlet of the MXT-5 column was connected to a FID module *via* another piece of DFS capillary (0.3 m × 250 µm ID, Trajan) and SilFlow union, as shown in Figure 4.

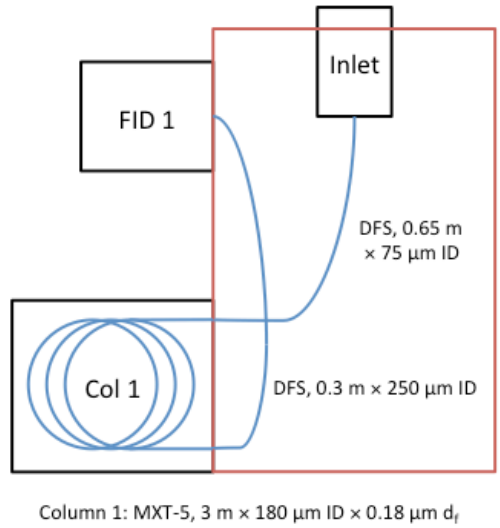

Figure 4 Schematic showing the connection of components within the Calidus™ transfer line oven (shown in red) for injection bandwidth measurement experiments using a single resistively heated column.

The carrier gas was hydrogen and the column flow rate was 1.6 mL min^{-1}, which required an inlet pressure of 25.81 PSI. The S/SL inlet, column module and associated transfer lines were all maintained at an isothermal temperature of 100 °C. The FID was maintained at a temperature of 250 °C and was supplied with purified air (130 mL min^{-1}) and hydrogen (13 mL min^{-1}) for flame operation.

A sample of natural gas (primarily comprised of methane) was diluted (20:1 in air) prior to sampling. A series of 5 µL injection to the Calidus™ S/SL inlet was performed at a range of different split ratios ranging from 10:1 to 200:1. The inlet liner was an ultra-inert split liner (Agilent, #5190-3165). Data were collected at a rate of 100 Hz, with a laptop computer running Chrom Perfect software (Justice Laboratory Software, USA). All peak statistics were calculated using the Chrom Perfect, and exported to Microsoft Excel for further data processing.

2.2.6 Agilent 6850 GC methane injection bandwidth measurements

An Agilent 6850 GC (Agilent) equipped with an S/SL inlet, and FID module was used for methane injection bandwidth studies. A piece of DFS (0.65 m × 75 µm ID, Trajan) was connected to the S/SL inlet of the Agilent GC. A RTX-5 column (3 m × 180 µm ID × 0.18 µm d_f, Restek) was then connected to the outlet of this piece of DFS *via* SilTite µ-union (Trajan). The outlet of the RTX-5 column was connected to an FID using another piece of DFS capillary (0.3 m × 250 µm ID, Trajan) as shown in Figure 5, to match the conditions of the Calidus™ GC in the previous section (2.2.5).

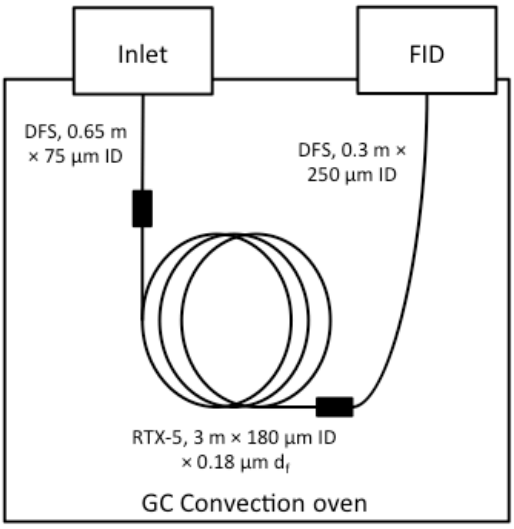

Figure 5 Diagram showing the installation of a capillary GC column within the Agilent 6850 GC instrument. Note that all respective capillary connections, unions (shown as black boxes) and columns are installed within the GC convection oven of the instrument.

The FID was maintained at a temperature of 250 °C, with 30 mL min^{-1} of hydrogen, 340 mL min^{-1} of purified air, and 30 mL min^{-1} of nitrogen makeup gas. The oven and S/SL inlet were maintained at an isothermal temperature of 100°C. The carrier gas was hydrogen with a column flow rate 1.6 mL min^{-1}, requiring an inlet pressure of 25.76 PSI.

A sample of natural gas (primarily comprised of methane) was diluted (20:1 in air) prior injection. A series of 5 µL injections to the Agilent S/SL inlet was performed at a range of different split ratios ranging from 10:1 to 200:1. The inlet liner was an ultra-inert split liner (Agilent, #5190-3165). Data were collected at a rate of 100 Hz, with a laptop computer running ChemStation software (Agilent). All peak statistics were calculated using the ChemStation software, and exported to Microsoft Excel for further data processing.

2.2.7 Planar microfluidic device controlled injection bandwidth studies using the Calidus™ GC

A Calidus™ GC (Falcon) equipped with a S/SL inlet, two column modules, two FID modules and an EPC module (Parker Hannifin, Part #990-005021-050) was used for planar microfluidic device (PMD) controlled injection bandwidth manipulation. A piece of DFS (0.6 m × 75 µm ID, Trajan) was used to connect the S/SL inlet of the Calidus™ GC to Port #B, of a Deans' switch PMD (Trajan). Port #A of the PMD was connected to a MXT-5 column (3 m × 180 µm ID × 0.18 µm d_f, Restek) with piece of DFS (0.3 m × 100 µm ID, Trajan). Port #C was connected to a MXT-1 column (3 m × 180 µm ID × 1.0 µm d_f, Restek), using another piece of DFS (0.3 m × 100 µm ID, Trajan). The MXT-1 and MXT-5 columns were connected to two FID modules using two pieces of DFS (0.3 m × 250 µm ID, Trajan) and a schematic showing the connectivity of each component is shown in

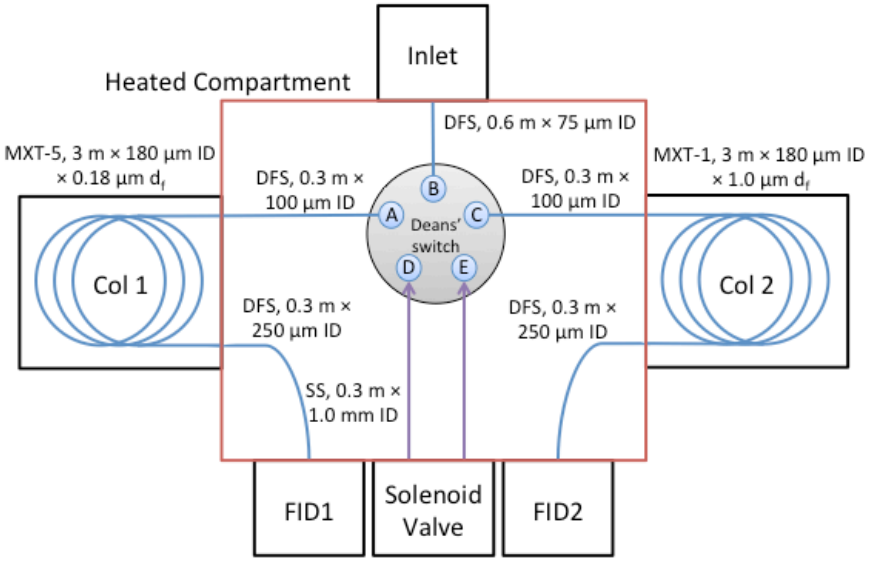

Figure 6 Schematic diagram showing the connections made between each component of the Calidus™ Deans' switch injection setup. Note that each column is resistively heated at a temperature independent of the central heated compartment.

The transfer lines, S/SL inlet and columns were all maintained at an isothermal temperature of 100 °C. The EPC unit and solenoid valve were connected to the Deans' PMD (Ports D and E) using two SS capillaries (30 cm × 1.0 mm ID, Trajan). The carrier gas was hydrogen for both the S/SL inlet and auxiliary EPC. The S/SL inlet was programmed to deliver a constant flow of 0.5 mL min^{-1}, which required a pressure of 10.05 PSI; while the auxiliary EPC channel was set to provide a constant flow of 1.6 mL min^{-1}, requiring a pressure of 18.06 PSI. The Deans' switch PMD state was controlled using a 12 V electronic solenoid valve (Lee Corporation, USA). Timing of the valve actuation was synchronised to the start-out signal of the Calidus™ GC instrument, and the duration of injection periods could be varied using a customised timing circuit and software (Arduino Uno microcontroller).

A sample of natural gas (primarily comprised of methane) was diluted (20:1 in air) prior to injection. A series of 5 µL injections to the Agilent S/SL inlet were performed at

a range of different split ratios ranging from 10:1 to 200:1. The inlet liner was an ultra-inert split liner (Agilent, #5190-3165). FID data was collected with Chrom Perfect Chromatography Data System version 6.0.4 (Justice Laboratory Software, USA). All peak statistics were calculated using the Chrom Perfect software, and exported to Microsoft Excel for further data processing.

2.2.8 PMD controlled injection bandwidth studies using the 6850 GC

An Agilent 6850 GC (Agilent) equipped with S/SL inlet, a FID module, and an auxiliary EPC was used for injection bandwidth control experiments. A piece of DFS capillary (65 cm × 75 µm ID, Trajan) was used to connect the S/SL inlet to Port #B of a Deans' switch PMD (Trajan) using. Port #A of the PMD was connected to a RTX-5 column (3 m × 180 µm ID × 0.18 µm d_f, Restek). Port #C was connected to a RTX-1 column (3 m × 180 µm ID × 1.0 µm d_f, Restek). Both columns were coiled into 8 cm diameter circular bundles that were carefully positioned within the GC convection oven to ensure they did not touch the walls of the oven cavity. The RTX-5 column was connected to a FID, while the RTX-1 column was vented to atmosphere outside the GC oven cavity. The EPC unit and solenoid valve were connected to the Deans' PMD using two deactivated SS capillaries (30 cm × 1.0 mm ID, Trajan). The inlet was set to a temperature of 250 °C and the GC oven cavity was set to an isothermal temperature of 100 °C. The carrier gas was hydrogen for both the S/SL inlet and auxiliary EPC. The S/SL inlet was programmed to deliver a constant flow of 0.5 mL min^{-1}, which required a pressure of 10.05 PSI, while the auxiliary EPC channel was set to provide a constant flow of 1.6 mL min^{-1}, requiring a pressure of 18.06 PSI. The Deans' switch PMD state was controlled using a 12 V electronic solenoid valve (Lee Corporation, USA). Timing of the valve actuation was synchronised to the start-out signal of the Calidus™ GC instrument, and the duration of injection periods could be varied using a customised timing circuit and software (Arduino Uno microcontroller). The FID was set to 250 °C, and

programmed to operate with 30 mL min^{-1} hydrogen and 340 mL min^{-1} of purified air. The Deans' switch PMD state was controlled using a 12 V electronic solenoid valve (Lee Corporation, USA). Timing of the valve actuation was synchronised to the start-out signal of the Calidus™ GC instrument, and the duration of injection periods could be varied using a customised timing circuit and software (Arduino Uno microcontroller).

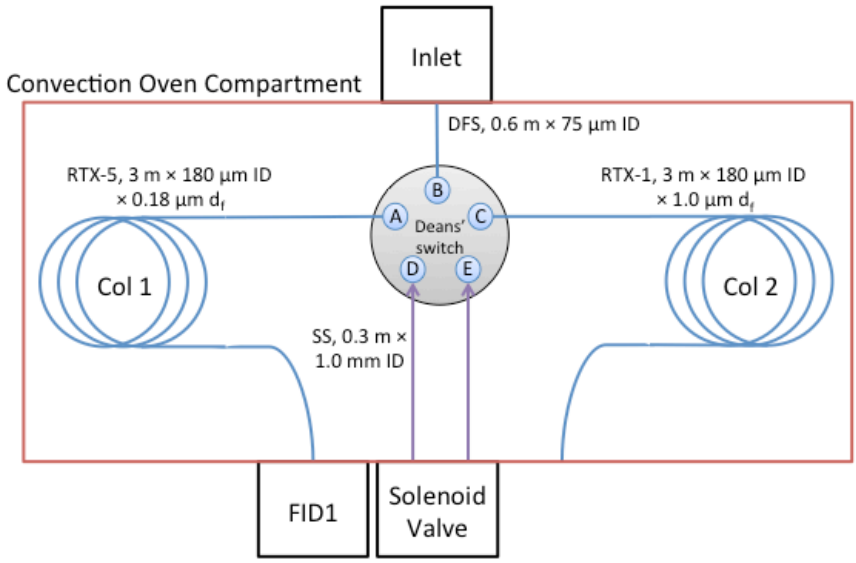

Figure 7 Schematic diagram showing the connections made between each component of the Agilent 6850 GC Deans' switch injection system. Note that all components are housed within the convection oven of the GC instrument that is used for column temperature programming, and that the outlet of column 2 is not connected to a detector in this experiment.

A sample of natural gas (primarily comprised of methane) was diluted (20:1 in air) prior injection. A series of 5 µL injections to the Agilent S/SL inlet were performed at a range of different split ratios ranging from 10:1 to 200:1. The inlet liner was an ultra-inert split liner (Agilent, #5190-3165). FID data was collected at a data-sampling rate of 100 Hz, with ChemStation software (Agilent) version B.04.03SP1. Peak statistics were measured with Agilent ChemStation software and then exported to Microsoft Excel for further processing.

2.2.9 Measuring the oven temperature tracking capabilities of PMDs installed within a convection oven

The instrument configuration described in Section 2.2.8 was used for testing oven temperature profiles of the Agilent 6850 GC instrument, with a few modifications. Both columns were vented to atmosphere since data acquisition from the FID was not required. The inlet and FID were set to a temperature of 250 °C to simulate typical GC conditions. The GC oven was temperature programmed from an initial temperature of 40 ° C (0.5 min hold duration) and then ramped at different rates, up to a temperature of 300 ° C (1 min hold duration). Temperature programming rates of 10, 15, 20, 25 and 30 °C min^{-1} were tested. The inlet was programmed to deliver a flow of 3.0 mL min^{-1} that was split equally between the two columns (1.5 mL min^{-1} each). A k-type thermocouple was installed on each wafer for temperature measurements using a multimeter (Digitech, QM1538) with RS232 data logging capabilities. Data was recorded using Electus distribution data logging software (2000) on a Dell notebook computer. All data was saved in comma separated values format, and imported into Microsoft Excel for processing.

2.2.10 Calidus™ resistively heated column module performance testing

The Calidus™ instrument setup described in Section 2.2.5 was used for testing the performance of the resistively heated modules. During the performance testing, the S/SL inlet, column module and associated transfer lines were all maintained at an isothermal temperature of 100 °C. The FID was maintained at a temperature of 250 °C and was supplied with air (130 mL min^{-1}) and hydrogen (13 mL min^{-1}) for flame operation, with a data sampling rate of 100 Hz.

A sample of *n*-tetradecane, 100 mg kg^{-1} in *n*-hexane (Sigma Aldrich, Castle Hill, Australia) was prepared gravimetrically for analysis and 1 µL was injected into the Calidus™ GC while operating the MXT-5 column at a variety of flow rates between 0.25

and 2.5 mL min^{-1}. These flow rates yielded average linear velocities between 20 and 200 cm s^{-1}. Data was collected using Chrom Perfect software (Justice Laboratory Software, USA), and the peak width of the *n*-tetradecane solute was measured using this software. The data was then exported and used to construct a plot of linear gas velocity against the height equivalent to a theoretical plate for the purpose of ascertaining the minimum plate height for the system.

The instrument configuration described in this section was then applied to the separation of a test mix with a flow rate of 1.2 mL min^{-1}, which required an inlet pressure of 21.15 PSI. The test mix contained ethylbenzene, *n*-nonane, *n*-undecane, *n*-dodecane, 1-decanol and *n*-tetradecane each 100 mg kg^{-1} in dichloromethane (Sigma Aldrich, Castle Hill, Australia, and 1 µL of this mixture was injected into the S/SL inlet using a 10 µL micro syringe (Trajan). The inlet liner was an ultra-inert split liner (Agilent, #5190-3165), and the split ratio was 100:1. FID Data was similarly collected with Chrom Perfect software (Justice Laboratory Software, USA), which was used for the measurement of peak statistics, and data was exported to Microsoft Excel for further processing.

2.3 Results and discussion

2.3.1 PMDs for injection bandwidth minimisation

Studies were carried out to determine whether PMDs could be utilised for manipulating the injection bandwidth of a GC system. Methane was selected as an ideal test compound due to its negligible retention within the present capillary columns. In this way, peak broadening experienced by methane in the following experiments can be attributed to diffusion in the longitudinal direction within the capillaries used to construct the GC system, rather than broadening *via* mass transfer mechanisms.

Before testing the Deans' switching injection system, the injection bandwidths obtainable with the S/SL injectors provided in the Calidus™ and 6850 GC instruments were evaluated. A series of methane injections were carried out, while varying the split ratios of each injector to ascertain the minimum peak widths attainable with each system. To simulate a liquid or headspace sample injection, a 500 µL injection of methane gas was injected into the GC liner (860 µL internal volume), which approximately matches the volume of space occupied by a vaporised 1 µL injection of acetonitrile (assumptions: Injector temperature 280 °C, inlet pressure 11 PSI, hydrogen carrier). Acetonitrile is a poor injection solvent for GC, as it generates a relatively large volume of vapour. Despite this drawback, acetonitrile is used in sample preparation procedures such as QECHERS to great effect, and this large sample vapour volume (500 µL) represents a worst-case scenario during GC sample injection.

A plot of the effect of inlet flow rate on methane peak width at half height is presented in Figure 8 for the Calidus™ and 6850 GC instruments.

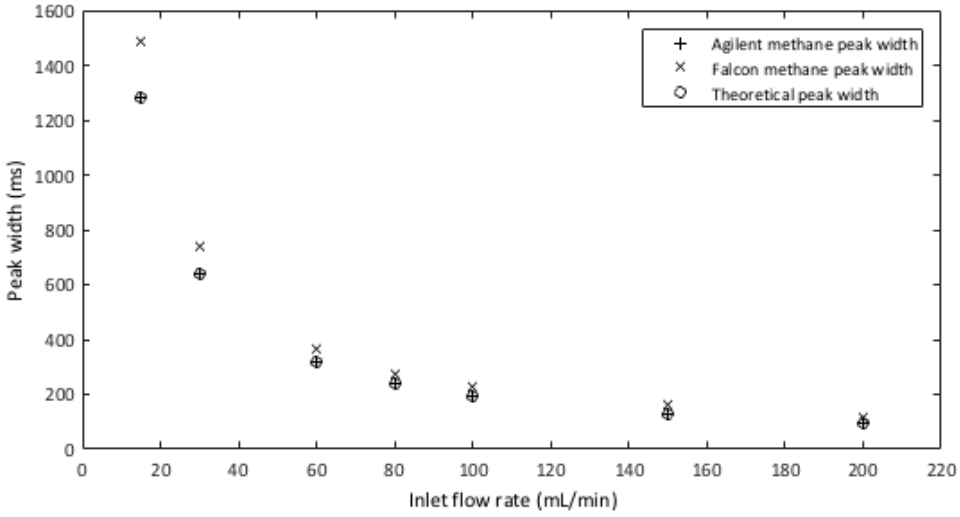

Figure 8 Plot of the effect of inlet flow rate on the peak width at half height for a series of methane injections performed on the Calidus™ and Agilent 6850 GC instruments compared the theoretical injection bandwidths.

The performance of the Calidus™ and 6850 GC injectors were similar, which is expected given the matching dimensions of each S/SL injector (both injectors use a 870 µL deactivated glass inlet liner). The injection bandwidths measured for each instrument were compared to the theoretical peak widths that would be obtained if no longitudinal band broadening occurred during a GC experiment. Theoretical injection bandwidths were calculated by dividing the sample vapour volume by total flow rate of carrier gas flowing through the inlet liner to give the time required to complete an injection. For the present experiments, a 500 µL sample injection was used, with a constant carrier gas flow rate of 1.6 mL min^{-1}. The split vent flow rates were varied from 16 to 320 mL min^{-1} to deliver a range of different split ratios. The carrier gas flow rate and split vent flow rate are added together to obtain the total inlet flow rate. A peak width of 112 ms ± 5 ms ($\alpha = 0.05$) at a split ratio of 200:1 was obtained on the 6850 GC system, which compared quite well with the theoretically achievable 96 ms. This suggests that the 6850 system is contributing approximately 16 ms of peak broadening. The Calidus™ system broadened peaks slightly more with a peak width of 120 ± 10 ms

($\alpha = 0.05$) at an equal split ratio. Both GC systems were approximately broadening initial injection bandwidths by 15 % compared to the bandwidths predicted by theory; however these experiments provided a good benchmark for the performance achievable with each GC instrument. A PMD type Deans' switch was then investigated for injection bandwidth manipulation. A schematic of the experimental setup is shown in Figure 9. A narrow bore capillary (70 cm long, 75 μm ID) was selected for the connection of the Deans' switch to the GC injector to provide sufficient restriction (flow restrictor 1) to prevent back flow from the Deans' switch to the GC injector during switching. Additionally, this restrictor allowed the injector to operate at a stable inlet pressure, since the present GC inlet and auxiliary pressure control modules (PCM) are unstable at pressures lower than 5 PSI.

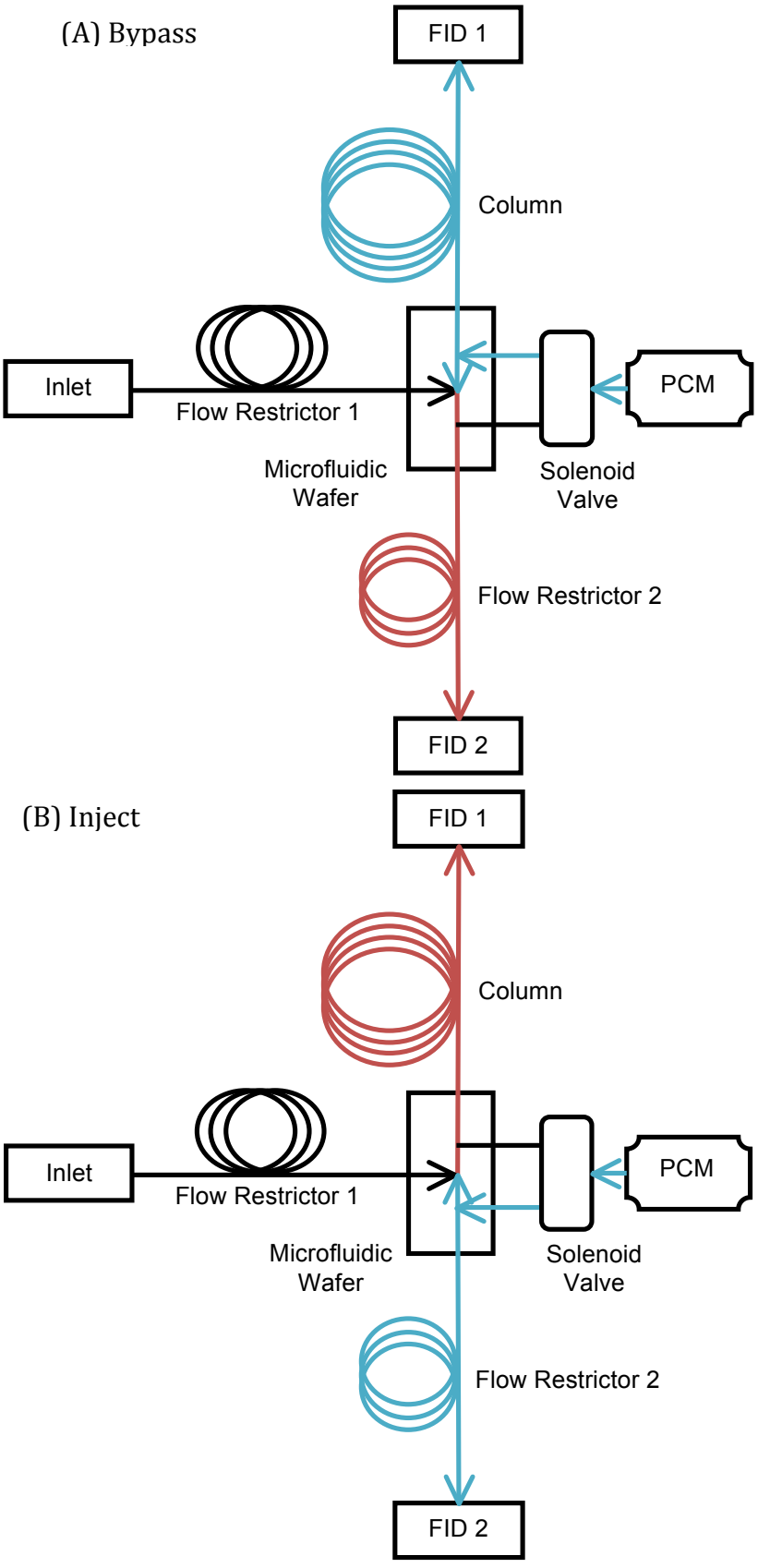

Figure 9 Heart-cut GC injection setup based on Deans' switching with an SGE PMD Deans' switch. The solenoid valve is used to apply a constant pressure at one

of two points within the microfluidic wafer. While in state (A) "Bypass" pressure is applied to the junction above the input from the inlet and restrictor 1, causing all effluent from this section to be directed to FID 2. Once the three way valve is switched to state (B) "Inject", the applied pressure is shifted to the junction below the input of the inlet and restrictor 1, causing all effluent to be to the column and FID 1 while in this state.

A second flow restrictor (flow restrictor 2) was used to balance the carrier gas flow rate of the column channel (FID 1) with the Deans' switch waste channel (FID 2). A restrictor with equal dimensions to the primary separation column was used as for flow restrictor 2 to balance the flows at each side of the PMD. Valve actuation was controlled using a programmable microcontroller that was capable of activating a 12 V solid-state relay for periods 1 ms or greater in length. Valve actuation was synchronised with the GC start out signal provided by the Calidus™ and 6850 GC instruments.

Ideally, the initial injection band provided by the Deans' switch should resemble a perfect cylindrical plug, and the valve actuation duration should predict the physical length of this plug. This initial cylindrical band then undergoes longitudinal broadening while being transported from the Deans' switch to the detector. The result of this broadening process is that the each peak assumes a Gaussian shape, which must be considered when comparing injection bandwidths. While peak broadening can be minimised by reducing the capillary volumes between Deans' switch and the detector by using a very short piece of narrow bore DFS capillary, that setup would not be realistic for a GC system using a separation column, which is generally quite long to ensure that adequate separation performance can be achieved. For this reason a short separation column was included in the present experimental setup, so that the peak broadening of the system matched the previous S/SL injection bandwidth studies.

Peak widths were measured at half height using the data processing software included with the Agilent and Calidus™ GC instruments. Since the Deans' switch is assumed to inject a cylindrical plug to the column, the post column peak widths, which are measured at half height, should be converted to peak widths at base to provide a fair comparison between the injection and final peak widths. Peak heights measured at half height and base can be conveniently converted using the following equations (Eq. 3-5).

$$N = 16 \times (t_R / w_b)^2 \qquad \text{(Eq. 3)}$$

$$N = 5.54 \times (t_R / w_{0.5})^2 \qquad \text{(Eq. 4)}$$

$$w_b = w_{0.5} / 0.5884 \qquad \text{(Eq. 5)}$$

Where N indicates the number of theoretical plates for a given peak, t_R is that peak's retention time, w_b is the width of the peak at the base, $w_{0.5}$ is that peak's corresponding half height and the constants 16 and 5.54 correspond to the theoretical plate number equations for peak widths measured at base and half height respectively [64]. By substitution of the two equations (Eq. 2 and 4) and solving for base peak width (w_b) a simple conversion between peak width measurements at half height and base width was obtained (Eq. 5).

Methane was infused into each GC injector for the heart-cut injection studies using a syringe pump. The peak widths of methane after heart cut injection is shown in Figure 10 with a minimum width of 216 ± 16 and 220 ± 16 ms being obtained for the Agilent and Calidus™ GC systems, respectively. Valve actuation times below 100 ms did not lead to proportional decreases in peak widths, indicating that the present solenoid valve was not able to switch faster than 100 ms, or that there is a dead volume present in the PMD design that inherently prevents lower switching times.

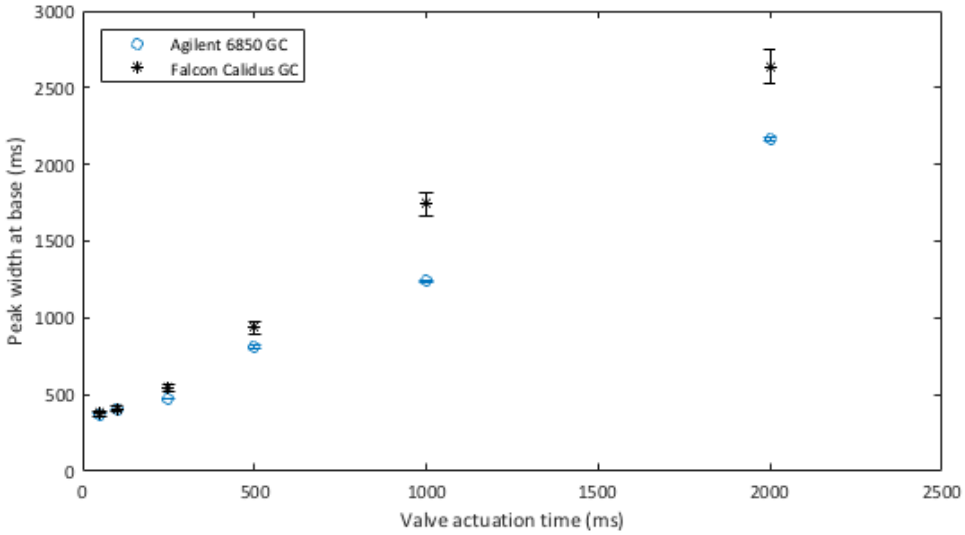

Figure 10 Plot of the effect of valve actuation duration on methane peak width after Deans' switch heart cutting. Peak widths at half height are reported along with confidence intervals (α = 0.05) for the Agilent and Calidus™ GC systems.

The methane peak widths obtained with the PMD were substantially broader than the methane peak widths obtained using S/SL injection alone. This peak broadening is best visualised by subtracting the valve actuation times, or injection bandwidths from methane peak widths following post injection band broadening, as shown in Figure 11. Since the column dimensions, carrier gas flow rates and detector modules were preserved between the S/SL benchmarking and PMD switching experiments, the PMD must be the source of this additional peak broadening.

Table 4 summarises the peak widths obtained with the Calidus™ and 6850 GC systems using S/SL injection and a PMD switching with a 100 ms actuation time.

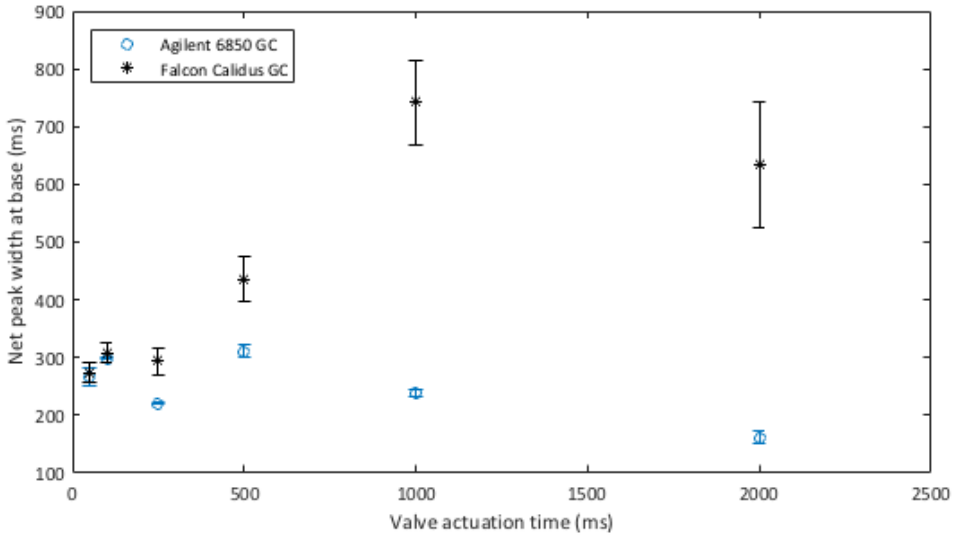

Figure 11 Plot showing the effect of valve actuation duration on peak broadening after subtraction of the valve actuation time from the final methane peak bandwidth.

Valve controlled injection using the present PMD yielded peak widths ($w_{0.5}$) of 250 ± 50 ms and 290 ± 40 for the 6850 and Calidus™ GC instruments respectively, which compares poorly with the 120 and 112 ms obtained using S/SL injection. This meant that the PMD was responsible for an additional 54 to 14 ms of peak broadening, after subtracting the off column broadening evident in the S/SL experiments. Therefore the PMD is more than doubling the longitudinal peak broadening experienced by methane.

Table 4 Summary of peak widths for methane injection bandwidths obtained on the Calidus™ and 6850 GC systems.

Injection type	Type of peak width value	Calidus™ GC		6850 GC	
		Peak width ($w_{0.5}$)	Peak width (w_b)	Peak width ($w_{0.5}$)	Peak width (w_b)
		ms			
Split (200:1)	Theoretical	96	163	96	163
	Experimental methane	120	204	112	190
	Experimental - theoretical	24	41	16	27
PMD (100 ms actuation time)	Theoretical	100	170	100	170
	Experimental methane	250	425	290	493
	Experimental - theoretical	190	255	150	323
N/A	Split - Deans' experimental methane	78	51	30	133

For these reasons the incorporation of the present PMDs and associated solenoids was abandoned as a means for reducing GC injection bandwidth. While this approach was not successful in providing injection bandwidths narrower than those achievable using S/SL injection, the switching speed obtained using planar microfluidics was sufficient for heart cut MDGC analysis, and was used for the analysis of trace aromatic species in industrial samples in Chapter 4.

2.3.2 Planar microfluidic devices and temperature programming

Two PMDs were evaluated for pneumatically controlled GC injection, specifically the Agilent Capillary Flow Technology™ (CFT) and SGE SilFlow™ Deans' switch microfluidic wafers. PMDs are constructed from a series of thin SS plates that are laser etched and carefully aligned to obtain the required flow path architecture. Diffusion bonding was used to form a single cohesive wafer with a complex internal architecture. Column

unions are then welded to the wafer inputs and outputs to allow connection to capillary columns, and a control stream of auxiliary carrier gas. The internal surfaces of the PMDs were also chemically deactivated to prevent possible analyte retention or degradation from occurring during separation.

GC convection ovens are constructed from SS sheets that are insulated with a glass fibre insulation material to minimise heat loss during temperature programming. The thermal mass of most GC ovens is greater than 2 kg, all of which must be accurately heated during temperature-programmed analysis, which limits the maximum temperature-programming rate of these GC instruments. While PMDs represent a relatively small thermal mass compared to a GC convection oven, their ability to accurately track oven temperatures has not been previously established in the academic literature. Insufficient temperature tracking leads to the development of cold spots in the carrier gas flow path and causes extra-column peak broadening. The surface area, mass and surface area to mass ratio of the Agilent and SGE PMD Deans' switch are shown in Table 5.

Table 5 Physical properties of Agilent and SGE Deans' switch microfluidic wafers

	Agilent	SGE
Wafer mass (g)	32.3	15.5
Wafer surface area (cm^2)	46.5	17.8
Surface area to mass ratio ($cm^2\ g^{-1}$)	1.4	1.1

To evaluate the ability of each PMD to track GC oven temperatures during temperature-programmed analysis, a κ-type thermocouple was attached to each PMD. The relative temperature of the PMD was plotted against time during a series of different temperature programs to determine the ability of the wafers to track the oven temperature set point during a typical GC run (Figure 12 and Figure 13).

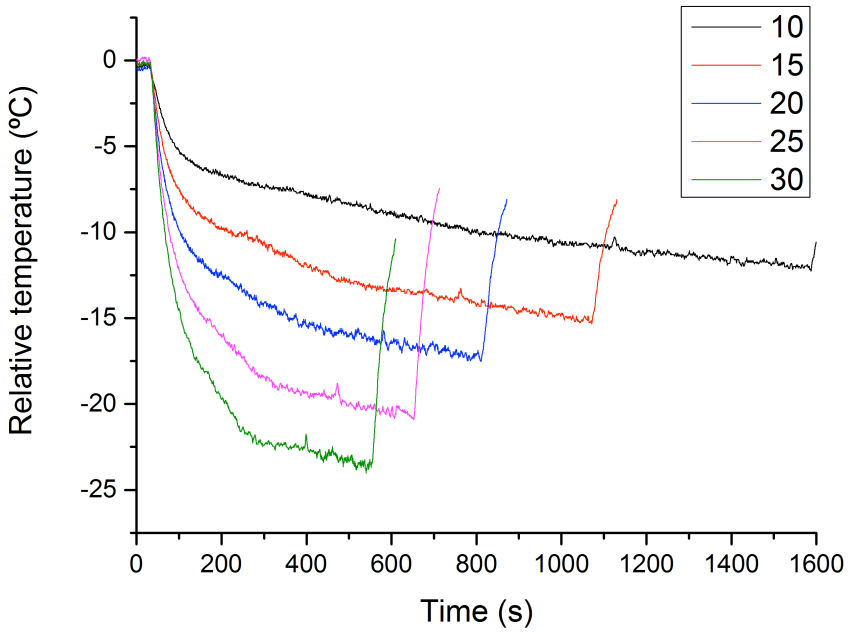

Figure 12 Temperature measurements of the Agilent Deans' switch PMD, relative to the programmed oven temperature for five linear temperature programs. Temperature programming rates (°C min^{-1}) are indicated in the figure legend. Initial oven temperature 40 °C with a 30 s hold, followed by temperature programming to a final temperature of 300 °C with a 60 s hold.

Figure 12 revealed some large temperature deficits between the PMD temperature and the oven temperature. Ideally, all of the plots should show a relative difference of 0 °C between the PMD and the oven temperature set point. However following the initiation of the temperature ramp, the PMD was unable to track the oven temperature accurately, which caused the wafer to trail the temperature set point of the oven by 6 to 22 °C, depending on the speed of the temperature ramp selected.

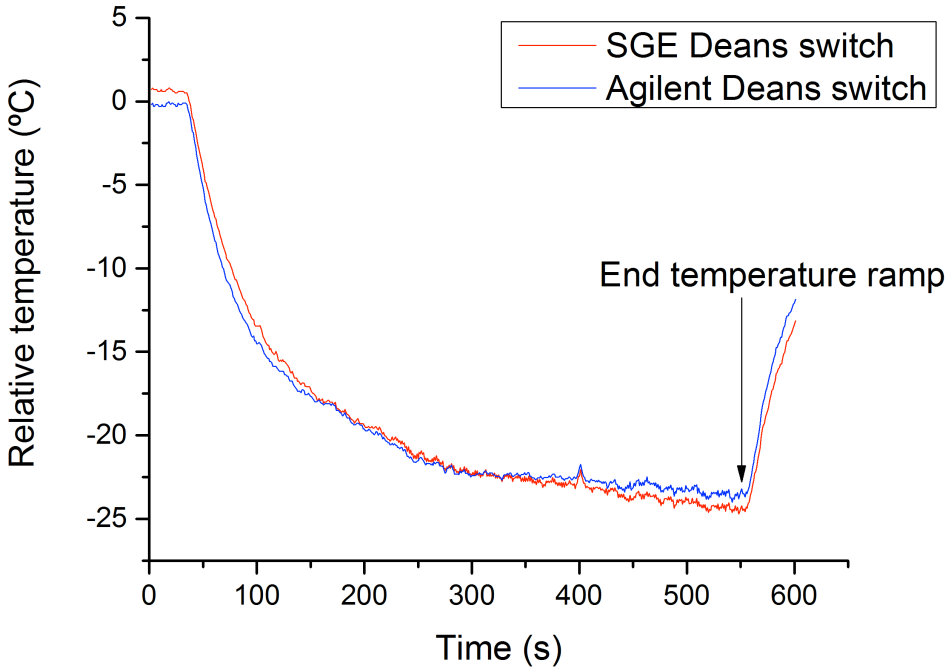

Figure 13 Comparing the temperature of the SGE and Agilent Deans 'switch wafers relative to the oven cavity during a fast temperature ramp. Initial temperature 40 °C for 60 s, then the oven was temperature programmed at a rate of 30 °C min^{-1} to 300 °C, with a final hold time of 60 s afterwards.

Figure 13 shows an overlay of the Agilent and SGE PMDs temperature during a 30 °C min^{-1} programming rate, relative to the oven temperature. Both microfluidic wafers exhibited thermal hysteresis after the temperature programming was initiated at 60 s, with an average temperature deficit of -22 °C. A difference of this magnitude would cause significant amounts of extra-column peak broadening. Initially it was expected that the SGE wafer would have superior temperature tracking capabilities compared to the Agilent wafer, since it was smaller and had a much lower mass (44 % less). This proved to not be the case, and both wafers had similar temperature tracking profiles as shown in Figure 13. To reconcile this observation, the surface area of each wafer was calculated and compared to each wafers' mass (Table 5) and the Agilent wafer was found to have a much larger surface area to mass ratio compared to the SGE wafer.

After 550 s, there is a steep return towards 0 °C relative temperature difference between the PMD and the oven temperature (Figure 13) that corresponds with reaching the final oven programmed temperature. A 60 s hold at 300 °C is then initiated. Both wafers equilibrate towards the 300 °C set point at a rate of approximately 12 °C min^{-1}, suggesting that 12 °C min^{-1} is the maximum heating rate that either PMD can be heated within the 6850 GC oven cavity, during temperature programmed GC. Further experiments showed that 2 min was sufficient to ensure that PMDs were equilibrated at the final temperature of 300 °C. The Agilent 6850 GC is specified to be capable of temperature ramps at rates between 1 and 70 °C min^{-1}, however this specification appears to only be accurate when a capillary column is the only item being heated. Larger items, such as PMDs or rotary valves are large thermal masses that limit the upper programming limit of fast convection oven heating. To overcome this limitation, auxiliary heating is necessary to ensure cold spots do not develop in the flow path within GC convection ovens, alternatively a high temperature compartment, such as an isothermal oven or heating block can be used to ensure that PMDs are maintained at a sufficiently high temperature compared to the oven.

2.3.3 Resistively heated GC for fast and portable analysis

Resistive column heating has been developed to satisfy the demands for faster temperature programming and reducing the power requirements for GC analysis, which is useful for portable GC analysis [6,7]. A Calidus™ GC was selected as a portable GC platform due to its rugged modular instrument design and form factor. The Calidus™ GC includes an isothermally controlled injector module, a small isothermal oven cavity for component connectivity, up to two resistively heated column modules, and up to two detector modules, which enable it to be configured for a wide range of applications. Each column module includes an independent temperature controller, an electric fan for post-analysis cooling, and a SS capillary column (up to 8 m in length) for separation. Column

heating was achieved by the application of electrical current to the SS column itself, which causes resistive heating and temperature increase [65]. Columns are wound into a tight coil on an aluminium ring for support [10,66,67]. Loops of the column are insulated from each other using glass fibre braid to prevent electrical short circuits. A platinum resistance temperature sensor is installed in a collinear fashion with the SS capillary to monitor the column temperature. Rapid temperature ramps of up to 600 °C min^{-1} were possible with the present column modules.

An isothermally controlled oven cavity (172 mm × 98 mm × 38 mm) was included in the Calidus™ GC to provide connectivity between the injector, column and detector modules. Additional valve and PMDs components were installed in this heated zone for the following experiments. This isothermal oven was expected to eliminate the thermal hysteresis exhibited by PMDs that are installed within temperature programmed convection ovens, as highlighted by Figure 12. Finally, the Calidus™ instrument included two FID detectors that were designed built for capillary format columns. The Calidus™ FID modules only require hydrogen and air for flame operation unlike conventional FID detectors that also require in inert make-up gas (nitrogen/helium/argon) to purge the internal volume of the detector.

Prior to the use of the Calidus™ instrument, a number of modifications were made to enhance connectivity and system flow path inertness. Graphite-Vespel ferrules were supplied for the connection of injectors, columns and detector modules. These polymeric based ferrules can thermally degrade over time and are sometimes reactive towards some chemical species, which complicates analysis. For this reason the unions and Graphite-Vespel ferrules were replaced with custom made deactivated SS SilFlow bulkheads, with SilFlow metallic ferrules, as shown in Figure 14. SilFlow ferrules are chemically inert and form low dead volume, gas tight connections between each GC component.

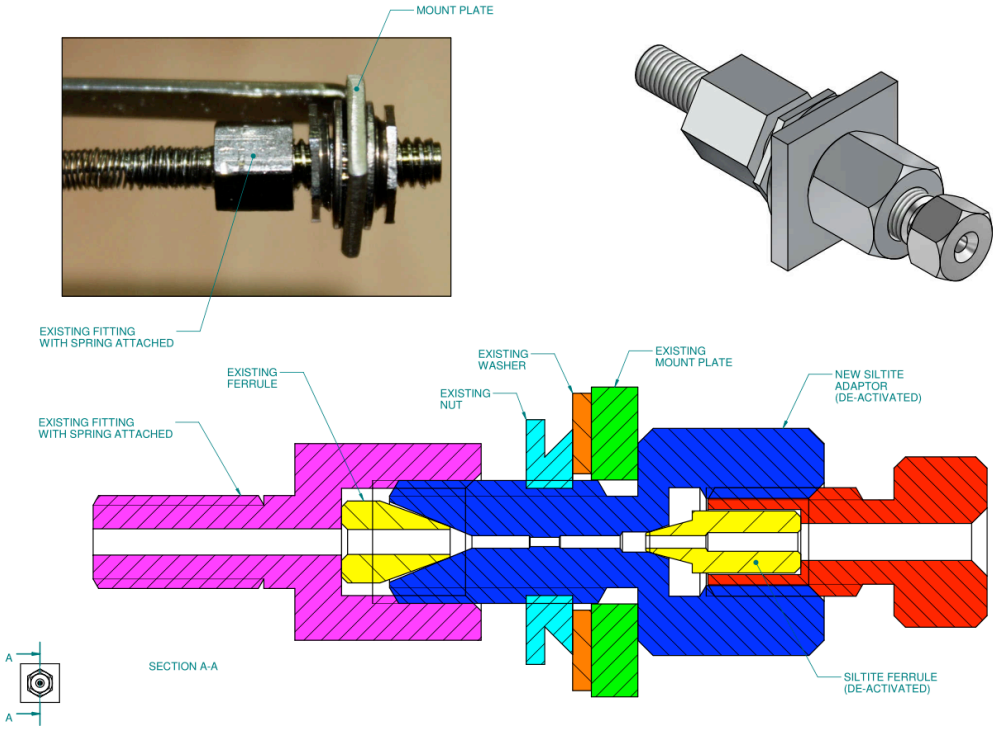

Figure 14 A low dead volume SilFlow™ bulkhead assembly, custom made for the Calidus™ GC (courtesy of SGE Analytical Sciences, Trajan Scientific and Medical).

The Calidus™ system was tested for cold spots in the carrier flow path due to detection of peak tailing during initial experiments. A κ-type thermocouple was used to measure the temperature of each component of the Calidus™ GC to ascertain whether all heated regions were accurately temperature controlled. This procedure revealed that the column modules used in the Calidus™ system had a cold spot within the design. Each module included an aluminium ring onto which the column coils were woven. During temperature-programmed analysis, it was noted that this aluminium ring did not accurately track the temperature specified by the GC system. The temperature of the aluminium ring trailed the programmed temperature set point by approximately 15 °C, even during isothermal temperature programming. The patent describing the Calidus™ GC column modules specifies that the aluminium ring be installed to enhance heat

distribution between the coils of the column. However it appeared that the ring was contributing a substantial cold spot within the column assembly [10,66,67].

The aluminium ring was subsequently removed from all column modules, and each column was coiled into a small toroid and insulated with a thin layer of aluminium foil, similar to the design of the Agilent LTM resistively heated column bundles. This minimised the size and mass of each column bundle, and eliminated the thermal hysteresis caused by the aluminium ring. The aluminium foil serves to trap a small mass of air between the interstitial spaces between each capillary column loop to facilitate the rapid convection of heat within the capillary column bundle, which reduces peak tailing. The Calidus™ instrument used SS capillary columns, unlike the polyimide coated glass fused silica columns that are more commonly used. SS capillaries were resistively heated using electrical current, which eliminated the need for a large convection oven and reduced the power requirements of the instrument. Additionally, SS capillaries are more robust than their fused silica counterparts making them ideal for portable instrumentation. Since the Calidus™ GC has not been used for academic research before, the performance of the resistively heated column modules needed to be evaluated.

Column performance for GC instruments operating with a low-pressure drop across the column, like the Calidus™ GC, can be described using the following equation (Eq. 6) [3].

$$HETP = (B / \bar{u}) + (C_s + C_m) \times \bar{u} \qquad \text{(Eq. 6)}$$

Where *HETP* describes the height equivalent to a theoretical plate, B defines the peak broadening due to longitudinal dispersion of the chromatographic band, $\bar{u}$ is the average linear velocity of the carrier gas, and C_s and C_m constants describing the resistance to mass transfer of a solute between the stationary and mobile phase of the column. To maximise *HETP*, longitudinal band broadening and resistance to mass transfer must be minimised. Practically that meant that a compromise in the carrier gas linear velocity

was required, since a low linear velocity was optimal for minimising the mass transfer component of the van Deemter equation (Eq. 6), while a fast linear velocity was ideal for minimising longitudinal band broadening. A plot of carrier gas average linear velocity against *HETP* is presented in Figure 15 for the solute *n*-tetradecane on a short separation column using the Calidus™ GC.

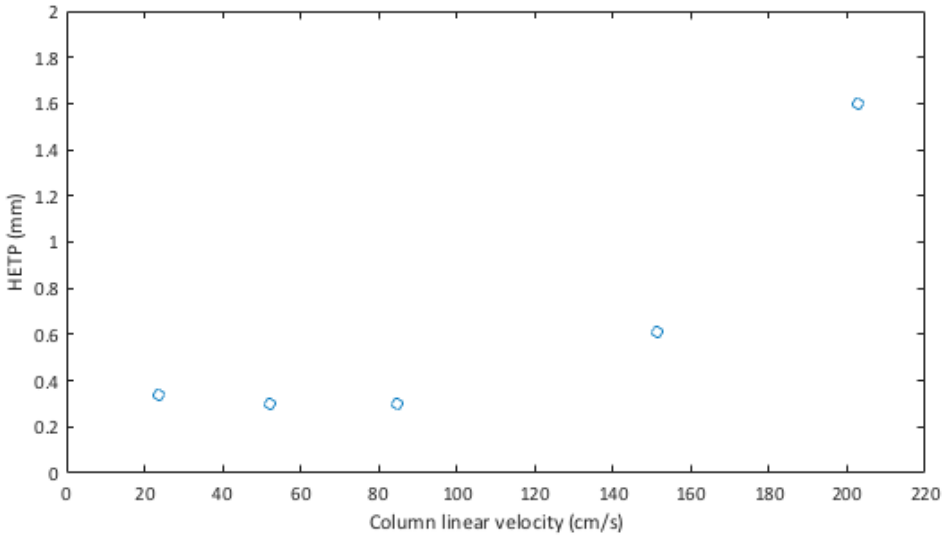

Figure 15 Average linear velocity plotted against column efficiency for the solute *n*-tetradecane, using an MXT-5 column (3 m × 180 µm ID × 0.18 µm d_f) at 100 °C isothermal oven conditions.

A minimum plate height was obtained at 0.22 mm, which was acceptable for a low-resolution separation column such as the 3 m long column utilised. From Figure 15, it was immediately apparent that a very flat van Deemter plot was obtained, which indicates that the contribution of longitudinal band broadening was negligible in the present column. This is likely due to the low residence time solutes have within such a short column. For example a 20 m long column with a 180 µm ID at 40 °C with a hydrogen carrier gas flow of 1.5 mL min^{-1} (linear velocity, 63 cm s^{-1}) has a void time of 32 s, while a corresponding short column with a length of 3 m with the same dimensions and conditions has a void time of only 3 s (linear velocity 93 cm s^{-1}). This means that a

column that is 6.6 times shorter has a void time that is 10 times less, therefore low carrier gas flow rates and linear velocities can be implemented in the Calidus™ GC, with little impact on the final column performance other than increasing the time of analysis. Meanwhile, operation of short columns at high flow rates causes a significant loss in column performance due to the elevated impact of the mass transfer component (C_s + C_m) of the van Deemter equation (Eq. 6) [3,4]. Blumberg and co-workers similarly observed that short columns are limited primarily by mass transfer and benefit from low flow rates, while longer columns typically have a much sharper loss of column performance at low flow rates due to longitudinal band broadening [1,5].

To determine the optimal trade-off between the time of analysis and column performance (in terms of *HETP*) it is useful to calculate the minimum time required to obtain a theoretical plate, this separation metric is known as plate duration (Q) [4].

$$Q = HETP / \bar{u} \qquad \text{(Eq. 7)}$$

This property is calculated using the following equation, where Q is the plate duration, *HETP* is the height equivalent to a theoretical plate, and $\bar{u}$ is the average linear velocity of the carrier gas. The minimum of Q reveals the linear velocity at which theoretical plates are generated at the maximum rate. In the case of the Calidus™ GC it was found that, the minimum plate duration was obtained at 120 cm s^{-1} (Figure 16), which corresponds to a flow rate of 1.8 mL min^{-1}, which agrees well with theoretical predictions [1,3,4]. It is also interesting to note that operation at a linear velocity of less than 75 cm s^{-1} results in negligible losses in column efficiency, as shown in Figure 15, of course this comes at the cost of a longer analysis time.

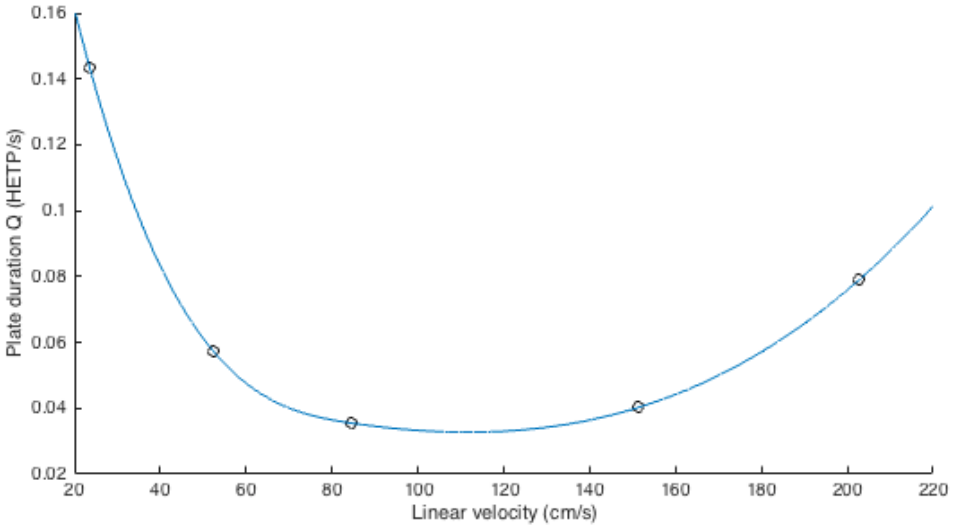

Figure 16 Average linear velocity plotted against plate duration for the solute *n*-tetradecane, using an MXT-5 column (3 m × 180 µm ID × 0.18 µm d_f) at 100 °C isothermal oven conditions.

The performance of the available Calidus™ column modules was evaluated with a range of different solutes to assess retention time and peak area repeatability as summarised in Table 6. The average peak retention time repeatability was 1.1 % and peak area repeatability was 3 %, and considering that manual injection technique was used for these experiments, the retention time and peak area repeatability was acceptable. The addition of an auto sampler unit would improve these statistics. Additional peak retention, theoretical plate counts, and peak shape statistics for each test compounds are shown in Table 7.

Table 6 Retention times, peak widths ($w_{0.5}$), peak areas and repeatability statistics for test compounds on MXT-5 column (3 m, 180 µm ID, 0.18 µm d_f; n = 3, α = 0.05).

Analyte	t_R (s)	t_R RSD (%)	Peak width (s)	Peak Area (µV s)	Peak Area RSD (%)
ethylbenzene	8.94	0.9	0.37 ± 0.01	11619	3.20
n-nonane	10.51	0.9	0.41 ± 0.07	15550	3.24
n-undecane	33.89	1.0	1.05 ± 0.01	17690	3.62
naphthalene	57.15	2.0	1.47 ± 0.05	14385	3.27
n-dodecane	70.76	1.0	2.3 ± 0.3	20846	3.85
1-decanol	103.30	0.8	3.2 ± 0.1	23478	1.10
n-tetradecane	147.08	1.0	4.5 + 0.1	15841	2.50

Table 7 Table of peak symmetry and column performance parameters for MXT-5 column (3 m, 180 µm ID, 0.18 µm d_f). Skew and Kurtosis statistics were calculated using Chrom Perfect Chromatography Data System software. Detailed information about the calculation of these statistics can be obtained in the following reference [68]

Analyte	Retention Factor (k)	Theoretical plates (N)	HETP (mm)	Symmetry	Kurtosis
Ethylbenzene	1.6	3174	0.95	2.09	0.95
n-nonane	2.1	3693	0.81	1.59	0.96
n-undecane	9.0	5729	0.52	1.18	1.01
Naphthalene	15.8	8363	0.36	1.31	0.96
n-dodecane	19.8	5145	0.59	1.49	1.00
1-decanol	29.4	5811	0.52	1.62	1.00
n-tetradecane	42.3	5790	0.52	1.03	0.99

The performance of the MXT-5 column was poor considering that the theoretically predicted number of plates for a 180 µm ID column is approximately 4400 N m^{-1}. The short separation column (3 m) was the cause of this poor separation performance. Short

columns have been previously observed to magnify the apparent stationary phase film thickness, which causes a substantial loss in the apparent plate height (HETP) of short columns relative to longer column systems [3]. Using low carrier gas flow rates can mitigate the poor mass transfer characteristics of short GC columns, however this also causes a proportionally increase analysis time, with limited gains in the plate height, as confirmed by the van Deemter plot shown in Figure 15. Therefore the carrier gas flow rate was maintained at the efficiency-optimised value of 1.2 mL min^{-1} (as is recommended for a 180 μm ID capillary [1]) as a compromise between analysis duration and performance.

The symmetry statistic (Table 7) indicates the degree of tailing a given peak displays. This is calculated by dividing a peak into two components by drawing a line, orthogonal to the baseline, from peak apex to the baseline. The ratio of the back peak width (right hand side of the centre line), to the front peak width (left hand side of the centre line) at 10 % of the peak apex maxima provides the symmetry value. A symmetry value 1 indicates a peak is symmetrical and values greater than 1.3 are said to be significantly tailing, while those that are less 1 are exhibiting peak fronting. Presently there is evidence for peak tailing in the data for all peaks other than *n*-tetradecane. This means that there is likely a cold spot or dead volume in the flow path that is causing mixing or non-specific retention. The Kurtosis factor indicates how Gaussian or flat a peak is, by comparing the ratio of a peak's width at 50 % height and peak width at 10 % of peak height. Peaks with a Kurtosis value that deviates significantly from 1 are said to be too sharp or too flat compared to an ideal Gaussian peak. Kurtosis values tend to deviate from 1, when peaks are not being sampled at a fast enough data rate, or the dynamic range of the detector or column is exceeded. Kurtosis values for the present peaks were acceptable, indicating ideal detection for the analysis.

2.4 Conclusions

The Calidus™ GC instrument was modified to reduce the dead volumes and other sources of peak broadening in the system. The ability of the Calidus™ GC to generate narrow injection bandwidths was evaluated *via* the injection of a non-retained compound (methane), which allowed an unbiased measurement of the peak widths that can be obtained using included S/SL injector, a Deans' switching approach with PMDs. Deans' switching with PMDs was not capable of providing injection bandwidths narrower than the native S/SL injector. This inability to reduce the peak widths with Deans' switching was likely caused by the switching speed of the solenoid used and the large mass of carrier gas between the solenoid and PMD, which is inertial mass that can experience compression during valve switching.

Diaphragm valves are an alternative method for providing pneumatically controlled switching, that are capable of the rapid actuation speeds (< 10 ms) needed for injection bandwidth control. Presently it appears that diaphragm valves are the preferred valve based strategy for injection bandwidth control, however future research should focus on the development and implementation of temperature stable membranes into PMDs to overcome the temperature limitations of the present diaphragm valve technologies.

The temperature programming capabilities of PMDs were evaluated, and it was discovered that these devices were not able to accurately track convection oven temperatures during fast temperature programming. This means that cold spots could develop in the carrier gas flow path, within PMDs whenever a rapid temperature program is used. Cold spots cause solute condensation and the degradation of chromatographic performance, therefore auxiliary heating is recommended to minimise this effect. The isothermal oven of the Calidus™ GC instrument was expected to prevent condensation of solutes in the GC flow path, which is discussed in Section 2.3.2.

Finally the separation capabilities of the Calidus™ GC's resistively heated column modules were evaluated using a test mixture comprised of a range of compounds. The retention times and peak area repeatabilitites for the Calidus™ column were relatively good considering the use of manual injection technique, and further improvements would likely be realised if an auto-sampler unit was incorporated into the instrument. The separation performance of a short column was found to be relatively poor compared to longer columns with similar internal diameters after normalising the number of theoretical plates for each solute with the length of column. This poor performance was attributed to the stationary film thickness inefficiency factor, which is magnified by using short columns with low-pressure drops. The addition of a second separation column to facilitate MDGC and GC × GC will be explored in the following research chapters as a means to increase the separation performance of the Calidus™ system to enable it to separate complex samples.

2.5 References

[1] L.M. Blumberg, Theory of fast capillary gas chromatography. Part 3. Column performance vs. gas flow rate, J. High Resolut. Chromatogr. 22 (1999) 403-413.

[2] L.M. Blumberg, Theory of fast capillary gas chromatography. Part 4. Column performance vs. liquid film thickness, J. High Resolut. Chromatogr. 22 (1999) 501-508.

[3] L.M. Blumberg, Theory of fast capillary gas chromatography. Part 1. Column efficiency, J. High Resolut. Chromatogr. 20 (1997) 597-604.

[4] L.M. Blumberg, Theory of fast capillary gas chromatography. Part 2. Speed of analysis, J. High Resolut. Chromatogr. 20 (1997) 679-687.

[5] M.S. Klee, L.M. Blumberg, Theoretical and practical aspects of fast gas chromatography and method translation, J. Chromatogr. Sci. 40 (2002) 234-247.

[6] M.R. Jacobs, E.F. Hilder, R.A. Shellie, Applications of resistive heating in gas chromatography: A review, Anal. Chim. Acta 803 (2013) 2-14.

[7] A. Wang, H.D. Tolley, M.L. Lee, Gas chromatography using resistive heating technology, J. Chromatogr. A 1261 (2012) 46-57.

[8] R.V. Mustacich, Temperature control system of gas chromatography column assembly, US5782964A (1998) RVM Scientific, Inc., USA, 10 pp.

[9] S.D. Stearns, H. Cai, J.A. Koehn, M. Brisbin, C. Cowles, C. Bishop, S. Puente, D. Ashworth, A direct resistively heated gas chromatography column with heating and sensing on the same nickel element, J. Chromatogr. A 1217 (2010) 4629-4638.

[10] N. Roques, J. Crandall, Fast micro gas chromatograph system, WO2010028398A2 (2010) Falcon Analytical Systems & Technology, USA, 50 pp.

[11] J. Luong, R. Gras, R.A. Shellie, H.J. Cortes, Applications of planar microfluidic devices and gas chromatography for complex problem solving, J. Sep. Sci. 36 (2013) 182-191.

[12] R.A. Shellie, H.J. Cortes, R. Gras, J. Luong, Planar microfluidic devices in flow modulated comprehensive two dimensional gas chromatography for challenging petrochemical applications, Anal. Methods 5 (2013) 6598-6604.

[13] W. Bertsch, V. Pretorius, Deactivation of metal surfaces for capillary columns for GC by deposition of silicon, HRC CC, J. High Resolut. Chromatogr. Chromatogr. Commun. 5 (1982) 498-500.

[14] V. Pretorius, J.W. Du Toit, J.H. Purnell, Gas chromatography in glass and fused silica capillary columns: deactivation of the inner surface using silicon films, HRC CC, J. High Resolut. Chromatogr. Chromatogr. Commun. 4 (1981) 344-345.

[15] W. Bertsch, V. Pretorius, G.C. Van Niekerk, The use of silicon in the preparation of apolar glass capillary columns, HRC CC, J. High Resolut. Chromatogr. Chromatogr. Commun. 5 (1982) 539-545.

[16] T. Welsch, High-temperature silylation in the production of inert glass capillary columns. From the first experiments to the chemical mechanism, HRC CC, J. High Resolut. Chromatogr. Chromatogr. Commun. 11 (1988) 471-479.

[17] C.F. Poole, S.K. Poole, Separation characteristics of wall-coated open-tubular columns for gas chromatography, J. Chromatogr. A 1184 (2008) 254-280.

[18] J.V. Seeley, S.K. Seeley, Multidimensional Gas Chromatography: Fundamental Advances and New Applications, Anal. Chem. 85 (2013) 557-578.

[19] R.C. Blase, K. Llera, A. Luspay-Kuti, M. Libardoni, The Importance of Detector Acquisition Rate in Comprehensive Two-Dimensional Gas Chromatography (GC×GC), Sep. Sci. Technol. 49 (2014) 847-853.

[20] G. Gaspar, P. Arpino, G. Guiochon, Study in high speed gas chromatography. I. Injections of narrow sample plugs, J. Chromatogr. Sci. 15 (1977) 256-261.

[21] A. Van Es, J. Janssen, C. Cramers, J. Rijks, Sample enrichment in high speed narrow bore capillary gas chromatography, HRC CC, J. High Resolut. Chromatogr. Chromatogr. Commun. 11 (1988) 852-857.

[22] M. Klemp, A. Peters, R. Sacks, High-speed GC analysis of VOCs: sample collection and inlet systems. 1, Environ. Sci. Technol. 28 (1994) 369A-376A.

[23] A. Grall, C. Leonard, R. Sacks, Peak capacity, peak-capacity production rate, and boiling point resolution for temperature-programmed GC with very high programming rates, Anal. Chem. 72 (2000) 591-598.

[24] K. Grob, Injection techniques in capillary GC, Anal. Chem. 66 (1994) 1009A-1019A.

[25] R. Bailey, Injectors for capillary gas chromatography and their application to environmental analysis, J. Environ. Monit. 7 (2005) 1054-1058.

[26] V.R. Reid, R.E. Synovec, High-speed gas chromatography: The importance of instrumentation optimization and the elimination of extra-column band broadening, Talanta 76 (2008) 703-717.

[27] K. Grob, G. Grob, Splitless injection on capillary columns. I. Basic technique; steroid analysis as an example, J. Chromatogr. Sci. 7 (1969) 584-586.

[28] K. Grob, G. Grob, Splitless injection on capillary columns. II. Conditions and limits, practical realization, J. Chromatogr. Sci. 7 (1969) 587-591.

[29] G.L. Pratt, J.H. Purnell, Sampling valve for use in gas chromatographic analysis of the products of gaseous reactions, Anal. Chem. 32 (1960) 1213.

[30] C.J. Penther, J.W. Hickling, New liquid-sampling valve extends usefulness of process chromatographs, Oil Gas J. 59 (1961) 130-133.

[31] G.M. Gross, V.R. Reid, R.E. Synovec, Recent advances in instrumentation for gas chromatography, Curr. Anal. Chem. 1 (2005) 135-147.

[32] M.C. Harvey, R.E. Robinson, M.C. Harvey, S.D. Stearns, Further studies on high-speed switching of chromatographic valves, J. Chromatogr. Sci. 32 (1994) 190-194.

[33] R. Tijssen, N. Van den Hoed, M.E. Van Kreveld, Theoretical aspects and practical potentials of rapid gas analysis in capillary gas chromatography, Anal. Chem. 59 (1987) 1007-1015.

[34] A. Peters, M. Klemp, L. Puig, C. Rankin, R. Sacks, Instrumentation and strategies for high-speed gas chromatography, Analyst 116 (1991) 1313-1320.

[35] M. Nowak, A. Gorsuch, H. Smith, R. Sacks, Stepper motor controlled micro gas valve inlet system for gas chromatography, Anal. Chem. 70 (1998) 2481-2486.

[36] J.V. Seeley, N.J. Primeau, S.V. Bandurski, S.K. Seeley, J.D. McCurry, Microfluidic Deans Switch for Comprehensive Two-Dimensional Gas Chromatography, Anal. Chem. 79 (2007) 1840-1847.

[37] A. Ghosh, C.T. Bates, S.K. Seeley, J.V. Seeley, High speed Deans switch for low duty cycle comprehensive two-dimensional gas chromatography, J. Chromatogr. A 1291 (2013) 146-154.

[38] A. Van Es, J. Janssen, R. Bally, C. Cramers, J. Rijks, Sample introduction in high speed capillary gas chromatography; input band width and detection limits, HRC CC, J. High Resolut. Chromatogr. Chromatogr. Commun. 10 (1987) 273-279.

[39] C.G. Fraga, B.J. Prazen, R.E. Synovec, Comprehensive Two-Dimensional Gas Chromatography and Chemometrics for the High-Speed Quantitative Analysis of Aromatic Isomers in a Jet Fuel Using the Standard Addition Method and an Objective Retention Time Alignment Algorithm, Anal. Chem. 72 (2000) 4154-4162.

[40] C.A. Bruckner, B.J. Prazen, R.E. Synovec, Comprehensive two-dimensional high-speed gas chromatography with chemometric analysis, Anal. Chem. 70 (1998) 2796-2804.

[41] R.E. Mohler, B.J. Prazen, R.E. Synovec, Total-transfer, valve-based comprehensive two-dimensional gas chromatography, Anal. Chim. Acta 555 (2006) 68-74.

[42] R.T. Lidster, J.F. Hamilton, A.C. Lewis, The application of two total transfer valve modulators for comprehensive two-dimensional gas chromatography of volatile organic compounds, J. Sep. Sci. 34 (2011) 812-821.

[43] R.B. Wilson, W.C. Siegler, J.C. Hoggard, B.D. Fitz, J.S. Nadeau, R.E. Synovec, Achieving high peak capacity production for gas chromatography and comprehensive two-dimensional gas chromatography by minimizing off-column peak broadening, J. Chromatogr. A 1218 (2011) 3130-3139.

[44] J.L. Hope, K.J. Johnson, M.A. Cavelti, B.J. Prazen, J.W. Grate, R.E. Synovec, High-speed gas chromatographic separations with diaphragm valve-based injection and chemometric analysis as a gas chromatographic "sensor", Anal. Chim. Acta 490 (2003) 223-230.

[45] V.R. Reid, A.D. McBrady, R.E. Synovec, Investigation of high-speed gas chromatography using synchronized dual-valve injection and resistively heated temperature programming, J. Chromatogr. A 1148 (2007) 236-243.

[46] G.M. Gross, B.J. Prazen, J.W. Grate, R.E. Synovec, High-Speed Gas Chromatography Using Synchronized Dual-Valve Injection, Anal. Chem. 76 (2004) 3517-3524.

[47] R.L. Wade, S.P. Cram, Fluidic logic sampling and injection system for gas chromatography, Anal. Chem. 44 (1971) 131-139.

[48] R. Annino, J. Leone, The use of coanda wall attachment fluidic switches as gas chromatographic valves, J. Chromatogr. Sci. 20 (1982) 19-26.

[49] C.P.M. Schutjes, C.A. Cramers, C. Vidal-Madjar, G. Guiochon, Fast "fluidic logic" injection at pressures up to 25 bar in high-speed capillary gas chromatography, J. Chromatogr. 279 (1983) 269-277.

[50] M. Poliak, M. Kochman, A. Amirav, Pulsed flow modulation comprehensive two-dimensional gas chromatography, J. Chromatogr. A 1186 (2008) 189-195.

[51] P.Q. Tranchida, G. Purcaro, A. Visco, L. Conte, P. Dugo, P. Dawes, L. Mondello, A flexible loop-type flow modulator for comprehensive two-dimensional gas chromatography, J. Chromatogr. A 1218 (2011) 3140-3145.

[52] R.J. Jonker, H. Poppe, J.F.K. Huber, Improvement of speed of separation in packed column gas chromatography, Anal. Chem. 54 (1982) 2447-2456.

[53] D.R. Deans, A new technique for heart cutting in gas chromatography, Chromatographia 1 (1968) 18-22.

[54] P.Q. Tranchida, D. Sciarrone, P. Dugo, L. Mondello, Heart-cutting multidimensional gas chromatography: A review of recent evolution, applications, and future prospects, Anal. Chim. Acta 716 (2012) 66-75.

[55] J.V. Seeley, Recent advances in flow-controlled multidimensional gas chromatography, J. Chromatogr. A 1255 (2012) 24-37.

[56] J. Luong, R. Gras, G. Yang, H. Cortes, R. Mustacich, Multidimensional gas chromatography with capillary flow technology and LTM-GC, J. Sep. Sci. 31 (2008) 3385-3394.

[57] J.D. McCurry, B.D. Quimby, Two-Dimensional Gas Chromatography Analysis of Components in Fuel and Fuel Additives Using a Simplified Heart-Cutting GC System, J. Chromatogr. Sci. 41 (2003) 524-527.

[58] SGE Analytical Science, SilFlow™ Stainless Steel Micro-fluidic Platform product note (2015) Accessed on: [12th November 2015] Website: http://sge.com/products/silflow-stainless-steel-micro-fluidic-platform.

[59] M. Hastings, R.E. Majors, The inert flow path story for GC and GC-MS: eliminating the weakest links, LCGC North Am. 31 (2013) 448, 450, 452-454.

[60] Restek Corporation, EZGC Method Translator and Flow Calculator (2014) Accessed on: [1st of October 2015] Website: http://www.restek.com/ezgc-mtfc.

[61] Agilent Technologies, GC Method Translation Software (2013) Accessed on: [1st of October 2015] Website: http://www.agilent.com/en-us/support/gas-chromatography/gcmethodtranslation.

[62] S.S. Stafford, P. Sandra, T.A. Berger, M.Q. Thompson, K.J. Klein, F. David, L.C. Doherty, J.V. Wisniewski, D.W. Snyder, P.A. Larson, Electronic Pressure Control in Gas Chromatography, Hewlett-Packard Company, Wilmington, DE, 1993.

[63] L.M. Blumberg, M.S. Klee, Optimal heating rate in gas chromatography, J. Microcolumn Sep. 12 (2000) 508-514.

[64] L.M. Blumberg, M.S. Klee, Metrics of separation in chromatography, J. Chromatogr. A 933 (2001) 1-11.

[65] F. Xu, W. Guan, G. Yao, Y. Guan, Fast temperature programming on a stainless-steel narrow-bore capillary column by direct resistive heating for fast gas chromatography, J. Chromatogr. A 1186 (2008) 183-188.

[66] N. Roques, J. Crandall, Trans-configurable modular chromatographic assembly, US20100256922A1 (2010) Falcon Analytical Systems & Technology, USA, 18pp.

[67] N.J. Roques, Flat spiral capillary column assembly with thermal modulator, US20060283324A1 (2006) Falcon Analytical Systems & Technology, USA, 25pp.

[68] S. Reichenbach, Q. Tao, "GCxGC Blob Metadata and Statistics in GC Image", white paper available from GC Image LLC (2011) Accessed on: [10th of December 2015] Website: http://www.gcimage.com/gcxgc/usersguide/statistics.pdf.

Chapter 3: Thermal focusing for gas chromatography injection optimisation

Summary

Thermal focusing strategies, unlike valve based switching, are capable of physically focusing a sample band, and then eluting these focused compounds in a narrow injection plug to a column. Injection band focusing leads to appreciable increases in separation performance compared to S/SL injection alone. Additionally, thermal focusing eliminates boiling point discrimination that is experienced during sample vaporisation and effluent transfer to the column. Finally, thermal modulators, unlike valve-controlled injectors, transfer an entire sample injection to the column maximising analytical sensitivity.

The present chapter explores the use of a trapping device that is based on a SS capillary, coated with a polydimethylsiloxane (PDMS) stationary phase. The trap's stationary phase was modified by applying a series of high temperature pulses, while flowing purified air through the SS capillary. After this procedure the morphology and chemistry of the stationary phase were modified substantially, which improved the thermal and retention properties of the trap. The performance and physical properties of this trap were evaluated using a range of techniques, and the trap was tested as a device for injection bandwidth minimisation in GC.

3.1 Introduction

In Chapter 2, PMDs were tested for the application of controlling the injection bandwidth of samples being introduced to a capillary GC column for fast GC analysis. This approach was not able to reduce injection bandwidths below 100 ms (half height) in duration, which was comparable to the performance achievable with S/SL injection. As a result of this PMDs were abandoned as a potential injection bandwidth control strategy in favour of S/SL injection. While S/SL injectors are effective and simple to use, they are not ideal for fast GC analysis due to their relatively wide injection bandwidths (100 ms peak widths at 200:1 split ratio). The need to operate at high split ratios can be limiting during trace analysis due to the small amount of sample that is transferred to the separation column with this splitting procedure.

Trace compound analysis often requires use of the splitless injection mode where an entire sample injection (≈ 1 µL) is vaporised and transferred to the column. Splitless injection takes a relatively long time to complete (> 1 min), which results in peaks having a wide injection bandwidth, despite on-column solute focusing [1,2]. Another alternative strategy is to utilise sample preparation techniques to pre-concentrate target analytes prior to injection, however such techniques are beyond the scope of the present research chapter. Finally, a sample injection can be focused prior to separation by using thermal focusing and retentive traps. This process of focusing peaks prior to separation and detection improves the signal to noise ratio by compressing peaks in the time dimension while maintaining the on-column mass. This leads to an increase in peak height thereby improving the detection of each peak, providing that an adequate data-sampling rate is provided by the detection system.

Injection bandwidth focusing has two distinct steps, the initial solute trapping step and the solute release step. Trapping has been achieved using a range of different stationary phases as well using condensation of analytes within uncoated inert traps

(Table 8). Early solute focusing designs were based on U-shaped tubes, and short columns packed with inert adsorbents that were cooled using cryogenic liquids [3-9]. The two main cryogens used for solute focusing are liquid nitrogen and solid carbon dioxide cryogens, both of which serve to increase the retention factor of volatile compounds within the focusing device and improve trap solute capacity. In terms of expense, carbon dioxide is a cheaper cryogen, however it is not well suited to the focusing of compounds with boiling points below -78 °C [10,11]. Liquid nitrogen despite being significantly more expensive, is capable of trapping highly volatile compounds with boiling points as low as -196 °C, and is therefore the cryogen of choice for such compounds [11].

While liquid cryogenic baths were effective for focusing injection bands, compound elution and the integration of these systems with GC systems was problematic and not repeatable. This led researchers to test cryogenically cooled nitrogen gas as an alternative, and this method proved to be simple to implement and control. [12-16]. A summary of the performances for modern cryogenically focused injection is given in Table 8. The selection of cooling strategy depends on the volatility of the analytes that need to be focused, and the retention capabilities of the focusing device that is being used. It is also possible to utilise ambient air, refrigerated air or thermoelectric cooling instead of cryogenic cooling to enhance the trapping of highly volatile components (Table 8), providing that the stationary phase of the focusing device is sufficiently retentive. Cramers and Vermeer tested air-cooling for solute trapping on a short segment of coated capillary column (SE-30 phase, 50 cm, 250 μm ID, 1 μm d_f), unfortunately focusing of volatile compounds proved unfeasible [17]. Valentin *et al.* tested air-cooling for controlling the retention of methane and other low molecular weight hydrocarbons with a SS column packed with highly retentive silver oxide, demonstrating the importance of appropriate stationary phase selection for peak focusing [18,19].

It is equally important that focused peaks, particularly low volatility solutes, can be quickly remobilised from the focusing device. Remobilisation can be achieved by applying heat supplied using resistive heating, or hot air provided by a blower or a GC oven compartment. Research on the performance of various modulator devices is summarised in Table 8, however it is worth noting the inconsistent conditions under which the injection bandwidths have been measured for each modulator. It is preferable to connect a DFS capillary between the modulator and detector to minimise any broadening due to chromatography to properly evaluate the injection bandwidths generated by a modulator, however it is common for researchers to connect a second-dimension column after the modulator, and then evaluate the modulator performance. For this reason, bandwidth measurements have been labelled in Table 8 as either injection or, post-column bandwidths. Furthermore, it is important to consider the flow rates, and void volumes present in GC systems following modulation, since these features can drastically broaden peaks following solute mobilisation.

Generally, the speed of solute remobilisation limits the injection plug bandwidth, while the retention and temperature of the trap limits the volatility range of solutes that can be focused using a given device [40-42]. As a compromise between these instrument types a number of researchers have developed a technique whereby a SS capillary trap used cryogenically cooled nitrogen gas for solute focusing, and resistive heating *via* electrical current application to the SS capillary solute remobilisation [26,28-30,43,44]. The main drawback of resistively heated solute release is the possibility of thermal degradation of labile compounds. In particular, the heating of metal capillaries to high temperatures while using hydrogen gas carrier, can lead to significant amounts of compound degradation in some instances, so care must be taken to minimise the desorption temperature used in addition to minimising the activity of SS capillaries [45].

Table 8 Summary of thermally focused peak widths obtained using a variety of different focusing strategies.

Cooling Strategy	Focusing device	Remobilisation strategy	Peak width (ms)	Solute	Bandwidth type	Ref
Ambient Air Cooling	WCOT FGS Capillary	Resistive heating, conductive painted capillary	1800	PCB	Post separation bandwidth	[20]
	WCOT SS capillary	Resistive heating, SS capillary	96	*n*-hexadecane		[21]
			60	*n*-octadecane	Injection bandwidth	[22]
			200	*n*-alkane	Post separation bandwidth	[23]
Cryogenic (LN_2)	Tenax packed SS Capillary		65	*n*-pentane	Injection bandwidth	[24]
	WCOT Aluminium clad capillary	Resistive heating, aluminium clad capillary	19.3	*n*-octane		[25]
			80	*n*-heptane	Post separation bandwidth	[26]
	WCOT SS capillary	Hot air jet	550	*n*-alkanes		[10]
		Latent heat from GC oven	6	Chlorodifluoromethane	Injection bandwidth	[27]
		Resistive heating, SS capillary	13.4	Acetone		[28]
			4.5	Toluene		[29]
			24	Methanol		[30]
Cryogenic jet (CO_2)	WCOT SS capillary	Latent heat from GC oven	800	n-dodecane	Post separation bandwidth	[9]
	WCOT FGS Capillary		1240	n-tridecane		[31]
			765	n-dodecane		[32]
		Hot air jet	86	n-dodecane	Injection bandwidth	[33]
			200	*n*-alkanes	Post separation bandwidth	[34]
GC oven only	WCOT SS capillary	Resistive heating, SS capillary	1450	Ethane		[18]
			350	*n*-alkanes		[34]
	WCOT FGS Capillary	Resistive heating, conductive painted capillary	410	*n*-decane		[35]
			28	*n*-heptane		[36]
			25	*n*-heptane		[37]
			22	*n*-nonane		[38]

		Hot air jet	200	*n*-alkanes		[34]
	WCOT Aluminium clad capillary	Resistive heating, aluminium clad capillary	800			[34]
Peltier assisted cooling	WCOT SS capillary	Resistive heating, SS capillary	215	PCB8		[39]

Focusing devices have also been constructed from inert fused silica capillary (FSC) coated with a layer of conductive paint to enable resistive heating [35,36,38]. This resulted in a low thermal mass trap that could be rapidly heated to enhance solute remobilisation, however this design was not robust and suffered from cracking of the conductive paint during repeated usage. Aluminium clad GC capillary columns were tested as alternatives to the coating strategy used by Phillips and co-workers; however these suffered from similar robustness issues [25].

Rather than relying on resistive heating for solute remobilisation, latent heat from convection ovens and auxiliary blowers have been used for solute remobilisation. Borgerding and Wilkerson utilised a cryogenically cooled narrow-bore capillary column (50 μm to 100 μm ID) for the trapping and focusing of analytes within a gas-sampling loop [27]. Solutes were remobilised from the loop using latent heat provided by the heated sampling valve. Marriott and Kinghorn developed a trapping device that used cryogenic carbon dioxide for solute focusing on FSC columns, which were housed within a GC convection oven, eliminating the need for auxiliary heating and a sampling loop [31]. Switching the cold jet off, after focusing an S/SL injection within a segment of capillary column allowed trapped solutes to be mobilised using latent heat present in the GC convection oven. This approach was later improved, with the development of the longitudinally modulated cryogenic system (LMCS), the position of a cryogenically cooled nitrogen jet could be mechanically moved back and forth over a segment of FSC to trap and release solutes [32].

The present research chapter focuses on the evaluation of a solute focusing trap that is constructed from a short (4 cm) segment of SS capillary column. This focusing device does not require cryogenic cooling for operation, and instead relies on ambient air or thermoelectric (Peltier) cooling to enhance solute retention. The trapping capillary is internally coated with a chemically modified stationary phase that is both highly retentive and temperature stable. The extent of stationary phase modification will be analysed using a range of techniques and the device's solute loading and remobilisation capabilities will be evaluated for a range of different solutes to determine the effectiveness of this device for injection bandwidth minimisation.

3.2 Materials and Methods:

3.2.1 Preparation of the thermally modified stationary phase

A focusing device that was capable of retaining volatile and semi-volatile species in a narrow injection bandwidth was constructed from SS capillary column (7 cm × 280 µm ID × 1.0 µm d_f, Restek) coated with a non-polar dimethylpolysiloxane (PDMS) coating, that was flattened and exposed to a thermo-oxidative treatment prior to use. A procedure described by Panic *et al.* was used to flatten 4 cm segment of a 7 cm long SS capillary [22]. Briefly, the capillary was placed in between a pair of parallel shims (4 cm long) and secured in place using masking tape. Two cover plates were then placed over the top and bottom of the trap and shim plates forming a sandwich with the modulator trap located in the centre. A vice was then used to apply pressure and flatten a 4 cm length of the trap from an outer diameter (wall to wall) of 540 µm to a wall distance of 360 µm, forming a flattened capillary surface, 4 cm long in the centre of the original 7 cm long piece of SS capillary. The internal wall-to-wall distance is 100 ± 5 µm, within the capillary after this procedure. A pair of SilTite mini unions (Trajan) was then connected to the ends of the flattened capillary to facilitate its connection with GC columns, and the final trap form is shown in Figure 17.

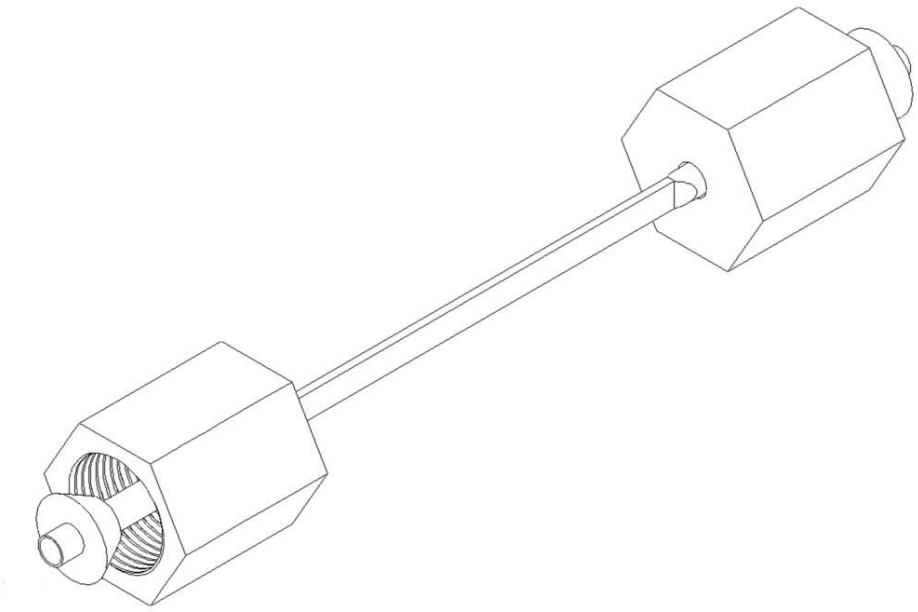

Figure 17 Schematic diagram of the flattened SS capillary complete with SilTite™ mini unions and ferrules. (Figure courtesy of Mr Matthew Edwards and Professor Tadeusz Gorecki; University of Waterloo, Canada).

The flattened SS capillary was then connected to a capacitive discharge power supply using a pair of solid core copper electrical leads that were insulated within a fiberglass braid to prevent electrical shorting, as shown in Figure 18.

Figure 18 Single core copper leads connected to the inlet and outlet of a SS capillary focusing device.

The capacitive discharge power supply was constructed from a bank of capacitors that were configured in parallel (4 × 44000 μF capacitors). A constant voltage power supply was used to provide a programmable charging voltage between 1.0 and 45 V. The stationary phase of the capillary was then thermally treated with a sequence of high current pulses. Initially 100 temperature pulses with a 30 V charging voltage were applied to the trap at a rate of 1 pulse every 6 s for 10 min. During this procedure the SS capillary visibly glows a hot red with each electrical discharge, which indicates a temperature of approximately 700 °C had been obtained periodically over the 10 min period. After this sequence of pulses was complete, the trap was connected to a source

of purified air, and an additional 50 electrical pulses were applied (once every 6 s) over a 5 min period. The airflow direction within the trap was then reversed and a final series of 50 capacitive discharges were applied to complete the thermal-oxidative treatment procedure. Further details on the preparation of the trap are given in the following reference [46].

3.2.2 Trap stationary phase characterisation

Characterisation of the modulator phase was carried out at the University of Waterloo, Canada. Scanning electron microscopy (SEM) imaging was performed on sections of SS capillary containing the PDMS stationary phase before and after modification using a Zeiss Ultra PLUS FESEM instrument (Zeiss, Germany) at excitation energy 10 kV. Energy dispersive X-ray electron spectroscopy (EDS) was subsequently carried out on the same samples. X-ray photoelectron spectroscopy (XPS) was carried out on the stationary phase before and after modification using an Oxford Instruments electron spectrometer (Argus, Oxford Instruments, United Kingdom) with monochromatic Al Kα (1486.6 eV) X-ray source, with a chamber pressure of 10^{-9} mbar.

3.2.3 Study of the heating and cooling profile of the resistively heated trap

The heating profile of the SS capillary trap was measured while the trap was installed within a holder device designed to dissipate heat away from the SS capillary after each capacitive discharge event. The holder was constructed from a pair of copper heat conduits that are held together using a spring mechanism as shown in Figure 19.

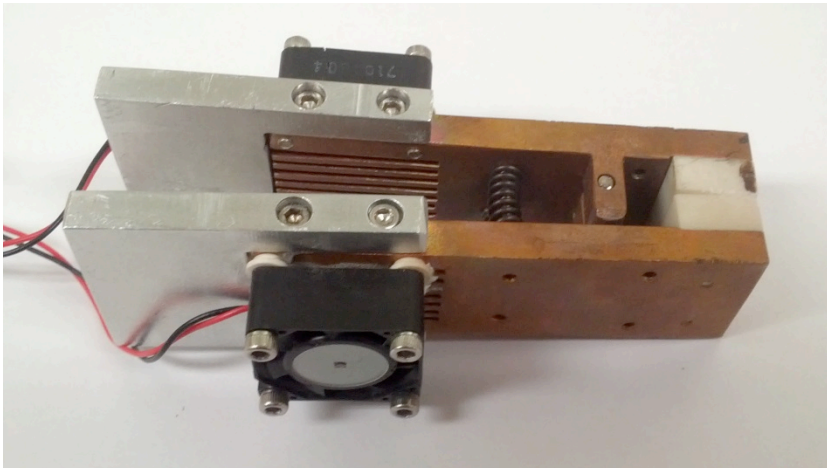

Figure 19 Heat sinking device for the SS capillary trap, showing the two copper heat conduits, ceramic pads and electric fans.

The heat conduits could be cooled either using ambient air *via* a pair of small electric fans (as shown in Figure 19), or using active cooling with Peltier thermoelectric cooling wafers. Both fans (12 V) and thermoelectric cooling pads (5 V, 2.6 A) were tested for cooling in the present research.

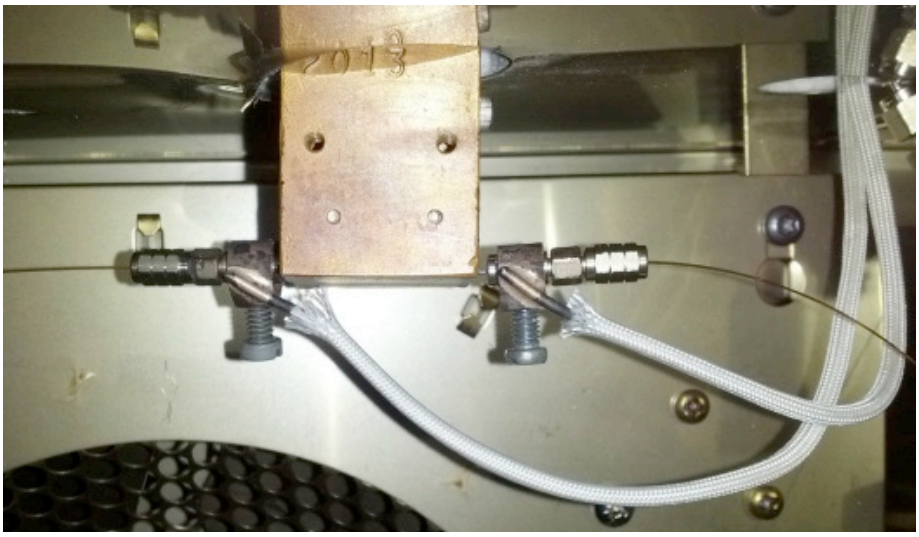

Figure 20 SS capillary trap supported within a GC convection oven. The heat-sinking device was installed through an unoccupied detector port. Heat is conducted through the copper heat sinks to the externally cooled side of the heat conduits.

The spring mechanism was used to compress and support the SS capillary trap within the heated compartment of a GC instrument as shown in Figure 20.

An Agilent 6850 GC with a S/SL inlet and FID was used as the platform for evaluating the heating and cooling capabilities of the SS capillary trap combined with the heat-sinking device. The S/SL inlet was connected to a DFS capillary (55 cm × 75 µm ID), which was then connected to an RTX-5 column (3 m × 180 µm ID × 0.2 µm d_f, Restek) using a SilTite µ-union. The carrier gas was hydrogen, which was delivered at a rate of 1.5 mL min^{-1}, which required an initial inlet pressure of 16.97 PSI. The RTX-5 column outlet was connected to a FID that was maintained at 250 °C and supplied with 30 mL min^{-1} of hydrogen, 320 mL min^{-1} of air, and 30 mL min^{-1} of nitrogen makeup gas for flame operation. The GC oven was set to an isothermal temperature of 40 °C for the duration of thermal modulation experiments.

A k-type thermocouple was spot welded to the midpoint of the SS trapping capillary for performing temperature measurements. A digital multimeter (Digitech, QM1538) with RS232 data logging capabilities was used for monitoring the temperature of the SS capillary during capacitive discharge events, at a range of different voltages from 15 to 32 V. Data was recorded using Electus distribution data logging software (2000) on a Dell notebook computer. All data was saved in comma separated values format, and imported into Microsoft Excel for processing. The maximum SS capillary temperatures for each discharge voltage were measures and the cooling rates of the SS capillary were calculated using this data.

3.2.4 Injection focusing studies using the single-stage thermal modulator

An Agilent 6850 GC with a S/SL inlet and FID was used as the platform for evaluating the heating and cooling capabilities of the SS capillary trap combined with the heat-sinking device. A piece of DFS capillary (55 cm × 75 µm ID) was connected to the S/SL inlet, which was then connected to an RTX-5 column (3 m × 180 µm ID × 0.2 µm

d_f, Restek) using a SilTite μ-union. The carrier gas was hydrogen, which was delivered at a rate of 1.5 mL min^{-1}, which required an initial inlet pressure of 16.97 PSI. The RTX-5 column outlet was connected to a FID that was maintained at 250 °C and supplied with 30 mL min^{-1} of hydrogen, 320 mL min^{-1} of air, and 30 mL min^{-1} of nitrogen makeup gas for flame operation.

A homologous series of linear alkanes was prepared containing: *n*-octane, *n*-nonane, *n*-decane, *n*-undecane, *n*-dodecane, *n*-tridecane, *n*-tetradecane, *n*-pentadecane, *n*-hexadecane, *n*-heptadecane, *n*-octadecane, *n*-nonadecane, *n*-eicosane (each 20 mg kg^{-1}, in *n*-hexane). This sample was injected (1 μL) at a split ratio of 100:1, onto the system described above. The GC oven was set to an initial temperature of 40 °C and was maintained at this temperature for a range of durations (0, 1, 2, 5 and 10 min). After this initial hold time had elapsed, the capacitive discharge power supply was actuated to heat the SS capillary and release the focused solutes from the focusing device. The GC oven was then temperature programmed at a rate of 10 °C min^{-1} up to 220 °C, to separate the focused analytes on the short RTX-5 column. FID data was collected with ChemStation software. Peak statistics were measured with Agilent ChemStation software and then exported to Microsoft Excel for further processing.

3.3 Results and discussion

3.3.1 Analytical characterisation of the focusing device

This solute focusing device was constructed from a short piece of SS capillary (6 cm, 280 μm ID) that was flattened to a nominal thickness of 100 μm ID as described in Section 3.2.1. The focusing device was installed between the GC injector and a short separation column during evaluation. The trap capillary was coated with thick film of PDMS polymer (1.0 μm d_f) that was modified using a proprietary process to enhance solute retention and stationary phase thermal stability [46]. The stationary phase of the device was analysed using a series of analytical techniques to evaluate the extent of stationary phase modification induced by the modification procedure described in Section 3.2.1.

Scanning electron microscopy (SEM) provided an insight into the effect of the thermal-oxidative treatment on the surface morphology of the PDMS stationary phase.

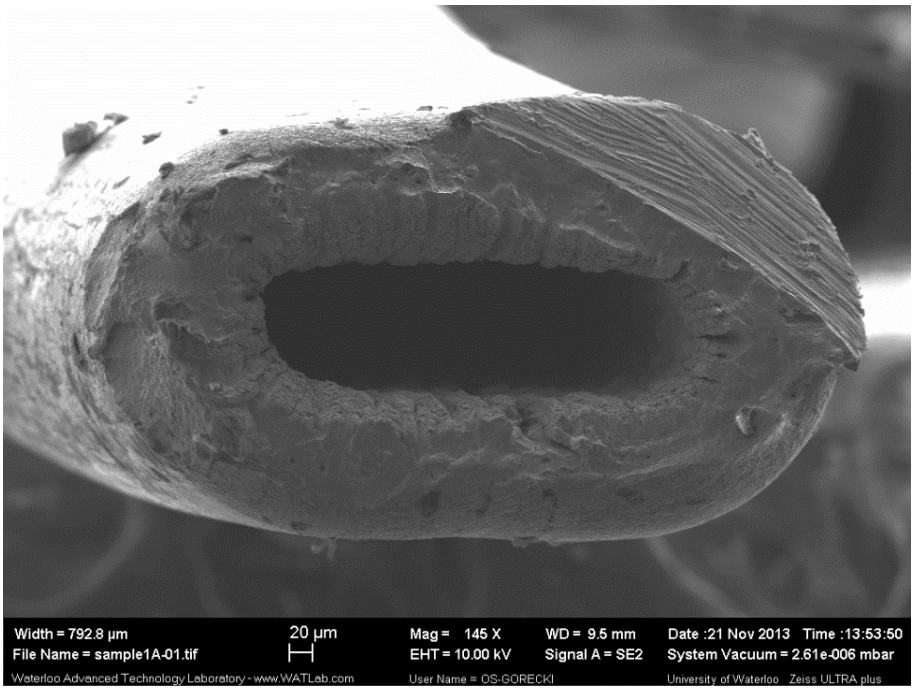

Figure 21 SEM cross-section of flattened modulator phase after chemical modification of the stationary phase surface.

Figure 21 shows an SEM image of a cross section of a flattened and chemically modified PDMS. The trap capillary revealed a rectangular geometry with dimensions of 100 ± 10 µm by 330 ± 10 µm, following flattening procedure described by Panic *et al.* [22]. The physical surface of the stationary phase appeared to be quite rough and irregular, with a number of small fissures visible in the stationary phase. These fissures were most likely formed as a result of the process of flattening the SS capillary from a cylindrical geometry to a rounded rectangular geometry using the procedure described in Section 3.2.1. The scored region on the upper right corner of the capillary was caused by the cutting procedure used to sever the SS capillary and obtain a cross-section, prior to SEM imaging.

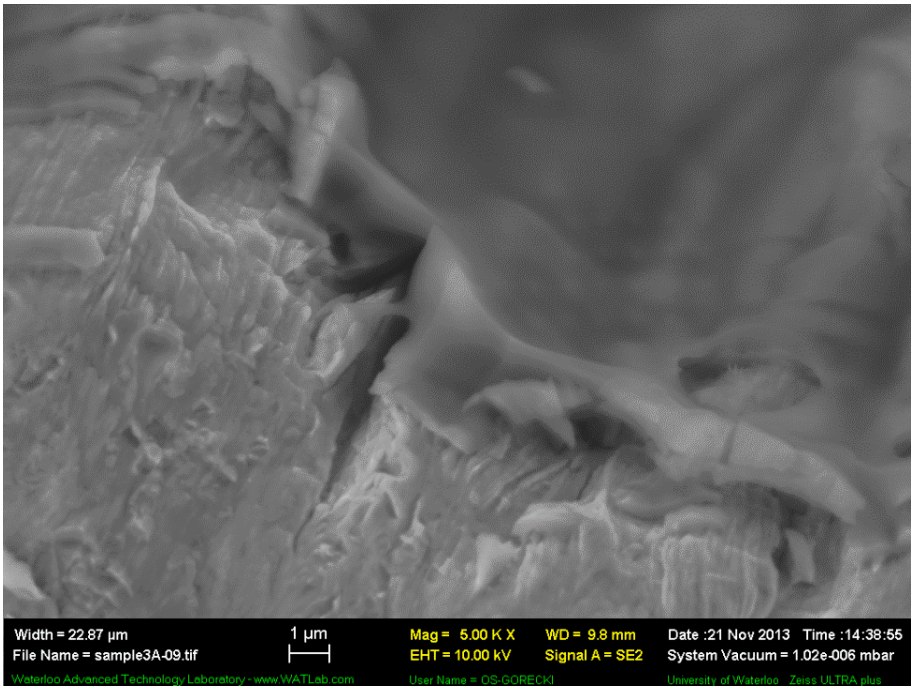

Figure 22 SEM image of a cross section of a SS capillary coated with a thick film of MXT-1 stationary phase (PDMS, 1 µm df) without the thermal treatment procedure.

A high magnification SEM image of an untreated segment of PDMS stationary phase is shown in Figure 22. The untreated PDMS stationary phase revealed a smooth, uniform coating of PDMS polymer with a thickness of approximately 1 µm. The rough area below

the smooth PDMS was the SS capillary after obtaining a capillary cross section. This was quite different to the rough texture of the stationary phase coating of a treated stationary phase capillary, shown in Figure 21.

Significant changes in the morphology of the stationary phase were evident, when compared with the untreated PDMS stationary phase (Figure 22). The rough surface of the stationary phase (Figure 21) after the treatment procedure was caused by the formation of spherical particles that are coating the interior walls of the stationary phase in the capillary. A high magnification image of the PDMS stationary phase after the thermal-oxidative procedure is shown in Figure 23. These spherical particles have diameters of approximately 500 ± 100 µm, and have formed a uniform layer throughout the capillary.

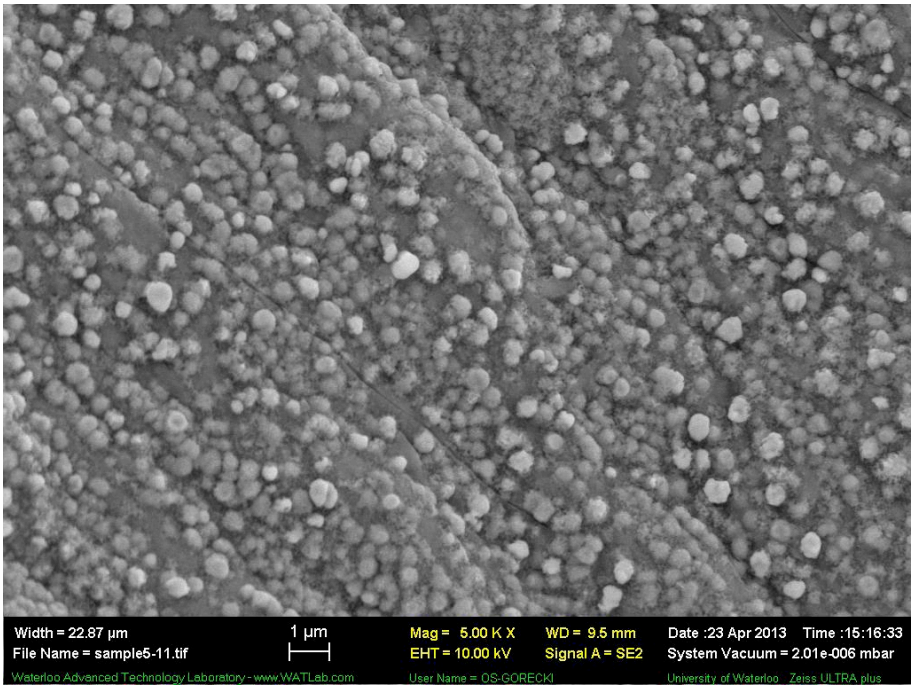

Figure 23 SEM image the internal surface morphology of a PDMS coated (1 µm d_f) capillary, after the thermal treatment procedure in the presence of air.

Energy dispersive X-ray spectroscopy (EDS) was used to analyse the chemical properties of the treated and un-treated PDMS stationary phase (Figure 24). EDS

supports the chemical modification of the PDMS stationary phase, with evidence for significant oxidation of the PDMS stationary phase.

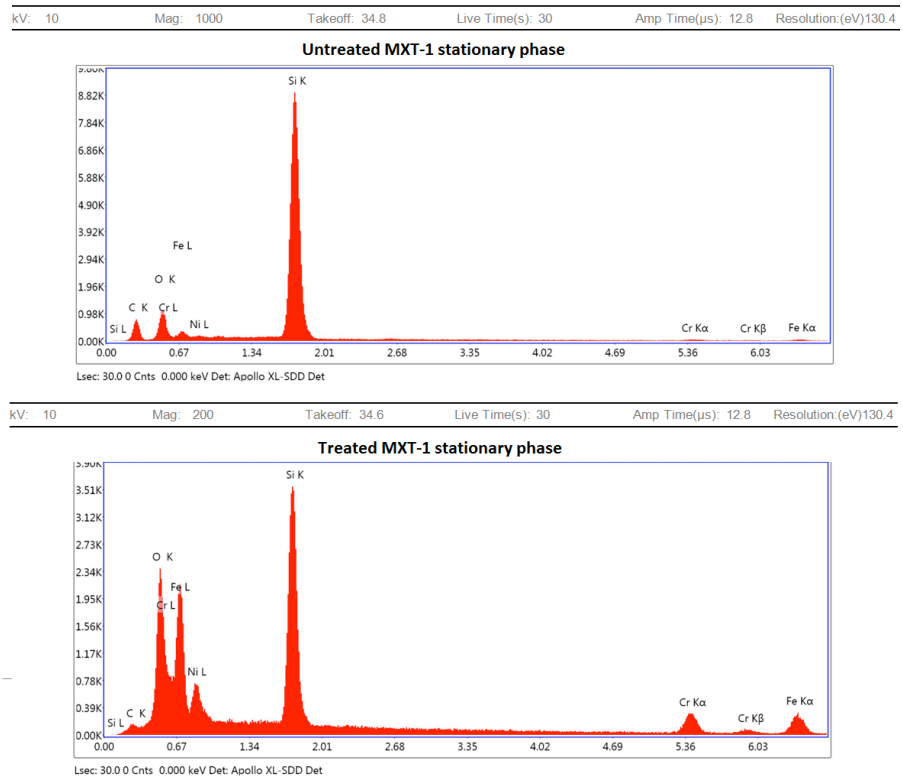

Figure 24 EDS spectra for untreated and treated MXT-1 stationary phase. Excitation energy 10 kV (y-axis label is: cps eV^{-1}) (x-axis label is: k eV).

The mass proportion of oxygen (κ-band) and carbon (κ-band) compared to silicon (κ-band) varies from an initial ratio of 0.45:0.18: 1, to 0.21:0.41:1 after the treatment procedure. This indicates that the amount of carbon present in the PDMS stationary phase is reduced by 50 % while the amount of oxygen increases by 260 % following the treatment procedure. Iron, nickel and chromium are present in the EDS spectra, which are expected, since these elements are components of the SS capillary. The signal of these metallic elements in the treated trap increased relative to the untreated trap, which suggested that the stationary phase film thickness was reduced during the treatment procedure, allowing a greater proportion of the signal to be obtained from the SS supporting capillary.

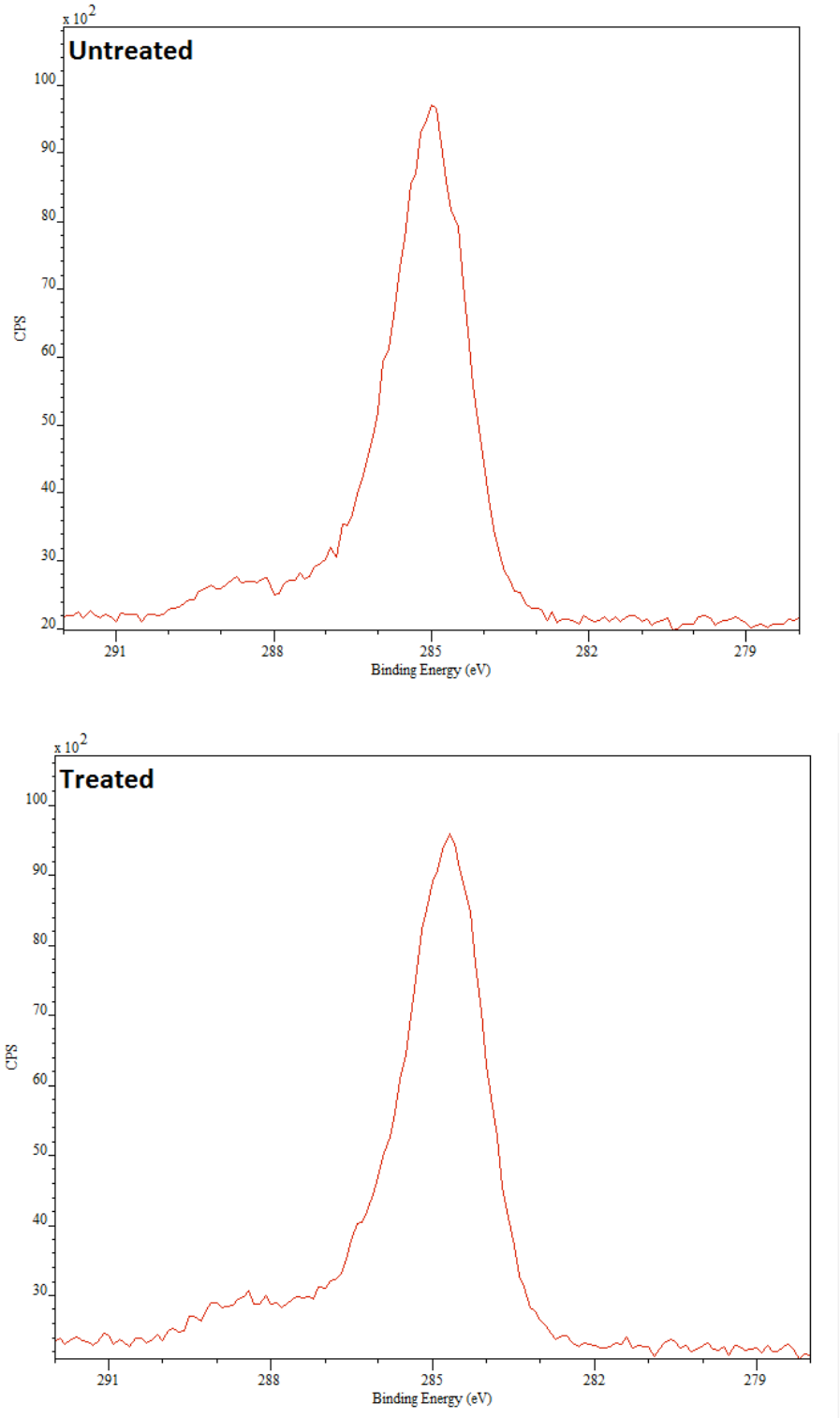

Figure 25 C1s XPS spectrum of untreated and treated PDMS stationary phase coating on a SS capillary.

It is also apparent that the absolute amount of silicon present in the treated sample has been substantially diminished compared to the untreated PDMS coated stationary phase, further supporting the reduction in stationary phase film thickness and oxidation of the PDMS coating.

Further analysis of the chemically modified stationary phase and nanoparticles that coat the capillary was carried out using X-ray photoelectron spectroscopy (XPS) analysis. XPS provides useful information on the chemical state of atoms that are present in the stationary phase coating by probing the binding energies of the various atoms that are present in a material. The C1s spectra of the untreated stationary phase revealed a binding energy of 284.8 eV, which is indicative of sp^3 hybridised carbon that is part of the PDMS polymer. After treatment this binding energy shifted to 284.0 eV (Figure 25) indicating the formation of sp^2 hybridised carbon. A small proportion of oxidised carbon C=O is also indicated at 288.3 eV further supporting modification of the stationary phase.

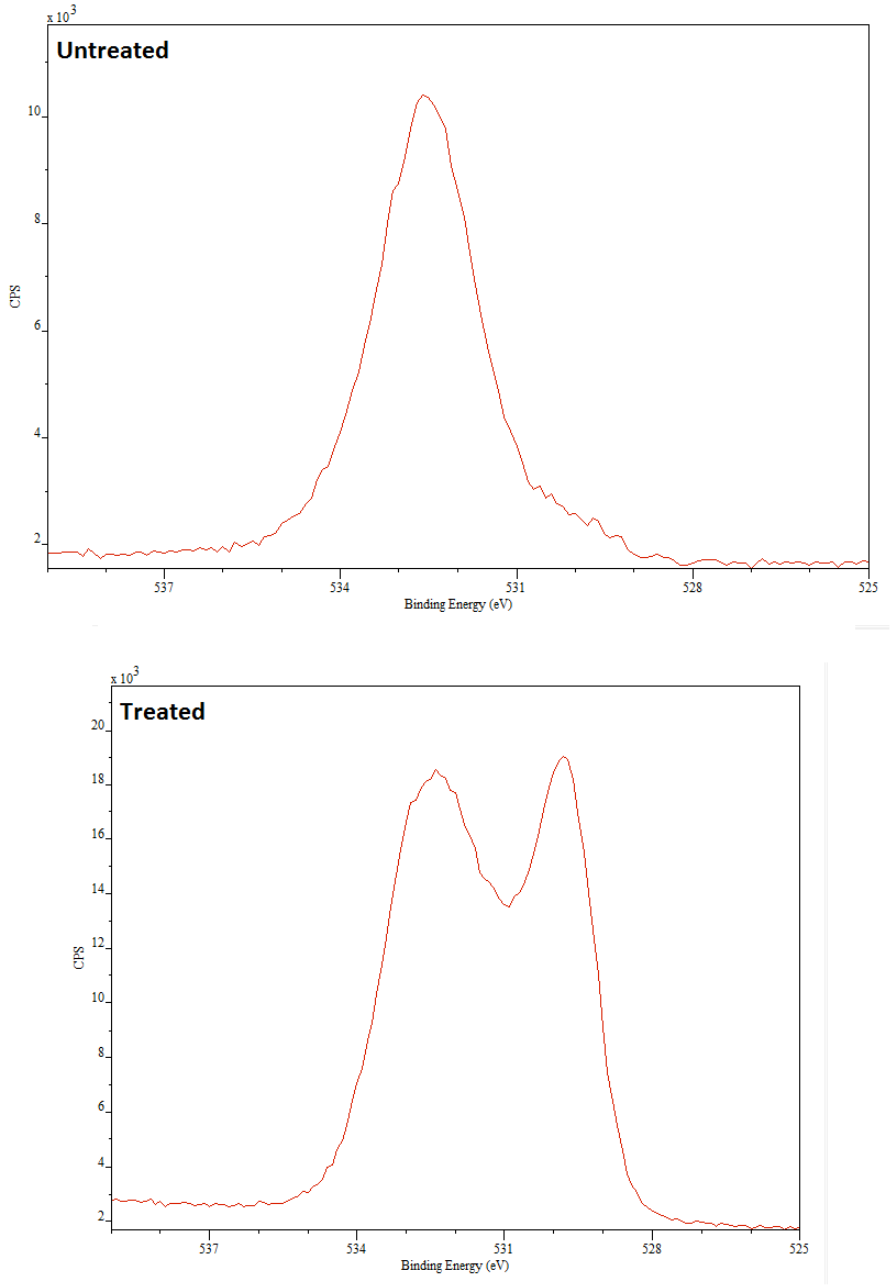

Figure 26 O1s XPS spectrum of untreated and treated PDMS stationary phase coating on a SS capillary.

The O1s spectrum (Figure 26) for the untreated PDMS displayed one broad peak at 533.0 eV, which is caused by Si-O bonds present in the PDMS polymer [47]. Additionally the deactivation procedure used to render SS capillaries inert also contributes to the Si-O due to the presence of a thin layer of SiO_2 that was deposited on the internal wall of the capillary to prevent compounds from coming into contact with a potentially active

metallic surface. After the treatment procedure, the peak at 533.0 eV increased in intensity suggesting that a greater amount of Si-O bonds had been formed during the treatment procedure (Figure 26). A second broad peak was also detected at 530.0 eV, which was indicative of the presence of metal oxides or carbonates that have likely formed due the oxidation of the SS capillary which is comprised of iron, chromium, nickel and molybdenum. Metal oxides were not present in the untreated SS capillary due to the deactivation procedure used by the manufacturer. The appearance of these metal oxides indicates that the deactivation procedure was compromised by the capacitive discharge induced heating. The rapid heating of the SS capillary caused a visible physical expansion and deformation of the capillary that could have exposed portions of the SS capillaries internal wall, thereby allowing the formation of metal oxides seen in Figure 26.

The Si2p spectrum (Figure 27) of the untreated stationary phase revealed a peak at 99.4 eV can be attributed to elemental silicon, which was present as an impurity in the PDMS polymer and the SiO_2 deposited with the capillary during the deactivation procedure [47]. Another peak at a higher binding energy of 103.5 eV is similarly caused by Si-O bonds in the material surface. Following the treatment procedure, this peak at 103.5 eV increased in intensity, while the peak at 99.4 eV was eliminated, suggesting that elemental silicon was completely oxidised to an Si-O state, most likely due to the formation of SiO_2 [47].

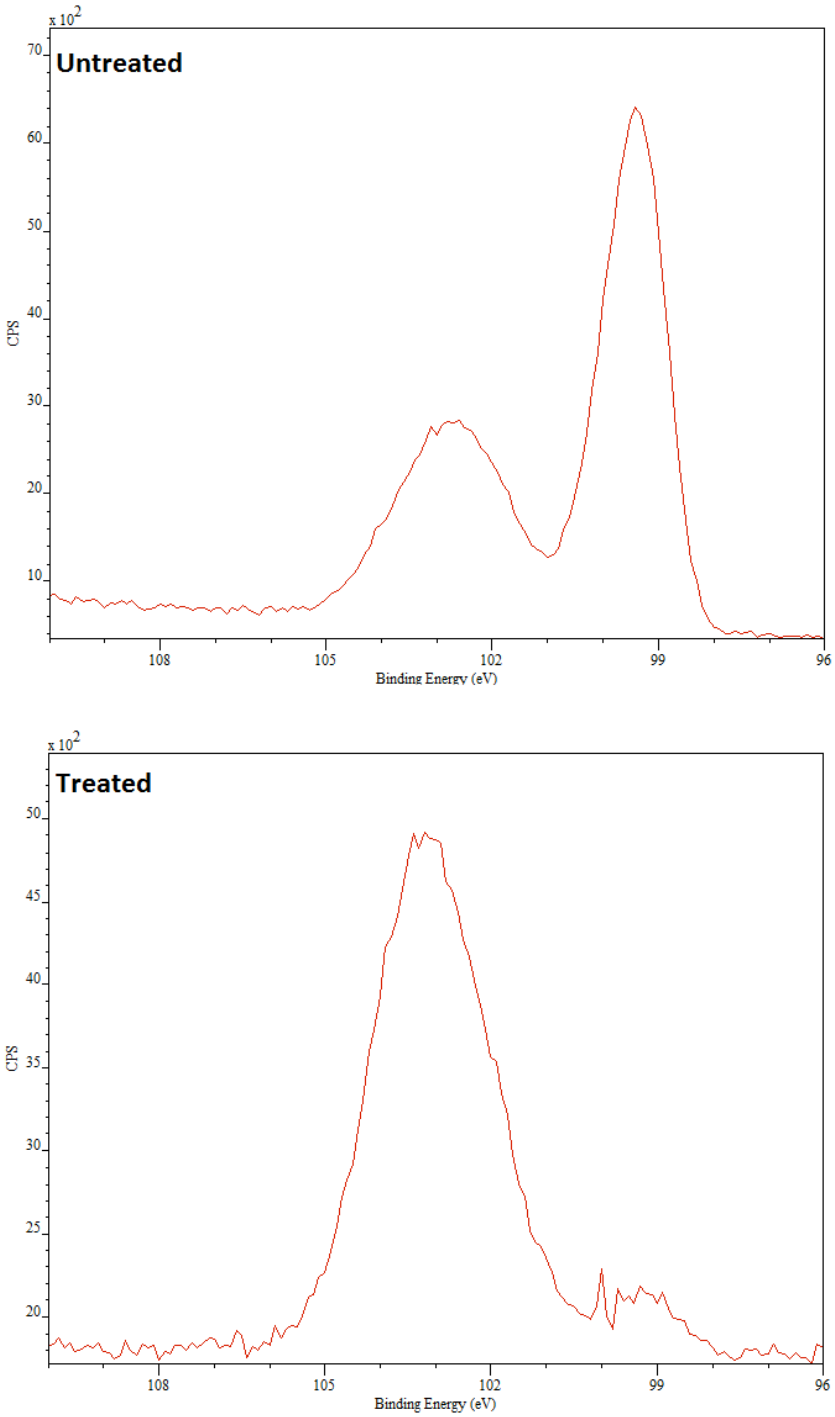

Figure 27 Silicon 2p XPS spectrum of untreated and treated PDMS stationary phase coating on a SS capillary.

There are two established mechanisms for PDMS degradation that have been identified. The first degradation pathway results from thermally initiated intermolecular reactions between terminal silanol groups (Si-OH) and Si-O bonds that are present

within the PDMS polymer. This reaction leads to the production a volatile cyclic trimethylsiloxane compound, along with other larger methylsiloxane oligomers [48-50]. These cyclic trimethylsiloxanes and methylsiloxane oligomers often manifest in GC experiments as an increase in the baseline signal as a function of column temperature that is referred to as column bleed [51].

The second PDMS degradation pathway occurs in situations where PDMS is heated rapidly to high temperature presence of oxygen, which causes homolytic cleavage of Si-CH_3 bonds to form methyl radicals [49,50,52,53]. The product methyl radicals quickly abstract a proton from the PDMS polymer to produce methane as shown in Figure 28.

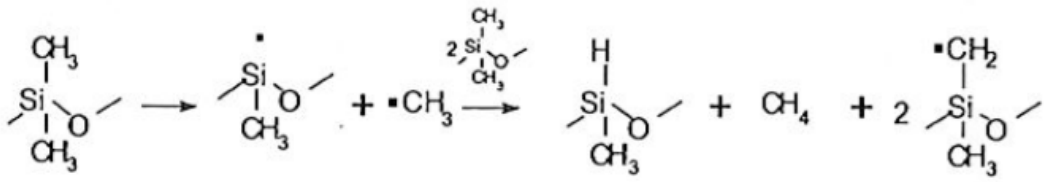

Figure 28 Mechanism for the homolytic formation of methane, Reproduced with permission from Elsevier Science Ltd. (2002) from reference [49].

The Si-H bond formed during this reaction is then cross-linked with Si-OH functionalities present in the PDMS polymer leading to crosslinking and ultimately the formation of SiO_2. The rapid heating rate of capacitive discharge was able to promote the homolytic cleavage reaction pathway as supported by XPS analysis of the treated and untreated PDMS stationary phases. Additionally, periodic heating using repetitive capacitive discharges caused the conversion of the uniform PDMS stationary phase coating to a nanoparticle morphology, as seen in Figure 23. This novel stationary phase modification was investigated for peak focusing applications in GC.

3.3.2 Resistive heating of SS capillaries using capacitive discharge

Resistive heating was selected as the elution strategy for the present focusing device due its proven speed and effectiveness in remobilising solutes from SS capillaries [24,29,42]. This particular technology employs a capacitive discharge power supply similar to that described by Ewels and Sacks [28]. The charging voltage of the system was programmed from 0 to 40 V, which affects the amount of current supplied to the SS capillary, and therefore the temperature obtained following a discharge event. Temperature pulses are useful for providing rapid heating due to the Joule heating effect described by Eq. 8.

$$P = I^2 \times R \quad \text{(Eq. 8)}$$

Where P is the power output, I is the current delivered and R is resistance of the segment through which power is applied. High currents are necessary to ensure the Joule heating effect is strong enough to cause a significant amount of heating. The resistance of a modulator trap was constant at approximately 8 Ω (Ohms), while the current delivered to the modulator was dependent on the charging voltage and capacitance of the capacitors used in the discharge unit. An array of four 22 000 µF capacitors were set up in parallel for the present system, to increase the amount of current delivered to the SS trap during capacitor discharge. The time required to charge a given capacitor is approximately 0.18 s, and the peak current provided by a charged 22 000 µF capacitor is 2.5 A, and this over a period of 100 ms approximately 1.1 A is discharged at an exponentially decaying rate, which yields a power output of 11.5 W J s^{-1}, for a total power of 1.15 J of energy delivered by each capacitor. The specific heat capacity of stainless steel is 0.466 J g^{-1} $°C^{-1}$ [11], therefore given the mass of the SS capillary ~ 12 mg, the combined 4.6 J of energy dissipated by the capacitor array should yield a temperature increase of approximately Δ 820 °C. Over a 100 ms period, an estimated heating rate of 8200 °C s^{-1} should be achieved using this setup. Of course the

actual temperature of the trap during discharge will be lower than this due to thermal losses to the environment, however this provides a useful guide on the efficiency of capacitive discharge heating for solute remobilisation. The rapid, high power delivered by capacitive discharge is essential for ensuring the remobilisation of semi-volatile compounds that are strongly retained by the stationary phase of the focusing device.

A study performed by Harynuk and Górecki reveals the rapid temperature increases that can be obtained using capacitive discharge and SS capillary traps [24]. Three different types of SS capillary were evaluated and the temperature rise achieved at a range of different capacitive discharge voltages were recorded and plotted as shown in Figure 29.

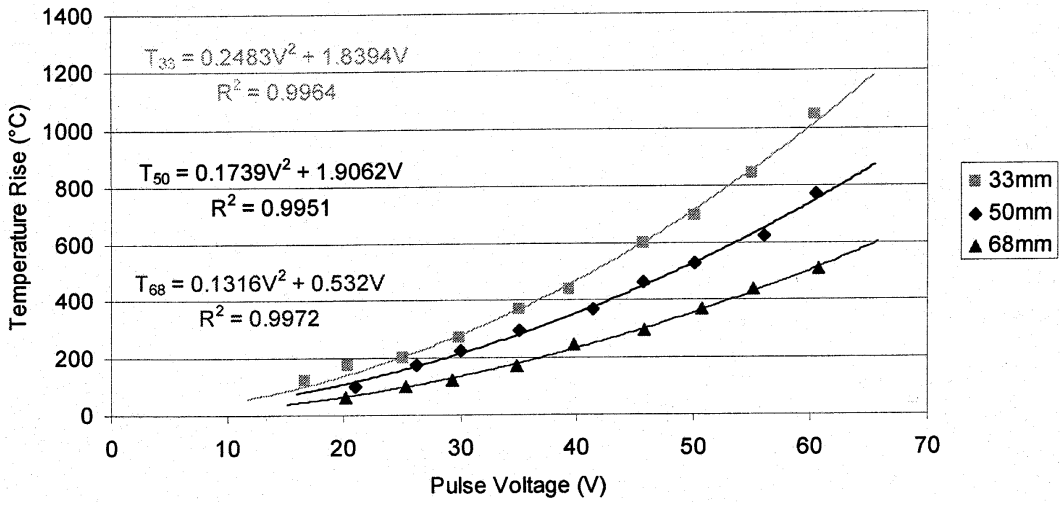

Figure 29 Pulse voltage plotted against peak trap temperature for three different SS capillary lengths. Reproduced with permission from Wiley & Sons, Inc. (2016) from reference [24].

In all three capillary lengths an exponential relationship was observed between pulse voltage and the temperature obtained for the SS capillary. This non-linearity was a result of the resistivity coefficient for SS (4×10^{-3} Ω K^{-1}), which caused the resistance of SS to double in value every ~250 °C [20]. Since the amount of electrical energy converted to thermal energy during capacitive discharge is linked to the resistance of

the SS capillary it makes sense that an exponential relation between discharge voltage and trap temperature was observed. Despite this, the relation between peak temperature and discharge voltage is relatively linear over the 15 to 40 V ranges, which simplifies the use of discharge voltage as a control parameter for temperature.

A study of the effect of discharge voltage on peak trap temperature was reproduced using the present focusing device with a 4 cm long SS capillary length. A small k-type thermocouple was installed with the trap to measure its temperature during capacitive discharge. The effect of charging voltage on the amount of heat generated resistively by the trap was measured (Figure 30), while maintaining the GC oven at an isothermal temperature of 40 °C.

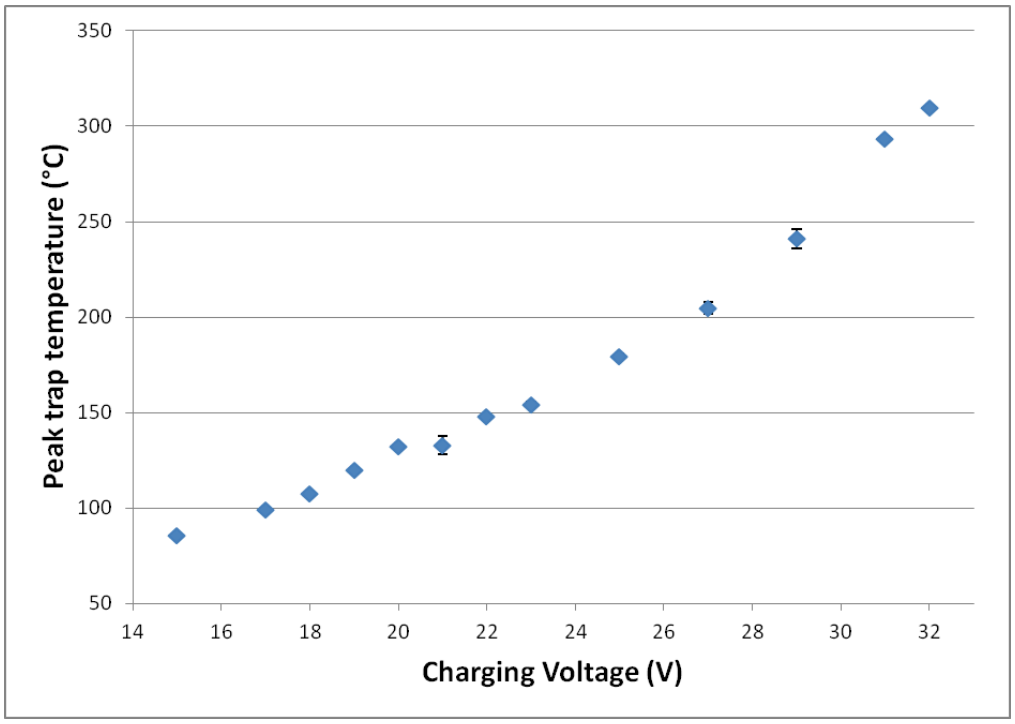

Figure 30 Charging voltage plotted against peak trap temperature for the SS capillary trap at a range of different charging voltages from 15 to 32 V.

A similar exponential relationship between the charging voltage and trap temperature was obtained compared to Figure 29. The correlation between the two variables was near linear between a range of 14 and 25 V. Selection of an appropriate

discharge voltage is crucial to ensuring that semi-volatile compounds are adequately remobilised following a discharge event. For an initial oven temperature of 40 °C, a 30 V discharge voltage yielded a trap temperature of 310 °C, which is sufficient to remobilise volatile and semi-volatile compounds, providing that the compounds are rapidly transferred from the focusing device to the head of the column, before the trap temperature returns to the low temperature state.

Measurement of the temperature profile of the SS capillary during a discharge was plotted in Figure 31 to determine the rate of heating trap heating induced by capacitive discharge as well as determine the rate of cooling following discharge.

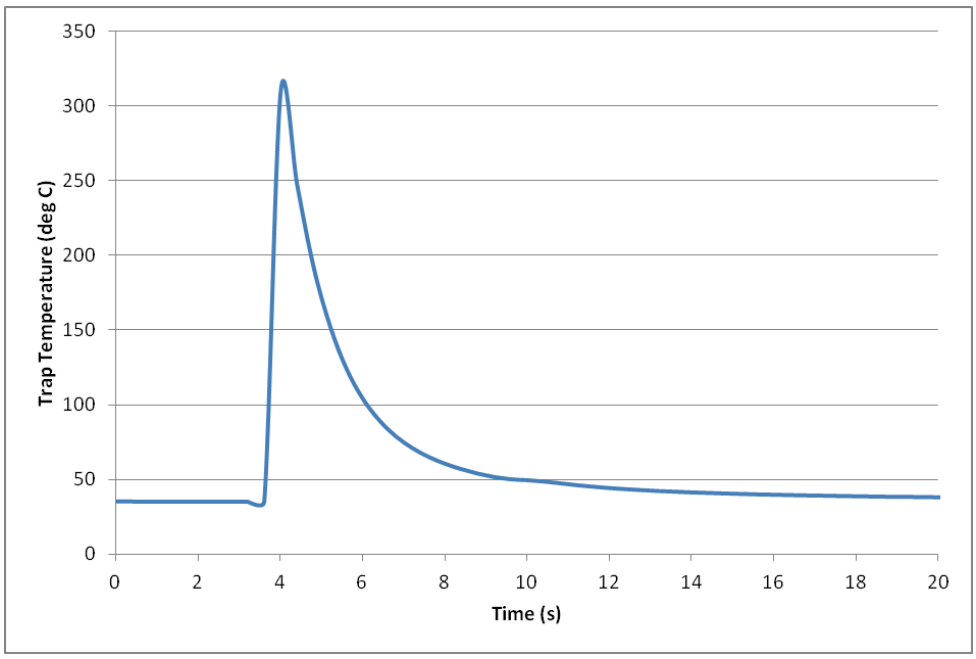

Figure 31 SS trap temperature plotted as a function of time. A charging voltage of 32 V was and GC oven temperature 40 °C was used.

The heating rate of the trap was measured to be approximately 900 °C s^{-1}, which was much slower than the estimated theoretical heating rate calculated previously (>8000 °C s^{-1}). A study carried out by van Es *et al.* calculated a heating rate of 270,000 C s^{-1} for an aluminium clad capillary design using resistive heating [25], while experimental measurements using a low mass thermocouple indicated a heating rate of 4000 °C s^{-1}.

Harynuk and Górecki used a high-speed oscilloscope and low mass thermocouple to measure the heating rate of a segment of SS capillary exposed to capacitive discharge [24]. They determined that the heating rate with capacitive discharge was in excess of 72,000 °C s^{-1}. Unfortunately the data logging speed of the multimeter used in the present experiment was 3 Hz, which limited the resolution of the temperature measurements. Substituting the 5 ms heating duration reported by Harynuk and Górecki into the calculation of the SS capillary heating rate calculation yielded a heating rate of 55,000 °C s^{-1}, compared to just 900 °C s^{-1} measured with the 3 Hz multimeter. This highlights the importance of utilising high speed data logging devices and low mass thermocouples for the study of heating rates, nevertheless the heating rate of the present capillary is very fast, which should be ideal for mobilising focused solutes.

It was also important that the time spent in the hot state is sufficient to elute all of the trapped components to the separation column. This data shows that the trap spends approximately 250 ms at temperatures above 300 °C before returning to oven temperature over a 10 s period. To determine whether 250 ms was enough time to enable solute remobilisation, the dimensions of the trap and flow rate of the carrier gas were considered. Given that the trap is 60 mm long, and SEM shows that the geometry was roughly that of an oblong rectangle with 100 µm height and 400 µm width, its internal volume is approximately 2.4 µL. If a flow rate of 1.0 mL min^{-1} (16.6 µL s^{-1}) of hydrogen was passed through trapping capillary while it was installed in a GC oven held at a temperature of 40 °C, the contents of the trap would be swept 4.2 times over a period of 250 ms at this carrier gas flow rate, which was more than enough time to ensure complete solute transfer.

Figure 31 shows that the focusing device cooled from its hot state (peak temperature 310 °C) at an initial rate of -180 °C s^{-1}, however this rate decreased at an exponential rate as the temperature of the trap approached oven temperature. Cooling from 310 °C to 50° C required approximately 4.5 s, yielding an average cooling rate of 58

°C s^{-1} using the passive cooling provided by the copper heat conduits and ambient air assisted heat dissipation. The addition of cryogenically assisted cooling has been shown to reduce the cooling time to just 1.3 s with similar SS capillaries, however cryogenic cooling was avoided for the present studies to maintain the possibility of portable GC analysis [24]. Rapid cooling times were not essential for the present injection bandwidth minimisation experiments, however cooling speeds do have ramifications for applications where rapid repetitive injections are required, such as in comprehensive two-dimensional GC × GC, as will be explored in Chapter 5.

3.3.3 Evaluation of the focusing device's retention capabilities

The effectiveness of a trap is dependent on its ability to focus a wide range of volatile and semi-volatile compounds for a requisite period of time. The length of time that a solute needs to be retained for depends on the time required to complete an injection. Following this focusing step, it is essential that focused solutes be rapidly remobilised in a narrow injection band to a column for separation. Narrow injection bandwidths and unbiased solute transfer are ideal for maximising chromatographic performance, particularly during fast GC analysis.

Currently, injection focusing is carried out using cryogenic focusing strategies such as those reported by Synovec and co-workers [40,42,54]. While these injection systems are without a doubt highly effective, the use of cryogen is an expensive and inconvenient requirement for injection bandwidth focusing. An ideal focusing device trap would be capable of trapping solutes around ambient temperature without the need for refrigeration units or cryogens. Synovec and co-workers also implement resistive heating for solute remobilisation due to the high-speed heat capabilities offered using this technique [29,40]. The present focusing device is prepared from a piece of SS capillary coated with a novel highly temperature stable stationary phase, that was connected to a cryogen free cooling device, and capacitive discharge power supply for

solute remobilisation. The focusing device is installed in the GC convection oven between the injector and separation column as shown in Figure 32. The focusing device, or trap, was supported within the oven using a pair of insulated copper heat sinks that were installed through the wall of the GC convection oven. Ambient air was used to cool the copper heat sinks, which act as a heat conduit to cool the in-oven focusing device.

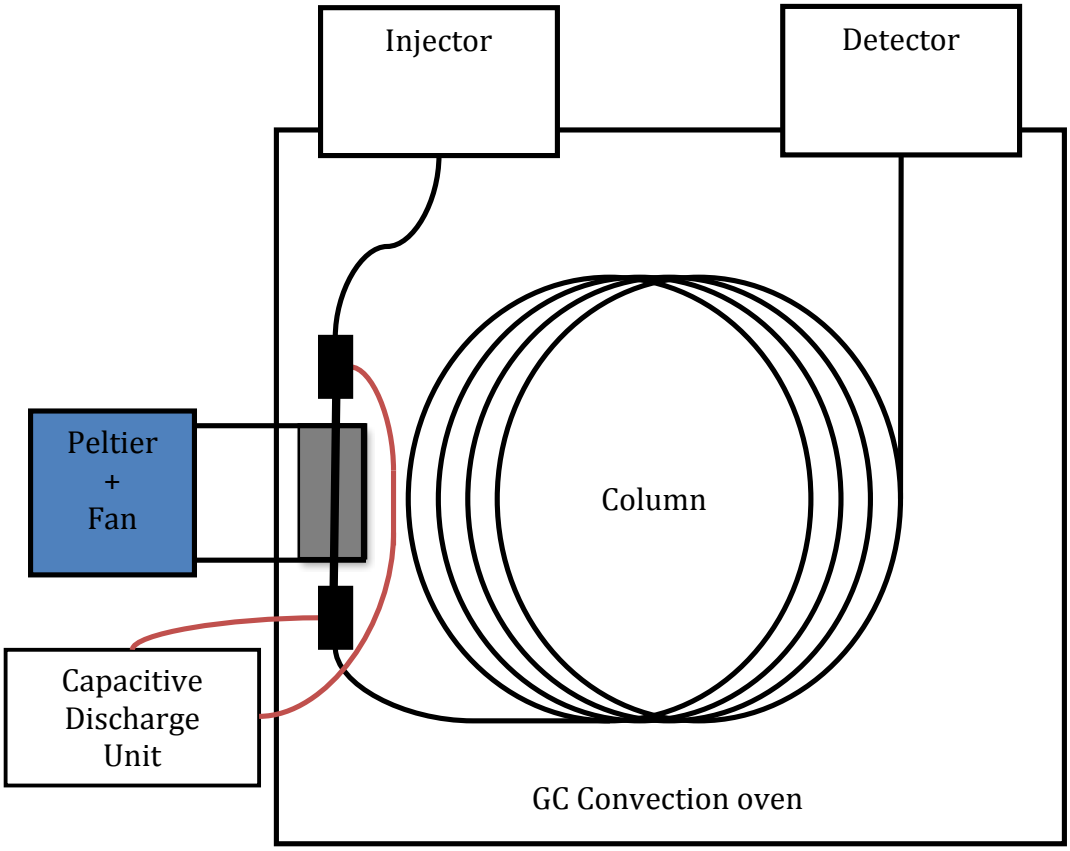

Figure 32 Schematic showing the installation of the focusing device through the wall of the GC convection oven. Two insulated solid copper core wires are used to connect the unions of the trap to an external capacitive discharge unit.

GC analyses commonly start at temperatures between 40 and 100 °C depending on the application, therefore the addition of trap cooling was expected to enhance the retention of volatile compounds. Two strategies were employed for the cooling of the copper heat sinks, air-cooling using a pair of electric fans and active cooling using two thermoelectric wafers. The temperature of the trap within the heat-sinking device was measured using a small thermocouple as described before (Section 3.3.2). For a GC oven

operated at an initial oven temperature of 40 °C ± 0.2 °C, the cooling provided by air cooling the heat sink (ambient air temperature 24 °C ± 1.1 °C) was able to facilitate a reduction in trap temperature to 36.7 °C ± 0.4 °C. This reduction in trap temperature was not expected to provide a substantial increase in solute retention, for this reason active cooling using thermoelectric (Peltier) cooling was tested. Two Peltier thermoelectric wafers (12 V, 3.6 A) facilitated the cooling of the in-oven trap to a temperature of 22.3 °C ± 0.2 °C for a net difference of – 17.7 °C relative to the oven temperature. This reduction in temperature was expected to enhance the retention of solutes compared to ambient air-cooling alone, however the focusing temperature was still high compared to the temperatures obtained with liquid nitrogen (-195.8 °C boiling point) or carbon dioxide (-78.5 °C sublimation temperature) cryogens [11]. Due to the relatively high focusing temperature it was important to evaluate the breakthrough conditions for this focusing device with a range of solutes with different vapour pressures. Additionally the temperature and properties of the focusing device's stationary phase affect the mass loading capacity of the focusing device. In cases where the solute capacity of the trap was exceeded, the remaining solute introduced to the device will pass through the device unfocused.

The ability of the present trap to retain volatile and semi-volatile compounds was tested by the injection of a mixture of *n*-alkanes (*n*-C_8 to C_{20}, each 20 mg L^{-1} in *n*-hexane), which were transferred to the trap using a piece of DFS capillary. The focusing device was cooled to 30 °C, while the oven was maintained at 40 °C, to enhance the trap's retention for low boiling point compounds. A series of experiments were carried out to determine the breakthrough times for a homologous series of *n*-alkanes, using 1, 2, 5 and 10 min duration focusing times, as well as a blank run with no solute focusing. The capacitive discharge power supply was activated at the end of the focusing period to remobilise trapped solutes to a column, while the trap was maintained in a hot state for the blank run.

A chromatogram of the separation obtained after the 10 min focusing time and capacitive discharge event is shown in Figure 33.

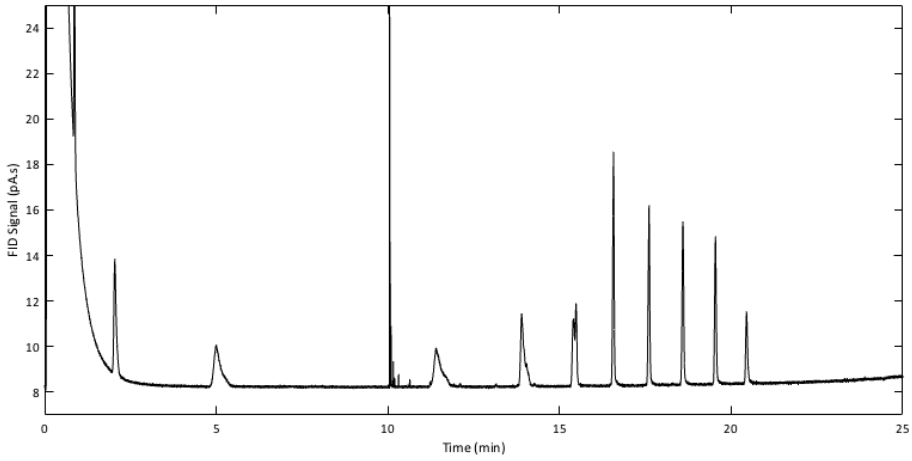

Figure 33 Trap breakthrough experiment with an initial 10 min focusing time, analytes *n*-alkanes 20 mg kg^{-1} each in *n*-hexane (C_8-C_{20}). The tall sharp peak at 10 min indicates the time at which the capacitive discharge power supply was activated.

The sharp peak at 10 min coincides with the capacitive discharge activation, which causes rapid heating of the capillary trap and a gas expansion that propagates through the GC column causing a small, sharp peak due to the increased flux of hydrogen gas to the FID. It was immediately apparent that a number of solutes were not retained for the 10 min focusing period. Solutes eluting *n*-tetradecane (13.9 min) completely broke through the focusing device and were then separated from one and other by the downstream separation column. It was also clear that the solutes *n*-tetradecane, *n*-pentadecane and *n*-hexadecane underwent some peak splitting which was caused by partial solute breakthrough during the focusing stage.

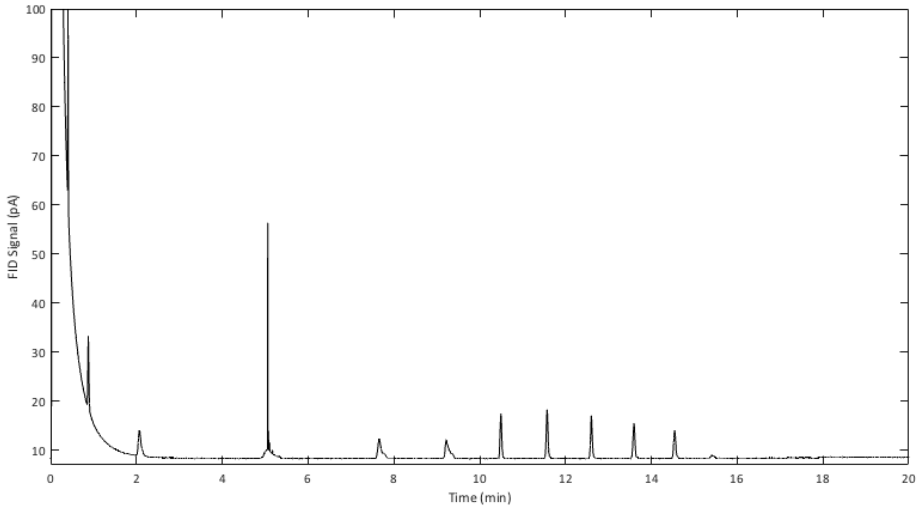

Figure 34 Trap breakthrough experiment with an initial 5 min focusing time, analytes *n*-alkanes 20 mg kg^{-1} each in hexane (C_8-C_{20}). The tall sharp peak at 5 min indicates the time at which the capacitive discharge power supply was activated.

In an effort to reduce the amount of solute breakthrough experienced using this trap with a 10 min focusing duration, the focusing time was progressively reduced to determine the breakthrough times of each *n*-alkane. In Figure 34, a 5 min focusing time was used; again there was evidence for the breakthrough of *n*-dodecane and more volatile *n*-alkanes. The breakthrough time of *n*-dodecane coincided with the 5 min discharge time. It was also worth noting that the peak area intensity of the solutes *n*-nonadecane and *n*-eicosane were diminished in this experiment compared to the previous experiment, which suggested that these solutes were not being properly focused and mobilised after the 5 min period. Peak splitting was eliminated for the solute *n*-pentadecane and reduced for *n*-tetradecane somewhat.

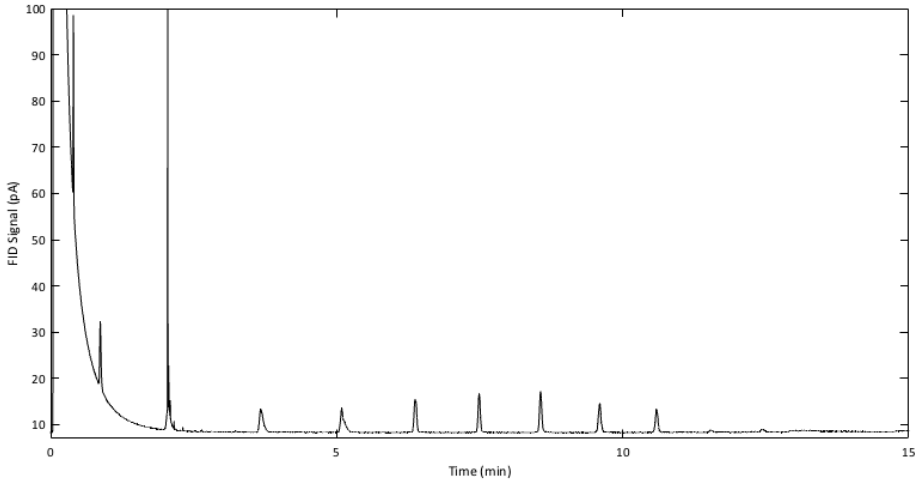

Figure 35 Trap breakthrough experiment with an initial 2 min focusing time, analytes *n*-alkanes 20 mg kg^{-1} each in hexane (C_8-C_{20}). The tall sharp peak at 2 min indicates the time at which the capacitive discharge power supply was activated.

Further reducing the focusing time to 2 min (Figure 35) eliminated the peak splitting seen for *n*-pentadecane and *n*-tetradecane, however the peak shapes for the solutes *n*-dodecane and *n*-tridecane are tailing and suggest that some solute breakthrough has occurred during the focusing time. The peak at 2.04 min was *n*-undecane, which coincided with the actuation of the discharge unit. Similar to the previous experiment, the peak intensity of the *n*-octadecane *n*-nonadecane and *n*-eicosane peaks was diminished supporting the deduction that incomplete focusing was occurring during the shorter focusing period.

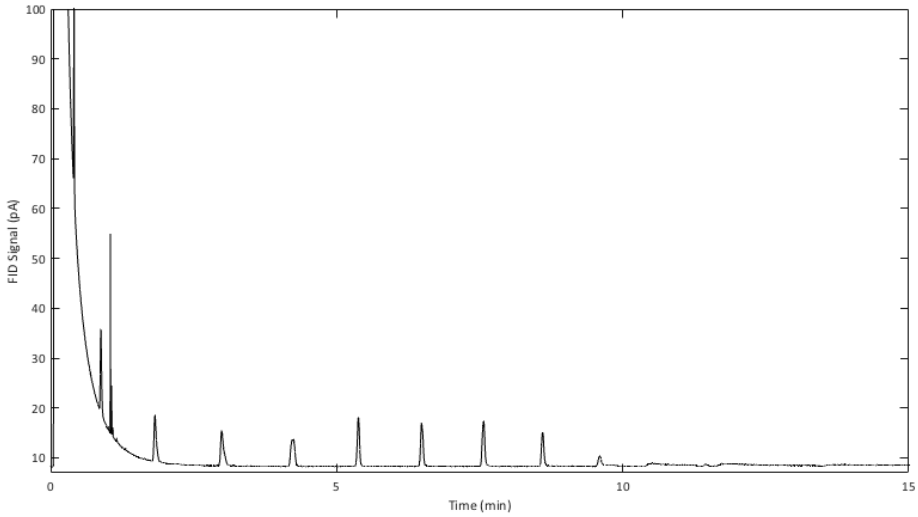

Figure 36 Trap breakthrough experiment with an initial 1 min focusing time, analytes *n*-alkanes 20 mg kg^{-1} each in hexane (C_8-C_{20}). The tall sharp peak at 1 min indicates the time at which the capacitive discharge power supply was activated.

Finally a 1 min focusing time was tested (Figure 36), and the peak shapes of the solutes *n*-undecane, *n*-dodecane were tailing, while *n*-tridecane was split, showing that even for the short period of 1 min, these solutes were not being adequately retained by the trap. Furthermore the 1 min focusing time led to an even greater reduction in peak intensity for the peaks *n*-heptadecane, *n*-octadecane, *n*-nonadecane and *n*-eicosane. This reduction in peak intensity was caused by the piece of DFS capillary (55 cm, 75 µm ID) that was used to connect the S/SL injector to the thermal focusing device. Since the initial oven temperature was 40 °C these high molecular weight solutes condensed within the capillary segment during the injection process. Heating the transfer line between the injector and the focusing device would prevent condensation of solutes before the focusing device, however this was not necessary for evaluating *n*-alkane retention using the present focusing device.

To calculate the breakthrough times of these solutes, the elution times of each *n*-alkane were then subtracted from the elution times of these solutes without the focusing device inline as shown in Figure 37.

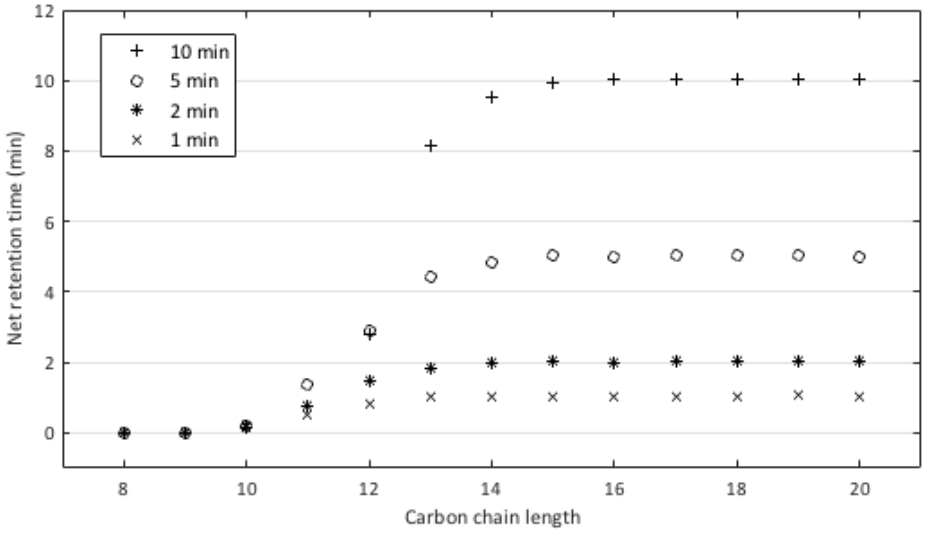

Figure 37 The effect of carbon chain length on the net elution times for a homologous series of *n*-alkanes after subtracting the retention times each solute without focusing. Four focusing times were tested, 10, 5, 2 and 1 min.

Any solutes that were not adequately retained by the trap during the focusing period (1, 2, 5 or 10 min) deviated from their expected net elution times (0 min). Based on Figure 37, it is clear that long focusing periods were detrimental towards the focusing of volatile solutes while using the present focusing device. The 5 and 10 min focusing times revealed solute breakthroughs for solutes more volatile than *n*-pentadecane as confirmed by Figure 33 and Figure 34. Shorter 1 and 2 minute focusing times reduced the incidence of solute breakthrough from solutes as volatile as *n*-tridecane, however this focusing performance was not ideal for trapping the volatile compounds that are often present in GC samples.

Finally the peak widths achieved using the focusing device were compared to the peak widths obtained without the focusing device in-line. Figure 38 was generated by subtracting the peak widths obtained without focusing from the peak widths with focusing and plotting this value for each *n*-alkane tested.

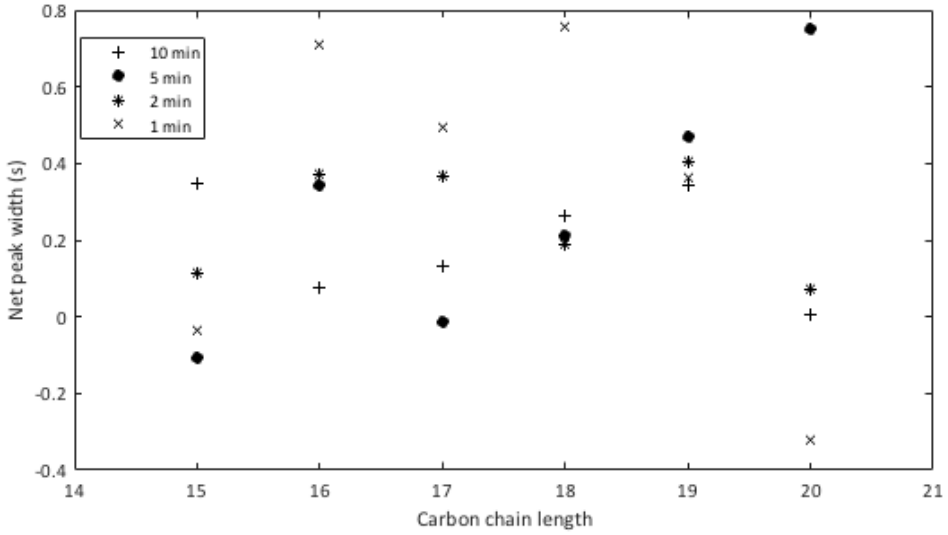

Figure 38 Net differences in peak widths for *n*-pentadecane, *n*-hexadecane, *n*-heptadecane, *n*-octadecane, *n*-nonadecane and *n*-eicosane, after subtracting the corresponding peaks widths for each compound without focusing. Four different peak focusing times were evaluated, 10, 5, 2 and 1 min.

Figure 38 revealed that peaks were broadened rather than focused with the trapping device, since the peak widths increased relative to an unfocused experiment. This figure was constructed using higher molecular weight compounds with volatilities equal or less than *n*-pentadecane, since there was evidence for peak splitting and breakthrough for the other more volatile compounds. Each of the compounds was broadened by an average of 210 ms ± 100 ms, relative to a separation without any focusing device. This broadening suggests that all of the present solutes broke through the focusing device and underwent peak broadening in the downstream column. The strong retention of each of these solutes at 40 °C in the downstream column prevented peak splitting from occurring. For this reason this focusing device was not pursued further for injection bandwidth focusing, given the greater flexibility and effectiveness of other existing technologies [25,32,40].

3.4 Conclusions

The chemistry and morphology of a novel stationary phase was evaluated after a high temperature pulsing treatment in the presence of purified air. This thermal-oxidative treatment caused significant changes to the physical structure of the stationary phase, leading to the formation of nanoparticle structures that were embedded on the internal walls of the PDMS coated capillary. The chemistry of the stationary phase was substantially modified from the initial PDMS polymer following the treatment procedure, in particular the PDMS polymer became highly oxidised and carbon deficient compared to the initial PDMS state.

The capillaries and stationary phase prepared were tested for applications in injection bandwidth minimisation, however the present stationary phase displayed limited retention for solutes less volatile that *n*-dodecane, severely limiting is effectiveness for this application. Previous research with cryogenic focusing has demonstrated narrow injection bandwidths on the order of 2.5 ms for *n*-hexane, using resistive heating of aluminium-clad capillaries for remobilisation confirming that the present single-stage thermal modulator is not appropriate for this application. [25]. The high temperature of the present focusing device (22.3 °C) relative to cryogenic alternatives such as liquid nitrogen lead to it having breakthrough times that were much too short for injection bandwidth focusing. Low temperatures, such as those provided by cryogen, are necessary to enable the trapping volatile and semi-volatile compounds for durations long enough to complete a S/SL injection. Another alternative would be to increase the capacity of the trap's stationary phase for solutes by increasing its length or reducing its' temperature using a better cooling device, however this option was not explored at this time. Instead the focusing device was employed as a modulator for comprehensive GC × GC analysis as described in Chapter 5.

3.5 References

[1] K. Grob, Injection techniques in capillary GC, Anal. Chem. 66 (1994) 1009A-1019A.

[2] E. Hoh, K. Mastovska, Large volume injection techniques in capillary gas chromatography, J. Chromatogr. A 1186 (2008) 2-15.

[3] R.L. Martin, J.C. Winters, Determination of Hydrocarbons in Crude Oil by Capillary-Column Gas Chromatography, Analyst 35 (1963) 1930-1933.

[4] M. Beroza, Trapping and transfering small amounts of volatile gas-chromatographic fractions, J. Gas Chromatogr. 2 (1964) 330-331.

[5] D.R. Rushneck, Cryogenic injection and chromatographic separation of cigaret smoke, J. Gas Chromatogr. 3 (1965) 318-319.

[6] D.E. Willis, R.M. Engelbrecht, Gas-chromatographic analysis of C1 to C10 hydrocarbons by open tubular columns with on-column injection, J. Gas Chromatogr. 5 (1967) 536-538.

[7] E.E. Bartel, S.J. Van der Walt, Reduction of plug length in capillary gas chromatography using an on-column micro-trap, J. Gas Chromatogr. 6 (1968) 396-398.

[8] D.E. Willis, Trapping technique for open tubular chromatographic columns, Anal. Chem. 40 (1968) 1597-1600.

[9] C.A. Cramers, M.M. Van Kessel, Direct sample introduction system for capillary columns, J. Gas Chromatogr. 6 (1968) 577-581.

[10] H.U. Buser, R. Soder, H.M. Widmer, Influence of a sophisticated cold trap on the shape of capillary chromatography peaks, HRC CC, J. High Resolut. Chromatogr. Chromatogr. Commun. 5 (1982) 156-157.

[11] W.M. Haynes, CRC handbook of chemistry and physics : a ready-reference book of chemical and physical data, Boca Raton, Florida CRC Press, 2014, 95th edition., 2014.

[12] R.E. Kaiser, Enriching volatile compounds by a temperature gradient tube, Anal. Chem. 45 (1973) 965-967.

[13] G. Schomburg, H. Husmann, F. Weeke, Aspects of double-column gas chromatography with glass capillaries involving intermediate trapping, J. Chromatogr. 112 (1975) 205-217.

[14] K.E. Murray, Concentration of headspace, airborne and aqueous volatiles on Chromosorb 105 for examination by gas chromatography and gas chromatography-mass spectrometry, J. Chromatogr. 135 (1977) 49-60.

[15] J.A. Rijks, J. Drozd, J. Novak, Versatile all-glass splitless sample-introduction system for trace analysis by capillary gas chromatography, J. Chromatogr. 186 (1979) 167-181.

[16] D. Kalman, R. Dills, C. Perera, F. DeWalle, On-column cryogenic trapping of sorbed organics for determination by capillary gas chromatography, Anal. Chem. 52 (1980) 1993-1994.

[17] C.A. Cramers, E.A. Vermeer, Direct sample introduction of high boiling compounds onto glass capillary columns. Comparison of manual and automatic sampling, Chromatographia 8 (1975) 479-481.

[18] J.R. Valentin, G.C. Carle, J.B. Phillips, A nonmechanical chemical concentration modulator for multiplex gas chromatography, HRC CC, J. High Resolut. Chromatogr. Chromatogr. Commun. 5 (1982) 269-271.

[19] J.R. Valentin, G.C. Carle, J.B. Phillips, Determination of methane in ambient air by multiplex gas chromatography, Anal. Chem. 57 (1985) 1035-1039.

[20] H.-J. de Geus, J. de Boer, U.A.T. Brinkman, Development of a thermal desorption modulator for gas chromatography, J. Chromatogr. A 767 (1997) 137-151.

[21] D.R. Worton, N.M. Kreisberg, G. Isaacman, A.P. Teng, C. McNeish, T. Górecki, S.V. Hering, A.H. Goldstein, Thermal desorption comprehensive two-dimensional gas chromatography: An improved instrument for in-situ speciated measurements of organic aerosols, Aerosol Sci. Technol. 46 (2012) 380-393.

[22] O. Panic, T. Górecki, C. McNeish, A.H. Goldstein, B.J. Williams, D.R. Worton, S.V. Hering, N.M. Kreisberg, Development of a new consumable-free thermal modulator for comprehensive two-dimensional gas chromatography, J. Chromatogr. A 1218 (2011) 3070-3079.

[23] A.H. Goldstein, D.R. Worton, B.J. Williams, S.V. Hering, N.M. Kreisberg, O. Panic, T. Górecki, Thermal desorption comprehensive two-dimensional gas chromatography for in-situ measurements of organic aerosols, J. Chromatogr. A 1186 (2008) 340-347.

[24] J. Harynuk, T. Górecki, Design considerations for a GC × GC system, J. Sep. Sci. 25 (2002) 304-310.

[25] A. Van Es, J. Janssen, C. Cramers, J. Rijks, Sample enrichment in high speed narrow bore capillary gas chromatography, HRC CC, J. High Resolut. Chromatogr. Chromatogr. Commun. 11 (1988) 852-857.

[26] C.L. Rankin, R.D. Sacks, Sample vapor introduction techniques for use with cryofocusing GC inlet systems, J. Chromatogr. Sci. 32 (1994) 7-13.

[27] A.J. Borgerding, C.W. Wilkerson, Cryogenically Cooled Microloop System for Sampling and Injection in Fast GC, Anal. Chem. 68 (1996) 701-707.

[28] B.A. Ewels, R.D. Sacks, Electrically-heated cold trap inlet system for high-speed gas chromatography, Anal. Chem. 57 (1985) 2774-2779.

[29] L.A. Lanning, R.D. Sacks, R.F. Mouradian, S.P. Levine, J.A. Foulke, Electrically heated cold trap inlet system for computer-controlled high-speed gas chromatography, Anal. Chem. 60 (1988) 1994-1996.

[30] H. Smith, R.D. Sacks, Column selectivity programming and fast temperature programming for high-speed GC analysis of purgeable organic compounds, Anal. Chem. 70 (1998) 4960-4966.

[31] P.J. Marriott, R.M. Kinghorn, Studies on cryogenic trapping of solutes during chromatographic elution in capillary gas chromatography, J. High Resolut. Chromatogr. 19 (1996) 403-408.

[32] P.J. Marriott, R.M. Kinghorn, Longitudinally Modulated Cryogenic System. A Generally Applicable Approach to Solute Trapping and Mobilization in Gas Chromatography, Anal. Chem. 69 (1997) 2582-2588.

[33] E.B. Ledford, Jr., C. Billesbach, Jet-cooled thermal modulator for comprehensive multidimensional gas chromatography, J. High Resolut. Chromatogr. 23 (2000) 202-204.

[34] A.L. Lee, A.C. Lewis, K.D. Bartle, J.B. McQuaid, P.J. Marriott, A comparison of modulating interface technologies in comprehensive two-dimensional gas chromatography (GC × GC), J. Microcolumn Sep. 12 (2000) 187-193.

[35] J.B. Phillips, D. Luu, J.B. Pawliszyn, G.C. Carle, Multiplex gas chromatography by thermal modulation of a fused silica capillary column, Anal. Chem. 57 (1985) 2779-2787.

[36] Z. Liu, J.B. Phillips, Sample introduction into a 5-μm i.d. capillary gas chromatography column using an on-column thermal desorption modulator, J. Microcolumn Sep. 1 (1989) 159-162.

[37] Z. Liu, J.B. Phillips, High-speed gas chromatography using an on-column thermal desorption modulator, J. Microcolumn Sep. 1 (1989) 249-256.

[38] Z. Liu, J.B. Phillips, Large-volume sample introduction into narrow-bore gas chromatography columns using thermal desorption modulation and signal averaging, J. Microcolumn Sep. 2 (1990) 33-40.

[39] A.M. Muscalu, M. Edwards, T. Górecki, E.J. Reiner, Evaluation of a single-stage consumable-free modulator for comprehensive two-dimensional gas chromatography: Analysis of polychlorinated biphenyls, organochlorine pesticides and chlorobenzenes, J. Chromatogr. A 1391 (2015) 93-101.

[40] R.B. Wilson, B.D. Fitz, B.C. Mannion, T. Lai, R.K. Olund, J.C. Hoggard, R.E. Synovec, High-speed cryo-focusing injection for gas chromatography: reduction of injection band broadening with concentration enrichment, Talanta 97 (2012) 9-15.

[41] B.D. Fitz, R.B. Wilson, B.A. Parsons, J.C. Hoggard, R.E. Synovec, Fast, high peak capacity separations in comprehensive two-dimensional gas chromatography with time-of-flight mass spectrometry, J. Chromatogr. A 1266 (2012) 116-123.

[42] B.D. Fitz, B.C. Mannion, K. To, T. Hoac, R.E. Synovec, Evaluation of injection methods for fast, high peak capacity separations with low thermal mass gas chromatography, J. Chromatogr. A 1392 (2015) 82-90.

[43] R.F. Mouradian, S.P. Levine, R.D. Sacks, Evaluation of a nitrogen-cooled, electrically heated cold trap inlet for high-speed gas chromatography, J. Chromatogr. Sci. 28 (1990) 643-648.

[44] A. Peters, M. Klemp, L. Puig, C. Rankin, R. Sacks, Instrumentation and strategies for high-speed gas chromatography, Analyst 116 (1991) 1313-1320.

[45] M. Klemp, R. Sacks, Sample decomposition in an electrically heated cold-trap inlet system for high-speed gas chromatography, J. High Resolut. Chromatogr. 14 (1991) 235-240.

[46] T. Górecki, M. Edwards, Material comprising thermally modified polymeric organosilicon, method for preparing said material and the uses thereof, Provisional US Patent 62/170,480 Filled June 3 (2015).

[47] C.Y.K. Lung, M. Heinonen, E. Kukk, J.P. Matinlinna, Surface modification of titanium with thermally treated polydimethylsiloxane coating and the effect on resin to titanium adhesion, Surf. Interface Anal. 47 (2015) 105-112.

[48] G. Camino, S.M. Lomakin, M. Lazzari, Polydimethylsiloxane thermal degradation Part 1. Kinetic aspects, Polymer 42 (2001) 2395-2402.

[49] G. Camino, S.M. Lomakin, M. Lageard, Thermal polydimethylsiloxane degradation. Part 2. The degradation mechanisms, Polymer 43 (2002) 2011-2015.

[50] K. Chenoweth, S. Cheung, A.C.T. van Duin, W.A. Goddard, III, E.M. Kober, Simulations on the Thermal Decomposition of a Poly(dimethylsiloxane) Polymer Using the ReaxFF Reactive Force Field, J. Am. Chem. Soc. 127 (2005) 7192-7202.

[51] S. Seethapathy, T. Górecki, Applications of polydimethylsiloxane in analytical chemistry: A review, Anal. Chim. Acta 750 (2012) 48-62.

[52] W.F. Manders, J.M. Bellama, Multiphoton infrared laser-induced degradation of polydimethylsiloxane and hexamethyldisiloxane, J. Polym. Sci., Polym. Chem. Ed. 23 (1985) 351-357.

[53] J.M. Bellama, W.F. Manders, On the thermal decomposition of poly(dimethylsiloxanes), Sci. Total Environ. 73 (1988) 87-93.

[54] R.B. Wilson, J.C. Hoggard, R.E. Synovec, High throughput analysis of atmospheric volatile organic compounds by thermal injection - isothermal gas chromatography - time-of-flight mass spectrometry, Talanta 103 (2013) 95-102.

Chapter 4: PMDs for heart cut MDGC analysis of trace aromatic compounds (adapted from Jacobs et al. [1])

Summary

PMDs coupled with modern electronic pressure control have allowed gas chromatography (GC) practitioners to easily manipulate chromatographic systems to achieve heart cut and back-flushing configurations. These PMDs have enhanced the connectivity between different components of GC instrumentation and have improved the inertness and minimised system dead volumes compared to classical chromatographic unions and valves. In the present contribution the setup and configuration of two multidimensional GC (MDGC) platforms is described for achieving the separation and quantification of trace level target C_6-C_8 alkylbenzenes in styrene monomer and Isoparaffin solvents, using flame ionisation detection (FID). The performance of these MDGC platforms indicated excellent retention time (0.2 % relative standard deviation, RSD) and peak area repeatability (1% RSD) for all analytes of interest. The limit of detection (LOD) was 0.8 mg kg^{-1} for benzene in styrene monomer, and 2.4 to 2.8 mg kg^{-1} for C_6-C_8 alkylbenzenes such as benzene, toluene, ethylbenzene and xylene in Isoparaffin solvent.

4.1 Introduction

While the separation power of one-dimensional gas chromatography is very formidable, many samples are so complex that peak co-elutions are not only frequent, but also expected [2]. There are three main strategies that can be used to reduce the incidence of peak co-elutions during chromatographic analysis; sample preparation techniques, selective detection strategies and MD analysis. Sample preparation techniques aim to simplify and selectively enrich target compounds in complex samples, prior to separation [3,4]. While sample preparation steps are very useful, these procedures are labour intensive and costly to implement. Selective detection such as mass spectrometers or chemically selective detectors can reduce the requirement from complete chromatographic separation however such detectors are relatively costly to implement. Alternatively, multidimensional (MD) analysis can be used to allow the analyst to use a series of separation steps to increase the amount of chromatographic separation prior to detection. The introduction of Deans' switching enabled robust implementation of heart cutting for GC analysis [5,6]. MDGC with Deans' switch heart-cutting has been utilised by many researchers and has since been the topic of a number of reviews highlighting its essential nature in modern MDGC research [7-9].

Heart cutting and back-flushing are important approaches to GC that are achieved by manipulating the net direction of carrier gas flow at the confluence of two or more capillary columns. Contemporary back-flushing and heart cutting approaches build on the work Deans described 50 years ago [5,10]. These once seemingly complicated approaches are readily accessible today using precise electronic pressure control (EPC) [11] and advanced capillary column connectivity using PMDs [12-18]. PMDs feature low connection void volumes that enhance carrier gas flow and pressure equilibration response times compared to classical setups. The thermal mass of each device is kept low to reduce the potential for thermal hysteresis during temperature programming,

and these devices are chemically deactivated to ensure inert surface chemistry, which prevents chemical activity during GC analysis.

PMDs are particularly useful when coupled with modern electronic pressure control, which is able to rapidly achieve and maintain accurate and precise pressure settings. Instrument control software can determine the pressures required to deliver user defined carrier gas flow rates after compartment temperatures, column dimensions, and connectivity between injector modules, microfluidic devices, and detector modules has been entered. Electronic pressure control and event control have enabled fast and simple implementation of column back-flushing, heart cutting or comprehensive two-dimensional GC configurations, minimising the need for laborious iterative system optimisation [17,19].

Multidimensional GC (MDGC) is increasingly required to address the complexity of samples to permit accurate compound identification and quantification. By utilising the stationary phase selectivity of two columns it is possible to reduce the probability of false-positive or false-negative results arising from peak co-elutions which enhances the confidence in solute identification based on retention time [7,20]. The present investigation uses planar microfluidic Deans' switching to achieve MDGC for the separation and quantification of trace levels of benzene in styrene monomer, and C_6-C_8 alkylbenzenes in Isoparaffin solvent. It is important to monitor styrene and Isoparaffin solvent for alkylbenzene content to ensure that these compounds are not incorporated into final products, since these compounds have health and hygiene implications that affects the quality of household, industrial, and automotive products [21-23].

Styrene monomer is an important industrial chemical that is used for the production of synthetic rubber. Styrene is synthesised industrially from benzene, and residual benzene can be found in crude styrene, intermediate process products, or as an undesirable impurity in purified styrene. Analysis of benzene in styrene is normally

performed using long, polar stationary phases, such polyethylene glycol (PEG), as specified by ASTM Method D5135-14 [24]. However these methods are not ideal for process monitoring and trace level quantification due to the high probability of false positive measurements arising from incomplete separation, and poor long-term method stability. The upper temperature limit (250 °C) for PEG phases limits the ability to elute high molecular weight compounds that are present in styrene and petroleum derived samples.

Isoparaffin solvents are light petroleum products that are derived from petroleum feedstock. They are industrially useful due to their high chemical stabilities, well-defined boiling points, low surface tensions, low freezing points and low electrical conductivities. They are used extensively in industrial applications during fuel refinery, process chemistry and are further used as cleaning agents, functional fluids, and fuels. The analysis of benzene and C_6-C_8 alkylbenzenes in Isoparaffin solvent is complicated by numerous peak co-elutions that are typical of one-dimensional separations. For this reason GC coupled with mass spectrometry (GC-MS) operated in the selective ion monitoring mode (SIM) is often utilised for the analysis of benzene and the alkylbenzenes [25]. GC-MS with SIM alleviates the need for complete temporal separation before detection, and reduces the possibility of false positive results. Unfortunately GC-MS systems have a high cost of ownership, which precludes them from being implemented universally; therefore other methods should be explored to complement GC-MS for routine analysis. An alternative MDGC method for the analysis of aromatic compounds in finished gasoline using FID is the ASTM D5580 method which uses a polar 1,2,3-tris (cyanoethoxy)propane (TCEP) column to selectivity trap aromatic compounds, which are then eluted to a polydimethylsiloxane (PDMS) column for additional separation. While this method is effective for the separation of a range of aromatic compounds, the temperature stability of the TCEP phase is limited (145 °C)

and prone to contamination by high molecular weight compounds making this method not ideal for routine analysis.

MDGC with a combination of non-polar PDMS columns and highly polar PEG or ionic sorbent PLOT columns can be effective at separating benzene and C_6-C_8 alkylbenzenes in styrene monomer and petroleum derived samples which lessens the need for expensive MS detection [26-29]. This approach enabled the quantitation of trace levels of C_6-C_8 alkylbenzenes compounds in styrene monomer and Isoparaffin solvent while using low cost flame ionisation detection. The approach is fast and robust, with potential for deployment in field quality control laboratories where time, space and resources are limited.

4.2 Materials and Methods:

4.2.1 Measurement of benzene in styrene monomer

An Agilent 7890A gas chromatograph (Agilent Technologies) equipped with a S/SL inlet, Agilent 7683B series Automated Liquid Sampler, two FID modules, and an auxiliary EPC was used for benzene analysis in styrene monomer. A VF-1ms column (30 m × 250 µm ID × 1 µm d_f, Agilent, #CP8913) was connected between the S/SL inlet and the central port of a Deans' switch PMD (Agilent, #G2855A). A VF-WAXms column (30 m × 250 µm ID × 1 µm d_f, Agilent, #CP9206) was connected between the Deans' switch and FID A, while a piece of DFS capillary (80 cm × 100 µm ID) (Agilent, #160-2635-5) was used as a transfer line and flow restrictor between the Deans' switch and FID B. The inlet was set to a temperature of 250 °C, and operated with a split ratio of 10:1. An ultra inert liner (Agilent, #5190-2295) and Moulded Thermogreen LB-2 septum (Supelco, Bellefonte, PA, USA) were incorporated into the inlet and the sample injection volume was 1 µL for all samples.

The carrier gas was helium (Air Liquide, Edmonton, Canada) and the first-dimension column was operated at a flow rate of 1.6 mL min^{-1} with an initial head pressure of 34.55 PSI for 8 min, after which the ^{1}D column was back-flushed at -2 mL min^{-1} for 7 min. The ^{2}D column was operated at a constant flow of 3 mL min^{-1} with an initial pressure of 25.91 PSI for 8 min, after which the flow rate was increased to 5 mL min^{-1} for 7 min during the back-flush cycle. The oven was temperature programmed from an initial temperature of 40 °C, which was held for 1 min, and then ramped at 15 °C min^{-1} to 250 °C. The total analysis time was 15 min. A three-way switching valve (Agilent, #G2399-60600) was used to change the direction of auxiliary carrier gas within the Deans' switch to facilitate redirection of first-dimension column effluent to either the transfer line or the second-dimension column. The valve was actuated between 6.3 and 6.6 min to transfer benzene and any interfering compounds to the second-dimension column.

FID A and B were each held at a temperature of 250 °C and operated at a data sampling rate of 20 Hz. Data were collected and processed with ChemStation software version B.04.03SP1.

A pure stock of benzene (Sigma Aldrich) was obtained and used for preparing standards *via* the standard additions technique. Different levels of benzene were spiked into pure styrene monomer (Fisher Scientific) to achieve final benzene concentrations ranging from 1 to 500 mg kg^{-1} benzene in styrene monomer. Crude, intermediate and purified styrene monomer samples were obtained from commercial vendors and injected into the GC system without dilution or modification to determine the levels of benzene present in these products.

4.2.2 Measurement of C_6-C_8 alkylbenzenes in Isoparaffin solvents

An Agilent 6890 GC (Agilent) equipped with a S/SL inlet, Agilent 7683B series Automated Liquid Sampler, two FID modules and an auxiliary EPC was used for analysis of C_6-C_8 alkylbenzenes in Isoparaffin solvents. A CP-Sil8 CB Low Bleed/MS column (30 m × 250 µm ID × 1 µm d_f, Agilent, #CP5862) was used as the ^{1}D separation column, which was connected between the inlet and a Deans' switch PMD (Agilent, PN# G2855A). A CP-Lowox column (9 m × 530 µm ID × 10 µm d_f, Agilent, #CP8587) was connected between the Deans' switch and FID A, while a piece of DFS capillary (63 cm × 250 µm ID, Agilent, #160-2255-5) was used as a transfer line between the Deans' switch and FID B. A three-way switching valve (Agilent, #G2399-60600) was installed in-line with the EPC and Deans' switch enabling redirection of first-dimension column effluent to either the transfer line or the ^{2}D column. The inlet was maintained at a temperature of 250 °C, a split ratio of 20:1 was used, with a 1 µL injection volume for all samples. The inlet was equipped with an Ultra Inert Liner (Agilent, #5190-2295) and a Moulded Thermogreen LB-2 septum (Supelco).

The carrier gas was helium (Air Liquide), which was held at a flow rate of 2 mL min^{-1}. The EPC was operated in the constant pressure mode at 4.6 PSI for flow switching. The oven was temperature programmed from an initial temperature of 60 °C, which was held for 0.2 min, and then ramped at 15 °C min^{-1} to 165 °C, and then ramped at a rate of 30 °C min^{-1} to 260 °C with a final hold time of 5 min. The total analysis time was 15 min. Four retention time windows were transferred from the first-dimension column to the second-dimension column by activating the three-way switching valve: benzene 2.90 to 3.05 min, toluene 3.95 min to 4.10 min, ethylbenzene/*m*-xylene/*p*-xylene 5.04 min to 5.24 min, *o*-xylene 5.44 min to 5.54 min. FID A and B were each held at a temperature of 250 °C and operated at a data sampling rate of 20 Hz. Data was collected and processed with ChemStation software.

Benzene, *p*-xylene, *o*-xylene and ethylbenzene were obtained from Sigma-Aldrich (Oakville, Canada). Toluene, cyclohexane, hexane, and methanol, were obtained from Fisher Scientific (Edmonton, Canada). A stock standard containing equal concentrations (1000 mg kg^{-1} each) of benzene, toluene, ethylbenzene, *m*/*p*-xylene and *o*-xylene was used for the preparation of a series standards with concentrations ranging from 1 to 200 mg kg^{-1} per component. These standard solutions and dilutions used cyclohexane (Sigma Aldrich, #65045) as the solvent. Two Isoparaffin solvents, Shell 2025 and Exxon Isopar E and were obtained from local commercial sources, and analysed without dilution or further modification.

4.3 Results and Discussion

4.3.1 Deans switch installation and GC configuration

Installing a PMD Deans' switch into a GC instrument is fast and straightforward. The Deans' switch is mounted inside the oven cavity and connected to a three-way solenoid valve and PCM mounted outside the GC oven. The first-dimension column is connected between a GC inlet and the central port of the Deans' switch, as shown in Figure 39. Columns are installed using metallic ferrules and nuts to ensure leak free and inert connections. Metallic ferrules ensure that ferrule particulates are not dislodged into the narrow device channels. A second-dimension column is connected between the top port of the Deans' switch and FID. Finally a third piece of DFS capillary, known as a flow restrictor, is connected to the bottom Deans' switch port and a second detector. The flow restrictor serves to balance the carrier gas flows between the restrictor and the second-dimension column. A short length of capillary, with a narrow internal diameter is used as the flow restrictor to minimise the dead volume between the Deans' switch and the second detector module.

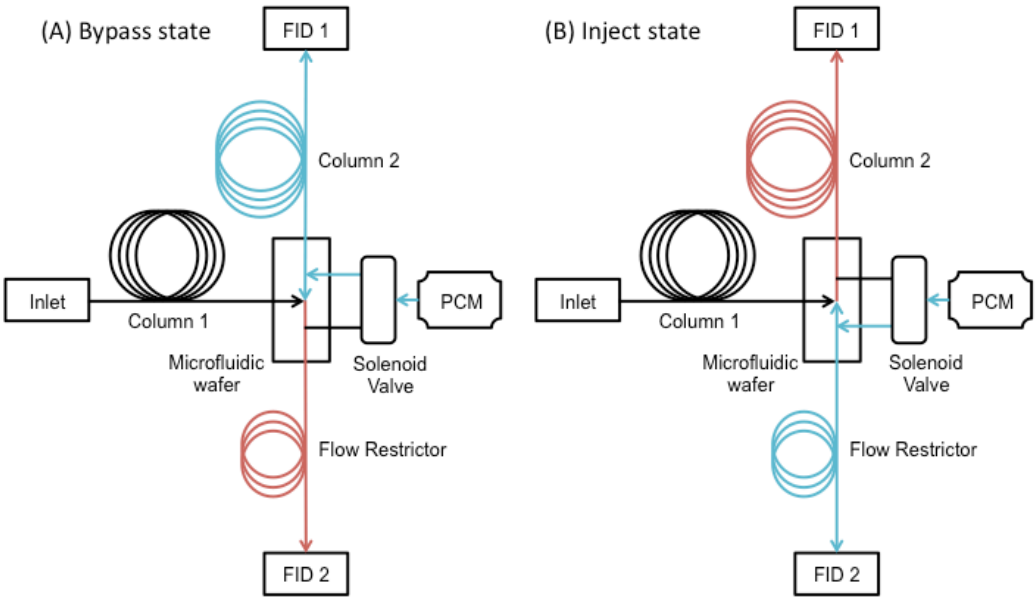

Figure 39 Pneumatic diagram of the MDGC system showing column connectivity and (A) "Bypass" and (B) "inject" states of the Deans' switch. Flow in the microfluidic Deans' switch is mechanically controlled *via* an electrically activated three-way switching valve connected in-line with the PCM.

The length and internal diameter of the flow restrictor can be calculated with freely available method calculator software [30,31]. To ensure that stable flow switching is achieved during heart cutting, the second-dimension column should be operated a flow rate higher than the first-dimension to prevent effluent splitting between the restrictor and second-dimension. Instrument control software provides an interface for mapping the layout of the instrument's connectivity including the inlet and detector modules, auxiliary PCMs, microfluidic wafers, and columns. The software then analyses the layout and programs the GC inlet and auxiliary PCM to provide precise carrier gas flows through the GC system, by considering the capillary dimensions, compartment temperatures and the outlet pressures of each segment of the system.

In the case of the analysis of benzene in styrene as described in Section 4.2.1, two system states are possible depending on whether a three-way switching valve is off (bypass) or on (inject). In the bypass state (Figure 39A) the three-way switching valve is off. Column 1 is operated at a constant flow rate of 1.6 mL min^{-1}, which is supplied by the GC inlet. To provide this carrier gas flow rate the software must consider the outlet pressure of Column 1, which corresponds to the pressure applied by the PCM. Meanwhile Column 2 is operated at a constant flow rate of 3.0 mL min^{-1}, with 1.6 mL min^{-1} provided by the inlet and an additional 1.4 mL min^{-1} provided by the PCM. Injection of effluent from Column 1 to Column 2 is achieved by activation of the inject state by energising the three-way switching valve (Figure 39B). After the desired peak has been transferred from the Column 1 to Column 2, the switching valve is deactivated, thereby reverting to the bypass state. To initiate the back-flush, the inlet pressure is reduced so that the pressure applied by the PCM is higher than the inlet pressure to reverse the direction of flow in Column 1 to - 2.0 mL min^{-1} while maintaining a constant flow of 3.0 mL min^{-1} in Column 2. This allows high molecular weight compounds to be vented through the split vent of the injector rather than transported to a detector.

4.3.2 Benzene analysis in styrene monomer sample

While the separation of styrene monomer from benzene is simple to achieve using one-dimensional GC, the separation of benzene from minor impurities present in commercial styrene is significantly more complicated. Styrene monomer has more than 100 potential trace impurities depending on the precursors used in its synthesis, and the procedure used [32]. Common contaminants include organic solvents such as diethyl ether, methanol, acetone, ethanol, chloroform; saturated and unsaturated hydrocarbons, alkyl benzenes, chlorinated benzenes, phthalates, and other aromatic compounds [32].

Due to the large number of potential compounds in styrene, a non-polar PDMS coated stationary phase was used as the first-dimension column to provide an initial boiling point based pre-separation. PDMS phases are both highly inert and temperature stable, which maximises method stability and column lifespan during repeated thermal cycles and sample injections. A one-dimensional separation of crude styrene is provided in Figure 40 (A), which shows a saturated styrene monomer peak as well as a large number of other peaks including benzene at 6.45 min.

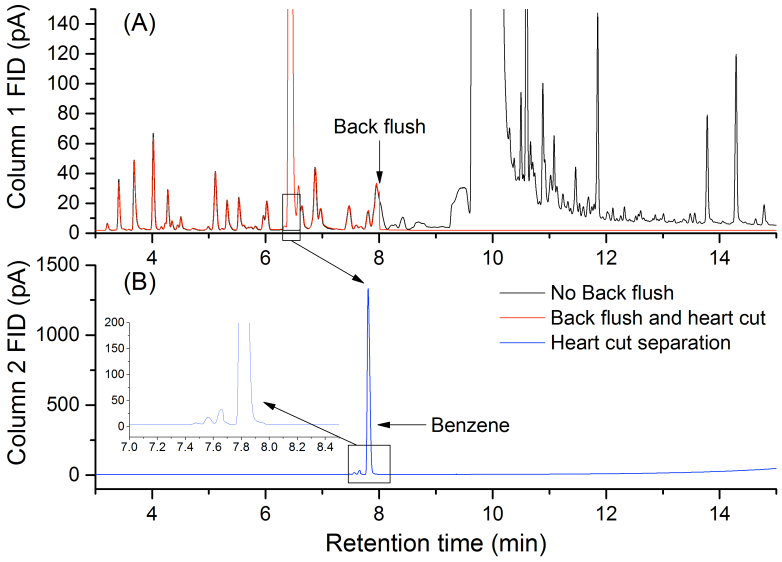

Figure 40 Separation of crude industrial styrene sample showing: (A) the one-dimensional separation on Column 1 (Vf-1ms, 30 m, 250 µm ID, 1.0 µm d_f) with and without back-flush initiation at 8 min. The heart cut window (6.3 to 6.6 min) is indicated by a box in panel (A). Panel (B) shows the heart cut separation on Column 2 (Vf-WAXms, 30 m, 250 µm ID, 1.0 µm d_f) showing the peak corresponding to benzene, and a zoomed view of the separation (7.79 min).

An 18 s heart-cut window at 6.3 to 6.6 min was sufficient for total transfer of benzene from Column 1 to Column 2, as shown in Figure 40 (B). Initially a 50% phenyl/50% dimethylpolysiloxane based column (Vf-17 ms) was tested as the second-dimension column, since it was expected to have favourable selectivity for benzene. This

column proved not to have sufficient selectivity to separate benzene from the aliphatic hydrocarbon interferences present in styrene monomer. A more polar PEG coated column (VF-WAXms) was tested and proved successful at resolving the benzene peak from the interfering aliphatic hydrocarbons present at 7.79 min, as shown in Figure 40 (B). After the elution of benzene, a back-flush cycle was initiated to eliminate styrene monomer and other high molecular weight compounds from Column 1. Back-flushing reduces sample carryover between injections and further prevents styrene from contaminating and degrading the PEG column after repeated sample injections. Back-flushing also reduces carbon formation in the detector jet by preventing high concentrations of styrene from being eluted into either FID, which increases long term method robustness. A conservative back-flush time of 7 min was selected to ensure that 5 column volumes of carrier gas passed through Column 1 *via* the split vent, while increasing the oven temperature to 250 °C to elute all remaining solutes.

Benzene was spiked into pure styrene monomer at concentrations between 0 and 500 mg kg^{-1} to prepare a nine-point calibration. Calibration linearity was tested using an F-test (F_{exp} = 1.77) and found to be linear over the calibration range used (F_{crit} = 2.89). The LOD was calculated based on IUPAC recommendations and the procedure outlined by Olivieri [33]. This method of LOD calculation, better controls for both false positive and false negative results compared to classical signal to noise based (3:1 signal to noise) LOD calculations. Specifically LODs calculated using the IUPAC recommendations are statistically more rugged than the 3:1 signal to noise. The LOD for benzene in styrene was 0.8 mg kg^{-1} and the limit of quantification (LOQ) was 2.4 mg kg^{-1}, which is sufficient for assuring the elimination of benzene from styrene monomer samples. This LOD and LOQ are sufficient for achieving current specification targets needed to ensure that styrene monomer is of sufficient quality for applications such as in food packaging [34,35]. Benzene was quantified in three commercial samples of crude (334.7 ± 0.2 mg kg^{-1}, α = 0.05) intermediate purity (165.0 ± 0.2 mg kg^{-1}, α = 0.05) and final purified

styrene (below LOD). A large amount of benzene was found in both the crude and the intermediate purity styrene samples, though the intermediate purity contained 50% less benzene. Most importantly, there was no detectable benzene in the final commercial styrene product, indicating that the purification steps were successful in removing the high levels of benzene that were present in the crude and intermediate styrene samples. The present approach improves on ASTM D5135-14 by substantially lowering the LOQ of the method to 2.4 mg kg^{-1}, which is substantially better than the 10 mg kg^{-1} limit outlined in the former method, especially considering the robust means of LOQ calculation used [24]. This approach minimises the opportunity for false positive measurements of benzene, and could be adapted to target additional polar compounds of interest as required.

4.3.3 Benzene and C_6-C_8 alkylbenzene analysis in Isoparaffin solvent

When a sample has a wide range of boiling points, such as in petroleum derived samples, the PEG phase used in the previous application can limit the upper temperature range required for the elution of all sample components, since PEG phases thermally degrade above 250 °C. There are two alternative column types with higher thermal stability that have sufficient polarity to separate benzene and C_6-C_8 alkylbenzenes from aliphatic hydrocarbon interferences: ionic liquid based columns, and ionic sorbent PLOT columns [36-38]. Ionic liquid phases have demonstrated equal or higher polarity and better thermal stability as compared to PEG based phases; however the column efficiencies, long-term phase stability and elevated chemical activity towards some compounds, is not ideal [38]. PLOT columns coated with ionic sorbent phases, such as the CP-Lowox, have been indicated as some of the most polar and retentive column phases available [39]. The CP-Lowox also displays high thermal stability (max 350 °C) and low chemical activity making it ideal for trace analysis of thermally labile polar compounds [39]. The CP-Lowox phase was developed for the

separation of oxygenated compounds, and has demonstrated exceptionally high polarity compared to existing stationary phases [16,17,40,41]. Further research utilising this column for the analysis of volatile organic compounds has revealed the potential of this column's unique ionic sorbent phase for benzene and alkylbenzene separations [37,42].

In the case of Isoparaffin solvents, the quantitation of benzene and C_6-C_8 alkylbenzenes, including toluene, ethylbenzene and the xylene isomers is important due to their health and hygiene impacts on industrial workers and products produced using these solvents. Similar to the previous approach (Section 4.3.2), a non-polar first-dimension column was employed to separate compounds based on their boiling point. A wide-bore CP-Lowox column with a thick stationary phase coating (10 m long, 530 µm ID, 10 µm d_f) was selected for the second-dimension to maximise the sample loading capabilities, since PLOT columns typically cannot accommodate high solute concentrations [43,44]. While the CP-Lowox could be used as the first-dimension column, similar to the use of TCEP column in the ASTM D5580 method, its limited sample loading capability would necessitate the use of high split ratios at the expense of analytical sensitivity. It is therefore preferable to use the CP-Lowox column as a second-dimension column, since this minimises the amount of solute loaded onto the column phase. Heart cutting target solutes to the CP-Lowox phase minimises the transfer of high molecular weight compounds that could irreversibly adhere to the PLOT phase, which reduces column efficiency and retention time stability. Finally by placing the PLOT column after the Deans' switch the possibility of particle shedding into the narrow channels within the Deans' switch was removed.

A one-dimensional separation of a Shell 2025 Isoparaffin sample overlaid with an injection of benzene, toluene, ethylbenzene and xylene isomer standard is shown in Figure 41 (A), revealing that the sample has numerous co-eluting peaks in the chromatogram. The heart-cut retention times were determined by measuring the retention time of each compound on the first-dimension column with the Deans' switch

operating in the bypass state (Figure 39A) for the duration of the experiment. A separation of Shell 2025 Isoparaffin spiked with 50 mg kg^{-1} of benzene, ethylbenzene, toluene and xylene isomers is shown in Figure 41 (B), with four heart cutting windows activated to separate benzene and the target C_6-C_8 alkylbenzene compounds from background aliphatic hydrocarbon interferences.

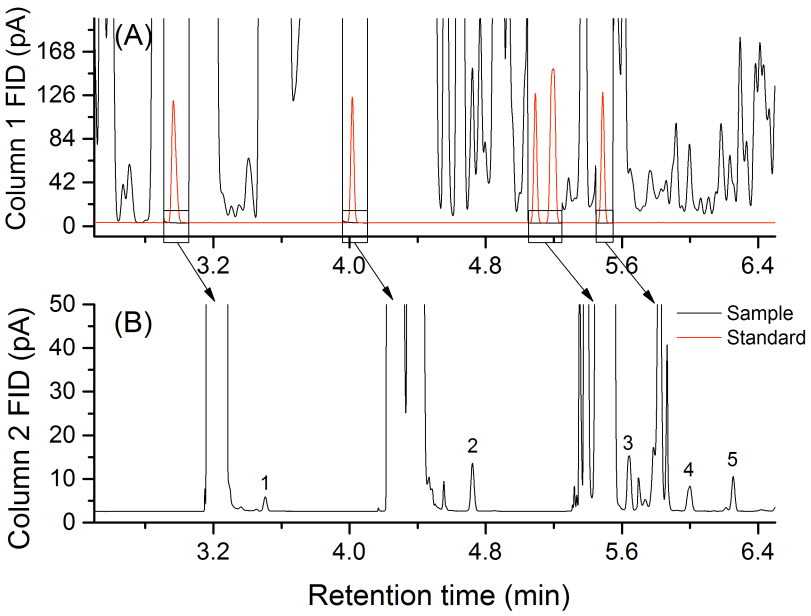

Figure 41 One-dimensional separation of an Isoparaffin solvent showing: (A) the separation on Column 1 with the four heart cutting windows activated at their respective times as indicated by black boxes. A separation of a standard containing benzene, toluene, ethylbenzene, *m/p*-xylene and *o*-xylene (200 mg kg^{-1} each) is overlaid in red over inset (A) showing where each solute would have eluted were it not for the heart cut windows. Inset (B) shows the separation of each heart cut window on Column 2 with labeled peaks for (1) benzene 3.56 min, (2) toluene 4.80 min, (3) ethylbenzene 5.86 min, (4) *m/p*-xylene 6.11 min, (5) *o*-xylene 6.37 min, all resolved from interfering compounds.

Back-flushing was explored for this approach as well, however due to the wide internal diameter (530 µm) of the second-dimension column, excessive second-

dimension carrier gas flows were required to allow a timely back-flush to be implemented, which caused instability in the FID's operation. Installation of a restrictor capillary after the second-dimension column would alleviate this problem and enable the addition of a back-flush cycle to this approach, but this requires additional column connectivity, which was deemed undesirable for the present application.

The retention time and peak area repeatability was assessed by replicate analysis (n = 10) of a benzene, toluene, ethylbenzene and *m/p/o*-xylene standard (5.0 mg kg^{-1}). In both cases the repeatability was better than 1 % RSD indicating acceptable experimental precision (Table 9). External calibration with linear regression analysis was used to quantitate the amounts of benzene and C_6-C_8 alkylbenzenes present in Isoparaffin solvent. A nine-point calibration including an un-spiked solvent injection as prepared, and the linearity of each calibration was tested using an F-test as described previously [33]. Table 9 summarises the F_{exp} values calculated, and all calibrations were found to be linear over the calibration range used (F_{crit} = 2.89).

Table 9 Calibration details for targeted aromatic compounds including: retention time RSD (n = 10), peak area RSD (n = 10), F-test values for calibration linearity, LOD and LOQ.

Analyte	Retention time RSD (%)	Peak area RSD (%)	$F_{experimental}$	LOD (mg kg^{-1})	LOQ (mg kg^{-1})
benzene	9.9×10^{-3}	0.8	5.4×10^{-4}	2.7	9.0
toluene	1.1×10^{-2}	0.4	4.4×10^{-4}	2.4	7.9
ethylbenzene	6.3×10^{-3}	0.5	5.5×10^{-4}	2.7	9.0
p-xylene	7.4×10^{-3}	0.3	5.6×10^{-4}	2.8	9.0
o-xylene	7.1×10^{-3}	0.2	6.0×10^{-4}	2.8	9.4

Similarly, the LODs and LOQs for each compound are tabulated in Table 9, with LOD values between 2.4 and 2.8 mg kg^{-1} and LOQs between 7.9 and 9.4 mg kg^{-1}. Some Isoparaffin solvent manufacturers specify that the total aromatic content (as measured

by UV spectrophotometry) is less than 10 mg kg^{-1} [45]. The present approach enables the monitoring of benzene and the C_6-C_8 alkylbenzene compounds, which indicate that an Isoparaffin solvent is likely unsuitable for industrial use, while the former UV spectrophotometry method yields more general information on the aromatic content of Isoparaffin solvent.

This approach improves on other published methods by achieving robust low detection limits to ensure Isoparaffin solvents are not contaminated with benzene and C_6-C_8 alkylbenzenes, without the need for expensive MS detection. The ASTM D5580 method is not well suited to low level quantitation since it is specified for concentrations of 100 mg kg^{-1} or greater of each respective component [27]. Analysis of two Isoparaffin solvents, Shell 2025 and Exxon Isopar™ E, revealed the presence of low levels of toluene, ethylbenzene and xylene isomers in the Exxon Isopar™ E Isoparaffin solvent, indicating that this solvent had undesirable levels of alkylbenzenes for industrial applications warranting further investigation (Table 10).

Table 10 Concentrations (mg kg^{-1}) and confidence intervals (mg kg^{-1}, n = 3, α = 0.05) of target aromatic compounds in four Isoparaffin samples, including two Isoparaffin solvents that have been used for process chemistry, and Isopar™ E Isoparaffin solvent.

Sample	Sample 1	Sample 2	Isopar™ E Isoparaffin solvent
benzene	< LOD		
toluene	2.7 ± 0.2	15.6 ± 0.2	8.1 ± 0.2
ethylbenzene	< LOD		9.8 ± 0.3
m/p-xylene	2.8 ± 0.3	8.1 ± 0.3	8.6 ± 0.3
o-xylene	n.d.	14.5 ± 0.3	3.1 ± 0.3

No benzene or C_6-C_8 alkylbenzenes were detected in the Shell 2025 sample, with all measurements below the LOD values specified within Table 9. Additionally, two Isoparaffin solvents that were used for industrial process chemistry were analysed to

determine whether they had become contaminated with benzene or C_6-C_8 alkylbenzenes during their use. In both samples low levels of toluene and xylene were found, indicating that they need to be purified prior to further use in industrial processes, or discarded in favour of new Isoparaffin solvent.

4.4 Conclusions

PMDs coupled with modern EPC and instrument control software were utilised for low cost, rapid, robust and, repeatable MDGC analysis of trace amounts of benzene in styrene monomer and C_6-C_8 alkylbenzenes in Isoparaffin solvent. MDGC separations utilising non-polar first-dimension columns coupled with polar second-dimension columns were demonstrated to be very effective for the separation of benzene in styrene monomer and benzene and C_6-C_8 alkylbenzenes in Isoparaffin solvent. A LOQ of 2.4 mg kg^{-1} for benzene in styrene monomer and 7.9 to 9.4 mg kg^{-1} for individual C_6-C_8 alkylbenzenes in Isoparaffin solvents was achieved using FID detection. This made the present approaches ideal for trace analysis without the need for MS based detection. The present MDGC method could also be adapted to target different polar analytes by adjusting the heart cut window appropriately, however this was not explored for the present applications. Both approaches are fast, with a total analysis time of only 15 min, enabling significant sample throughput that would be useful for monitoring of industrial process chemistry and product quality.

4.5 References

[1] M.R. Jacobs, R. Gras, P.N. Nesterenko, J. Luong, R.A. Shellie, Back-flushing and heart cut capillary gas chromatography using planar microfluidic Deans' switching for the separation of benzene and alkylbenzenes in industrial samples, Journal of Chromatography A 1421 (2015) 123-128.

[2] J.M. Davis, J.C. Giddings, Statistical theory of component overlap in multicomponent chromatograms, Anal. Chem. 55 (1983) 418-424.

[3] J. Pawliszyn, H.L. Lord, Handbook of sample preparation, Hoboken, N.J. : Wiley, c2010., 2010.

[4] S. Moldoveanu, V. David, Modern Sample Preparation for Chromatography, Burlington : Elsevier Science, 2014., 2014.

[5] D.R. Deans, A new technique for heart cutting in gas chromatography, Chromatographia 1 (1968) 18-22.

[6] G. Schomburg, H. Husmann, F. Weeke, Aspects of double-column gas chromatography with glass capillaries involving intermediate trapping, J. Chromatogr. 112 (1975) 205-217.

[7] P.Q. Tranchida, D. Sciarrone, P. Dugo, L. Mondello, Heart-cutting multidimensional gas chromatography: A review of recent evolution, applications, and future prospects, Anal. Chim. Acta 716 (2012) 66-75.

[8] W. Bertsch, Two-dimensional gas chromatography. Concepts, instrumentation, and applications - part 1: fundamentals, conventional two-dimensional gas chromatography, selected applications, J. High Resolut. Chromatogr. 22 (1999) 647-665.

[9] G. Schomburg, Two-dimensional gas chromatography: principles, instrumentation, methods, J. Chromatogr. A 703 (1995) 309-325.

[10] D.R. Deans, Improved technique for back-flushing gas chromatographic columns, J. Chromatogr. 18 (1965) 477-481.

[11] S.S. Stafford, P. Sandra, T.A. Berger, M.Q. Thompson, K.J. Klein, F. David, L.C. Doherty, J.V. Wisniewski, D.W. Snyder, P.A. Larson, Electronic Pressure Control in Gas Chromatography, Hewlett-Packard Company, Wilmington, DE, 1993.

[12] G. Schomburg, F. Weeke, F. Mueller, M. Oreans, Multidimensional gas chromatography (MDC) in capillary columns using double oven instruments and a newly designed coupling piece for monitoring detection after preseparation, Chromatographia 16 (1982) 87-91.

[13] J.V. Seeley, N.J. Primeau, S.V. Bandurski, S.K. Seeley, J.D. McCurry, Microfluidic Deans Switch for Comprehensive Two-Dimensional Gas Chromatography, Anal. Chem. 79 (2007) 1840-1847.

[14] B. Quimby, J. McCurry, W. Norman, Capillary Flow Technique for Gas Chromatography: Reinvigorating a Mature Analytical Discipline, LC-GC The Peak (2007) 7-10.

[15] J. Luong, R. Gras, G. Yang, L. Sieben, H. Cortes, Capillary flow technology with multi-dimensional gas chromatography for trace analysis of oxygenated compounds in complex hydrocarbon matrices, J. Chromatogr. Sci. 45 (2007) 664-670.

[16] J. Luong, R. Gras, H. Cortes, R.A. Shellie, Multi-dimensional gas chromatography with a planar microfluidic device for the characterization of volatile oxygenated organic compounds, J. Chromatogr. A 1255 (2012) 216-220.

[17] J. Luong, R. Gras, R.A. Shellie, H.J. Cortes, Applications of planar microfluidic devices and gas chromatography for complex problem solving, J. Sep. Sci. 36 (2013) 182-191.

[18] R.A. Shellie, H.J. Cortes, R. Gras, J. Luong, Planar microfluidic devices in flow modulated comprehensive two dimensional gas chromatography for challenging petrochemical applications, Anal. Methods 5 (2013) 6598-6604.

[19] K. Sasamoto, N. Ochiai, Selectable one-dimensional or two-dimensional gas chromatography-mass spectrometry with simultaneous olfactometry or element-specific detection, J. Chromatogr. A 1217 (2010) 2903-2910.

[20] C. Bicchi, A. Binello, A. D'Amato, P. Rubiolo, Reliability of Van den Dool Retention Indices in the Analysis of Essential Oils, J. Chromatogr. Sci. 37 (1999) 288-294.

[21] D. Sciarrone, P.Q. Tranchida, C. Ragonese, L. Schipilliti, L. Mondello, Multidimensional GC coupled to MS for the simultaneous determination of oxygenate compounds and BTEX in gasoline, J. Sep. Sci. 33 (2010) 594-599.

[22] J. Huff, Benzene-induced Cancers: Abridged History and Occupational Health Impact, International Journal of Occupational and Environmental Health 13 (2007) 213-221.

[23] F.F. Liu, B.I. Escher, S. Were, L. Duffy, J.C. Ng, Mixture Effects of Benzene, Toluene, Ethylbenzene, and Xylenes (BTEX) on Lung Carcinoma Cells via a Hanging Drop Air Exposure System, Chem. Res. Toxicol. 27 (2014) 952-959.

[24] ASTM D5135-14 Standard Test Method for Analysis of Styrene by Capillary Gas Chromatography, West Conshohocken, PA, USA (2014).

[25] ASTM D5769-10 Standard Test Method for Determination of Benzene, Toluene, and Total Aromatics in Finished Gasolines by Gas Chromatography/Mass Spectrometry, West Conshohocken, PA, USA (2010).

[26] N.S. Chary, A.R. Fernandez-Alba, Determination of volatile organic compounds in drinking and environmental waters, Trends Anal. Chem. 32 (2012) 60-75.

[27] ASTM 5580-13 Test Method for Determination of Benzene, Toluene, Ethylbenzene, p/m-Xylene, o-Xylene, C9 and Heavier Aromatics, and Total Aromatics in Finished Gasoline by Gas Chromatography, West Conshohocken, PA, USA (2013).

[28] K. Shiomi, M. Shimono, H. Arimoto, S. Takahashi, High resolution capillary gas chromatographic hydrocarbon-type analysis of naphtha and gasoline, J. High Resolut. Chromatogr. 14 (1991) 729-737.

[29] R.E. Pauls, G.J. Weight, P.S. Munowitz, A comparison of methods to determine benzene in gasoline boiling range material, J. Chromatogr. Sci. 30 (1992) 32-39.

[30] Restek Corporation, EZGC Method Translator and Flow Calculator (2014) Accessed on: [1st of October 2015] Website: http://www.restek.com/ezgc-mtfc.

[31] Agilent Technologies, GC Method Translation Software (2013) Accessed on: [1st of October 2015] Website: http://www.agilent.com/en-us/support/gas-chromatography/gcmethodtranslation.

[32] A. Zlatkis, J.W. Anderson, G. Holzer, Concentration and analysis of trace impurities in styrene monomer, J. Chromatogr. 142 (1977) 127-129.

[33] A.C. Olivieri, Practical guidelines for reporting results in single- and multi-component analytical calibration: A tutorial, Anal. Chim. Acta 868 (2015) 10-22.

[34] Chevron Phillips Chemical Company LP, Styrene momomer specification (2004) Accessed on: [1st of October 2015] Website: http://www.cpchem.com/bl/aromatics/en-us/tdslibrary/StyreneMonomer.pdf.

[35] Lyondell Chemical Company, U.S. sales specification: Styrene Monomer (2008) Accessed on: [1st of October 2015] Website: http://www.lyondellbasell.com/techlit/techlit/SalesSpecs/3371.pdf.

[36] J. Krupcik, R. Gorovenko, I. Spanik, I. Bockova, P. Sandra, D.W. Armstrong, On the use of ionic liquid capillary columns for analysis of aromatic hydrocarbons in low-boiling petrochemical products by one-dimensional and comprehensive two-dimensional gas chromatography, J. Chromatogr. A 1301 (2013) 225-236.

[37] K. Dettmer, U. Felix, W. Engewald, M. Mohnke, Application of a unique selective PLOT capillary column for the analysis of oxygenated compounds in ambient air, Chromatographia 51 (2000) S221-S227.

[38] C.F. Poole, N. Lenca, Gas chromatography on wall-coated open-tubular columns with ionic liquid stationary phases, J. Chromatogr. A 1357 (2014) 87-109.

[39] J. de Zeeuw, The Development and Applications of PLOT Columns in Gas-Solid Chromatography, LC-GC Europe 24 (2011) 38-45.

[40] J. de Zeeuw, C. Duvekot, M. Mohnke, D. Estel, N. Vonk, Analysis of ppm-ppb levels of oxygenates in C1-C5 hydrocarbons using a highly selective multilayer PLOT column, Am. Lab. 31 (1999) 81C-82C.

[41] J. Luong, R. Gras, H. Cortes, R. Mustacich, Stacked injection with low thermal mass gas chromatography for ppb level detection of oxygenated compounds in hydrocarbons, J. Chromatogr. Sci. 44 (2006) 219-226.

[42] J.R. Hopkins, A.C. Lewis, K.A. Read, A two-column method for long-term monitoring of non-methane hydrocarbons (NMHCs) and oxygenated volatile organic compounds (o-VOCs), Journal of Environmental Monitoring 5 (2003) 8-13.

[43] Z. Ji, R.E. Majors, E.J. Guthrie, Porous layer open-tubular capillary columns: preparations, applications and future directions, J. Chromatogr. A 842 (1999) 115-142.

[44] J. de Zeeuw, J. Luong, Developments in stationary phase technology for gas chromatography, Trends Anal. Chem. 21 (2002) 594-607.

[45] ExxonMobil Chemical Company, Isopar E, Isoparaffin™ fluid specification (2010) Accessed on: [1st of October 2015] Website: http://exxonmobilchemical.ides.com/en-US/ds248005/Isopar%E2%84%A2 E.aspx?I=22455&U=0.

Chapter 5: Resistively heated flow modulated comprehensive two-dimensional gas chromatography

Summary

Comprehensive two-dimensional chromatography GC × GC has been demonstrated to deliver exceptionally high peak capacity without substantially increasing the time of analysis. This is achieved by multiplying the peak capacity of two separation columns, a long first-dimension column and a shorter second dimension column that is capable of completing a very rapid separation. The success of a GC × GC system is contingent on the ability of a device known as a modulator to sample, focus and inject solutes eluting from the first-dimension column in a narrow bandwidth for additional separation.

In this chapter, a resistively heated single-stage thermal modulator was investigated as a device for achieving comprehensive two-dimensional GC × GC analysis. This device was constructed from a SS capillary that was coated with the novel stationary phase described in Chapter 4. The stationary phase of this trap was demonstrated to be capable of focusing and retaining solutes for periods long enough to achieve GC × GC modulation (3-5 s). The modulator utilised a capacitive discharge power supply, to provide rapid resistive heating of the modulator to periodically elute focused solutes to a second separation column. The capacitive discharge power supply, its integrated timing circuit and the SS capillary enabled precise repeatable modulation period for GC × GC modulation without the requirement for refrigerated cooling units or cryogenically cooled modulators. The peak volume repeatability was similarly excellent (~ 1% RSD), while the peak widths obtained with this modulator were as narrow as 60 ms.

The modulator was capable of focusing a wide variety of different chemical compounds with concentrations ranging from 5 to 1300 pg on column mass, without the

need for a secondary trapping stage, which simplifies modulator design. The main limitation of the modulator was its ability to focus volatile compounds such as *n*-octane, which could not be retained by the present stationary phase. However, the modulator was found to be very effective for the modulation of petroleum, essential oil, and food aroma type samples, demonstrating the versatility of the trap. Excellent peak area enhancements were obtained using the trap, which enabled the low level quantification of total petroleum hydrocarbon and target analytes in soil extracts compared to 1D GC analysis.

The modulator was installed in a portable Calidus™ GC instrument since access to electrical power was the only requirement for its operation and it was anticipated that the addition of comprehensive GC × GC would increase the separation power of this instrument. Despite the success of the modulator when utilised in a bench top GC instrument, the modulator was not similarly effective in the Calidus™ GC, due to the isothermally controlled convection oven in which the modulator was installed. The requirement for maintaining the transfer line oven at a high temperature reduced the ability of the modulator to provide narrow injection bandwidths, which impacted on the two-dimensional GC performance that could be obtained.

5.1 Introduction

Multidimensional gas chromatography (MDGC) and comprehensive two-dimensional gas chromatography (GC × GC) has been a topic of great interest due to the expanded possibilities of this technique to analyse very complex mixtures of compounds [1-3]. One-dimensional gas chromatography (GC) separations with long (60 to 100 m) columns often fail to resolve large numbers of compounds due to limited peak capacity, which necessitates the use of MDGC and GC × GC techniques [4,5]. Heart-cut MDGC analysis differs from GC × GC by the throughput of injections to the second-dimension column. The long, high resolution second-dimension columns used in MDGC analysis limits the number of heart-cut injections that can be performed, since all solutes must be eluted before additional injections can take place. If the contents of the second-dimension column are not completely eluted before an additional injection is performed the analyst runs the risk of recombining previously separated solutes during the second-dimension separation. For this reason typical MDGC analyses are limited to between 1 and 4 heart cuts depending on the sample and the second-dimension column's stationary phase and dimensions [3]. Therefore heart-cut MDGC is best suited to the separation of target compounds in complex samples by leveraging the selectivity of two high-resolution columns.

Efforts to increase throughput of heart-cut injections in MDGC have been on-going and one potential strategy is to initiate stop-flow conditions in the first-dimension column during the elution of solutes from the second-dimension column that would otherwise be recombined [6-9]. This is achieved by setting the mid-point pressure to the same value as the inlet pressure, while solutes are being eluted from the second-dimension column to prevent co-elutions from occurring. Multiple stop flow events can be programmed using this setup, however such systems require careful optimisation.

Additionally, stop flow conditions cause a proportional increase in experimental run time, since the first-dimension separation is paused while in the stop flow state.

Comprehensive GC × GC performs second-dimension separations on the timescale of a few seconds which allow on-line, continuous sampling of the first-dimension column to obtain a complete two-dimensional data output. As a result of this GC × GC is able to increase the peak capacity of GC by an order of magnitude, without significantly increasing the time of analysis [1,10,11]. The vast range of stationary phases and column dimensions complicate method development due to the large number of combinations can be used. Generally a non-polar or weakly polar column is selected for the first-dimension, to provide a separation that is based primarily on the vapour pressure or boiling point of analytes during a temperature programmed separation [12]. A polar or mid-polarity column is then used in the second-dimension, which provides an additional dimension of separation based on solute polarity [13-15]. The selection of columns and conditions for GC × GC is challenging given the large number of parameters that can be changed to affect the separation obtained (inlet pressures, column dimensions, column lengths, phases, outlet pressures *etc.*), however a number of researchers have devised an excellent set of guidelines that can be used to simplify the method development process [11,16-19].

The critical component of any GC × GC system is a component known as a modulator that is installed at the interface between the first- and second-dimension columns. The modulator is responsible for sampling the first-dimension effluent and injecting the sampled effluent in a narrow band to the second-dimension column. The narrower the injection bandwidth provided by the modulator, the better the quality of second-dimension separation [10,11,20]. Due to the importance of the modulator for GC × GC they have been a topic of intense research [1,21]. In addition to providing narrow injection bandwidths, GC × GC modulators must also be capable of repetitively sampling

peaks eluting from the first-dimension at least three times to ensure that the separation resolution obtained in the first-dimension is not lost, and first-dimension retention times can be reconstructed accurately [22,23]. The duration of each sampling cycle is known as the modulation period, and the selection of this period defines the time available for a second dimension separation. The selection of a short modulation period limits the separation space of the second dimension and furthermore, sampling a peak more than four times leads to a reduction in peak intensity due to a reduction in flux to detector during each modulation cycle [24]. As a result the modulation period and second-dimension separation need to be carefully selected for each given application.

There are two types of GC × GC modulators that are based on either valve manipulation or solute focusing. This research chapter will focus on solute focusing modulation and Chapter 7 will address valve-based modulation. Solute-focusing modulation traps solutes in a narrow band within the GC × GC modulator, while allowing the carrier gas to flow through unimpeded. The trap is periodically heated to mobilise trapped solutes to the second-dimension column, thereby providing modulation. GC × GC modulation was first demonstrated using a capillary column trap that was coated with a thick film of a non-polar stationary phase [25]. The outside of the capillary was painted with a layer of conductive paint, through which an electrical current was periodically passed to resistively heat and mobilise trapped solutes. The robustness of this modulator was limited due to peeling of the conductive paint and limited capacity for highly volatile solutes [12], which prompted research into GC × GC modulation techniques. The two distinct steps in GC × GC modulation, focusing and mobilisation, have been addressed using a range of different strategies. Focusing can be achieved either by relying on retentive stationary phases, or it can be enhanced with the application of cooling provided by cryogen or cooling devices. Mobilisation on the other hand has been achieved using heat provided by convection ovens, hot air jets and resistive heating.

Following the initial resistively heated modulator reported by Liu and Phillips [25], Phillips and co-workers developed a more robust modulator known as a rotating thermal modulator [26,27]. This device (Figure 42) provided modulation by sweeping a segment of capillary with a hot metallic sweeper that provided heat to a trapping capillary to mobilise solutes to the second dimension column. This modulator was commercialised and proved very effective, although its ability to modulate very volatile solutes such as pentane (boiling point 36 °C) was limited. Furthermore the elution of less volatile solutes was not possible due to the temperature stability of capillary column polyimide coatings that could be damaged by the heated sweeper device. An investigation by de Geus *et al.* reported a number of alternative resistive capillary coatings that were more robust than original thermal modulator design, however these modifications were never commercialised due to their complexity [28].

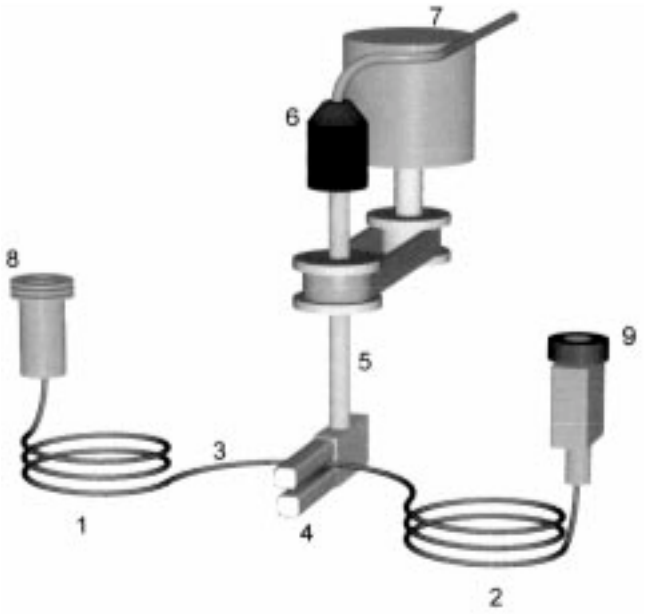

Figure 42 Schematic of a rotating heater thermal modulation system configured for GC × GC. 1. First-dimension capillary column; 2. Second-dimension capillary column; 3. Modulator tube; 4. Rotating heater ("sweeper"); 5. Machined ceramic shaft; 6. Rotating electrical feed-through with electrical cable; 7. Stepper motor; 8. Injector; 9. Detector.

To improve the modulation of volatile species a number of researchers have reported GC × GC modulators that utilise cryogen to enhance solute trapping. Marriott and Kinghorn developed the longitudinally modulated cryogenic system (LMCS) that provided modulation by controlling the position of a cryogenically cooled focusing region that could be shifted along the axis of a GC capillary column [29]. Solutes were mobilised by latent heat provided by the GC convection oven, whenever the cryogenic region was shifted to expose a previously cooled region as show in Figure 43.

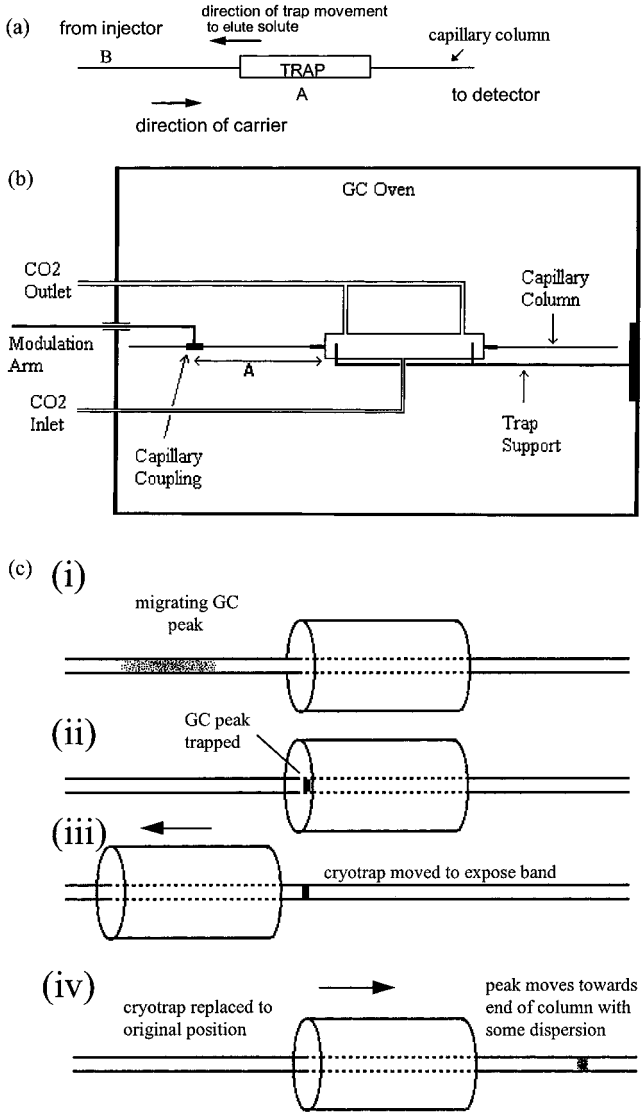

Figure 43 LMCS modulator operation diagram showing (a) movement of the trap within a GC convection oven, (b) schematic design of the LMCS modulator, (c) the operation of the modulator. (i) Migration of a solute towards the trap, (ii)

trapping of a solute in a narrow band within the cryotrap, (iii) movement of the cryotrap upstream from the focused peak and remobilisation of the solute, (iv) movement of cryotrap back to its original position after remobilisation focused solute. Reproduced with permission from the American Chemical Society (1997) from [29].

A series of iterations of cryogenic modulators have been prepared using carbon dioxide [30-34] and liquid nitrogen cryogen [35-38], both of which can provide effective modulation for GC × GC. Of the two cryogenic options, liquid nitrogen is more effective for focusing highly volatile species such as organic compounds with less than five carbon units, due to the lower boiling point of liquid nitrogen (-195.8 °C) compared to carbon dioxide's sublimation point (-78.5 °C), for this reason most commercial GC × GC systems employ liquid nitrogen [37,39].

While mobilisation of focused solutes has been achieved using both latent heat from the convection oven used for column heating or a hot jet of air, resistive heating has the potential to speed up the solute mobilisation step due to the extremely rapid heating that can be achieved with this technique [40]. The development and commercialisation of SS capillary columns presented a new opportunity for resistively heated GC × GC modulators, since they eliminated the need for resistive coatings. Harynuk and Górecki used a SS capillary (530 μm ID) that was packed with a macro porous organic polymer (Tenax TA) as the basis for a GC × GC modulator [36]. Liquid nitrogen cryogen was used to maximise the trapping of volatile compounds, and this modulator proved to be very effective. Libardoni *et al.* developed a single-stage thermal modulator based on a SS capillary (180 μm ID) coated with a non-polar stationary phase (MXT-1, 0.2 μm d_f) that was mounted in an aluminium block [41]. Refrigerated air was pumped through the block to enhance retention of solutes within the trap. This modulator exhibited some solute breakthrough for high concentration solutes and highly volatile species, however

it was still relatively effective. Later modifications of the Libardoni *et al*. design eliminated breakthrough with the addition of liquid cooling [42] and dual-stage modulation [43].

The addition of liquid nitrogen, carbon dioxide cryogen or other cooling devices are effective at enhancing solute focusing, however this comes at the significant cost of cryogen or refrigeration units. It would be more desirable from a cost and convenience perspective to be able to achieve modulation without the need for cryogenic cooling or refrigeration units. The initial embodiment of GC × GC utilised resistive heating for solute mobilisation [25] and the subsequent rotating modulator design [27] and alternate coating strategies [28] improved the robustness of cryogen free modulation, unfortunately modulation performance of these devices were not as good as cryogenic focusing methods. Burger *et al.* prepared a ten-stage modulator with a fused silica capillary (200 μm ID) coated with a film of non-polar phase (DB-1 equivalent, 3 μm d_f) [44]. The capillary was resistively heated using a SS capillary sleeve (530 μm ID) through which the silica capillary was threaded. Heating was applied to each segment using a series of electrical contacts and computer control to provide modulation as narrow as 145 ms at half height. The large number of stages in this modulator was reported to reduce the possibility for stationary phase burn out and eliminate solute breakthrough, however the complexity of the design prevented uptake of the technique.

A dual stage modulator prepared from a SS capillary column with a non-polar stationary phase (MXT-1, 280 μm ID, 3 μm d_f) was constructed and used for aerosol analysis [45]. Rather than using cryogen for trap cooling, a vortex fan that was supplied with ambient air was used. The peaks generated with this system were on the order of 200 ms at half height after the second-dimension separation was carried out.

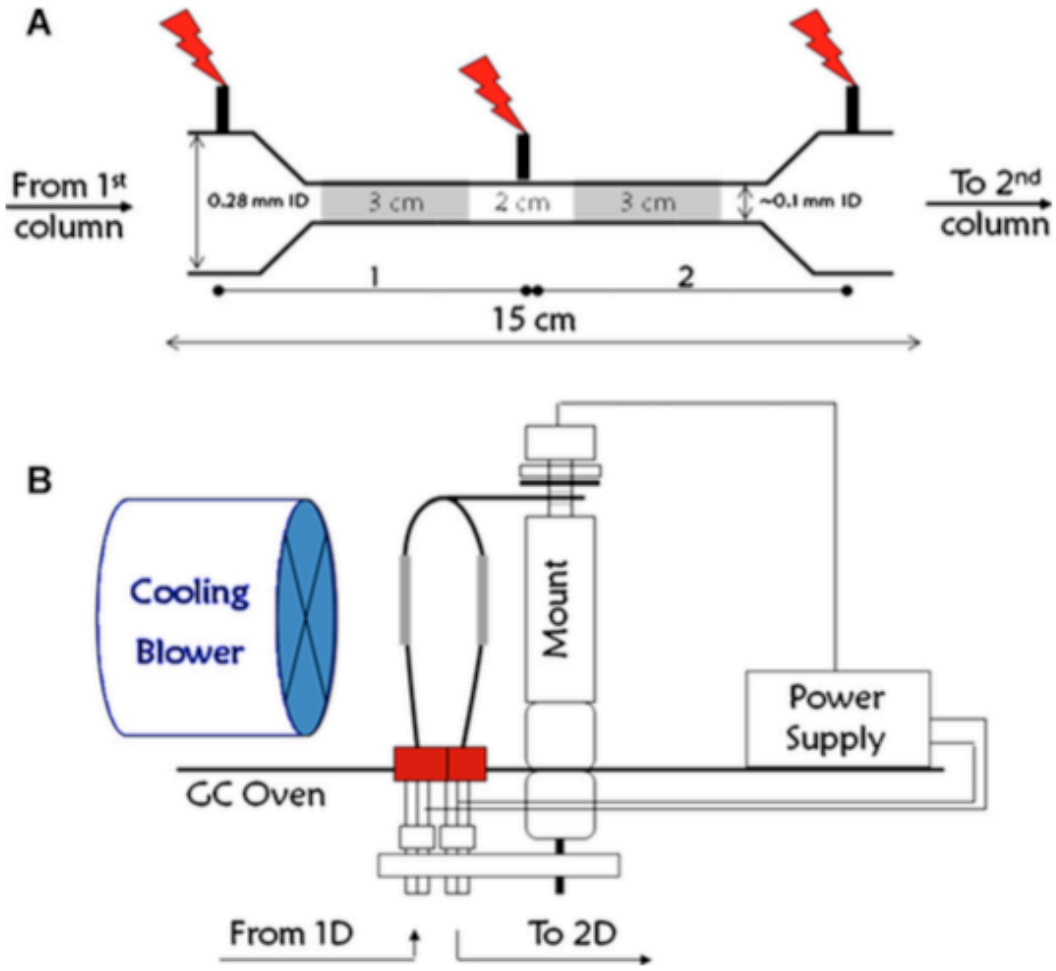

Figure 44 Schematic diagrams of a dual stage, resistively heated GC × GC modulator. (A) The flattened trapping capillary with two trapping zones. There are 3 electrical contact points on the trap enabling dual-stage modulation using resistive heating. (B) The modulator was installed through the roof of a GC oven. A cooling blower was mounted next to the trap. Reproduced with permission from Elsevier (2011) [46].

Another iteration of the resistively heated modulator used a flattened SS capillary trap (280 µm ID, flattened to a nominal ID of 100 µm ID) that was coated with a non-polar stationary phase (MXT-1, 280 µm ID, 3 µm d_f), as shown in Figure 44 [46]. The injection bandwidths delivered by this modulator were just 60 ms at half height.

Table 11 Summary of thermal modulator focusing devices, trapping stationary phase and trap cooling strategies.

Authors	Modulator construction	Trapping stationary phase	Trap cooling	Ref
Liu and Phillips	FS column, 100 um ID, conductive paint, dual stage, 15 cm	PDMS 0.5 µm	GC oven only	[25]
de Geus *et al.*	FS column, 220 um ID, conductive paint, 30 cm	CP-Sil8 CB (5% phenyl, PDMS) 0.5 um	Air cooling	[28]
Phillips *et al.*	FS column, 100 um ID, rotating modulator, 10 cm	PDMS 3.5 µm	GC oven only	[27]
Harynuk and Gorecki	SS tube, 530 um ID, 2.0 cm	Micro packed TENAX TA	Liquid nitrogen	[36]
Burger *et al.*	SS tube, 530 um ID, 11 cm; FS column 200 um ID	DB-1 (PDMS) 3 µm d_f	GC oven only	[44]
Libardoni *et al.*	SS column, 180 um ID, single-stage, 5.5 cm	MXT-1 (PDMS) 0.2 µm d_f	Refrigerated air	[41]
Libardoni *et al.*	SS column, 180 um ID, single-stage, 5.5 cm	MXT-1 (PDMS) 0.2 µm d_f	Refrigerated ethylene glycol	[42]
Goldstein *et al.*	SS column, 530 um ID, dual stage, 15 cm	MXT-1 (PDMS) 3 µm d_f	Air cooling	[45]
Libardoni *et al.*	SS column, 100 um ID, dual stage, 5.5 and 2.2 cm	MXT-1 (PDMS) 0.2 µm d_f	Refrigerated air	[43]
Panic *et al.*	SS column, 280 um ID, dual stage, 15 cm	MXT-1 (PDMS) 1 µm d_f	Air cooling	[46]
Worton *et al.*	SS column, 280 um ID, single-stage, 15 cm	Deactivated SS	Air cooling	[47]
Mascalu *et al.*	SS column, 280 um ID, flattened to 100 um, 15 cm	Chemically modified PDMS	Air and thermoelectric cooling	[48]
Present modulator	SS column, 280 um ID, flattened to 100 um, 4 cm	Chemically modified PDMS	Air and thermoelectric cooling	N/A

The flattened capillary design enhanced the mobilisation of solutes as a result of the reduced internal volume of the capillary, which enabled solutes to be transported in a narrow injection band to the second-dimension column [46]. It was later reported that

this modulator was effective in the single-stage modulation mode, for solutes as volatile as *n*-hexane [47].

Both single- and dual-stage thermal modulators (summarised in Table 11) have been shown to be effective for GC × GC modulation, although dual-stage modulation has the advantage of preventing solute breakthrough during the cooling period following a heating event. A number of single-stage thermal modulators have been investigated that deliver adequate performance without the need for a second stage which significantly simplifies modulator operation [34,36,41,47,49-52]. Ensuring that a modulator trapping capillary is rapidly cooled after a heating event is essential to preventing solute breakthrough in single stage modulators [46,52]. Generally non-polar or weakly polar stationary phases with a thick coating (between 1 and 3 μm d_f) are used as trapping phases for GC × GC modulators (see Table 11 for a summary of modulator stationary phases). These phases have better thermal stability and chemical inertness than other polar stationary phases [53]. There has been limited research on the development of stationary phases specifically for GC × GC modulation, however preliminary research has shown that peak shape, and the solute loading capability of a trap could potentially be enhanced with novel temperature stable stationary phase coatings [48]. Muscalu *et al.* utilised a modified PDMS based stationary phase for the modulation and separation of polychlorinated biphenyls (PCB), chlorinated pesticides and organochlorine compounds in complex waste and sediment samples [48].

The aim of the present chapter is to qualitatively and quantitatively evaluate a miniaturised single-stage thermal modulator with a novel thermally treated stationary phase for applications in GC × GC analysis. This will be achieved by evaluating its ability to provide modulation for a range of different chemical compounds, with a range of boiling points. The operation and use of the modulator will be optimised and applied to the analysis of a variety of different samples to evaluate its effectiveness. Finally the

modulator will be tested as a potential tool for providing fast, high-throughput GC × GC analysis with potential for portable analysis using the Calidus™ GC platform. The combination of two separation columns in the comprehensive GC × GC format can vastly increase the ability of GC systems to separate complex samples, which is critical for the analysis of complex samples in the field.

5.2 Materials and Methods:

5.2.1 Single-stage thermal modulator installation and evaluation in the comprehensive two-dimensional analysis (GC × GC) mode

An Agilent 6850 GC (Agilent) equipped with a S/SL inlet, an automatic liquid sampler 7683B Series (Agilent) and an FID was used for evaluation of the modulation capabilities of a single-stage thermal modulator device. A DB5-MS column (25 m × 250 μm ID × 0.25 μm d_f, Agilent) was connected to the S/SL inlet of the GC using a graphite vespel ferrule (Trajan). The outlet of the DB5-MS column was connected to a single stage thermal modulator using a SilTite mini-union (Trajan). The outlet of the thermal modulator was connected to a Rxi17Sil MS column (1 m × 100 μm ID × 0.1 μm d_f, Restek) *via* another SilTite mini union (Trajan). Finally the outlet of the Rxi17Sil MS column was connected to a FID unit using a graphite vespel ferrule (Trajan). A heat-sinking device was installed through the MS interface port on the 6850 GC, as described previously (Section 3.2.3). The heat-sinking device was actively cooled using a pair of fans (12 V) and pair of thermoelectric cooling pads (5 V, 2.6 A) that were mounted in contact with the copper heat conduits, outside of the GC convection oven. The single-stage modulator was gripped and supported by the heat-sinking device between a pair of electrically insulating ceramic pads. The trap was connected to a programmable (0 to 80 V) capacitive discharge power supply (4 x 44,000 μF capacitor array) using two fiberglass braid insulated copper wires.

The inlet temperature was 250 °C, and a 4 mm split liner (Trajan) was used. The carrier gas was hydrogen, with a constant flow rate of 1.0 mL min^{-1}, requiring an initial inlet pressure of 12.63 PSI. The initial oven temperature was 30 °C which was held for 1 min and then ramped at a rate of 5 °C min^{-1} to 200 °C. The FID temperature was 250 °C, and was supplied with hydrogen (30 mL min^{-1}), air (320 mL min^{-1}) and nitrogen makeup

gas (30 mL min^{-1}). The capacitive discharge power supply was programmed to provide a modulation period of 3.0 s, with a discharge voltage of 21.0 V.

A sample containing a mixture of toluene, *n*-octane, ethylbenzene, 2-heptanone, pentylacetate, *n*-decane, 2-octanol, 2-nonanone, 1,6-hexanediol, *n*-docecane, 2-decanol, 4-chlorophenol and *n*-tetradecane (Sigma Aldrich, Castle Hill, Australia) were used to prepare a stock solution containing all of these compounds (nominal concentration 10,000 mg kg^{-1} each in dichloromethane (Sigma Aldrich)). This stock was diluted with dichloromethane (Sigma Aldrich), to obtain a series of standards where each individual component was between 100 to 0.5 mg kg^{-1}. These standards were then injected (1 µL) into the 6850 S/SL inlet at a split ratio of 100:1. All experiments were performed in triplicate. FID data were acquired using ChemStation Software at a data sampling rate of 200 Hz. All data files were then imported into GC Image R2.5b4 software (GC Image LLC, Lincoln NE, USA) for two-dimensional visualisation, baseline correction peak detection, integration and analysis. Chromatograms were generated for all samples and the peak statistics generated were exported to Microsoft Excel for calibration and processing purposes.

5.2.2 Petroleum spill analysis

A 6850 GC (Agilent) equipped with a S/SL inlet, an automatic liquid sampler 7683B Series (Agilent) and an FID was used for the separation of solvent extracts from petroleum-contaminated soil at Macquarie Island. The S/SL inlet was connected to a DB5-MS column (25 m × 250 µm ID × 0.25 µm d_f, Agilent). The outlet of the DB5-MS column was connected to a single stage thermal modulator using a SilTite mini union (Trajan). The outlet of the thermal modulator was connected to an Rxi17Sil MS column (1 m × 100 µm ID × 0.1 µm d_f, Restek) *via* another SilTite mini union (Trajan). Finally the outlet of the Rxi17Sil MS column was connected to a FID unit. A heat-sinking device was installed through the MS interface port on the 6850 GC, as described. The heat-sinking

device was actively cooled using a pair of fans (12 V) and pair of thermoelectric cooling pads (5 V, 2.6 A) that were mounted in contact with the copper heat conduits, outside of the GC convection oven. The single-stage modulator was gripped and supported by the heat-sinking device between a pair of electrically insulating ceramic pads. The trap was connected to a programmable (0 to 80 V) capacitive discharge power supply (4 x 44,000 μF capacitor array) using two fiberglass braid insulated copper wires.

The carrier gas was hydrogen, with a constant flow of 0.8 mL min^{-1}; the initial head pressure was 9.59 PSI at 40 °C. The GC temperature was initially 40 °C for 1 min and then ramped at a rate of 5 °C min^{-1} to 320 °C, and held for 3 min. The FID temperature was 280 °C and was supplied with hydrogen (30 mL min^{-1}), air (320 mL min^{-1}) and nitrogen makeup gas (30 mL min^{-1}). The capacitive discharge power supply was programmed to provide a modulation period of 3.0 s, with a discharge voltage of 21.0 V.

Samples and standards were injected (1 μL) into a S/SL inlet with a split ratio of 20:1. The inlet temperature was 280 °C, and a 4 mm split liner (Trajan) was used. All samples were analysed in triplicate, while the facilitator sample was analysed ten times throughout the analytical sequence. Soil extracts were obtained from the Australian Antarctic Division (Kingston, Tasmania). Soil samples were prepared using the method described in [54]. Each soil sample (10 g) was spiked with 1-bromoeicosane 25 mg kg^{-1} (Sigma-Aldrich), and then extracted using *n*-hexane (Mallinckrodt Baker, USA). The soils originated from two sites, indicated as the Fuel Farm (FF) and Main Power House (MPH), on Macquarie Island (see [55] for details on each sampling site). A sample of Special Antarctic Blend (SAB) diesel was obtained from the Macquarie Island research station. A series of SAB diesel dilutions were prepared, ranging in concentration from 100 to 3000 mg kg^{-1} in *n*-hexane (Mallinckrodt Baker). Each SAB diesel sample was spiked with 1-bromoeicosane 25 mg kg^{-1} (Sigma-Aldrich) for internal standardisation purposes. Two fuel spill sample extracts, containing approximately 3,000 mg kg^{-1} of

petroleum hydrocarbon, from the FF and MPH sites were combined in a 1:1 ratio and used as a facilitator sample as described by Furbo *et al.* [56].

A 10 mg kg^{-1} standard containing *n*-octane, *n*-nonane, *n*-decane, *n*-undecane, *n*-dodecane, *n*-tridecane, *n*-tetradecane, *n*-pentadecane *n*-hexadecane *n*-heptadecane *n*-octadecane, *n*-nonadecane and *n*-eicosane (Sigma Aldrich) as well as a range of polycyclic aromatic hydrocarbons including: naphthalene, fluoranthene, acenaphthene, chrysene, benzo(k)fluoranthene, dibenz(a,h)anthracene, benzo(g,h,i)perylene, benzo(a)pyrene, anthracene, phenanthrene, indeno(1,2,3-c,d)pyrene, benzo(b)fluoranthene, fluorene, pyrene, benz(a)anthracene, 2-methylnaphthalene and acenaphthylene (Restek, catalogue #31458) was prepared in *n*-hexane (Sigma Aldrich). FID data were acquired at a 200 Hz data sampling rate, using ChemStation Software. The data were then imported into GC Image (GC Image LLC) to perform baseline correction and peak detection and integration. Peak volumes, retention times and chromatograms were generated for the modulator performance testing mixture, which were then exported to Microsoft Excel for calibration and analysis.

The Image Investigator feature of GC Image was used to analyse the petroleum spill samples. A composite chromatogram was constructed using ten replicate analyses of the facilitator sample. This composite chromatogram was used for constructing a peak and feature template, which was used for analysing all petroleum spill samples. All chromatograms were manually reviewed to ensure correct template alignment and peak assignment. Peak and feature tables were compiled using Image Investigator and exported to Excel format for further data processing. Principal Component Analysis was performed using the Matlab software package R2015b build 8.3.0.532 (The Math Works Inc., Natick, MA, USA).

5.2.3 Installation of single-stage thermal modulator in the Calidus™ GC

A Calidus™ GC equipped with a S/SL inlet, and an FID was modified to include a single-stage thermal modulator for comprehensive GC × GC. The modulator was installed within the Calidus™ transfer line oven to ensure that the SilTite mini unions used for connectivity would be maintained at a high temperature during analysis. A new cover plate was prepared for Calidus™ transfer line oven to facilitate the installation of the single-stage thermal modulator's heat-sinking device. A piece of SS sheet was cut to match the dimensions of the original oven door, and this cover plate was then insulated with a piece of Teflon sheet (0.6 mm diameter thickness).

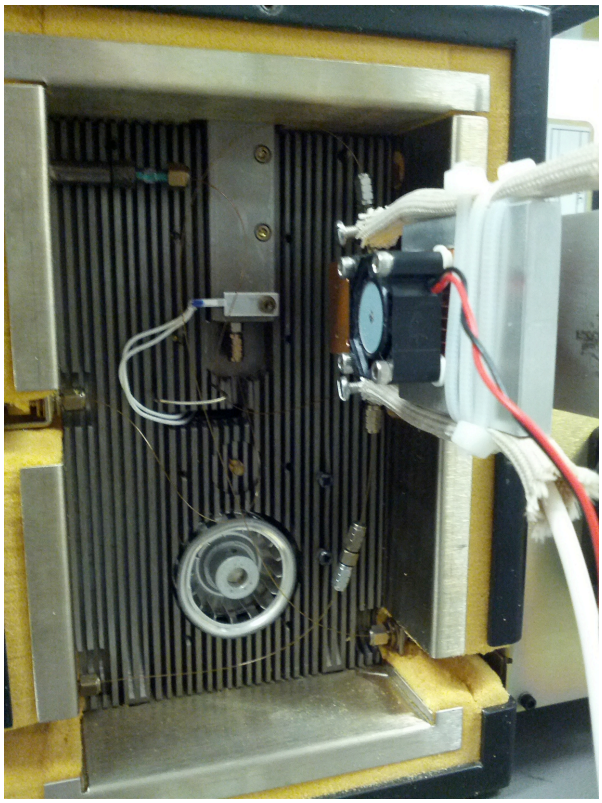

Figure 45 Image showing the installation of the thermal modulator and its associated heat sink within the Calidus™ GC's convection oven.

A rectangular section was cut out of this cover place to facilitate the installation of the heat sink device through the wall of the convection oven cover plate. The single-stage thermal modulator's heat sink device was attached to the internal wall of the

convection oven using two M4 thread nuts through a pair of holes that were drilled in the side of the oven wall. This allowed secured attachment of the modulator within the GC oven as shown in Figure 45.

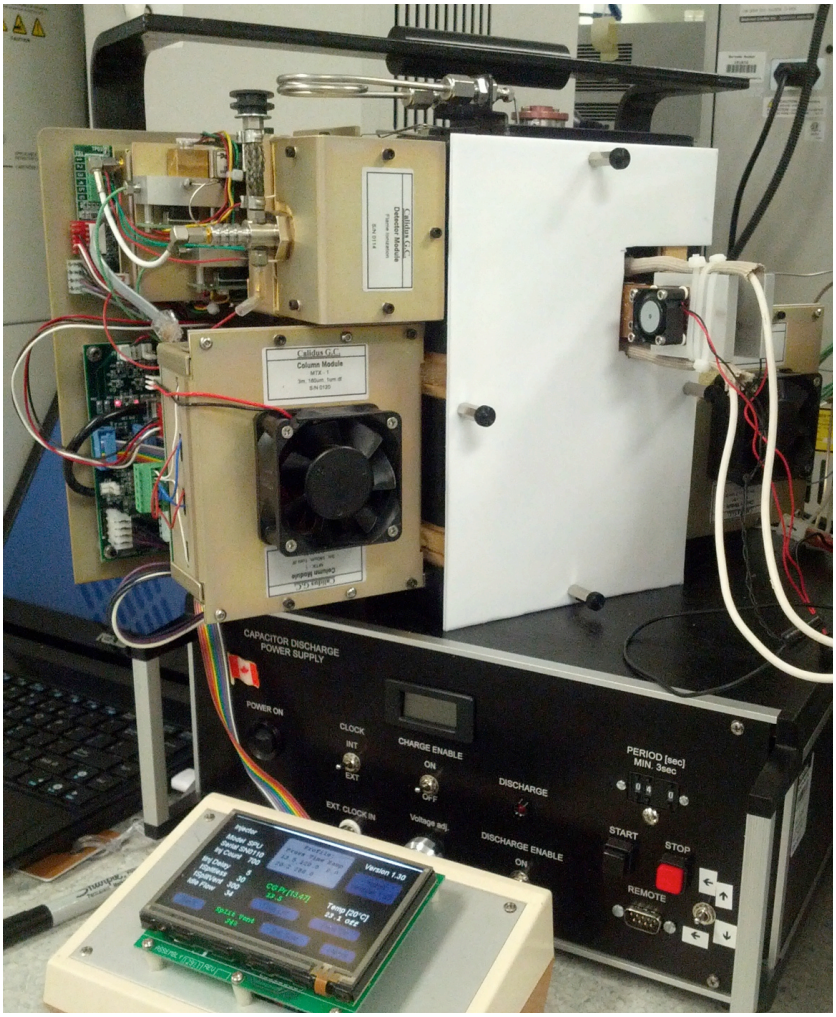

Figure 46 Single-stage thermal modulation system integrated with the Calidus™ GC instrument, with the casing removed to reveal the instrument modifications. The instrument is sitting on top of a laboratory capacitive discharge power supply and a touch screen is attached by ribbon cable to the Calidus™ GC for instrument control.

The SS capillary of the modulator trap was supported within the Calidus™ convection oven by compression between the ceramic plates of the heat sink device, as described before (Section 3.2.3). This ensured that electrical short circuits could not

occur during capacitive discharge, and allowed the modulator to be cooled below the convection oven temperature *via* the copper heat conduits of the heat sink device. The single-stage modulator was connected to a capacitive discharge power supply using a pair of single core copper wires that were insulated with fiberglass braid as shown in Figure 46.

The S/SL inlet was connected to the first dimension column using a piece of DFS (13 cm × 180 µm ID, Trajan) using SilTite ferrules (Trajan). A MXT-1 column (3 m × 180 µm ID × 1.0 µm d_f, Restek) was used as the first-dimension column and its outlet was connected using a piece of DFS (10 cm × 250 µm ID). A DFS restrictor capillary (5 cm × 50 µm ID) was installed in front of the single-stage thermal modulator to prevent backflow during capacitive discharge, and was connected using a SilTite mini union (Trajan). The modulator was then connected to an MXT-1701 column using a DFS capillary (25 cm × 250 µm ID). The MXT-1701 column (3 m × 250 µm ID × 0.1 µm d_f, Restek) was connected to the Calidus™ FID *via* a piece of DFS (12 cm × 250 µm ID). Column module to capillary connections were made using SilFlow connections and bulkheads that were installed on each column module. All transfer lines were installed in the Calidus™ GC transfer line oven which was maintained at a constant temperature of 250 °C throughout the analysis.

The initial temperature of the MXT-1 column was 30 °C (1 min hold) after which the temperature was ramped at a rate of 0.4 °C s^{-1} to a temperature of 250 °C. The second-dimension column was programmed to lead the first-dimension column by +20 °C. Pressure programming was used to deliver a constant system flow of 1.0 mL min^{-1}, which required an initial head pressure of 14.5 PSI. The transfer line, oven and inlet were maintained at a temperature of 250 °C for the duration of the analysis. The FID, was set to a temperature of 270 °C and supplied with hydrogen at (13 mL min^{-1}) and air (130 mL min^{-1}) for flame operation.

Two samples were prepared for analysis. A sample of SAB Diesel was obtained from the Australian Antarctic division. This diesel sample was diluted to a concentration of 2250 mg kg^{-1} in dichloromethane. Another sample was prepared that was comprised of a homologous series of *n*-alkanes including *n*-octane, *n*-nonane, *n*-decane, *n*-undecane, *n*-dodecane, *n*-tridecane, *n*-tetradecane, *n*-pentadecane *n*-hexadecane *n*-heptadecane *n*-octadecane, *n*-nonadecane and *n*-eicosane (20 mg kg^{-1} each, Sigma Aldrich) diluted in dichloromethane (Sigma Aldrich). These two samples were injected (1 µL) into the Calidus™ GC, at a split ratio of 20:1 using a 10 µL micro syringe. FID data were collected at a data sampling rate of 100 Hz, using Chrom Perfect software (Justice Laboratory Software, USA).

5.3 Results and Discussion

5.3.1 A resistively heated single-stage thermal modulator for GC × GC

The SS capillary trap that was used for injection focusing studies in Chapter 2, was utilised as a modulator for comprehensive GC × GC. While this trap was not able to retain solutes for extended durations (> 60 s), the ability to retain volatile and semi-volatile compounds for the short durations required during GC × GC modulation is well established using similar capillary column traps [25,28,36,41,45-47]. The key to effective single-stage modulation is to ensure that the remobilisation step is very rapid, and that the return to trapping temperature is fast enough to prevent solute breakthrough from the first-dimension column. A SS capillary column (280 μm ID) was used as the basis for the present modulator, similar to research carried out by Górecki and co-workers [48]. The SS capillary was rapidly heated using a capacitive discharge power supply [57] that was able to heat the capillary to high temperatures (> 400 °C) in less than 5 milliseconds [36].

The cooling rate for the modulator was approximately -180 °C s^{-1} after the heating induced by a capacitive discharge event, with an exponential decrease in the cooling rate as the trap approaches ambient temperature (as established in Chapter 4). The time required to return to 50 °C after a 32 V capacitive discharge event was approximately 4.5 s, which could limit the modulators ability to trap and focus volatile compounds. A schematic of the present single-stage GC × GC modulator is shown in Figure 47. Trap cooling was enhanced using a heat sink device that was installed through the wall of the GC convection oven. The heat sink was cooled externally using a pair of small electric fans and ambient air. Two Peltier cooling wafers were added to the heat sinks to provide the option for active cooling to enhance the cooling capabilities of the heat sink. Installation of the modulator within the GC convection oven allows the modulator to

trail the oven temperature by 10 to 50 ° C, depending on the temperature of the convection oven and level of cooling provided by the heat sink device.

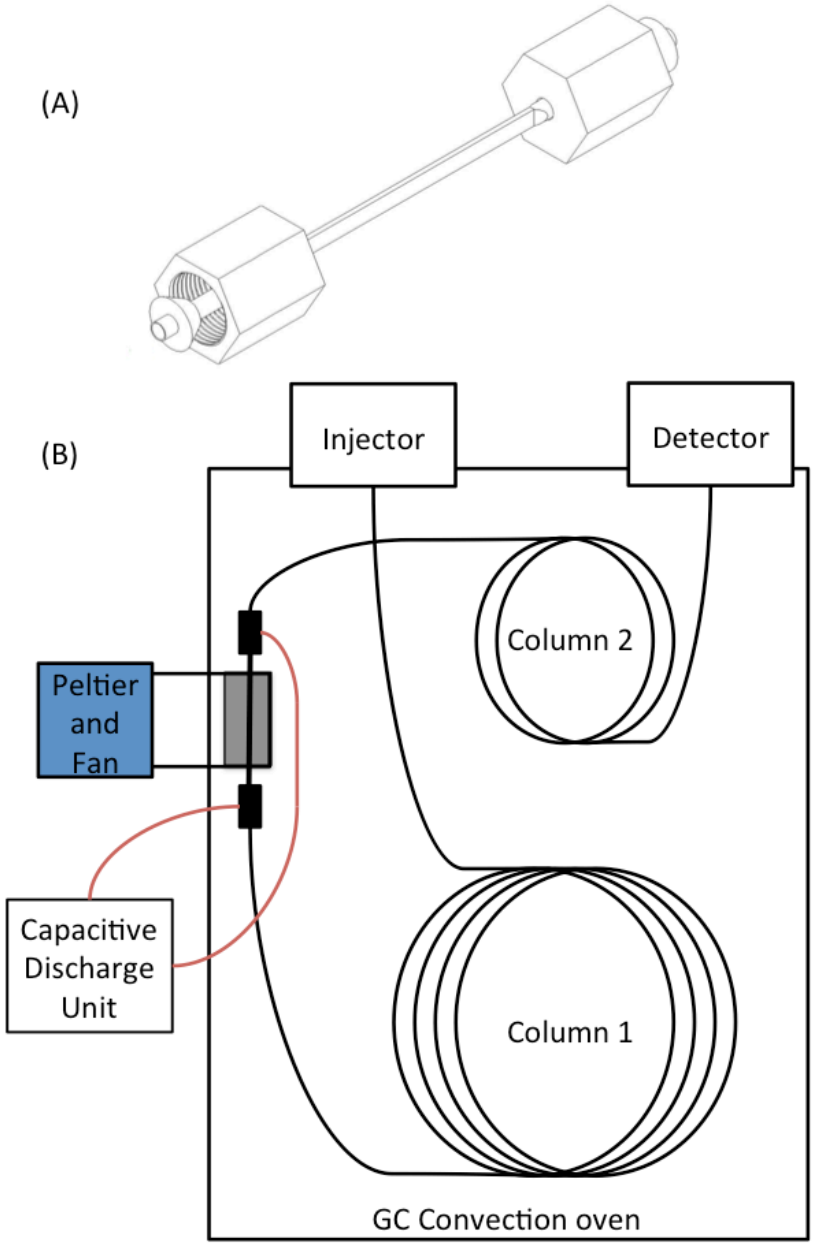

Figure 47 Schematic diagram of the single-stage thermal modulator (A) and its installation in a GC convection oven (B).

The modulator differs substantially from the previous incarnations of SS capillary modulators [41,43,45-47,52]. In particular the chemistry of the stationary phase was substantially modified (as discussed in Chapter 4) compared with the initial MXT-5

stationary phase. The thermal-oxidative treatment resulted in the formation of nanoparticles embedded within the SS capillary stationary phase coating, and the oxidation of the PDMS phase resulted in a more polar stationary phase compared to the initial stationary phase. The stationary phase used in this modulator is identical to the coating used by Muscalu *et al*. however the size of the modulator was substantially reduced compared to that device [48]. Specifically, the trapping capillary was reduced in length from 13 cm to 6 cm long, and the mass of the heat sink device was reduced from 1.6 kg to just 0.43 kg and it was made to be more compact in size. This reduction in size was intended to enable the possibility of portable GC × GC analysis using the Calidus™ GC instrument.

5.3.2 Modulator performance evaluation

The ability of this modulator to trap and mobilise focused solutes was assessed by analysing a test mixture composed of 13 compounds with different chemical functionalities, to determine the modulators ability to trap and focus a variety of solutes. A range of concentrations (0.5 to 100 mg kg^{-1}) were analysed in triplicate to determine the trap's solute loading capabilities and measure its repeatability. A one-dimensional chromatogram of a separation obtained using this modulator is shown in Figure 48.

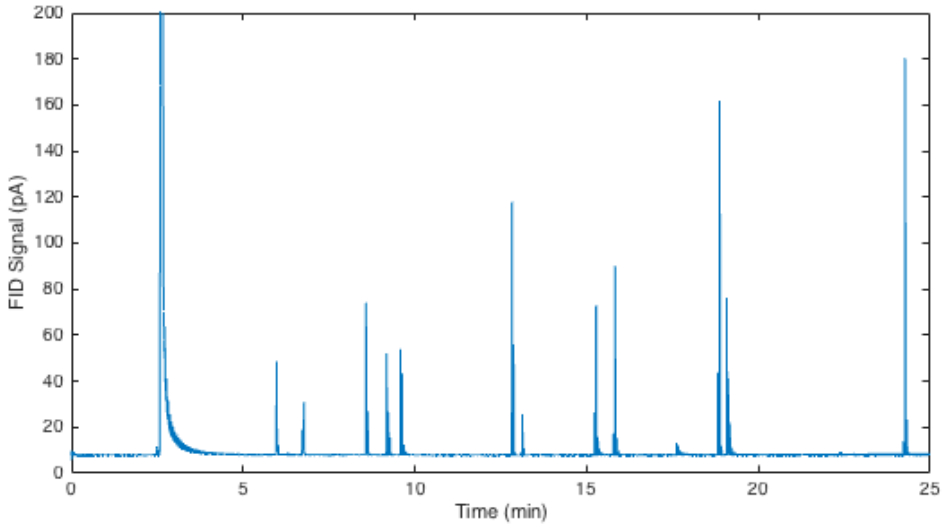

Figure 48 One-Dimensional chromatogram of a modulated GC × GC experiment. The sample was a 13-component test mix (100 mg kg^{-1}, 1 µL injection at 100:1 split ratio), see Table 12 for component list, retention times and peak statistics.

All solutes were well modulated with the exception of *n*-octane (boiling point 125 °C [39]), which showed substantial amounts of solute breakthrough. Approximately 21% of the mass of *n*-octane was passing through the trap without being focused, despite the stationary phase coating and cooling provided by the modulator device. Interestingly, toluene (boiling point 110 °C [39]) was well focused by the modulator, suggesting that the stationary phase of the trap has enhanced solute loading capacity for more polar aromatic compounds, compared to volatile non-polar solutes such as *n*-octane. The first peak that eluted in the chromatogram was toluene at 5.96 min (Figure 49). The modulation of this volatile solute was not 100 % successful, as seen in the chromatogram; some of the toluene effluent broke through the modulator as shown by the fronting component of the peak at 5.975 min. Additionally once the heating event was initiated the cooling of the modulator was not quick enough to prevent further solute breakthrough in the form of peak tailing. The boiling point of toluene is 110° C,

which is not particularly volatile given the preferred goal of being able to modulate solutes as volatile as *n*-pentane (boiling point 36 °C).

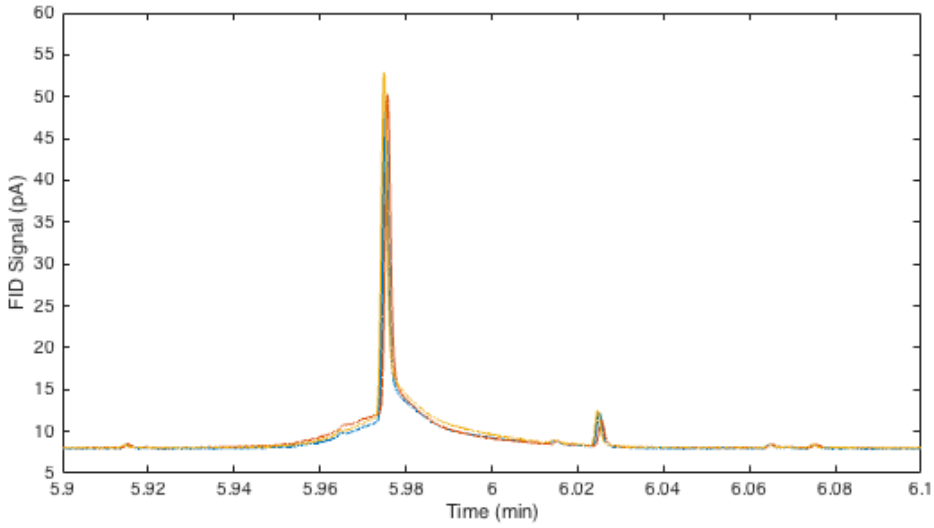

Figure 49 Zoom in view of Figure 48 region (5.9 to 6.1 min) showing the toluene peak modulated (P_m = 3.0 s), 3 runs are overlaid to show repeatability.

The second peak in the test mix was *n*-octane, which had an elution time of 6.750 min and this peak showed significant breakthrough (Figure 50), even more than the earlier eluting toluene peak shown in Figure 49. The boiling point of *n*-octane is 125 ° C which led to *n*-octane eluting after the more volatile toluene solute, however it was interesting to note that the more polar toluene solute exhibited far less breakthrough compared the less volatile *n*-octane. This indicates that the modulator itself has some selectivity and increased solute capacity for more polar compounds compared to aliphatic hydrocarbon compounds.

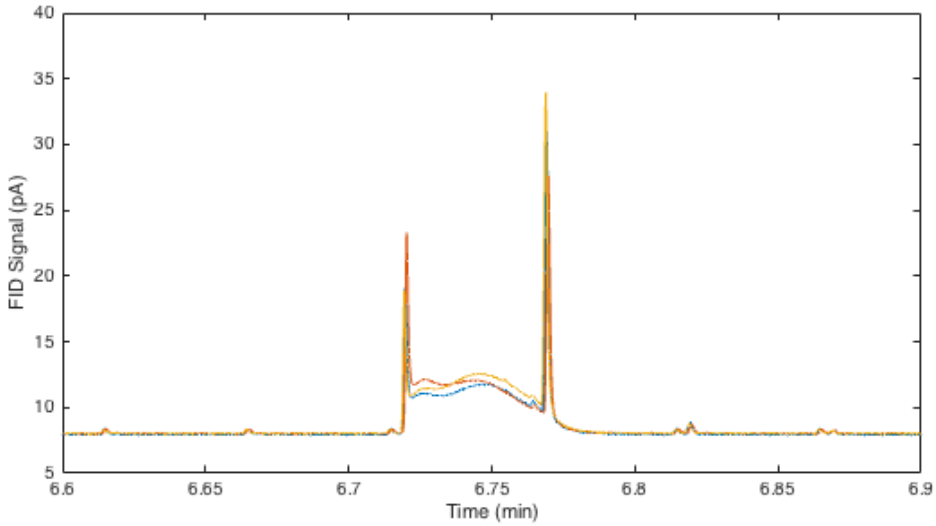

Figure 50 Zoom in view of Figure 48 region (6.6 to 6.9 min) showing the *n*-octane peak modulated (P_m = 3.0 s), 3 runs are overlaid to show repeatability.

The next solute to elute was another volatile aromatic species, ethylbenzene (boiling point 136 °C), with a retention time of 8.592 min (Figure 51), showing improved peak shape compared to the more volatile aromatic compound, toluene. The slight tailing present for the first modulated peak (8.58 min) indicated that the cooling speed of the modulator trap was not fast enough to prevent a small portion of breakthrough from occurring.

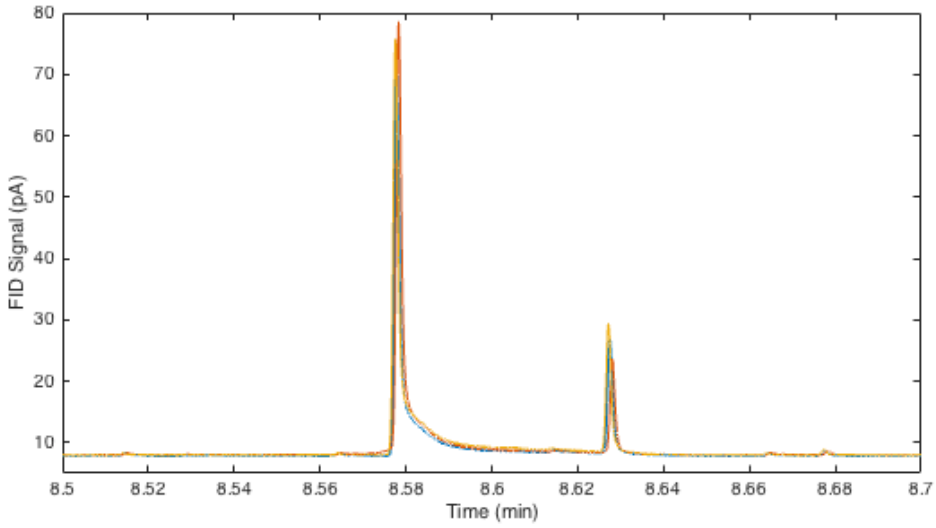

Figure 51 Zoom in view of Figure 48 region (8.5 to 8.7 min) showing the ethylbenzene peak modulated (P_m = 3.0 s), 3 runs are overlaid to show repeatability.

Modulation of 2-heptanone (boiling point 151 °C) eluting at 9.20 min revealed excellent second-dimension peak symmetry for a polar solute with a ketone functionality (Figure 52). Peak symmetry was substantially improved for this solute compared to the earlier eluting solutes.

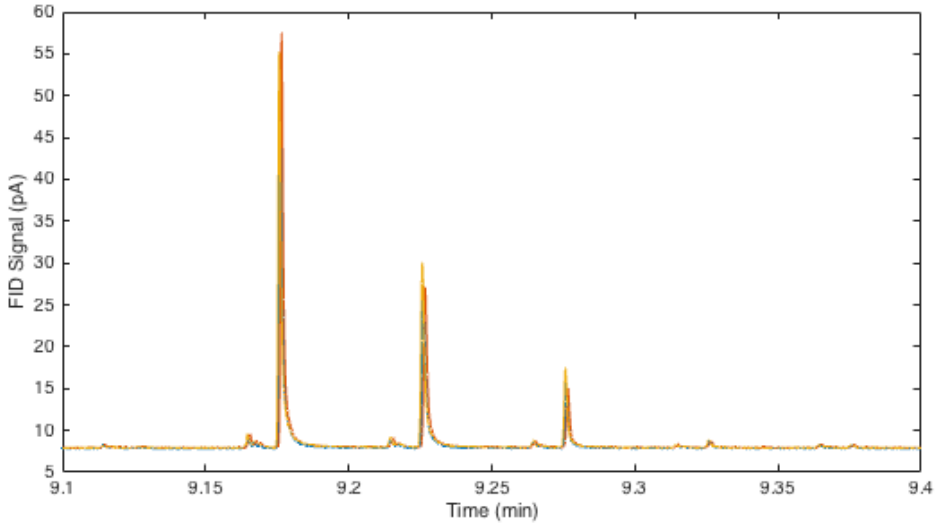

Figure 52 Zoom in view of Figure 48 region (9.1 to 9.4 min) showing the 2-heptanone peak modulated (P_m = 3.0 s), 3 runs are overlaid to show repeatability.

The remaining polar solutes (pentylacetate, 2-octanol, 2-nonanone, 1,6-hexanediol, 2-decanol, 4-chlorophenol) also displayed similar peak symmetry and were well-modulated first-dimension peaks with minimal breakthrough evident in the one-dimensional chromatogram. Since the polar solutes were retained more strongly by the second-dimension column than *n*-alkane compounds, due to the polar Rxi17Sil MS stationary phase (35 % diphenyl- 65 % dimethylpolysiloxane equivalent), which caused second-dimension peak broadening compared to non-polar analytes.

The modulation of *n*-decane is shown in Figure 53, showed clean modulation of this solute, with some tailing on the most concentrated modulation peak at 12.83 min. This tailing indicated solute breakthrough during the cool down of the trap following capacitive discharge.

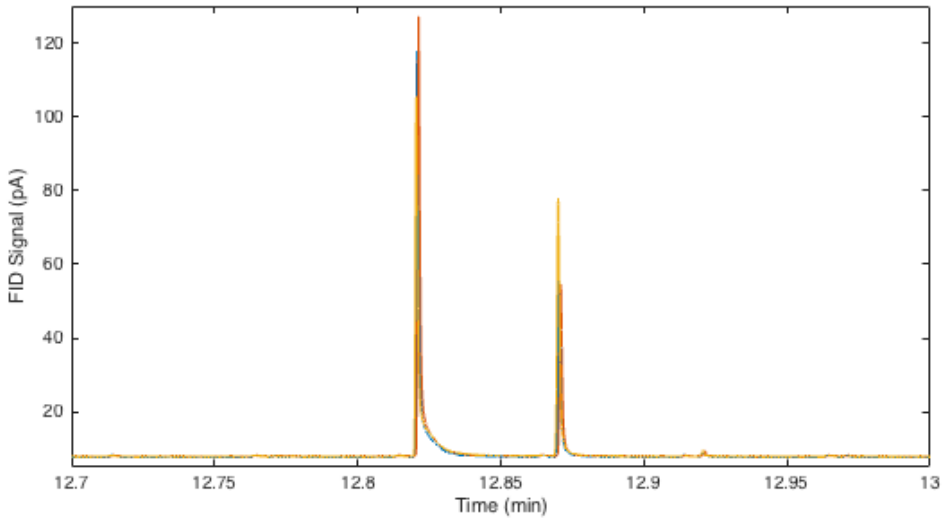

Figure 53 Zoom in view of Figure 48 region (9.1 to 9.4 min) showing the *n*-decane peak modulated (P_m = 3.0 s), 3 runs are overlaid to show repeatability.

The other non-polar solutes in the test mix (*n*-dodecane, *n*-tetradecane) with volatilities less than that of *n*-decane (boiling point 174 °C) displayed reduced breakthrough levels during modulator capillary cooling, although some small tailing was still present for these solute modulations.

Average relative standard deviations (RSD %) of 9×10^{-5} and 2.7 % were achieved for the first- and second-dimension retention times respectively, which compared favourably with other GC × GC modulators [25,41,48,52]. The second-dimension peak widths of each solute are summarised in Table 12, with average values on the order of 72 ± 3 ms measured at half height. The peak symmetry factors for polar solutes were on average 1.9 ± 0.3, while non-polar solutes displayed greater asymmetry with a symmetry factor of 2.8 ± 0.5. These symmetry factors showed that all of the modulated peaks were tailing, which caused a corresponding loss in second dimension separation efficiency. Ideally a symmetry factor of 1 should be obtained, with values of up to 1.3 being considered excellent depending on the solute and stationary phase. The improved symmetry statistics for the polar solutes was likely due to the compatibility of each of these solutes with the polar modulator phase and polar second-dimension column. Presently the narrow peaks generated by the modulator are still able to provide good resolution of solutes despite the evident tailing as shown in Figure 54.

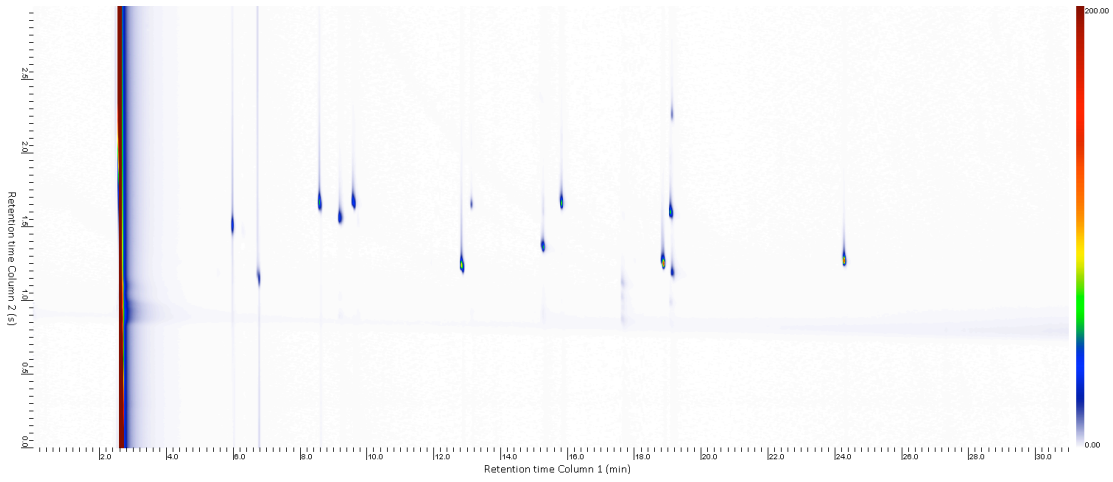

Figure 54 Two-dimensional chromatogram of a 13-component test mix (100 mg kg^{-1}, 1 µL injection at 100:1 split ratio), with a 3.0 s modulation period. See Table 12 for component list, retention time, and peak width and peak symmetry statistics.

The tailing of the peaks generated by the present modulator was caused by the slow cooling speed of the modulator trap following each heating event. Attempts to enhance the cooling of the heat sink device with Peltier cooling were not successful due to the limited rate of heat transfer through the ceramic grips that are used to hold the modulator within the GC convection oven. This consumable free system provided comparable performance to cryogenic and thermal modulation GC × GC systems for solutes with volatilities less than *n*-octane. Cryogenic modulators produce peaks with widths between 20 and 120 ms at half height depending on the solute, second-dimension column properties, and the optimisation of the hot and cold jets [11,34].

Previous work using capacitive discharge thermal modulation demonstrated peak widths between 60 to 160 ms at half height indicating that the present design provided significant improvements over previous designs, although the reduction in trap length reduced its capacity for volatile solutes [43,47]. Average relative standard deviations (RSD %) of 9×10^{-5} and 2.7 were achieved for the first- (^1t_R) and second dimension (^2t_R) retention times respectively, which compared favourably with other thermal and cryogenic modulators [25,41,48,52]. An average peak volume repeatability of 3 % RSD (Table 13) was obtained, which is sufficient for quantitative analysis. Ranges of different test mix concentrations were injected to determine mass loading capabilities of the GC × GC modulator. A bi-logarithmic plot of peak volume (V_p) *versus* solute mass (m_s) was used to assess the loss of solute mass to breakthrough, where slopes of plots lower than 1 represent solute losses to breakthrough [43,52].

Table 12 Peak statistics for test compounds for Figure 54 including: retention time and peak volume repeatability (n = 12); Log-Log slope and linearity test (n = 12, F_{crit} = 3.45); the second-dimension peak widths at half peak height (300 pg solute mass of *n*-octane, and 150 pg solute mass for all other solutes, n = 3, α = 0.05) and the symmetry factor (300 pg solute mass of *n*-octane and 150 pg for all other solutes, n = 3, α = 0.05).

Compound	^1t_R (min)	^1t_R (RSD %)	^2t_R (RSD %)	^{2}D Peak width (ms)	^{2}D Peak Symmetry
toluene	5.959	1.7×10^{-4}	2.3	93 ± 3	1.5 ± 0.2
n-octane	6.750	1.5×10^{-4}	3.4	88 ± 3	1.7 ± 0.2
ethylbenzene	8.592	1.2×10^{-4}	2.3	88 ± 6	1.6 ± 0.3
2-heptanone	9.200	1.1×10^{-4}	2.6	77 ± 3	2.5 ± 0.3
pentylacetate	9.625	1.0×10^{-4}	2.4	110 ± 1	1.7 ± 0.7
n-decane	12.850	7.8×10^{-5}	3.1	52 ± 3	3.3 ± 0.9
2-octanol	13.139	7.6×10^{-5}	2.3	67 ± 3	1.6 ± 0.5
2-nonanone	15.305	6.5×10^{-5}	2.9	55 ± 1	2.4 ± 0.3
1,6-hexanediol	15.857	6.3×10^{-5}	2.3	72 ± 3	2.2 ± 0.1
n-dodecane	18.904	5.3×10^{-5}	3.2	45 ± 1	3.4 ± 1.3
2-decanol	19.150	5.2×10^{-5}	2.3	70 ± 1	2.0 ± 0.6
4-chlorophenol	19.168	1.5×10^{-4}	2.8	72 ± 3	1.6 ± 0.3
n-tetradecane	24.350	4.1×10^{-5}	3.2	47 ± 3	2.7 ± 0.4

The calibrations were linear across the concentration range of 5 to 1300 pg (mass on column) for most solutes with an average limit of detection (LOD) of 70 pg of solute mass (on column) using a FID.

Table 13 Quantitative performance for each component of the 13-component test mix.

Compound	Peak Volume (RSD %)	Log-Log Slope (Peak volume *vs.* mass)	$F_{experimental}$	LOD (pg)
toluene	5.3	1.00 ± 0.02	2.61	132
n-octane	3.0	0.79 ± 0.01	1.04	207
ethylbenzene	4.3	0.96 ± 0.01	1.80	113
2-heptanone	3.9	1.06 ± 0.01	1.10	37
pentylacetate	4.3	1.24 ± 0.03	2.51	43
n-decane	0.9	1.03 ± 0.01	2.30	34
2-octanol	1.9	1.19 ± 0.03	1.14	62
2-nonanone	2.4	1.28 ± 0.02	3.05	29
1,6-hexanediol	3.0	1.12 ± 0.01	2.45	19
n-dodecane	1.7	1.02 ± 0.01	3.10	29
2-decanol	1.9	1.18 ± 0.02	1.26	22
4-chlorophenol	4.9	1.19 ± 0.03	1.38	160
n-tetradecane	2.6	0.97 ± 0.01	1.17	21

Approximately 20% of the mass of *n*-octane was being lost in the form of component breakthrough as was expected after inspecting the one-dimensional chromatogram. A number of test compounds also revealed log V_p - log m_s slopes greater than 1, indicating that the modulator improving the mass sensitivity of the FID used during the GC analysis, and this effect was particularly pronounced for the more polar compounds in the test mix.

The optimisation of this capacitive discharge-based thermal modulator is very simple compared to other modulators. Cryogenic modulation requires careful optimisation of the cryogen flow rate and hot jet durations, and flow modulated GC

systems require careful balancing of system pressures to ensure that proper modulation is achieved. The present modulator only requires adjustment of the capacitive discharge voltage to ensure that focused compounds are adequately mobilised in a narrow injection band. It is important that the voltage selected is not too high so as to cause analytes to be pyrolysed during desorption from the trap, or destruction of the metal capillary by over heating. A charging voltage of 21 V was sufficient to provide solute remobilisation for the present analysis. Finally, it is important to ensure that the trapping capillary is carefully aligned between the two ceramic pads to ensure that it is satisfactorily cooled.

5.3.3 Method development for GC × GC analysis of petroleum spill samples

To develop a method for the separation of a light fraction of diesel, known as Special Antarctic blend (SAB) diesel, a range of conditions and stationary phase columns were tested. Initially a combination of a BPX5 (equivalent to a 5% diphenyl- 95% dimethylpolysiloxane stationary phase coating), 25 m × 220 μm ID × 0.25 μm d_f first-dimension column and a Stabilwax (a cross-bonded polyethylene glycol stationary phase coating) 1 m × 150 μm ID × 0.15 μm d_f second-dimension was selected as a column ensemble that could potentially provide a good separation of the components in the diesel based sample [1]. The choice of a BPX5 column matched with the existing one-dimensional GC method used by the Australian Antarctic Division (AAD) for petroleum spill analysis [58-61].

Hydrogen was used as the carrier gas due to the high efficiency separations that it enables, while maintaining a high speed of analysis. The column flow rate was set to a flow of 0.9 mL min^{-1} to minimise the possibility of solute breaking through the GC × GC modulator given its low capacity for solutes. Additionally, the operation of the system at a low carrier gas flow rate is necessary to ensure that the peaks generated by the first

dimension are sufficiently broad enough at the point of elution that three or more modulations can be obtained using the modulator.

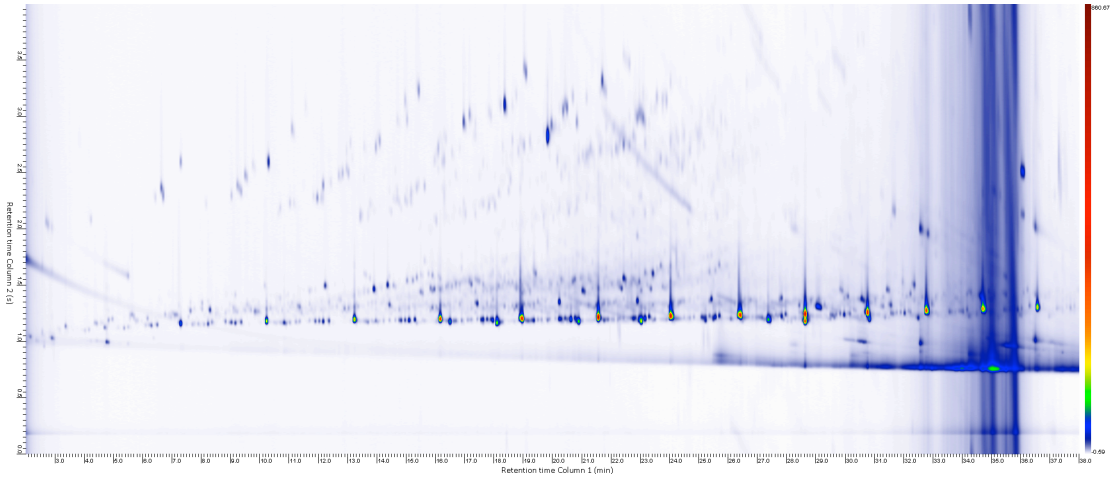

Figure 55 Two-dimensional chromatogram of a separation of SAB diesel (1 µL, 20:1 split ratio, 2250 ppm). ^{1}D column BPX5, 25 m × 220 µm ID × 0.25 µm d_f, ^{2}D column Stabilwax, 1.0 m × 150 µm ID × 0.15 µm d_f. Carrier gas hydrogen, flow rate 0.9 mL min^{-1}, temperature program 40 °C (1 min) then ramped at a rate of 4 °C min^{-1} to 280 °C (hold 1 min). P_m = 4.0 s, 24 V discharge voltage.

There was evidence of solute wraparound in the second dimension column so the second dimension was trimmed down to 70 cm in length to yield the following separation. There were a number of late eluting peaks in this chromatogram that were artifacts from the previous sample injection that were not eluted from the first-dimension column at a temperature of 280 °C which was used in the previous experiment. Unfortunately 280 °C is the maximum stable temperature for a polyethylene glycol based stationary phase such as the Stabilwax column, therefore a different second-dimension column had to be selected despite the favourable two-dimensional separation that had been obtained for the more volatile components of the SAB sample.

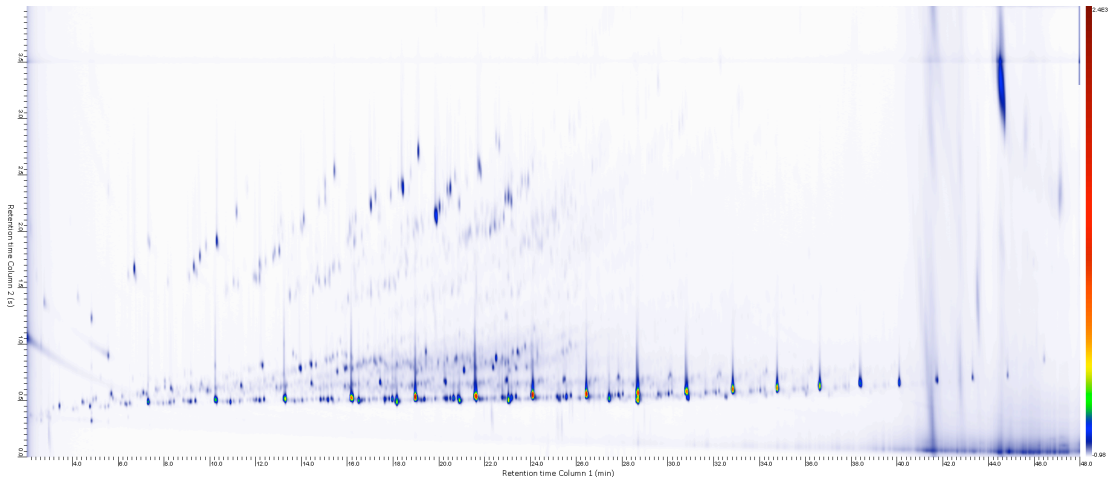

Figure 56 Two-dimensional chromatogram of a separation of SAB diesel (1 µL, 20:1 split ratio, 2250 ppm). ^{1}D column BPX5, 25 m × 220 µm ID × 0.25 µm d_f, ^{2}D column Stabilwax, 0.7 m × 150 µm ID × 0.15 µm d_f. Carrier gas hydrogen, flow rate 0.9 mL min^{-1}, temperature program 40 °C (1 min) then ramped at a rate of 4 °C min^{-1} to 280 °C (hold 1 min). P_m = 4.0 s, 24 V discharge voltage.

The second-dimension column was changed to a more temperature stable Rxi17SIL MS column (equivalent stationary phase to a 50 % diphenyl- 50 % dimethylpolysiloxane column) 1 m × 150 µm ID × 0.15 µm d_f that had a maximum operating temperature of 330 °C, similar to the first-dimension column. This column combination allowed the temperature range of the analysis to be extended and provided the following separation (Figure 57).

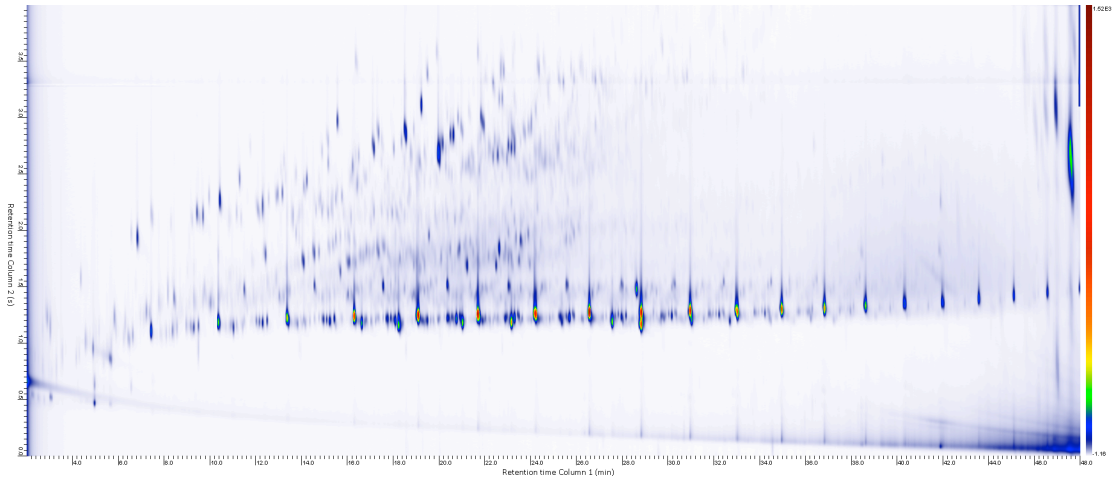

Figure 57 Two-dimensional chromatogram of a separation of SAB diesel (1 µL, 20:1 split ratio, 2250 ppm). ^{1}D column BPX5, 25 m × 220 µm ID × 0.25 µm d_f, ^{2}D column Rxi17SIL MS, 1.0 m × 150 µm ID × 0.15 µm d_f. Carrier gas hydrogen, flow rate 0.9 mL min^{-1}, temperature program 40 °C (1 min) then ramped at a rate of 4 °C min^{-1} to 280 °C (hold 1 min). P_m = 4.0 s, 24 V discharge voltage.

Similarly, this chromatogram showed that some solutes were being retained for an excessive time on the second-dimension column and were wrapping around. The second-dimension column was again trimmed to 70 cm to yield the following separation (Figure 58). The separation obtained using the Rxi17Sil stationary phase was superior for the present sample due to its excellent selectivity for the aromatic components that are constituents of the SAB diesel sample. The chromatographic run time and final temperature were then extended to ensure that the artifact compounds from previous runs were eluted in a single run (Figure 59).

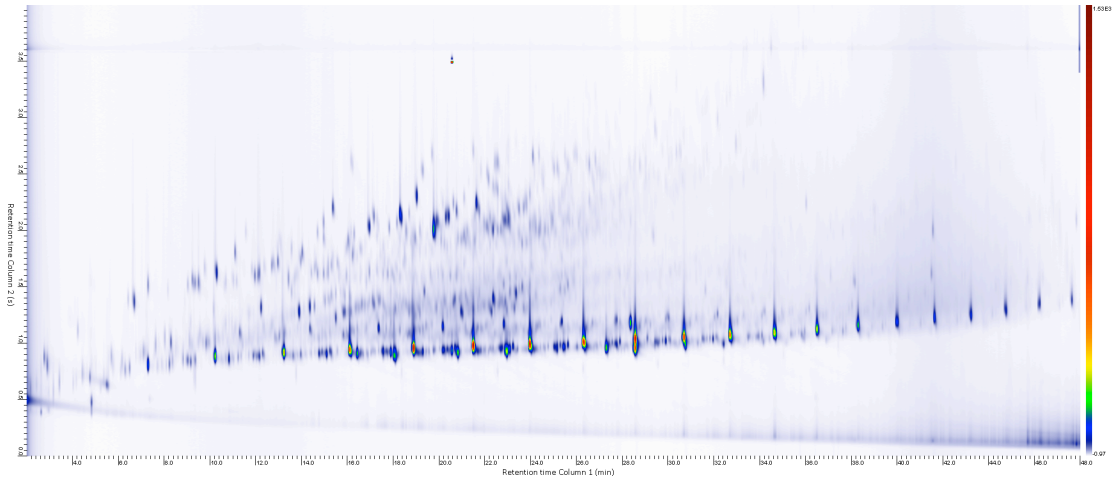

Figure 58 Two-dimensional chromatogram of a separation of SAB diesel (1 µL, 20:1 split ratio, 2250 ppm). ^{1}D column BPX5, 25 m × 220 µm ID × 0.25 µm d_f, ^{2}D column Rxi17Sil ms, 0.7 m × 150 µm ID × 0.15 µm d_f. Carrier gas hydrogen, flow rate 0.9 mL min^{-1}, temperature program 40 °C (1 min) then ramped at a rate of 4 °C min^{-1} to 280 °C (hold 1 min). P_m = 4.0 s, 24 V discharge voltage.

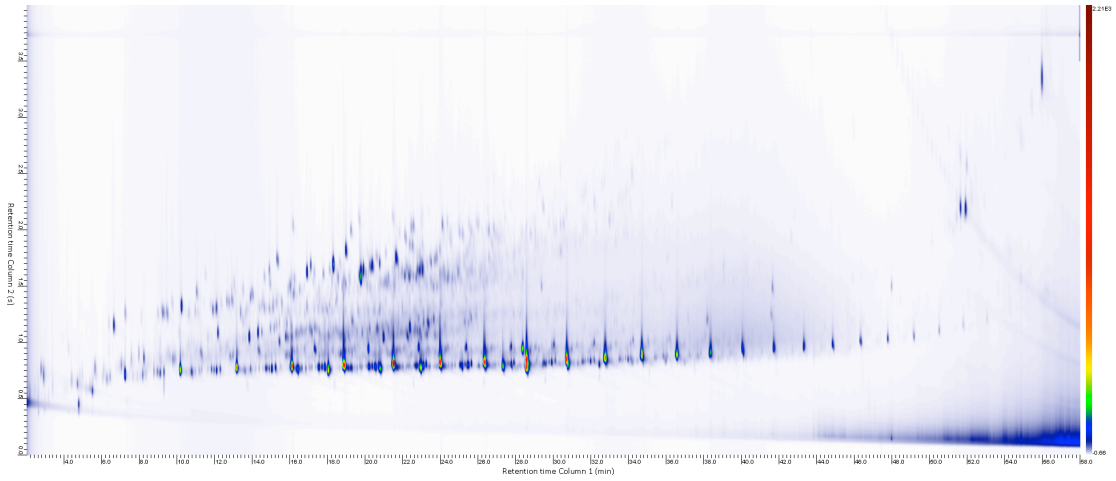

Figure 59 Two-dimensional chromatogram of a separation of SAB diesel (1 µL, 20:1 split ratio, 2250 ppm). ^{1}D column BPX5, 25 m × 220 µm ID × 0.25 µm d_f, ^{2}D column Rxi17SilMS, 0.6 m × 150 µm ID × 0.15 µm d_f. Carrier gas hydrogen, flow rate 0.9 mL min^{-1}, temperature program 40 °C (1 min) then ramped at a rate of 5 °C min^{-1} to 330 °C (hold 1 min). P_m = 4.0 s, 24 V discharge voltage.

Increasing the final temperature of analysis substantially increased the column bleed from the first-dimension column, however the second-dimension easily resolved the components of the sample from the column bleed in the second-dimension separation. The speed of the temperature ramp was also increased from 4 to 5 °C min^{-1} so as to not increase the time of analysis substantially. Additionally, the second-dimension column was trimmed to 60 cm to compensate for the additional retention that would be experienced in the second dimension due to solutes being eluted at an earlier retention time as a result of the faster temperature ramp rate.

The effect of changing the discharge voltage on the GC × GC modulation and two-dimensional separation was then assessed in a series of injections of the SAB sample using a range of different discharge voltages from 24 to 16 V (Figure 60, Figure 61 and Figure 62).

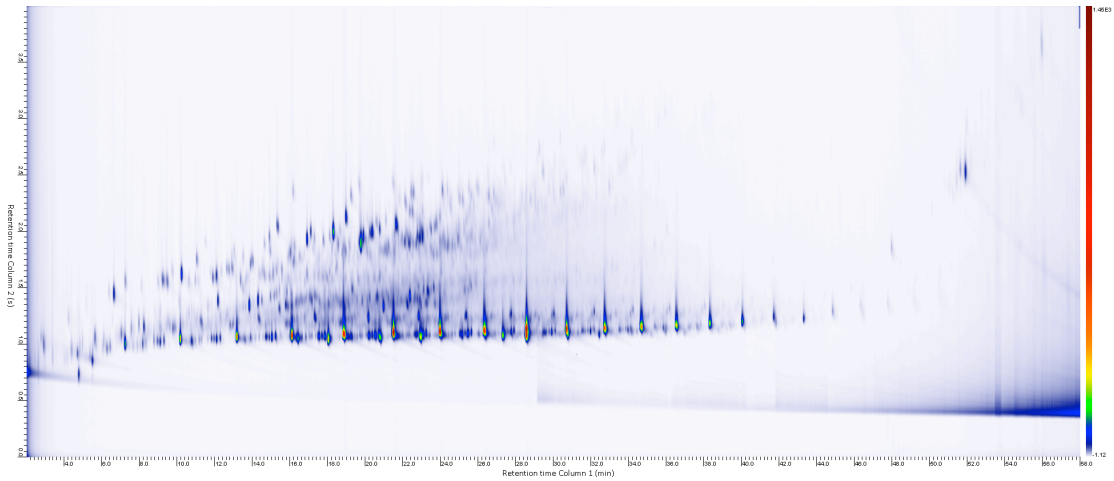

Figure 60 Two-dimensional chromatogram of a separation of SAB diesel (1 µL, 20:1 split ratio, 2250 ppm). Discharge voltage changed to 22 V.

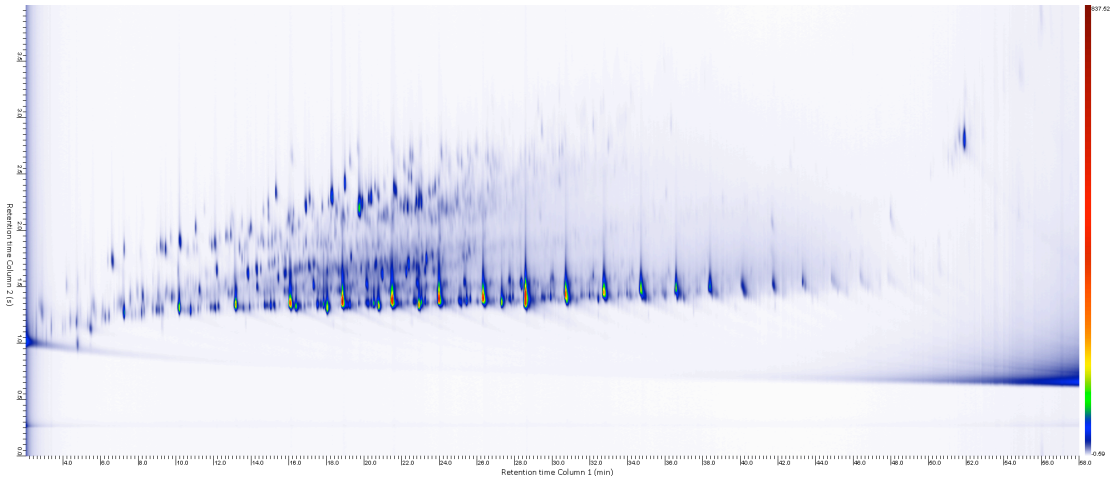

Figure 61 Two-dimensional chromatogram of a separation of SAB diesel (1 µL, 20:1 split ratio, 2250 ppm). Discharge voltage changed to 20 V.

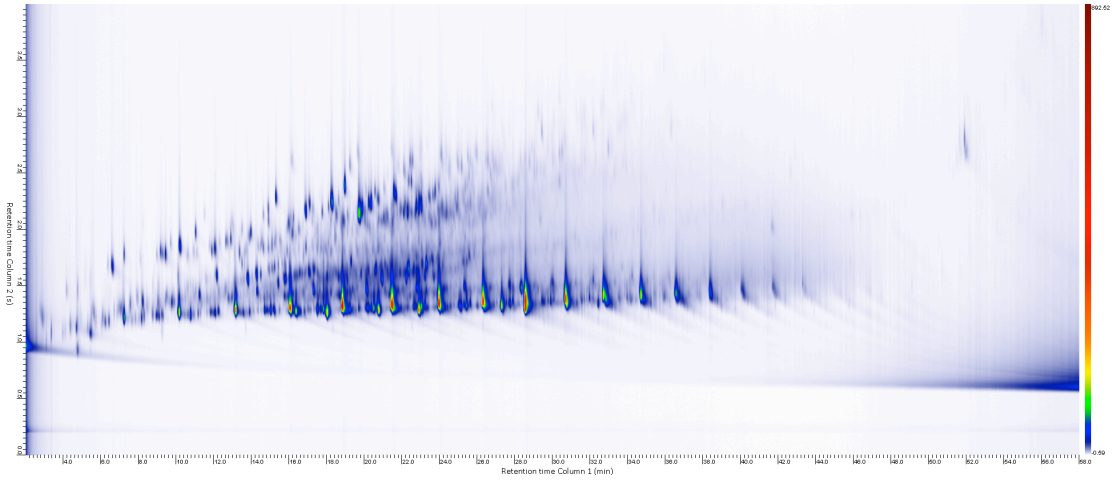

Figure 62 Two-dimensional chromatogram of a separation of SAB diesel (1 µL, 20:1 split ratio, 2250 ppm). Discharge voltage changed to 18 V.

The reduction in discharge voltage from 24 to 18 V did not cause a substantial reduction in the performance of the modulator (Figure 62). Peak widths and symmetries were maintained for all of the solutes. A discharge voltage of approximately 18 V was capable of yielding trap heating to temperatures in excess of 330 °C which should be sufficient for the present sample, therefore this voltage was utilised for further experiments. Operation at lower discharge voltages reduces the maximum temperature of the modulator during capacitive discharge, which is beneficial for preserving the

stationary phase of the trap, and minimising the possibility of solute degradation during the heating of the SS capillary. Libardoni *et al.* previously explored the possibility of programming the discharge voltage throughout a temperature-programmed GC experiment to ensure that discharge temperatures better matched the temperature required to mobilise solutes [52]. The addition of this programmable discharge setting could be very useful for preserving the integrity of the SS capillary and stationary phase coating.

The modulation period was varied between 6 and 3 s to determine the optimum setting for the diesel sample. To select an appropriate modulation it is important to know the width of peaks eluting from the first-dimension column, so that a duration can be selected that allows each peak to be sampled at least three times by the modulator. Long modulation periods provide a longer time to complete a second-dimension separation, however this comes at the cost of separation resolution in the first-dimension. The peaks generated by the first-dimension column were approximately 14 s wide at the base of each peak, which meant that a modulation period of 6 s was not able to obtain the requisite 3 to 4 modulations for each peak. A modulation period of 4 s was expected to provide a sufficient number of modulations per first dimension peak, and this was verified by injecting a mixture of *n*-alkanes (Figure 63). At least 3 modulation slices were obtained per first-dimension peak using the present experimental conditions.

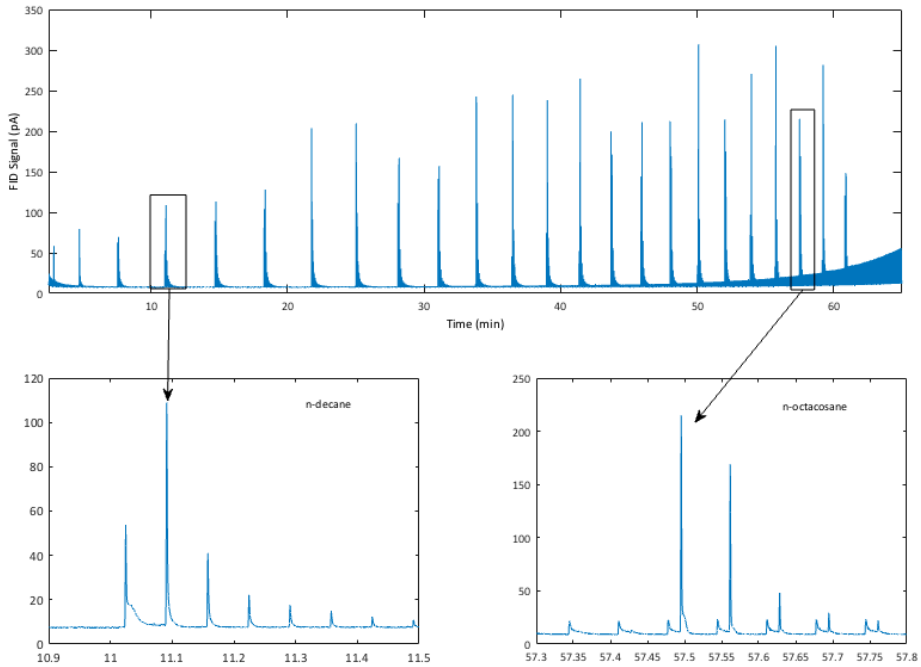

Figure 63 One-dimensional chromatogram of *n*-alkane test mixture (C7 to C30) with select insets of *n*-decane and *n*-octacosane showing the number of modulation slices obtained per peak.

The second-dimension column was further modified to a BPX50 stationary phase (equivalent to the RxiSIL MS stationary phase or 50% diphenyl- 50% dimethyl polysiloxane coating) with a narrower diameter to enhance the separation efficiency and speed of the column (1 m × 100 µm ID × 0.1 µm d_f) after experiments revealed significant wraparound for polyaromatic hydrocarbon species. To verify that the separation method would be effective for a wide variety of potential diesel based samples it was important to ensure that polar compounds such as naphthalene and other polyaromatic species would not be excessively retained by the second-dimension column. A mixture of *n*-alkanes, and prevalent aromatic and polyaromatic species was prepared to gauge the utilisation of the two-dimensional separation space and separation of this mixture is shown in Figure 64.

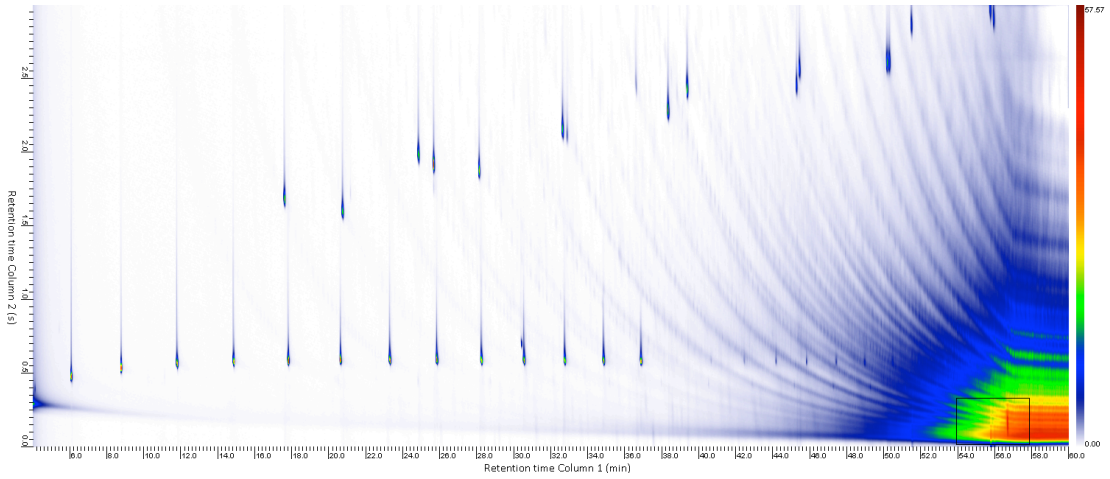

Figure 64 Two-dimensional chromatogram of a separation of a mixture of extractable petroleum hydrocarbon (EPH) aromatics (10 ppm, Restek # 31458) and *n*-alkanes (10 ppm, C_8 to C_{20}) SAB diesel (1 µL, 20:1 split ratio, 2250 ppm). ^{1}D column DB5-MS, 25 m × 250 µm ID × 0.25 µm d_f, ^{2}D column Rxi17Sil ms, 1.0 m × 100 µm ID × 0.1 µm d_f. Carrier gas hydrogen, flow rate 1.0 mL min^{-1}, temperature program 40 °C (1 min) then ramped at a rate of 5 °C min^{-1} to 280 °C (hold 1 min). P_m = 3.0 s, 18 V discharge voltage. The black box in the chromatogram highlights three peaks (Indeno(1,2,3-cd)pyrene, Dibenz(a,h)anthracene and Benzo(g,h,i)perylene) that are showing wraparound.

The modulation period was reduced to 3 s to ensure that three modulations were obtained for each first-dimension peak, including trace components that are present in the SAB sample. This had the unfortunate effect of causing three polyaromatic hydrocarbon species (Indeno(1,2,3-cd)pyrene, Dibenz(a,h)anthracene and Benzo(g,h,i)perylene) to wraparound on the second-dimension column. Wraparound into the first-dimension column bleed region complicated quantification, however these components were not expected to be present in SAB diesel as confirmed by Figure 65. However it was still useful to have information about the distribution of polar (polyaromatic) species in the separation space of this GC × GC separation.

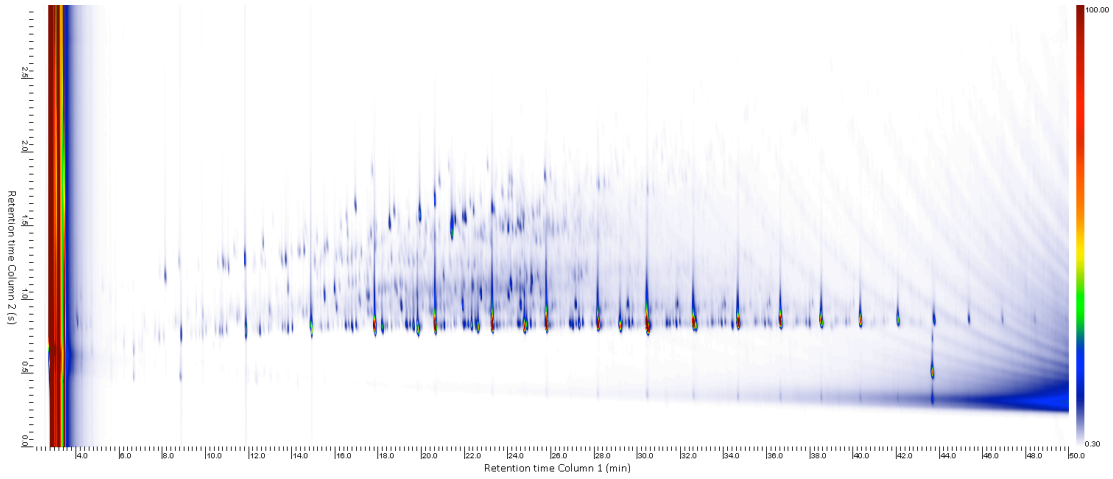

Figure 65 Two-dimensional chromatogram of Special Antarctic Blend (SAB) diesel (3000 mg kg^{-1} in *n*-hexane). ^{1}D column DB5-MS, 25 m × 250 µm ID × 0.25 µm d_f, ^{2}D column Rxi17Sil ms, 1.0 m × 100 µm ID × 0.1 µm d_f. Carrier gas hydrogen, flow rate 1.0 mL min^{-1}, temperature program 40 °C (1 min) then ramped at a rate of 5 °C min^{-1} to 280 °C (hold 1 min). P_m = 4.0 s, 18 V discharge voltage.

This stationary phase combination and experimental conditions were very effective for separating the petroleum spill samples of interest as demonstrated by a number of other authors in the literature [1,56,62-64]. This method was then applied to the analysis of a range of soil extracts obtained from Macquarie Island that had experienced petroleum contamination, with the goal of fingerprinting the type, quantifying the amounts, and mapping the position of petroleum contamination at two locations on Macquarie Island.

5.3.4 Petroleum mapping of spill sites at Macquarie Island

Petroleum hydrocarbon (PHC) contamination of Antarctic and sub-Antarctic terrestrial environments is a significant problem arising from human polar exploration and research [65,66]. Conventional single-dimensional GC is unable to adequately separate the components of these PHC contaminated soils due to the complexity of

petroleum and its degradation products [67,68]. GC × GC can be used to enhance the separation of complex petroleum spills, by separating compounds in two temporal dimensions [1,69]. Analysis of petroleum based samples using GC × GC has been well established in a number of studies, and offers benefits in terms of signal enhancement as well as simplifying the integration of peak volumes, due to the constant presence of a reliable baseline throughout the GC × GC chromatogram [67,70-75]. Furthermore, the two-dimensional chromatograms that are generated can be used to fingerprint samples and determine the source or type of petroleum contamination at a location [76].

The present GC × GC platform was applied to the separation of PHC present in contaminated soil sample extracts sourced from Macquarie Island. Macquarie Island is a small sub-Antarctic island that is located 1,500 km southeast of Australia. It serves as a critical breeding location for seals and sea birds, and a permanent research station has been maintained there since 1948 for the purposes of studying sub-Antarctic wildlife, and as a resupply station for Antarctic operations. There have been a number of petroleum spill incidents with release volumes ranging from 100 to 10,000 L, and remediation of these petroleum spills is on-going [54]. The risk posed by PHC has been evaluated using microbial and invertebrate species that are indigenous to Macquarie Island [55,77,78]. PHC levels from 50 to 200 mg kg^{-1} (of soil) have been found to pose significant risk to the health of the islands' ecosystem, and these threshold values indicate the need to actively remediate an area of contaminated soil. A map of the location of Macquarie Island in the southern ocean and the position of the two fuel spill sites evaluated herein is shown in Figure 66.

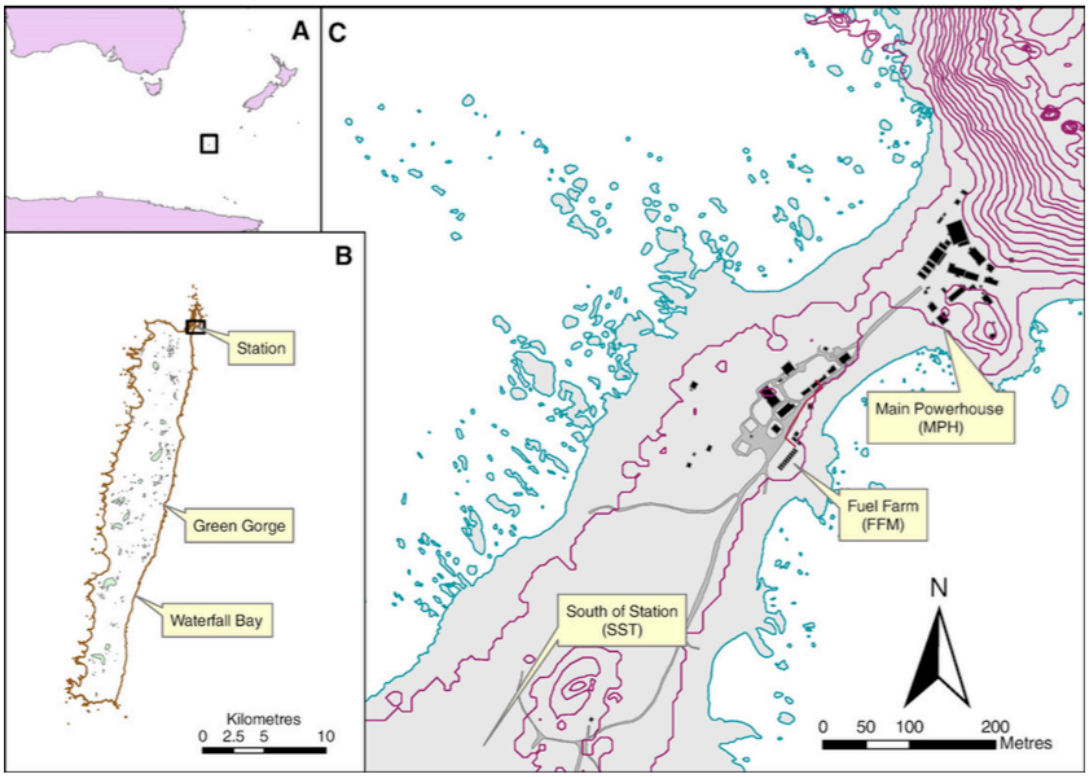

Figure 66 A, location of Macquarie Ocean in the Southern Ocean; B, location of Macquarie Island Station and reference sample sites south of the station; C, location of the contaminated areas investigated at the main power house (MPH) and fuel farm (FF) sites. Reproduced with permission from Elsevier (2007) from reference [54].

The FF site is centred at a fuel bunker containing eight fuel tanks (35,000 L each) that are surrounded by a containing wall constructed in 1991. The soil at this location is mostly sandy and free draining, with a water table 10-30 cm below the surface, with fuel contamination estimated to be between 500 and 15,800 mg kg^{-1} (of soil) (total estimated soil contamination 600 tonnes of soil)[54]. The MPH site is centred on the research station's generator location, which has similar sand soil types to the FF site on the north, east and south sides, while the western side of the site is characterised by peat type soil. PHC contamination levels up to 7000 mg kg^{-1} soil are expected at the MPH site, with an estimated 180 tonnes of contaminated soil [54].

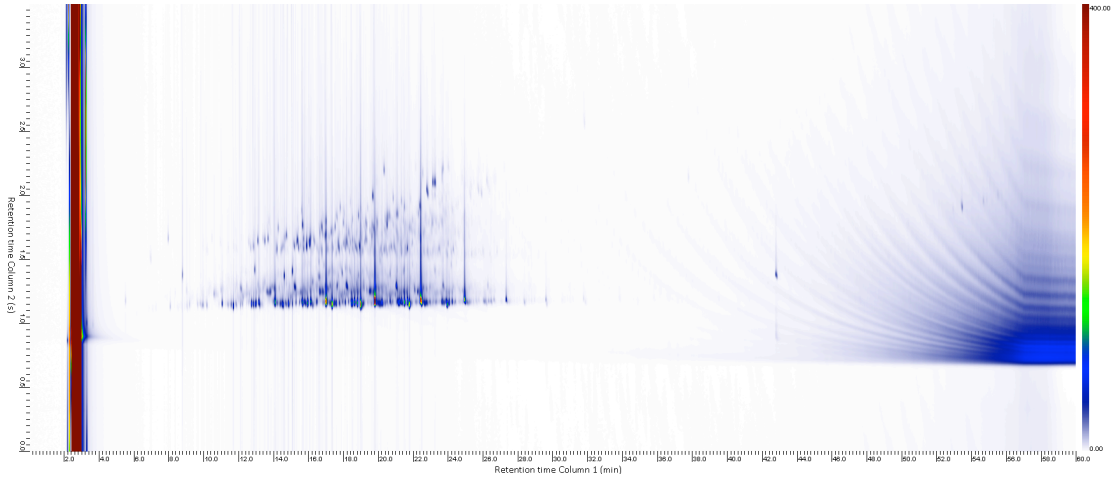

Figure 67 Sample derived from FF site, soil extract (FF87698), note that most of the PHCs present are eluting before the 26 min mark indicating that this fraction of petroleum is a lighter fraction of diesel, potentially SAB in this case. There is substantial evidence for the presence of polar molecules such as aromatic and polyaromatic compounds due to the large number of solutes being retained on the ^{2}D column in the chromatogram.

Figure 67 and Figure 68 show two GC × GC separations of soil extracts obtained from two sites at Macquarie Island. Inspection of these two chromatograms reveals that the contaminants present at the MPH site are substantially different from one another. Specifically, the proportion of polar peaks in the MPH chromatogram (Figure 68) is very low compared to the FF chromatogram (Figure 67), which has significantly more polar solutes present in the sample, as suggested by the large number of peaks that displayed retention on the second-dimension column. This indicates that different remediation strategies might be required for each site, given that the chemistry of each spill site is quite different. Some overloading of the modulator stationary phase is apparent in the form of peak tailing in the second-dimension for the more abundant components of the petroleum-based sample. This overloading occurs when a solute exceeds the stationary

phase capacity of the modulator stationary phase while the trap is cooling down from the hot state after capacitive discharge [41]. Dilution of the samples or the use of a higher split ratio would alleviate solute overloading issue and minimise peak tailing, but this would also reduce analytical sensitivity. Since the main goal of this work was to characterise low levels of PHC, further dilution was not explored. The majority of peaks in the two-dimensional chromatogram exhibited good peak symmetry with minimal peak tailing.

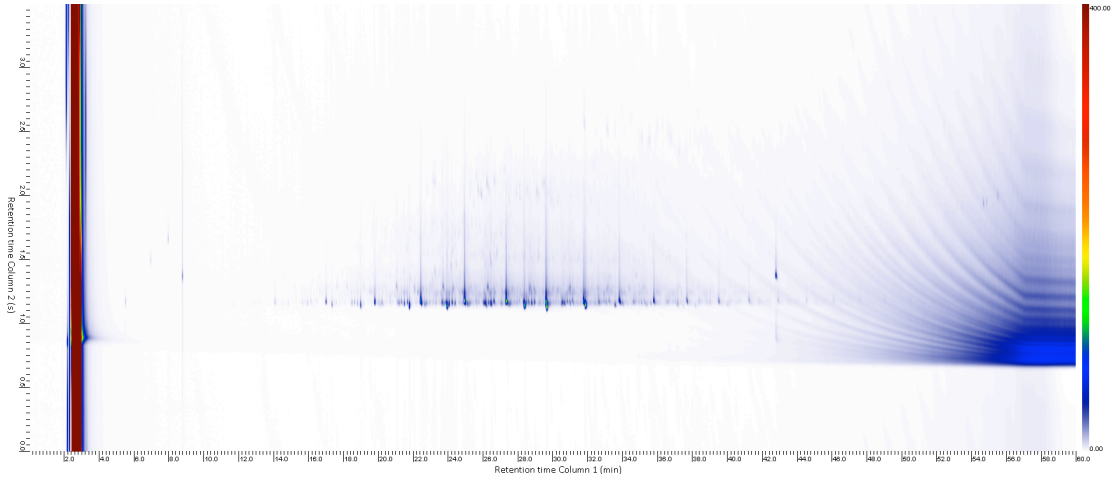

Figure 68 Sample derived from MPH site, soil extract (MPH88246). The distribution of PHC at the MPH site however reveals that the components of the sample are higher molecular weight compounds than those indicated in the FF sample (Figure 67), furthermore that the sample is predominantly made up of aliphatic hydrocarbon since few compounds are being retained for appreciable periods on the ^{2}D column.

A calibration was prepared using a series of SAB diesel standards spanning concentrations from blank to 3,000 mg kg^{-1}. The integrated peak volume of each of these SAB diesel standards was normalised using a 1-bromoeicosane internal standard used to construct a calibration graph to estimate the concentration of PHC's in contaminated soil. A linear calibration was constructed using three-dimensional peak volumes that were integrated using GC Image software with default settings. LOD values were

calculated using these peak volume responses and the calibration procedure outlined in the following reference [79] (8 level calibration, n = 16, 2 replicates for each level, F_{exp} = 2.5, F_{crit} = 3.2, blank leverage 0.0017). The LOD was 11 mg kg^{-1} compared to the 64 mg kg^{-1} LOD achieved using 1D GC analysis [61]. This lower LOD is important for being able to quantify low levels of PHCs in samples to ensure that remediation efforts have been sufficient for the cleanup of petroleum spill sites as outlined by Mooney *et al.* [78].

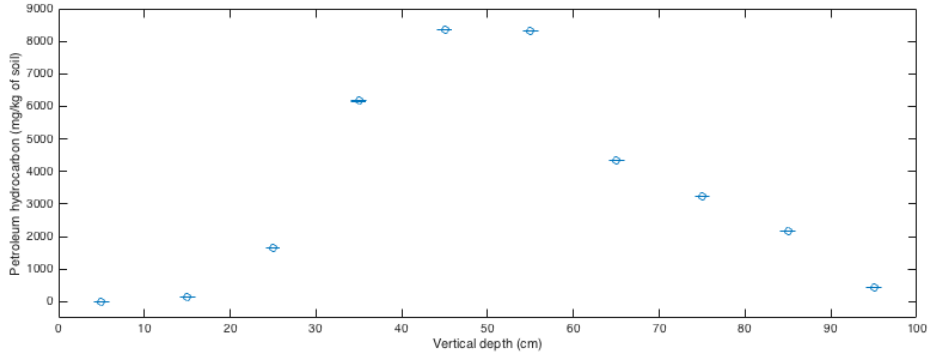

Figure 69 Vertical petroleum hydrocarbon concentration profile for the FF site on Macquarie Island.

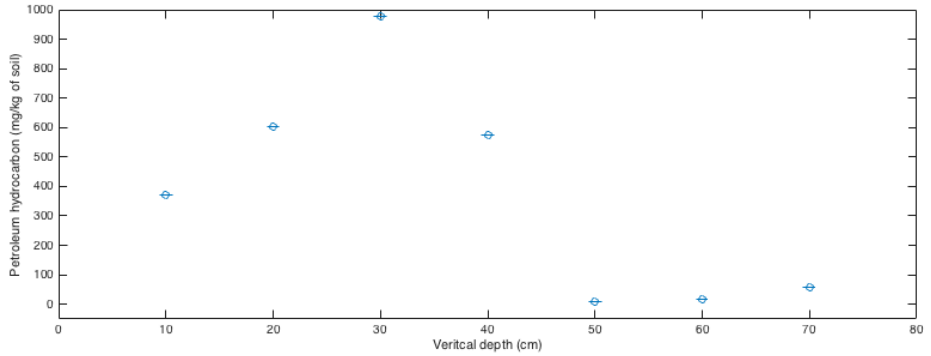

Figure 70 Vertical petroleum hydrocarbon concentration profile for the Main Power House site on Macquarie Island.

The calibration was used to determine the amounts of PHC present at two sites on Macquarie Island, and the GC × GC determinations were compared to one-dimensional GC analysis, as shown in Table 14**.** The vertical profiles of the FF (Figure 69) and MPH (Figure 70) sites revealed that petroleum contamination accumulated 30 to 50 cm

below surface of the site. The lower proportion of petroleum at the surface of each site is likely due to removal mechanisms such as evaporation or transportation away from the site *via* rainwater run off. The petroleum contamination that penetrated the soil could not be similarly removed and remained bound with the clay type soil underneath the topsoil, highlighting the need for its removal by alternative mechanisms.

There were significant differences between the GC × GC and one-dimensional GC PHC determinations; with the one-dimensional GC method generally predicting lower PHC values for samples with PHC concentrations below 1500 mg kg^{-1}. While it could be possible that the GC × GC method is over-predicting the concentration of PHC in each sample, this seems unlikely given that the FID is a mass sensitive detector. Instead it is more likely that the 1D-GC method is under predicting the amounts of PHC in low concentration PHC contaminated samples due to the broadening of low-level peaks in the 1D chromatogram. The peak focusing effect provided by the modulator in GC × GC is able to correct this broadening and increase the flux of mass to the detector allowing the FID to better detect eluting PHC compounds. Samples FF87711 and FF87712 were found to contain PHC levels that were significantly lower than the expected PHC levels indicated by 1D-GC analysis. This discrepancy was most likely due to analyte loss during storage, despite the best efforts to preserve the sample extracts in refrigeration.

Table 14 PHC determinations for FF and MPH sites measured using GC × GC and one-dimensional GC calibration. An asterisk (*) indicates a determination that was extrapolated rather than interpolated for the GC × GC calibration.

Sample ID	PHC Concentration by GC × GC (mg kg^{-1})	PHC Concentration by one-dimensional GC (mg kg^{-1})
FF87695	< 11.0 (LOD)	< 64 (LOD)
FF87696	138.5 ± 0.2	109 ± 2
FF87697	1641.2 ± 0.2	1400 ± 20
FF87698*	6165.2 ± 0.8	5230 ± 73
FF87699*	8355.5 ± 0.9	4690 ± 65
FF87700*	8334.3 ± 0.8	6040 ± 84
FF87701*	4325.2 ± 0.5	4040 ± 56
FF87702*	3237.9 ± 0.7	4740 ± 66
FF87703	2156.3 ± 0.3	1160 ± 16
FF87704	451.1 ± 0.2	300 ± 4
FF87705	59.7 ± 0.2	< 64 (LOD)
FF87706	1112.8 ± 0.2	990 ± 14
FF87707	1413.7 ± 0.2	1080 ± 15
FF87708*	3162.3 ± 0.6	3500 ± 48
FF87709*	4898.5 ± 0.7	4320 ± 59
FF87710*	12045.9 ± 1.1	13100 ± 180
FF87711	1998.5 ± 0.2	3010 ± 42
FF87712	1594.9 ± 0.4	2150 ± 30
FF87713*	5217.7 ± 0.3	3960 ± 55
FF87714	360.5 ± 0.8	380 ± 5
FF87715	< 11	< 64
MPH88237	371.5 ± 0.2	349 ± 5
MPH88238	602.8 ± 0.2	490 ± 7
MPH88239	976.0 ± 0.2	1070 ± 15
MPH88240	574.6 ± 0.2	473 ± 7
MPH88241	< 11	< 64
MPH88242	18.9 ± 0.2	< 64
MPH88243	58.4 ± 0.2	< 64

MPH88244	142.4	±	0.2	98	±	1
MPH88245	509.8	±	0.2	429	±	6
MPH88246*	3061.1	±	0.2	3080	±	40
MPH88247	693.4	±	0.2	600	±	8
MPH88248	386.6	±	0.2	301	±	4
MPH88249	1098.9	±	0.2	918.8	±	13
MPH88250	2790.7	±	0.2	2082.0	±	30
MPH88251	1559.8	±	0.2	1443.1	±	20
MPH88252	672.4	±	0.2	580	±	8
MPH88253	40.2	±	0.2	< 64		
MPH88254	37.7	±	0.2	< 64		
MPH88255	< 11			< 64		
MPH88256	< 11			< 64		
MPH88257	275.9	±	0.2	142	±	2
MPH88258	799.8	±	0.2	488	±	7

The chromatograms generated from the GC × GC separations were then analysed using principal component analysis (PCA) to determine whether there were discrete features present that could be used to fingerprint petroleum sources and spill sites. GC image software was used to automatically align a feature template to each chromatogram. This template was constructed using a facilitator and SAB diesel sample, using the most constrained and total volume correction settings in GC Image's Image Investigator software package.

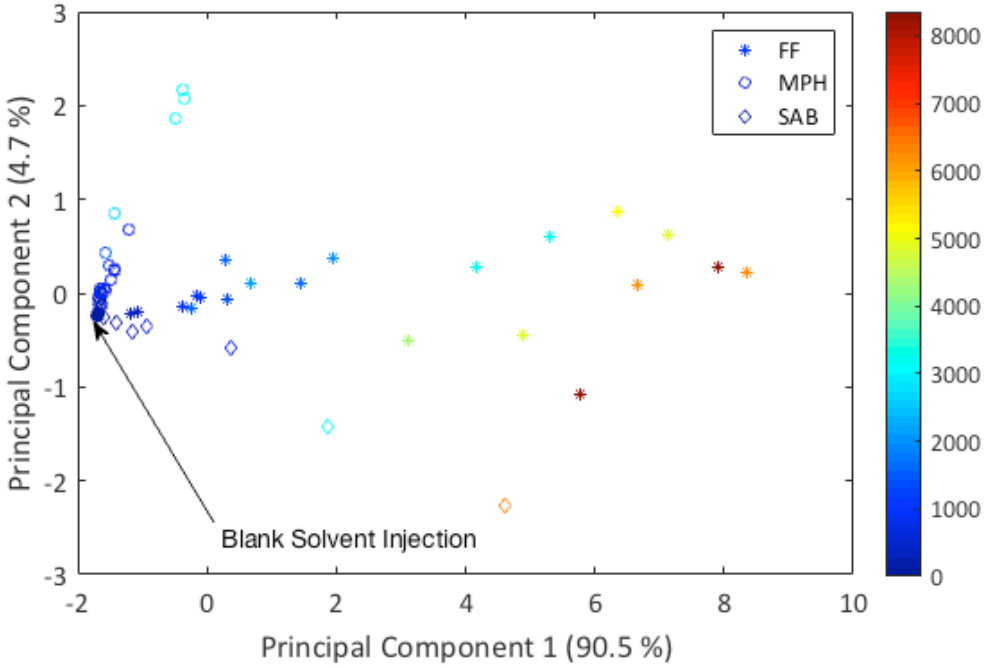

Figure 71 Principal component analysis scores plot for the Special Antarctic Blend diesel, FF and MPH site samples,

PCA was able to distinguish between standards of authentic SAB diesel and petroleum contaminated soil from each of the two sampling sites as shown in Figure 71**.** Principal component 1 (PC1) accounted for 90.5 % of the variability in the data and was correlated with the total amount of PHC in each of the samples and the molecular weight distribution of compounds within each sample. Principal component 2 (PC2) described another 4.7% of sample variance, and was predominantly linked to the different proportions of polar compounds present in each sample. Generally speaking, the SAB diesel had a higher proportion of polar compounds relative to the total amount of PHC FID signal compared to both the FF and MPH sites, which accounts for the differentiation between the SAB, FF and MPH samples. Furthermore there were a relatively low proportion of polar compounds present in the MPH sample causing the differentiation seen in between MPH, FF and SAB samples in PC2. Samples with low levels of total PHC gravitated towards the blank injection solvent (indicated in Figure 71) as expected, since few peaks were detected in the two-dimensional chromatograms

generated from these samples. PCA was a useful tool for categorising the amount of PHC, the proportion of polar compounds in the sample. The proportion of polar components present in a sample could be used to categorise what type (FF, MPH or SAB) of sample had been analysed, providing that the level of PHC was above a threshold level. This allows an analyst to quickly gauge the level of PHC contamination levels and degree of polar compounds, which has ramifications for the remediation of a particular site as to the methods used and whether remediation is required at all [73].

5.3.5 Other applications of the thermal modulator for complex samples

In addition to the separation of petroleum based samples, the GC × GC modulator was applied to the separation of a range of other different samples including tea tree oil, and coffee headspace analysis to determine whether the modulator would be appropriate for the analysis of a wide range of solutes.

Tea tree oil samples are comprised of a range of polar species such as terpenes, alcohols, acetates and ketones, with more than 130 components that have been identified thus far [80-83]. A sample of tea tree oil was injected into the previously described system using a weakly polar BPX5 column (25 m × 220 µm ID × 0.25 µm d_f) column coupled with an Rxi17SIL MS column (0.6 m × 150 µm ID × 0.15 µm d_f) as shown in Figure 72.

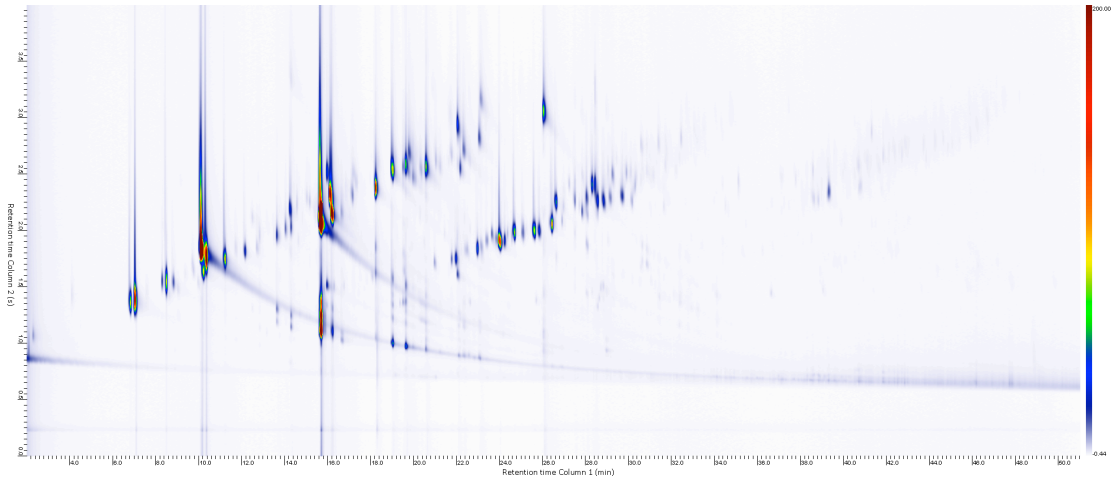

Figure 72 Two-dimensional chromatogram of a separation of Tea Tree Oil sample (1 % v/v in dichloromethane, 1 µL, 50:1 split ratio). ^{1}D column BPX5, 25 m × 220 µm ID × 0.25 µm d_f, ^{2}D column Rxi17SilMS, 0.6 m × 150 µm ID × 0.15 µm d_f. Carrier gas hydrogen, flow rate 1.0 mL min^{-1}, temperature program 45 °C and ramped at a rate of 4 °C min^{-1} to 253 °C (hold 1 min). P_m = 4.0 s, 18 V discharge voltage.

This separation showed some poor utilisation of the two-dimensional space with most compounds being eluted in two diagonal series in the chromatogram. This indicates there was some correlation between the retention mechanisms of each dimension. This is undesirable for maximising the amount of information obtained by the second-dimension separation, so the second-dimension column was changed to a high polarity polyethylene glycol coated column (Stabilwax, 0.6 m × 150 µm ID × 0.15 µm d_f), and the effect that this change had on the separation is shown in Figure 73. The conditions use by Shellie *et al.* and Tranchida *et al.* utilised similar first-dimension columns with 5% diphenyl- 95%dimethylpolysiloxane stationary phase (30 m × 250 µm ID× 0.25 µm d_f) and polyethylene glycol coated second-dimension columns (1 m × 100 µm ID × 0.1 μm d_f) that was operated at an overall flow rate of 0.8 mL min^{-1} using helium carrier gas [83]. This meant that the dead time of the second-dimension column was approximately 1 s, which is very compatible with the 4.5 s modulation period they

selected for their separation. The present chapter utilised hydrogen carrier gas with an overall flow rate of 1.0 mL min^{-1} which yields a similar second dimension dead time of 0.9 s, which should be appropriate for the 4.0 s modulation period selected.

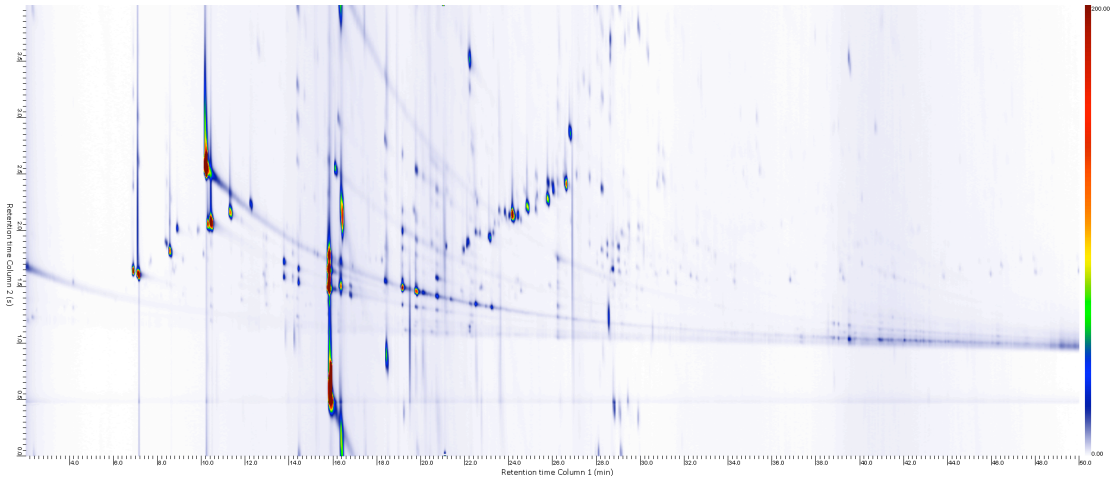

Figure 73 Two-dimensional chromatogram of a separation of Tea Tree Oil sample (1 % v/v in dichloromethane, 1 µL, 50:1 split ratio). ^{1}D column BPX5, 25 m × 220 µm ID × 0.25 µm d_f, ^{2}D column Stabilwax, 0.6 m × 150 µm ID × 0.15 µm d_f. Carrier gas hydrogen, flow rate 1.0 mL min^{-1}, temperature program 45 °C and ramped at a rate of 4 °C min^{-1} to 253 °C (hold 1 min). P_m = 4.0 s, 18 V discharge voltage.

The separation in Figure 73 revealed a significant amount of solute wraparound that needed to be addressed. To rectify this wraparound, the temperature programming rate was incrementally increased in 2 °C min^{-1} increments. Increasing the temperature-programming rate has the effect of increasing the elution temperatures of solutes when they are eluted from the first-dimension column. This means that solutes should experience less retention on the second dimension column, as their retention factor would have been proportionately reduced.

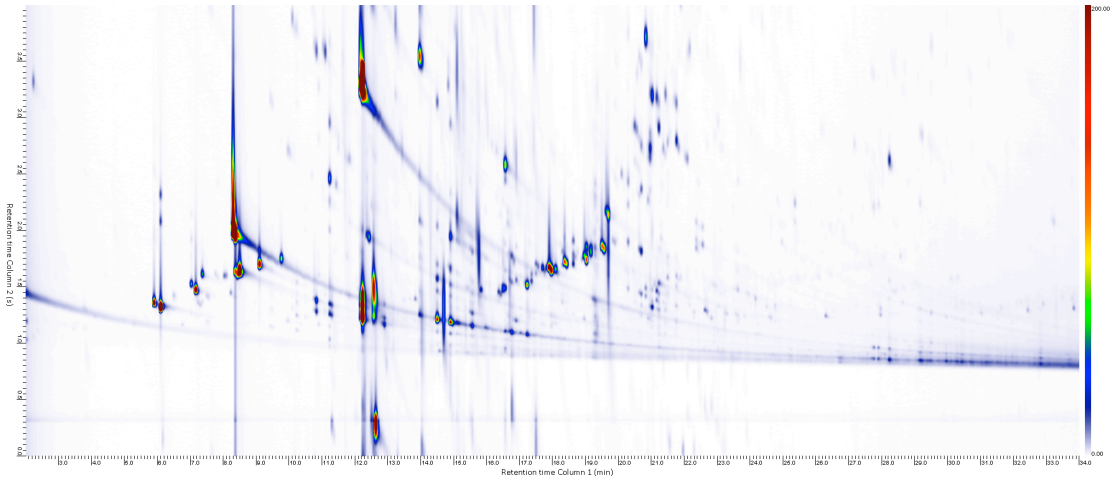

Figure 74 Two-dimensional chromatogram of a separation of Tea Tree Oil sample (1 % v/v in dichloromethane, 1 µL, 50:1 split ratio). ^{1}D column BPX5, 25 m × 220 µm ID × 0.25 µm d_f, ^{2}D column Stabilwax, 0.6 m × 150 µm ID × 0.15 µm d_f. Carrier gas hydrogen, flow rate 1.0 mL min^{-1}, temperature program 45 °C and ramped at a rate of 6 °C min^{-1} to 253 °C (hold 1 min). P_m = 4.0 s, 18 V discharge voltage.

Increasing the temperature programming rate reduced solute wraparound to a degree, however there were still a number of solutes that were being retained for multiples of the modulation period that were still wrapping around (Figure 74 and Figure 75). The faster narrow-bore (100 µm ID) columns used by Tranchida *et al*. could potentially have alleviated this wraparound further, however narrower ID columns were not explored at this time [83]. Alternatively a less polar stationary phase could have been selected or present stationary phase could be trimmed in length to ensure that solutes eluted faster from the second-dimension column. The present separation however was still able to demonstrate the effectiveness of the modulator for this complex tea tree oil sample.

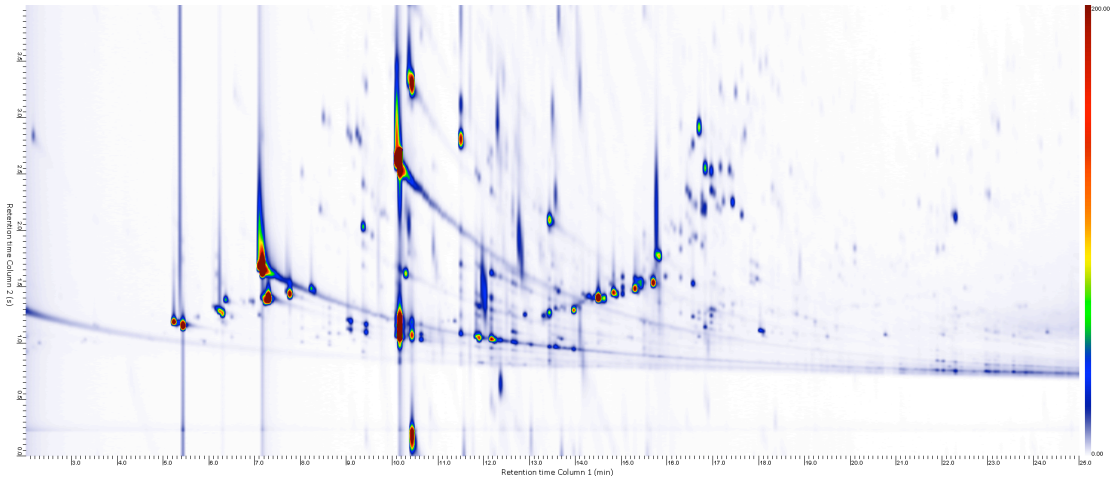

Figure 75 Two-dimensional chromatogram of a separation of Tea Tree Oil sample (1 % v/v in dichloromethane, 1 µL, 50:1 split ratio). ^{1}D column BPX5, 25 m × 220 µm ID × 0.25 µm d_f, ^{2}D column Stabilwax, 0.6 m × 150 µm ID × 0.15 µm d_f. Carrier gas hydrogen, flow rate 1.0 mL min^{-1}, temperature program 45 °C and ramped at a rate of 8 °C min^{-1} to 253 °C (hold 1 min). P_m = 4.0 s, 18 V discharge voltage.

The thermal modulator was applied to the separation of coffee headspace, with the addition of incorporating a mass spectrometer as the detector. The addition of a mass spectrometer results in vacuum outlet conditions that have been demonstrated to be very effective for improving the speed and efficiency of GC × GC separations due to the enhanced speed of diffusion of solutes between the stationary and mobile phases in the second-dimension column [84]. The combination of a mid-polarity cyanopropylphenylpolysiloxane based phase with high-polarity polyethylene glycol phase yielded an impressive utilisation of the two-dimensional space. Generally a non-polar and polar column combination is recognised as being the best means for obtaining a two-dimensional separation since this maximises the difference between retention mechanisms. However, this often leads to some solutes having strong retention on the second-dimension, which causes solute wraparound. Research on the differences between column phase characteristics has identified that the selection of stationary

phases with similar overall polarity but different selectivity is another robust method for obtaining two-dimensional separations [14,85,86].

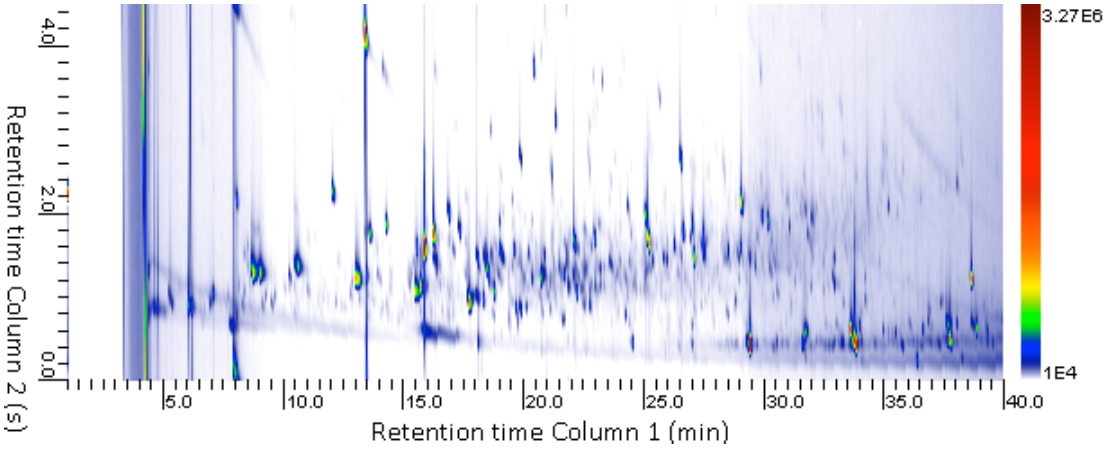

Figure 76 Headspace solid phase micro extraction (HS-SPME) GC × GC separation of cold coffee extract. ^{1}D column BP10, 30 m × 250 µm ID × 0.25 µm d_f, ^{2}D column BP20, 0.8 m × 100 µm ID × 0.1 µm d_f. Carrier gas hydrogen, flow rate 1.0 mL min^{-1}, temperature program 45 °C and ramped at a rate of 5 °C min^{-1} to 240 °C. P_m = 4.5 s, 18 V discharge voltage.

The polyethylene glycol phase (BP-20) promotes retention through dipole-dipole interactions, the formation of hydrogen bonds with basic solutes and electron lone-pair interactions with polarisable solutes [87]. Similarly the 14% cyanopropylphenyl (BP10) based phase retains solutes capable of having dipole-dipole interactions, and hydrogen bonding with basic solutes, however its selectivity for solutes compared to the BP-20 phase is substantially diminished [87]. A clear difference between the two stationary phases is the lack of lone pair interactions provided by the BP-10 phase [87]. The differences between the two columns used led to the excellent distribution and utilisation of two-dimensional separation space, as shown in Figure 76.

While the addition of MS detection led to a substantial reduction in second-dimension peak width and increase in column efficiency, this had the side effect of complicating the detection of peaks with the relatively slow scanning speeds provided

by quadrupole mass spectrometers. The trade off between sensitivity, mass scanning range and scan speed is very significant [88,89]. The library match factors obtained for the present sample were very poor < 80% using the NIST08 and Wiley229 libraries, since only 4 to 5 mass spectra were being obtained over the duration of each peak.

5.3.6 Integrating the thermal modulator into the Calidus™ GC system for portable GC × GC

Unlike a conventional convection oven GC that houses columns and connectivity within a temperature controlled oven, the Calidus™ GC is built in a modular format were each column has independent temperature programming capabilities and connectivity between instrument components is achieved using a central heated compartment. A custom face plate was constructed for the heated compartment that had a cut out section to facilitate installation of the modulator within the Calidus™ GC's connectivity oven, as described in section 5.2.3, and shown in Figure 45.

Installation of the modulator in the heated region was critical for preventing solutes from condensing in capillary connections between various instrument components. The Calidus™ instrument included two temperature-programmable column modules, containing an MXT-1 column (3 m × 180 μm ID × 1.0 μm d_f) and an MXT-1701 column (3 m × 250 μm ID × 0.1 μm d_f). The MXT-1 column was used as the first-dimension column since it would provide a separation based on dispersive interactions that are correlated primarily with solute boiling point (100 % dimethylpolysiloxane polymer). Additionally the thick stationary phase coating was expected to have larger solute loading capacity and stronger retention for solutes than the MXT-1701 column. The MXT-1701 column was used as the second-dimension column due to its different selectivity for polar solutes due to its capacity for dipole-dipole interactions and hydrogen bonding which should enable a good two-dimensional separation. Ideally the second-dimension column would be shorter and have an internal diameter that is equal to or lesser than the

diameter of the first-dimension column to increase the speed of second-dimension separation, however additional column modules were not available at the time. A two-dimensional separation of SAB diesel is shown in Figure 77.

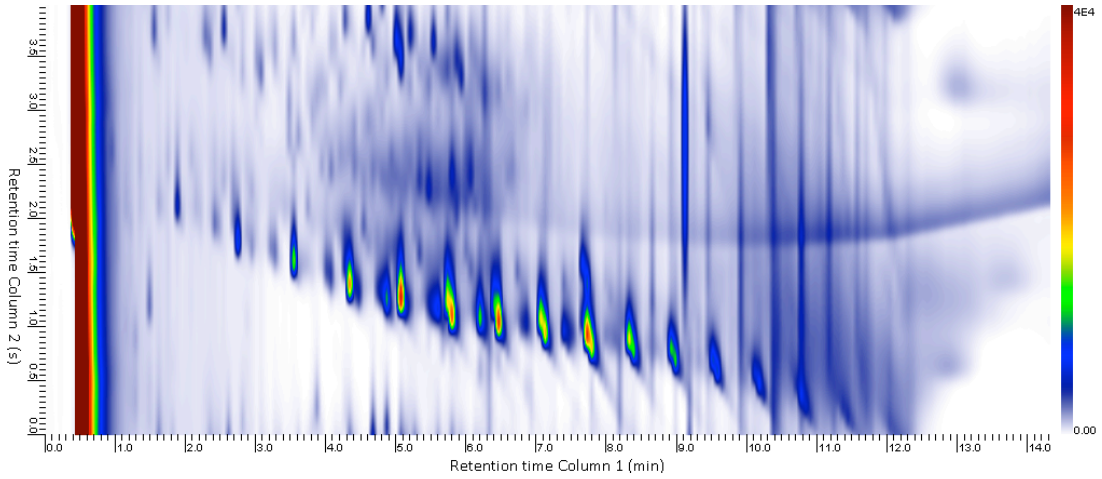

Figure 77 Two-dimensional GC × GC chromatogram of a SAB diesel sample (1 µL injection of 2250 ppm in *n*-hexane with a 20:1 split ratio) on the Calidus™ GC with single-stage thermal modulation.

It was immediately apparent from Figure 77 that solutes were being retained very strongly by the second-dimension column and many peaks were wrapping around within the two-dimensional separation space. Furthermore the peak widths were very broad peak (>300 ms at half height), compared to the peak widths obtained using the 6850 GC system described in section 5.3.2 (~60 ms, ^{2}D column Stabilwax 60 cm × 180 µm ID 0.18 µm d_f). Part of the cause for the wraparound and wide peaks obtained using the present system was due to the sub-optimal second-dimension column (3 m × 250 µm ID) that was used. At a flow rate of 1.0 mL min^{-1} this column has a dead time of 8.5 s, while the modulation period used in the experiment was 4.0 s. This means that by design, it was impossible for the present system not to exhibit wraparound. A substantial increase of the modulation period to a value greater than the second-dimension column dead time would be required to correct this issue, or the second-dimension separation speed would need to be increased substantially.

An injection of an *n*-alkane test mix was used to evaluate whether the modulation period could be increased. As always, 3 to 4 modulations per first-dimension peak were desired for preserving the first-dimension separation.

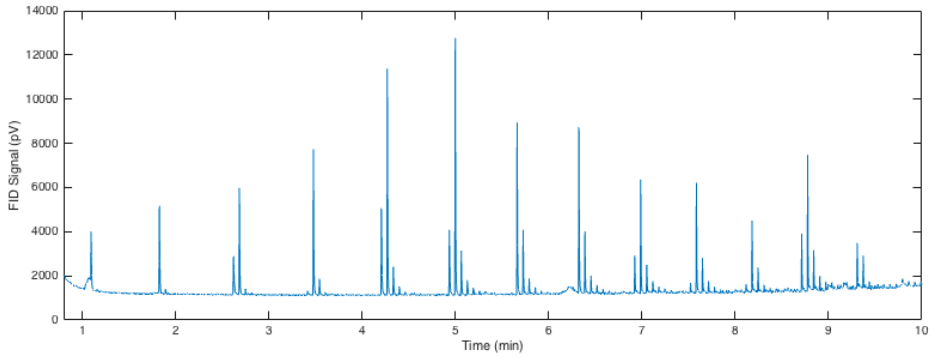

Figure 78 One-dimensional chromatogram showing the modulations of *n*-alkanes (C_8 to C_{20}, 20 mg kg^{-1} each, in dichloromethane) on the Falcon GC × GC system with single-stage thermal modulation. The modulation period was 4 s for this experiment.

Figure 78 reveals that increasing the modulation period was not feasible, since this would lead to the under sampling of the first-dimension column. This meant that either the first-dimension separation needed to be modified to yield wider peaks before modulation to enable access to longer modulation periods; or the second-dimension separation speed needed to be increased. Reduction of the 1D flow rate would lead to a widening of peaks delivered by the first-dimension but this would similarly slow down the flow rate of the second-dimension column, eliminating flow control as a useful parameter. A longer first-dimension column would increase the peak width and separation obtained during the ^{1}D separation; unfortunately no such column was available at the present time from Falcon Analytical.

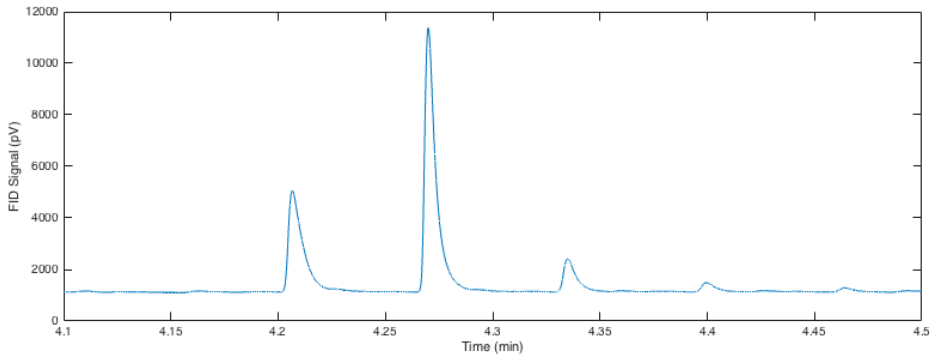

Figure 79 Zoomed in chromatogram 4.1 min to 4.5 min from Figure 78, showing the modulations of the solute *n*-dodecane.

The *n*-alkanes peaks displayed similar peak widths (300 ms, at half height) and poor peak symmetry values (2.0 ± 0.2) to the previous SAB separation shown in Figure 77. These broad, tailing peaks, highlighted in Figure 79, could have arisen from a number of causes, including the modulation process, the connections between each instrument component, the column, and the detector. The presence of dead volumes, cold spots and chemically active regions all contribute to the broadening and tailing of peaks. Every effort was made to ensure that inert capillary connections were made between instrument components with DFS capillaries. Minimal dead volumes were introduced to the system with the connection capillaries. Cold spots were minimised using heated transfer lines between the column modules and the central convection oven was maintained at a high temperature (> 250 °C) to prevent solute condensation.

A better approach was to enhance the speed of the second-dimension column. This can be achieved by either using a shorter column, applying vacuum outlet conditions, or by adding an auxiliary flow of carrier gas to the column. The use of an auxiliary flow of carrier gas was undesirable due to the additional pressure controller and connectivity that was required for providing such a flow. Therefore a shorter second-dimension column (MXT-50, 1.0 m × 180 µm ID × 0.18 µm d_f) was acquired for use in the Calidus™ GC. This new column was coated with a 50 % diphenyl- 50 % dimethylpolysiloxane

phase with a temperature stability up to 310 °C compared to the MXT-1701 phase (270 °C) which was expected to be useful for potential applications in the separation of petroleum based samples. The theoretical dead time of this column was approximately 1.5 s (column flow rate 1.0 mL min^{-1}, atmospheric outlet conditions, FID) making it more amenable towards the 4.0 s modulation duration required. Unfortunately this modification did not offer significant improvements in the peak widths obtained (240 ± 10 ms at half height, peak symmetry values of 1.9 for non-polar solutes) from the second-dimension column, which suggested that the ^{2}D column was not the primary source of the wide peaks being obtained in the second-dimension separation.

An experiment was carried out where the modulator was connected to the Calidus™ FID directly using a piece of DFS (15 cm × 250 µm ID), to measure the peak widths emanating from the modulator itself. A series of *n*-alkanes were once again injected and the peak widths and tailing factors were measured. Peak widths were approximately 220 ± 15 ms (*n*-alkane solutes at half height), with evidence for substantial peak tailing (symmetry values ~ 2.0). This indicated that the MXT-1701 and MXT-50 columns were responsible for broadening peaks by approximately 90 to 30 ms respectively. The remaining 220 ms worth of peak width was therefore linked to the either the modulation process, or the dead volumes present within the system.

In Chapter 2 the performance of the Calidus™ GC system and Agilent 6850 system were evaluated in the one-dimensional GC mode without the inclusion of the single-stage thermal modulator. Peak widths of 112 ms ± 5 ms (α = 0.05) were obtained on the 6850 GC system, while the Calidus™ system broadened peaks slightly more with a peak width of 120 ± 10 ms (α = 0.05) at similar split ratio. This indicated that Calidus™ FID and internal DFS connections were not responsible for the wide peaks obtained during a GC × GC experiment. The single-stage modulator was demonstrated in the previous section (5.3.2) to be capable of achieving post-separation peak widths of 60 ms using the 6850 GC. Therefore the procedure of installing the thermal modulator in the Calidus™

GC substantially widened the injection bandwidths provided by the modulator by up to 220 ms at half height. The main difference between the Calidus™ and 6850 GC instruments is the compartment where the modulator and heat sink was installed. In the case of the Agilent 6850 GC, the modulator was installed in a temperature-programmed oven along with the column and other connections. When the modulator was installed in the Calidus™ GC, it was mounted within in an isothermally controlled transfer-line oven that was maintained at a high temperature (250 °C). This difference between the thermal conditions of the modulator reduced the performance of the modulator substantially. To rectify this problem the single-stage thermal modulator would need to be installed in a temperature-programmed compartment similar to the 6850 GC. The addition of another temperature-controlled compartment was deemed to be undesirable for the Calidus™ GC, given that it already has a large number of temperature controlled zones, and it lacks the native capability to add another. For this reason, the incorporation of the single-stage modulator was abandoned in favour of exploring pulsed flow GC × GC with PMDs (Chapter 6) since these devices do not suffer from the same thermal constraints as the single-stage modulator.

5.4 Conclusions

A resistively heated single-stage thermal modulator was prepared using a novel stationary phase coating within a short SS capillary trap. The hardware required for modulation was simple and more compact than the cryogenic modulation GC × GC instruments that are commercially available. This resistively heated modulator delivered retention time and peak volume repeatability comparable or better than commercially available GC × GC modulators. Capacitive discharge facilitated rapid, repeatable remobilisation of trapped solutes in narrow reinjection bands (72 ± 3 ms average peak widths) as is required for GC × GC analysis. The present modulator is able to focus a wide range of chemically different solutes at different concentrations (5 to 1300 pg on column mass) without the need for a secondary trapping stage, which simplified the modulator design. The main limitation of the modulator is its ability to focus highly volatile solutes, specifically the solute *n*-octane (boiling point 125.1 °C) was not successfully modulated, while cryogenic GC × GC modulators have been shown to modulate solutes as volatile as *n*-pentane. Nevertheless the modulator was able to focus and release semi-volatile solutes such as triacontane (C_{30}, boiling point 449.7 °C) and benzo(g,h,i)perylene (C_{22}, boiling point 500 °C) without issue, making it an appropriate device for a wide variety of samples.

The single-stage resistively heated modulator was applied for the separation of soil samples that had been contaminated with PHC. It was found to be very effective for categorising petroleum spill sources and measuring low concentrations of petroleum compared to one-dimensional GC analysis. The LOD of the present technique was 11 mg kg^{-1}, while the LOQ was 36 mg kg^{-1}, which compares very well with the one-dimensional GC method that had a LOD of 64 mg kg^{-1} PHC in soil. Additionally the modulator was applied for the separation of complex tea tree oil distillates and coffee headspace samples using headspace solid phase micro extraction. This wide variety of samples

demonstrated the single stage thermal modulators ability to modulate a wide variety of chemical species in a repeatable manner allowing quantitative and qualitative GC × GC analysis. Additionally a range of different column combinations and analytical conditions were tested and these setups were evaluated for providing GC × GC separation of the aforementioned samples.

Since access to electrical power was the only consumable needed for operation of this modulator, it was installed within a portable Calidus™ GC and tested to see whether it would be capable of providing GC × GC modulation in the Calidus™ GC. The isothermal convection oven in which the modulator was installed limited the ability of the modulator to provide narrow injection bandwidths to the second-dimension column of the Calidus™ GC. Additionally, the availability of appropriate column dimensions for two-dimensional GC × GC limited the capabilities of the Calidus™ GC × GC system. Both longer first-dimension columns (> 10 m) and shorter second-dimension columns (< 1 m) would be ideal, however the limited flexibility in column dimensions and phases prevented the development of a high quality GC × GC system. Rather than modifying the Calidus™ GC instrument to better accommodate the single-stage resistively heated modulator, an alternate GC × GC modulation strategy (valve-based flow modulation) will be pursued in Chapter 6.

5.5 References

[1] J.V. Seeley, S.K. Seeley, Multidimensional Gas Chromatography: Fundamental Advances and New Applications, Anal. Chem. 85 (2013) 557-578.

[2] M. Edwards, H. Boswell, T. Górecki, Comprehensive Multidimensional Chromatography, Curr. Chromatogr. 2 (2015) 80-109.

[3] P.Q. Tranchida, D. Sciarrone, P. Dugo, L. Mondello, Heart-cutting multidimensional gas chromatography: A review of recent evolution, applications, and future prospects, Anal. Chim. Acta 716 (2012) 66-75.

[4] J.M. Davis, J.C. Giddings, Statistical method for estimation of number of components from single complex chromatograms: theory, computer-based testing, and analysis of errors, Anal. Chem. 57 (1985) 2168-2177.

[5] J.M. Davis, J.C. Giddings, Statistical method for estimation of number of components from single complex chromatograms: application to experimental chromatograms, Anal. Chem. 57 (1985) 2178-2182.

[6] T. Veriotti, R. Sacks, High-speed GC and GC/MS with a series-coupled column ensemble using stop-flow operation, Anal. Chem. 73 (2001) 3045-3050.

[7] T. Veriotti, R. Sacks, High-Speed Characterization and Analysis of Orange Oils with Tandem-Column Stop-Flow GC and Time-of-Flight MS, Anal. Chem. 74 (2002) 5635-5640.

[8] T. Veriotti, R. Sacks, Characterization and Quantitative Analysis with GC/TOFMS Comparing Enhanced Separation with Tandem-Column Stop-Flow GC and Spectral Deconvolution of Overlapping Peaks, Anal. Chem. 75 (2003) 4211-4216.

[9] F.L. Dorman, R. Wittrig, C.M. English, T. Veriotti, R.D. Sacks, High-speed gas chromatographic analysis using a tandem column ensemble and stop-flow modulation, Organohalogen Compd. 60 (2003) 363-366.

[10] L.M. Blumberg, Multidimensional gas chromatography: theoretical considerations, Comprehensive Chromatography in Combination with Mass Spectrometry, John Wiley & Sons, Inc., 2011, p. 13-63.

[11] M.S. Klee, J. Cochran, M. Merrick, L.M. Blumberg, Evaluation of conditions of comprehensive two-dimensional gas chromatography that yield a near-theoretical maximum in peak capacity gain, Journal of Chromatography A 1383 (2015) 151-159.

[12] J.B. Phillips, J. Beens, Comprehensive two-dimensional gas chromatography: a hyphenated method with strong coupling between the two dimensions, J. Chromatogr. A 856 (1999) 331-347.

[13] C.J. Venkatramani, J. Xu, J.B. Phillips, Separation Orthogonality in Temperature-Programmed Comprehensive Two-Dimensional Gas Chromatography, Anal. Chem. 68 (1996) 1486-1492.

[14] S.K. Poole, C.F. Poole, The orthogonal character of stationary phases for gas chromatography, J. Sep. Sci. 31 (2008) 1118-1123.

[15] N.E. Watson, J.M. Davis, R.E. Synovec, Observations on "orthogonality" in comprehensive two-dimensional separations, Anal. Chem. 79 (2007) 7924-7927.

[16] L.M. Blumberg, F. David, M.S. Klee, P. Sandra, Comparison of one-dimensional and comprehensive two-dimensional separations by gas chromatography, J. Chromatogr. A 1188 (2008) 2-16.

[17] L.M. Blumberg, Theory of fast capillary gas chromatography. Part 3. Column performance vs. gas flow rate, J. High Resolut. Chromatogr. 22 (1999) 403-413.

[18] M.S. Klee, L.M. Blumberg, Theoretical and practical aspects of fast gas chromatography and method translation, J. Chromatogr. Sci. 40 (2002) 234-247.

[19] A. Mostafa, M. Edwards, T. Górecki, Optimization aspects of comprehensive two-dimensional gas chromatography, J. Chromatogr. A 1255 (2012) 38-55.

[20] L.M. Blumberg, Accumulating resampling (modulation) in comprehensive two-dimensional capillary GC (GC × GC), J. Sep. Sci. 31 (2008) 3358-3365.

[21] P.Q. Tranchida, G. Purcaro, P. Dugo, L. Mondello, G. Purcaro, Modulators for comprehensive two-dimensional gas chromatography, Trends Anal. Chem. 30 (2011) 1437-1461.

[22] R.E. Murphy, M.R. Schure, J.P. Foley, Effect of Sampling Rate on Resolution in Comprehensive Two-Dimensional Liquid Chromatography, Anal. Chem. 70 (1998) 1585-1594.

[23] W. Khummueng, J. Harynuk, P.J. Marriott, Modulation ratio in comprehensive two-dimensional gas chromatography, Anal. Chem. 78 (2006) 4578-4587.

[24] R.C.Y. Ong, P.J. Marriott, A review of basic concepts in comprehensive two-dimensional gas chromatography, J. Chromatogr. Sci. 40 (2002) 276-291.

[25] Z. Liu, J.B. Phillips, Comprehensive two-dimensional gas chromatography using an on-column thermal modulator interface, J. Chromatogr. Sci. 29 (1991) 227-231.

[26] J.B. Phillips, E.B. Ledford, Thermal modulation: a chemical instrumentation component of potential value in improving portability, Field Anal. Chem. Technol. 1 (1996) 23-29.

[27] J.B. Phillips, R.B. Gaines, J. Blomberg, F.W.M. van der Wielen, J.-M. Dimandja, V. Green, J. Granger, D. Patterson, L. Racovalis, H.-J. de Geus, J. de Boer, P. Haglund, J. Lipsky, V. Sinha, E.B. Ledford, A Robust Thermal Modulator for Comprehensive Two-Dimensional Gas Chromatography, J. High Resolut. Chromatogr. 22 (1999) 3-10.

[28] H.-J. de Geus, J. de Boer, U.A.T. Brinkman, Development of a thermal desorption modulator for gas chromatography, J. Chromatogr. A 767 (1997) 137-151.

[29] P.J. Marriott, R.M. Kinghorn, Longitudinally Modulated Cryogenic System. A Generally Applicable Approach to Solute Trapping and Mobilization in Gas Chromatography, Anal. Chem. 69 (1997) 2582-2588.

[30] J. Beens, M. Adahchour, R.J.J. Vreuls, K. van Altena, U.A.T. Brinkman, Simple, non-moving modulation interface for comprehensive two-dimensional gas chromatography, J. Chromatogr. A 919 (2001) 127-132.

[31] J. Beens, J. Dalluge, M. Adahchour, R.J.J. Vreuls, U.A.T. Brinkman, Moving cryogenic modulator for the comprehensive two-dimensional gas chromatography (GC × GC) of surface water contaminants, J. Microcolumn Sep. 13 (2001) 134-140.

[32] T. Hyoetylaeinen, M. Kallio, K. Hartonen, M. Jussila, S. Palonen, M.-L. Riekkola, Modulator Design for Comprehensive Two-Dimensional Gas Chromatography: Quantitative Analysis of Polyaromatic Hydrocarbons and Polychlorinated Biphenyls, Anal. Chem. 74 (2002) 4441-4446.

[33] M. Kallio, T. Hyoetylaeinen, M. Jussila, K. Hartonen, S. Palonen, M. Shimmo, M.-L. Riekkola, Semi-rotating cryogenic modulator for comprehensive two-dimensional gas chromatography, Anal. Bioanal. Chem. 375 (2003) 725-731.

[34] M. Adahchour, J. Beens, U.A.T. Brinkman, Single-jet, single-stage cryogenic modulator for comprehensive two-dimensional gas chromatography (GC × GC), Analyst 128 (2003) 213-216.

[35] E.B. Ledford, Jr., C. Billesbach, Jet-cooled thermal modulator for comprehensive multidimensional gas chromatography, J. High Resolut. Chromatogr. 23 (2000) 202-204.

[36] J. Harynuk, T. Górecki, Design considerations for a GC × GC system, J. Sep. Sci. 25 (2002) 304-310.

[37] J. Harynuk, T. Górecki, New liquid nitrogen cryogenic modulator for comprehensive two-dimensional gas chromatography, J. Chromatogr. A 1019 (2003) 53-63.

[38] M. Pursch, P. Eckerle, J. Biel, R. Streck, H. Cortes, K. Sun, B. Winniford, Comprehensive two-dimensional gas chromatography using liquid nitrogen modulation: set-up and applications, J. Chromatogr. A 1019 (2003) 43-51.

[39] W.M. Haynes, CRC handbook of chemistry and physics : a ready-reference book of chemical and physical data, Boca Raton, Florida CRC Press, 2014, 95th edition., 2014.

[40] B.A. Ewels, R.D. Sacks, Electrically-heated cold trap inlet system for high-speed gas chromatography, Anal. Chem. 57 (1985) 2774-2779.

[41] M. Libardoni, J.H. Waite, R. Sacks, Electrically Heated, Air-Cooled Thermal Modulator and at-Column Heating for Comprehensive Two-Dimensional Gas Chromatography, Anal. Chem. 77 (2005) 2786-2794.

[42] M. Libardoni, P.T. Stevens, J.H. Waite, R. Sacks, Analysis of human breath samples with a multi-bed sorption trap and comprehensive two-dimensional gas chromatography (GC × GC), J. Chromatogr. B 842 (2006) 13-21.

[43] M. Libardoni, C. Fix, J.H. Waite, R. Sacks, Design and performance evaluation of a two-stage resistively-heated thermal modulator for GC × GC, Anal. Methods 2 (2010) 936.

[44] B.V. Burger, T. Snyman, W.J.G. Burger, W.F. van Rooyen, Thermal modulator array for analyte modulation and comprehensive two-dimensional gas chromatography, J. Sep. Sci. 26 (2003) 123-128.

[45] A.H. Goldstein, D.R. Worton, B.J. Williams, S.V. Hering, N.M. Kreisberg, O. Panic, T. Górecki, Thermal desorption comprehensive two-dimensional gas chromatography for in-situ measurements of organic aerosols, J. Chromatogr. A 1186 (2008) 340-347.

[46] O. Panic, T. Górecki, C. McNeish, A.H. Goldstein, B.J. Williams, D.R. Worton, S.V. Hering, N.M. Kreisberg, Development of a new consumable-free thermal modulator for comprehensive two-dimensional gas chromatography, J. Chromatogr. A 1218 (2011) 3070-3079.

[47] D.R. Worton, N.M. Kreisberg, G. Isaacman, A.P. Teng, C. McNeish, T. Górecki, S.V. Hering, A.H. Goldstein, Thermal desorption comprehensive two-dimensional gas chromatography: An improved instrument for in-situ speciated measurements of organic aerosols, Aerosol Sci. Technol. 46 (2012) 380-393.

[48] A.M. Muscalu, M. Edwards, T. Górecki, E.J. Reiner, Evaluation of a single-stage consumable-free modulator for comprehensive two-dimensional gas chromatography: Analysis of polychlorinated biphenyls, organochlorine pesticides and chlorobenzenes, J. Chromatogr. A 1391 (2015) 93-101.

[49] J.B. Phillips, D. Luu, J.B. Pawliszyn, G.C. Carle, Multiplex gas chromatography by thermal modulation of a fused silica capillary column, Anal. Chem. 57 (1985) 2779-2787.

[50] Z. Liu, J.B. Phillips, Sample introduction into a 5-μm i.d. capillary gas chromatography column using an on-column thermal desorption modulator, J. Microcolumn Sep. 1 (1989) 159-162.

[51] Z. Liu, J.B. Phillips, Large-volume sample introduction into narrow-bore gas chromatography columns using thermal desorption modulation and signal averaging, J. Microcolumn Sep. 2 (1990) 33-40.

[52] M. Libardoni, E. Hasselbrink, J.H. Waite, R. Sacks, At-column heating and a resistively heated, liquid-cooled thermal modulator for a low-resource bench-top GC × GC, J. Sep. Sci. 29 (2006) 1001-1008.

[53] J. Luong, R. Gras, W. Jennings, An advanced solventless column test for capillary GC columns, J. Sep. Sci. 30 (2007) 2480-2492.

[54] J.L. Rayner, I. Snape, J.L. Walworth, P.M. Harvey, S.H. Ferguson, Petroleum-hydrocarbon contamination and remdiation by microbioventing at sub-Antarctic Macquarie Island, Cold Reg. Sci. Technol. 48 (2007) 139-152.

[55] S.M. Powell, J.P. Bowman, S.H. Ferguson, I. Snape, The importance of soil characteristics to the structure of alkane-degrading bacterial communities on sub-Antarctic Macquarie Island, Soil Biol. Biochem. 42 (2010) 2012-2021.

[56] S. Furbo, A.B. Hansen, T. Skov, J.H. Christensen, Pixel-Based Analysis of Comprehensive Two-Dimensional Gas Chromatograms (Color Plots) of Petroleum: A Tutorial, Anal. Chem. 86 (2014) 7160-7170.

[57] L.A. Lanning, R.D. Sacks, R.F. Mouradian, S.P. Levine, J.A. Foulke, Electrically heated cold trap inlet system for computer-controlled high-speed gas chromatography, Anal. Chem. 60 (1988) 1994-1996.

[58] C.P. McIntyre, P.M. Harvey, S. Ferguson, A.M. Wressnig, I. Snape, S.C. George, Determining the extent of weathering of spilled fuel in contaminated soil using the diastereomers of pristane and phytane, Org. Geochem. 38 (2007) 2131-2134.

[59] C.P. McIntyre, P.M. Harvey, S.H. Ferguson, A.M. Wressnig, H. Volk, S.C. George, I. Snape, Determining the Extent of Biodegradation of Fuels Using the Diastereomers of Acyclic Isoprenoids, Environ. Sci. Technol. 41 (2007) 2452-2458.

[60] I. Snape, S.H. Ferguson, P.M. Harvey, M.J. Riddle, Investigation of evaporation and biodegradation of fuel spills in Antarctica: II-Extent of natural attenuation at Casey Station, Chemosphere 63 (2006) 89-98.

[61] I. Snape, P.M. Harvey, S.H. Ferguson, J.L. Rayner, A.T. Revill, Investigation of evaporation and biodegradation of fuel spills in Antarctica I. A chemical approach using GC-FID, Chemosphere 61 (2005) 1485-1494.

[62] G.S. Frysinger, R.B. Gaines, Comprehensive two-dimensional gas chromatography with mass spectrometric detection (GC × GC/MS) applied to the analysis of petroleum, J. High Resolut. Chromatogr. 22 (1999) 251-255.

[63] J.H. Christensen, G. Tomasi, Practical aspects of chemometrics for oil spill fingerprinting, J. Chromatogr. A 1169 (2007) 1-22.

[64] Z. Wang, M. Fingas, D.S. Page, Oil spill identification, J. Chromatogr. A 843 (1999) 369-411.

[65] J.M. Aislabie, M.R. Balks, J.M. Foght, E.J. Waterhouse, Hydrocarbon Spills on Antarctic Soils: Effects and Management, Environ. Sci. Technol. 38 (2004) 1265-1274.

[66] T. Tin, Z.L. Fleming, K.A. Hughes, D.G. Ainley, P. Convey, C.A. Moreno, S. Pfeiffer, J. Scott, I. Snape, Impacts of local human activities on the Antarctic environment, Antarctic Science 21 (2009) 3-33.

[67] G.S. Frysinger, R.B. Gaines, L. Xu, C.M. Reddy, Resolving the Unresolved Complex Mixture in Petroleum-Contaminated Sediments, Environ. Sci. Technol. 37 (2003) 1653-1662.

[68] M.A. Gough, S.J. Rowland, Characterization of unresolved complex mixtures of hydrocarbons in petroleum, Nature 344 (1990) 648-650.

[69] M. Adahchour, J. Beens, U.A.T. Brinkman, Recent developments in the application of comprehensive two-dimensional gas chromatography, J. Chromatogr. A 1186 (2008) 67-108.

[70] G.S. Frysinger, R.B. Gaines, Forensic analysis of ignitable liquids in fire debris by comprehensive two-dimensional gas chromatography, J. Forensic Sci. 47 (2002) 471-482.

[71] R.K. Nelson, B.M. Kile, D.L. Plata, S.P. Sylva, L. Xu, C.M. Reddy, R.B. Gaines, G.S. Frysinger, S.E. Reichenbach, Tracking the weathering of an oil spill with comprehensive two-dimensional gas chromatography, Environ. Forensics 7 (2006) 33-44.

[72] S.K. Seeley, S.V. Bandurski, R.G. Brown, J.D. McCurry, J.V. Seeley, A comprehensive two-dimensional gas chromatography method for analyzing extractable petroleum hydrocarbons in water and soil, J. Chromatogr. Sci. 45 (2007) 657-663.

[73] P.M. Harvey, R.A. Shellie, Data reduction in comprehensive two-dimensional gas chromatography for rapid and repeatable automated data analysis, Anal. Chem. 84 (2012) 6501-6507.

[74] C. Aeppli, R.K. Nelson, J.R. Radović, C.A. Carmichael, D.L. Valentine, C.M. Reddy, Recalcitrance and Degradation of Petroleum Biomarkers upon Abiotic and Biotic Natural Weathering of Deepwater Horizon Oil, Environ. Sci. Technol. 48 (2014) 6726-6734.

[75] J. Gros, C.M. Reddy, C. Aeppli, R.K. Nelson, C.A. Carmichael, J.S. Arey, Resolving Biodegradation Patterns of Persistent Saturated Hydrocarbons in Weathered Oil Samples from the Deepwater Horizon Disaster, Environ. Sci. Technol. 48 (2014) 1628-1637.

[76] W. Zhang, S. Zhu, S. He, Y. Wang, Screening of oil sources by using comprehensive two-dimensional gas chromatography/time-of-flight mass spectrometry and multivariate statistical analysis, J. Chromatogr. A 1380 (2015) 162-170.

[77] A.N. Harvey, I. Snape, S.D. Siciliano, Validating potential toxicity assays to assess petroleum hydrocarbon toxicity in polar soil, Environ. Toxicol. Chem. 31 (2012) 402-407.

[78] T.J. Mooney, C.K. King, J. Wasley, N.R. Andrew, Toxicity of diesel contaminated soils to the subantarctic earthworm Microscolex macquariensis, Environ. Toxicol. Chem. 32 (2013) 370-377.

[79] A.C. Olivieri, Practical guidelines for reporting results in single- and multi-component analytical calibration: A tutorial, Anal. Chim. Acta 868 (2015) 10-22.

[80] R. Shellie, P. Marriott, G. Zappia, L. Mondello, G. Dugo, Interactive use of linear retention indices on polar and apolar columns with an MS-library for reliable characterization of Australian tea tree and other Melaleuca sp. oils, J. Essent. Oil Res. 15 (2003) 305-312.

[81] R. Shellie, P. Marriott, C. Cornwell, Application of comprehensive two-dimensional gas chromatography (GC √ó GC) to the enantioselective analysis of essential oils, J. Sep. Sci. 24 (2001) 823-830.

[82] R. Shellie, P. Marriott, C. Cornwell, Characterization and comparison of tea tree and lavender oils by using comprehensive gas chromatography, J. High Resolut. Chromatogr. 23 (2000) 554-560.

[83] P.Q. Tranchida, R.A. Shellie, G. Purcaro, L.S. Conte, P. Dugo, G. Dugo, L. Mondello, Analysis of fresh and aged tea tree essential oils by using GC × GC-qMS, J. Chromatogr. Sci. 48 (2010) 262-266, 264 plates.

[84] L.M. Blumberg, Comprehensive two-dimensional gas chromatography: metrics, potentials, limits, J. Chromatogr., A 985 (2003) 29-38.

[85] J.V. Seeley, C.T. Bates, J.D. McCurry, S.K. Seeley, Stationary phase selection and comprehensive two-dimensional gas chromatographic analysis of trace biodiesel in petroleum-based fuel, J. Chromatogr. A 1226 (2012) 103-109.

[86] A. Ghosh, S.K. Seeley, S.R. Nartker, J.V. Seeley, Analysis of siloxanes in hydrocarbon mixtures using comprehensive two-dimensional gas chromatography, J. Chromatogr. A 1360 (2014) 258-263.

[87] C.F. Poole, S.K. Poole, Separation characteristics of wall-coated open-tubular columns for gas chromatography, J. Chromatogr. A 1184 (2008) 254-280.

[88] R.A. Shellie, P.J. Marriott, C.W. Huie, Comprehensive two-dimensional gas chromatography (GC × GC) and GC × GC-quadrupole MS analysis of Asian and American ginseng, J. Sep. Sci. 26 (2003) 1185-1192.

[89] R.A. Shellie, P.J. Marriott, Comprehensive two-dimensional gas chromatography-mass spectrometry analysis of Pelargonium graveolens essential oil using rapid scanning quadrupole mass spectrometry, Analyst 128 (2003) 879-883.

Chapter 6: Resistively heated columns and planar microfluidic devices for comprehensive two-dimensional gas chromatography

Summary

Comprehensive GC × GC using PMDs was investigated as a means of improving the separation capabilities of the Calidus™ GC instrument. Forward fill flush (FFF) and reversed fill flush (RFF) pulsed flow GC × GC configurations were both tested as strategies for achieving modulation in the Calidus™ instrument. Both configurations were successful, although the two-dimensional separation performance of the Calidus™ GC × GC system was not able to match that of commercial bench top instruments. A systematic analysis of the components comprising the Calidus™ GC instrument suggested that the design of the central convection oven and connectivity between the various components of the system are limiting the separation capabilities of the instrument.

A number of GC × GC column sets and analysis conditions were tested, for the purposes of developing a portable GC × GC instrument capable of characterising petroleum spill sites at Macquarie Island. The limited selection of short resistively heated column modules was not ideal for developing an instrument with sufficient separation capabilities. For this reason, a means of preparing customised resistively heated column modules was devised that utilised conventional fused silica GC columns. The fused silica columns were co-linearly wound with the SS columns included with the Calidus™ GC and insulated with a thin layer of aluminium foil. This procedure allowed for any commercially available fused silica capillary to be incorporated into the Calidus™ GC instrument.

6.1 Introduction

As discussed in Chapter 5, GC × GC is a technique that is able to vastly increase the separation performance of traditional one-dimensional GC analysis. The critical component that enables the operation of any GC × GC system is the modulator, which serves to continuously sample effluent from the first-dimension column and reproducibly transfer the sampled effluent to a second-dimension column. While the Chapter 5 focused on the development of a modulator that uses thermal principles to focus and release solutes to achieve modulation, it is also possible to use high-speed switching valves to achieve a similar modulation effect. These valve-based GC × GC modulators incorporate three components, an electronic pressure control unit (EPC), switching valve, and control/timing electronics. This simplifies the construction of GC × GC systems vastly since the need for capillary cooling, or retentive stationary phases are removed, however the control parameters are somewhat more complicated.

Switching devices must be very quick, and a number of valve designs have been developed that are based on rotary, diaphragm and pneumatic control principles as discussed in Chapter 2. Out of these options pneumatic switching valves have the advantage of eliminating moving parts from the high temperature compartments that are present within GC instruments. There are two dominant strategies for achieving pneumatically controlled GC × GC modulation: Deans' switch GC × GC and pulsed flow comprehensive two-dimensional GC × GC. Deans' switching is perhaps the simplest method for achieving GC × GC, and further information on the principles of Deans' switching is detailed in Chapter 2 and Chapter 4. Deans' switch PMDs have been developed to facilitate the construction of GC × GC systems [1]. A diagram of a typical Deans' switching GC × GC modulator is shown in Figure 80.

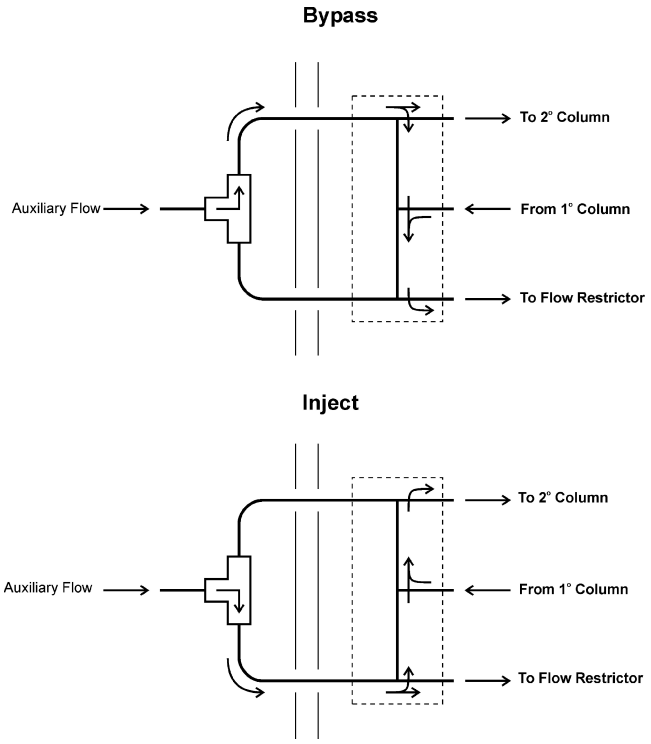

Figure 80 Deans' switch GC × GC modulator diagram showing the bypass (top) and injection (bottom) states for the PMD device (shown as the dashed box). When the modulator is in the bypass state effluent from the primary column is directed away from the secondary column. When the modulator is in the inject state effluent from the primary column is directed into the secondary column. Modulation is achieved by periodically switching between the two states. Reproduced with permission from the American Chemical Society (2007) from reference [1].

A high speed, three-way solenoid is used to control the "inject" and "bypass" state of the Deans' GC × GC PMD. Only a small percentage of ^{1}D column effluent (5-10 %) is redirected to the second-dimension column to ensure that injection bandwidths to the ^{2}D column are narrow, and to provide sufficient time for a ^{2}D separation to be completed for each injection to the ^{2}D [1,2]. The remainder of the effluent from the ^{1}D column is directed to a flow restrictor that matches the pneumatic resistance of the second-dimension column for pressure balancing of the system. This modulation strategy is

simple and effective at providing modulation however the mass sensitivity of the GC × GC analysis is reduced by 90 to 95 % since a large portion of effluent is not transferred to the second-dimension column. GC × GC techniques that modulate all of the effluent from the first-dimension column are said to "comprehensively" sample the first-dimension effluent, maximising mass sensitivity. To overcome the loss in sensitivity, while avoiding the requirement for thermal focusing with cryogenic modulation, pulsed flow comprehensive GC × GC modulation was developed.

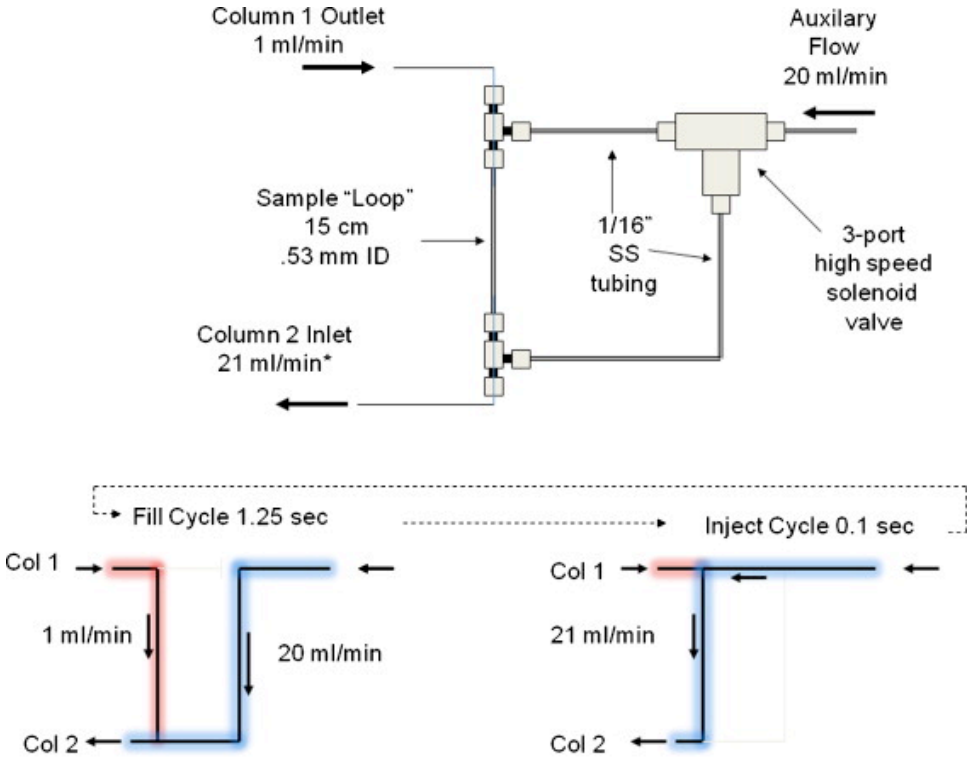

Figure 81 Schematic of a FFF-GC × GC modulation, showing the original design proposed by Seeley *et al.* [3], (Top) connectivity of the auxiliary EPC unit and sample loop. (Bottom) shows the flow through the sample loop during the loop "fill" and "inject" cycles. Reproduced with permission from Elsevier B.V. (2012) from reference [5].

Pulsed flow GC × GC has the benefit of transferring 100 % of the effluent from the ^{1}D column to the ^{2}D column. Pulsed flow modulation can be achieved using one of two configurations known as the FFF and RFF configurations [3-5]. The FFF-GC × GC design

was the first pulsed flow system to be developed in a PMD format similar to the Deans' switch PMD [6]. A schematic diagram of a FFF-GC × GC modulator configuration is shown in Figure 81. Control of the pressure at the junction between the first-dimension column and sample loop are critical to ensuring optimal GC × GC modulation. During the "fill" stage of modulation operation, effluent from the ^{1}D column is transferred to the sample loop at 1.0 mL min^{-1} (Figure 81). The contents of the sample loop are then periodically injected to the ^{2}D column by activating a three-way solenoid valve, which changed the system to the "inject" state. A flow of 21 mL min^{-1} (1 mL min^{-1} from the first dimension column, 20 mL min^{-1} from the auxiliary EPC unit) enables the contents of the 15 cm × 0.45 mm loop to be completely emptied in 100 ms. During the injection phase the carrier gas flow from the ^{1}D column is briefly halted by the application of pressure to the ^{1}D and sample loop junction by the auxiliary EPC, which ensures that effluent is not able to pass from the ^{1}D to the ^{2}D column without being modulated. A FFF-GC × GC PMD was commercialised based on the Seeley *et al.* modulator design [3,7,8]. This device included ports for connecting a ^{1}D and ^{2}D column, an integrated sample loop and connections for auxiliary carrier gas to control the "inject" and "fill" state of the PMD. This device has been used to great effect in a number of applications as summarised by a recent review [9].

An alternative pulsed flow GC × GC modulation configuration is the RFF modulator design in which the flow direction within the sample loop is inverted during the inject cycle [5]. Figure 82 shows a RFF-GC × GC modulator setup that was constructed from two PMDs (a four-port and three-port PMD).

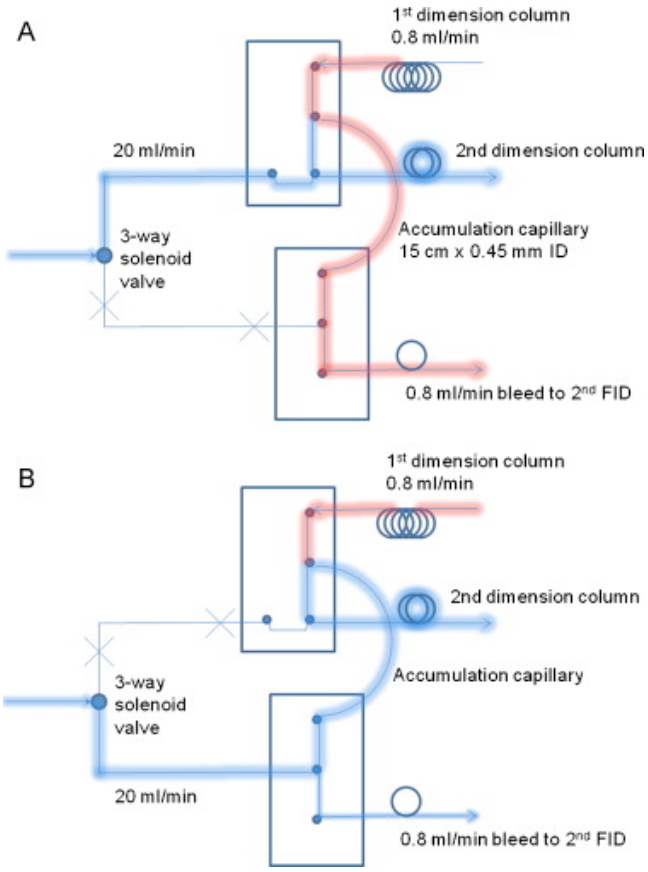

Figure 82 Schematic of a RFF-GC × GC modulation system, using a four-port and three-port PMD and customisable sample loop. Inset (A) shows the "fill" cycle of modulation, while (B) shows the "inject" cycle. Reproduced with permission from Elsevier B.V. (2012) from reference [5].

The RFF-GC × GC system includes an additional outlet for the sample loop (accumulation capillary) that is referred to as a bleed capillary. The pneumatic resistance of the bleed capillary is optimised to ensure that it has a constant flow of carrier during both the "inject" and "fill" state of the modulator. The bleed line enables the reversal of the flow direction within the sample loop during the inject cycle, which is advantageous, as shorter injection periods can be used in situations were the sample loop is not completely filled with effluent from the ^{1}D column during the "fill" cycle. Shorter injection periods reduce the risk of effluent breaking through from the ^{1}D column during the "inject" phase, since the length of time that the flow needs to be stopped is shorter.

Experiments carried out and detailed in Chapter 5 revealed that the Calidus™ GC is capable of achieving comprehensive two-dimensional GC × GC. Unfortunately the GC × GC separations obtained were limited by the lack of flexibility in column dimensions and the ability of the single-stage thermal modulator to provide narrow injection bandwidths to the ^{2}D column. Additionally, the Calidus™ GC lacked flexibility in the selection of column phases, lengths, internal diameters and film thicknesses, which vastly complicated method optimisation. In particular the limitation of short first-dimension columns (3 m) meant that low carrier gas flow rates were required to ensure that peaks were sufficiently broad so that 3 to 4 modulations could be obtained for each peak. Additionally, the 3 and 1 m long columns that were available for use as ^{2}D columns had large void times (~ 8 to 2.4 s) that were not compatible with the target modulation periods of 1 to 4 s. These long second-dimension columns caused substantial wraparound of peaks that reduced the two-dimensional performance of the system compared to bench top GC × GC instruments.

In this research chapter the previous weaknesses of the Calidus™ GC × GC system will be addressed by investigating PMD technology for achieving pulsed flow GC × GC modulation with the Calidus™ GC platform. The use of pulsed flow modulation removes the need for thermal modulation, which was not able to provide good modulation performance; furthermore the only additional hardware required for this modification is an extra EPC module. The high auxiliary carrier gas flow rates that are used to elute effluent from the sample loop will be beneficial in reducing the void times of the ^{2}D columns, which should improve the ^{2}D column performance compared to the previous thermal modulation system. Finally, a means of preparing in-house resistively heated columns with customisable lengths, dimensions and stationary phases will be developed and tested in order to overcome the limited column options caused by the prohibitive cost of resistively heated column modules.

6.2 Materials and Methods

6.2.1 MXT-5 (^{1}D) and MXT-1701 (^{2}D) method with FFF modulation for the separation of SAB diesel

A Calidus™ GC equipped with a S/SL inlet, two column modules, a FID module and an EPC module (Parker Hannafin, VSO-GC Valve 0-50 PSI, Part #990-005021-050) was used for forward fill flush (FFF) GC × GC experiments. The S/SL inlet of the Calidus™ GC was connected to a MXT-5 column (3 m × 180 µm ID × 0.18 µm d_f, Restek) using a piece of DFS capillary (13 cm × 180 µm ID, Trajan). The MXT-5 column was connected to a FFF pulsed flow modulation PMD Port #A (Agilent, PN# G3440A), using another piece of DFS capillary (35 cm × 50 µm ID, Trajan). The outlet port of the FFF-GC × GC PMD (Port #B) was connected to an MXT-1701 column (3 m × 180 µm ID × 0.18 µm d_f, Restek) using a piece of DFS capillary (12 cm × 250 µm ID, Trajan). Finally the MXT-1701 column was connected to the Calidus™ FID via another piece of DFS (12 cm × 250 µm ID, Trajan), as shown in Figure 83.

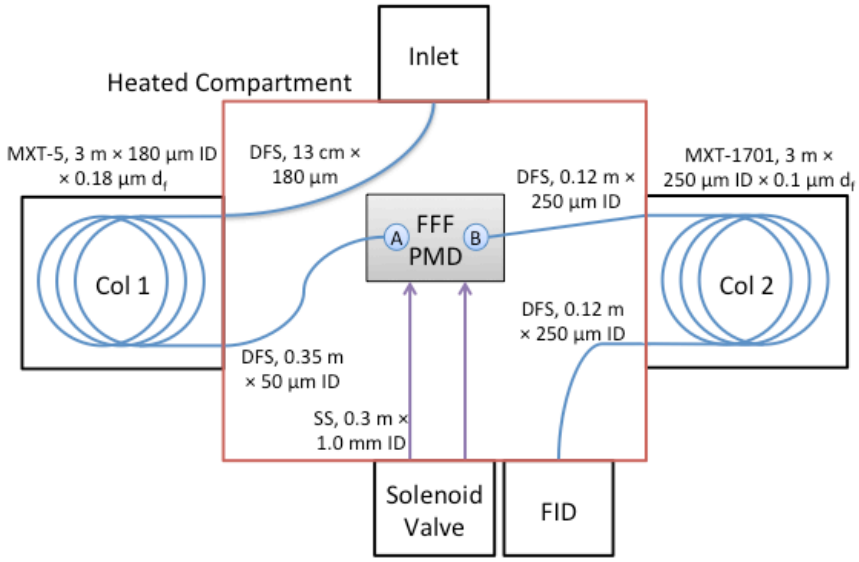

Figure 83 Schematic diagram of the connections between the Calidus™ GC Inlet, MXT-5 column, MXT-1701 column, FFF-GC × GC PMD, valve and FID modules.

The FID was supplied with 13 mL min^{-1} of hydrogen and 130 mL min^{-1} air for flame operation. The transfer lines, PMD, S/SL inlet and FID were all maintained at 280 °C. The pulsed flow PMD was connected to a three-way solenoid valve (Lee Corporation, Westbrook, Connecticut, USA) and auxiliary EPC using two SS capillaries (30 cm × 1.0 mm ID, Trajan). Valve actuations were controlled using a custom built programmable timer (Scielex, Kingston, Tasmania) that was synchronised to a start-out signal provided by the Calidus™ GC. A modulation period of 2.1 s with a 100 ms injection period was used for the present experiments.

The ^{1}D column module was set to an initial temperature of 60 °C (hold for 1 min) and then ramped at a rate of 0.2 °C s^{-1} to 270 °C (hold for 1 min). The ^{2}D column was temperature programmed similarly at 0.2 °C min^{-1}, however its initial and final temperatures were varied to achieve a 0, 10, 20 and 30 °C offset from the ^{1}D column as shown in Table 15. Hydrogen carrier gas was supplied to the GC *via* the S/SL inlet and the auxiliary EPC connected to the solenoid valve. The S/SL inlet was programmed to deliver a constant flow of 0.25 mL min^{-1} through the ^{1}D column, while the auxiliary EPC was programmed to provide 25 mL min^{-1}; the initial pressure set points for the ^{1}D and ^{2}D columns are tabulated in Table 15.

Table 15 Initial temperature and pressure set points for the present Calidus™ GC system.

^{1}D Temperature and pressure		^{2}D Temperature and pressure	
Temperature (° C)	Pressure (PSI)	Temperature (° C)	Pressure (PSI)
60	29.66	60	15.91
60	29.34	50	15.44
60	29.03	40	14.99
60	28.69	30	14.53

A sample of SAB diesel (Australian Antarctic Division, Kingston, Australia) was diluted to a concentration of 1000 mg kg^{-1} in *n*-hexane (Sigma Aldrich), and injected (1µL) into the Calidus™ S/SL inlet at a split ratio of 200:1. FID data was collected with a sampling rate of 100 Hz, using Chrom Perfect software (Justice Laboratory Software, USA) on a laptop computer. Data files were exported in CDF format for processing and visualization in GC image software (GC Image LLC, USA).

6.2.2 Peak width performance evaluation using MXT-5 (^{1}D) and MXT-1701 (^{2}D) column set with FFF modulation

The same experimental setup that was described in Section 6.2.1 was used for the evaluation of the peak width performance provided by the FFF-GC × GC modulator in the Calidus™ instrument, with the following changes. The initial temperature for both the MXT-5 and MXT-1701 columns was 60 °C (1 min hold), which was then ramped to 270 °C at a rate of 12 °C min^{-1} to 270 °C (1 min hold).

A mixture of a homologous series of *n*-alkanes including *n*-octane, *n*-nonane, *n*-decane, *n*-undecane, *n*-dodecane, *n*-tridecane, *n*-tetradecane, *n*-pentadecane *n*-hexadecane *n*-heptadecane *n*-octadecane, *n*-nonadecane and *n*-eicosane 20 mg kg^{-1} each (Sigma Aldrich, Castle Hill, Australia) diluted in dichloromethane (Sigma Aldrich) were injected (1µL) at a split ratio of 20:1.

6.2.3 Analysis of column elution temperatures for a series of n-alkanes using the Calidus™ and Agilent 6850 GC instruments

Calidus™ GC: A piece of DFS (65 cm × 75 µm ID, Trajan) was connected to the inlet of the Calidus™ GC. The outlet of this piece of DFS was then connected to a MXT-5 column (3 m × 180 µm ID × 0.18 µm d_f, Restek). The outlet of the column was then connected to a FID module *via* a piece of DFS (30 cm × 250 µm ID, Trajan). Hydrogen was used as the carrier gas, and a constant flow rate of 0.25 mL min^{-1} was used. The inlet and FID were

set to a temperature of 250 °C. The MXT-5 column was set to an initial temperature of 60 °C (1 min) and then temperature programmed at a rate of 12 °C min^{-1} to a final temperature of 270 °C (1 min). FID data was collected with a sampling rate of 100 Hz, using Chrom Perfect software (Justice Laboratory Software, USA) on a laptop computer.

Agilent 6850 GC: The inlet of the 6850 GC was connected to a DB5-ms column (25 m × 250 µm ID × 0.25 µm d_f). The outlet of this column was then connected to a FID module. Hydrogen was used as the carrier gas with a constant flow rate of 1.0 mL min^{-1}. The convection oven was set to an initial temperature of 40 ° C (1 min), and then ramped at 5 °C min^{-1} to a final temperature of 320 °C (1 min). FID data were acquired at a 20 Hz data-sampling rate, and data was processed using ChemStation Software.

6.2.4 MXT-1 (^{1}D) and MXT-1701 (^{2}D) column set with FFF modulation

A Calidus™ GC equipped with a S/SL inlet, a resistively heated column module and a FID module was used for developing a GC × GC method for the separation of a 13-component test mixture and SAB diesel. The experimental setup described in Section 6.2.1 was used with an MXT-1 column (3 m × 180µm ID × 1.0 µm d_f, Restek) in place of the MXT-5 column used previously. The carrier gas was hydrogen; the MXT-1 was operated at a flow rate of 0.6 mL min^{-1}, while the MXT-1701 was operated at a flow rate of 20 mL min^{-1}. The initial ^{1}D column temperature was 40 °C (1 min) then ramped at 30 °C s^{-1} to 280 °C (1 min); The MXT-1701 was programmed to trail the MXT-1 column by +10 °C. The modulation period was 1.5 s and the injection period 110 ms.

A 13-component test mix comprised of benzene, toluene, *n*-octane, 1-hexenol, *o*-xylene, *n*-decane, 1-octanol, naphthalene, 1-decanol, *n*-tetradecane, acenaphthene, fluorene, *n*-octadecane (Sigma Aldrich, Castel Hill, Australia) was prepared (each component 100 mg kg^{-1} diluted in dichloromethane) and injected (1 µL) into the Calidus™ system for analysis. SAB diesel was diluted to a concentration of 2250 mg kg-1 in dichloromethane (Sigma Aldrich, Castel Hill, Australia) prior to injection (1 µL) to the

Calidus™ GC. FID data was collected with a sampling rate of 100 Hz, using Chrom Perfect software (Justice Laboratory Software, USA) on a laptop computer. Data files were exported in CDF format for processing and visualization in GC image software (GC Image LLC).

6.2.5 RTX-1 (^{1}D) and RTX-1701 (^{2}D) column set with FFF using the 6850 GC

An Agilent 6850 GC with a S/SL inlet, auxiliary EPC and FID module were used for testing whether narrow peak widths could be obtained using a combination of short GC columns similar to the Calidus™ GC system. The S/SL inlet was connected to a Rtx-1 column (3 m × 180 μm ID × 1.0 μm d_f, Restek). The outlet of the RXT-1 column was then connected to a piece of DFS capillary (0.7 m × 100 μm ID, Trajan) that served as a flow restriction to allow a stable head pressure to be obtained. The outlet of this flow restrictor was then connected to Port #A of a three-port SilFlow PMD(1) (Trajan). Port #C was connected to a DFS sample loop (1 m × 250 μm ID, Trajan), which was then connected to Port #E of another three-port SilFlow PMD(2) (Trajan). Port #B of PMD(1) and Port #E of PMD(2) were both connected to a three-way solenoid valve (Lee Corporation, USA) for flow switching *via* two pieces of SS capillary (30 cm × 1.0 mm ID, Trajan). A Rtx-1701 column (1 m × 180 μm ID × 0.18 μm d_f, Restek) was connected to Port #F of PMD2, and the outlet of the RTX-1701 column was then connected to a FID module, as shown in Figure 84.

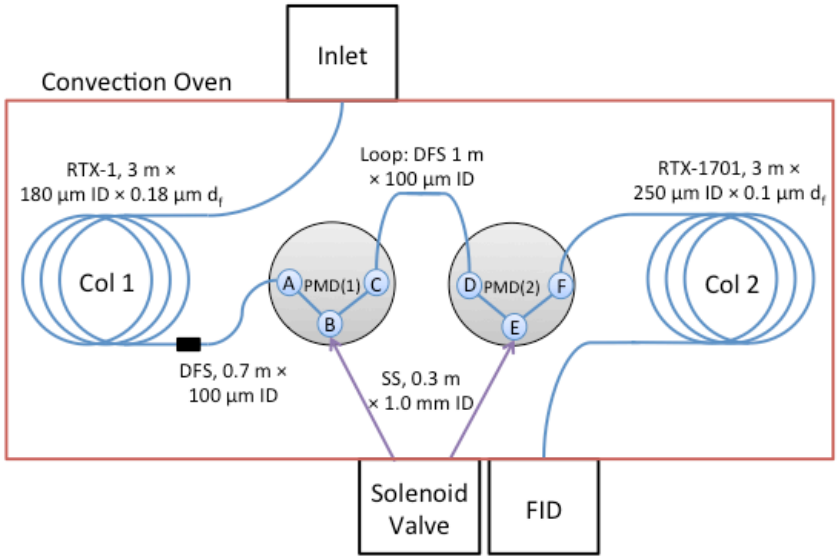

Figure 84 Schematic diagram of the FFF-GC × GC setup developed with the Agilent 6850 GC system showing the connectivity between the inlet, columns, three-port PMDs, solenoid valve and FID module. This instrument configuration was used replicate the FFF-GC × GC system constructed in section 6.2.4.

The FID was operated with 30 mL min^{-1} of hydrogen, 320 mL min^{-1} of air and 30 mL min^{-1} of nitrogen makeup gas, and set to a temperature of 280 °C. Modulation timings were controlled using a custom build timing circuit (Scielex, Kingston, Tasmania). The modulation period was 1.5 s with an injection period of 110 ms. The carrier gas hydrogen and the first dimension was set to a flow rate of 0.6 mL min^{-1}, while the second- dimension was maintained at a flow of 16 mL min^{-1}. The convection oven was set to an initial temperature of 40 °C for 1 min, after which the oven was temperature programmed at a rate of 10 ° C min^{-1} to 280 °C, followed by a 5 min hold.

A 10-component test mixture comprised of *n*-octane, 1-hexanol, 4-ethyltoluene, (+)-β -pinene, *n*-decane, 1-octanol, 1-bromooctane, naphthalene, *n*-dodecane, 1-bromodecane (Sigma Aldrich, Castel Hill, Australia) was prepared in a headspace vial for sampling *via* SPME. A 7 µm PDMS SPME fibre (Green, Sigma Aldrich) was used for sampling the headspace of the sample vial. The SPME fibre was exposed to the

headspace of the vial for 30 s, and then exposed in the Calidus™ GC inlet. The inlet was operated in the splitless mode with a SPME liner (Agilent) and 2 min desorption time. A second sample comprised of Special Antarctic blend diesel diluted in dichloromethane (Sigma Aldrich) to a concentration of 2250 mg kg^{-1} was also analysed, while utilising a split liner (Agilent) and a split ratio of 100:1. FID data was collected with a sampling rate of 200 Hz using ChemStation Software and a laptop computer. Data files were exported in CDF format for processing and visualization in GC image software (GC Image LLC, USA).

6.2.6 MXT-1 (^{1}D) and MXT-50 (^{2}D) column set with RFF modulation

A Calidus™ GC equipped with a S/SL inlet, a resistively heated column module and a FID was used for developing a GC × GC method capable of separating SAB diesel. A piece of DFS capillary (13 cm × 180 µm ID, Trajan) was connected to the S/SL inlet. The outlet of this DFS capillary was then connected to a MXT-1 column (3 m × 180 µm ID × 1.0 µm d_f, Restek). The MXT-1 column was connected to a Port #A of a four-port SilFlow PMD(1) (Trajan) using a piece of DFS capillary (35 cm × 50 µm ID, Trajan). Port #B was connected to a DFS sample loop (1 m × 250 µm ID, Trajan), which was then connected to Port #E of a three-port SilFlow PMD (Trajan). Port #C of PMD(1) was connected to the inlet a MXT-50 column (1 m × 180 µm ID × 0.18 µm d_f, Restek) using a piece of DFS capillary (12 cm × 250 µm ID, Trajan). Port #D of PMD(1) and Port F of PMD(2) were connected to a three-way solenoid valve using two pieces of SS capillary (30 cm × 1.0 mm ID, Trajan). Port #G of the PMD(2) was connected to a bleed capillary (DFS, 55 cm × 75 µm ID, Trajan). The outlet of the MXT-50 column was connected to an FID using a piece of DFS (12 cm × 250 µm ID, Trajan).

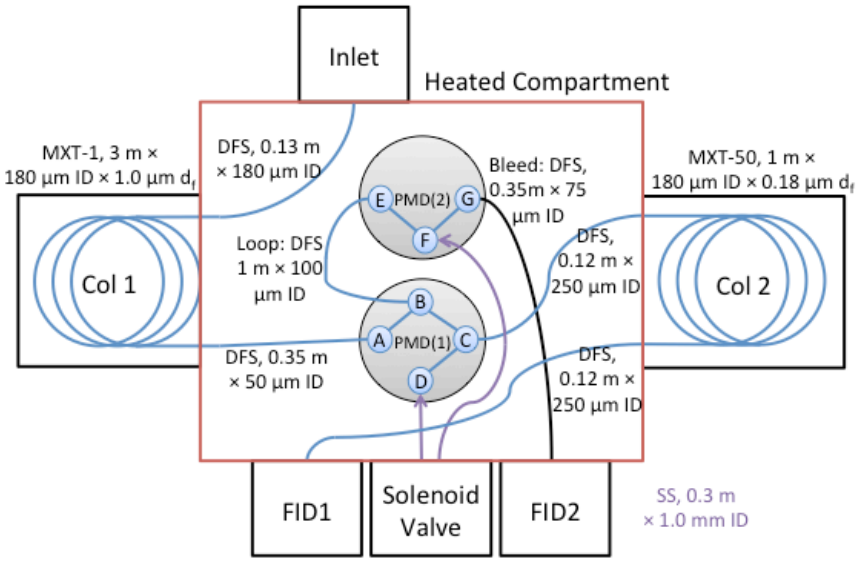

Figure 85 Schematic diagram of the RFF-GC × GC system developed using the Calidus™ GC platform, showing the connections between the inlet, columns, PMDs, solenoid valve and FID modules.

The FID was supplied with 13 mL min^{-1} of hydrogen and 130 mL min^{-1} air for flame operation. The transfer lines, PMD, S/SL inlet and FID were all maintained at 280 °C. The RFF pulsed flow PMD was connected to a three-way solenoid valve (Lee Corporation) and auxiliary EPC using two SS capillaries (30 cm × 1.0 mm ID, Trajan). The carrier gas was hydrogen; the MXT-1 was operated at a flow rate of 0.5 mL min^{-1}, which required an initial inlet pressure of 21.06 PSI. The MXT-50 column was operated at a flow rate of 20 mL min^{-1}, requiring an initial pressure of 14.23 PSI. The initial ^{1}D and ^{2}D column temperatures were 40 °C (1 min), both columns were then ramped at 30 °C s^{-1} to 280 °C (1 min). The modulation period was 2.0 s and the injection period 110 ms.

A 13-component test mix comprised of benzene, toluene, *n*-octane, 1-hexenol, *o*-xylene, *n*-decane, 1-octanol, naphthalene, 1-decanol, *n*-tetradecane, acenaphthene, fluorene, *n*-octadecane (Sigma Aldrich, Castle Hill, Australia) was prepared, each component 100 mg kg^{-1} diluted in dichloromethane (Sigma Aldrich) and injected (1 µL) into the Calidus™ system for analysis. Additionally a sample of SAB diesel (Australian

Antarctic Division) was analysed which was diluted to a concentration of 2250 mg kg^{-1} in dichloromethane (Sigma Aldrich) prior to being injected (1 µL) at a split ratio of 100:1. FID data was collected with a sampling rate of 100 Hz, using Chrom Perfect software (Justice Laboratory Software, USA) on a laptop computer. Data files were exported in CDF format for processing and visualization in GC image software.

6.2.7 Custom column modules

A Calidus™ resistively heated column module containing a 3 m long 180 µm ID column was disassembled and modified to incorporate a long BP1 column (12 m × 220 µm ID × 0.25 µm d_f, Trajan). The BP1 column was co-linearly wound with the Calidus™ GC's SS capillary into a toroid shape with a 6 cm diameter. This toroid was then covered with a thin layer of aluminium foil, which served to hold the assembly together and form an insulated cohesive bundle. The column toroid was then installed in the Calidus™ column module as shown in Figure 86.

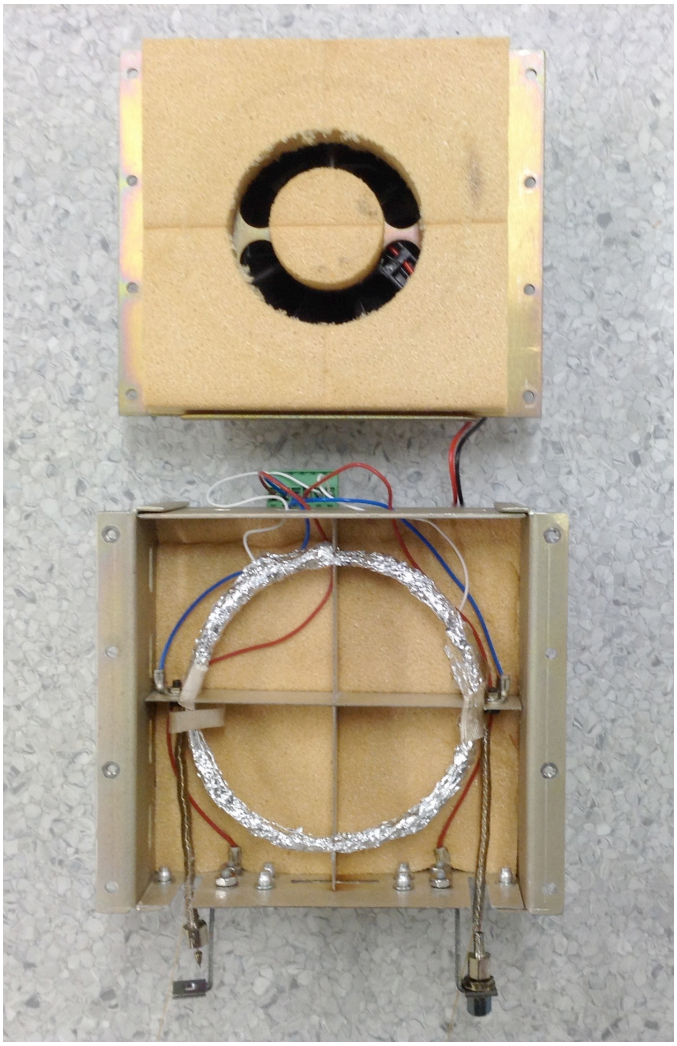

Figure 86 Modified column module showing the column module cover plate with (top) electric fan; and (bottom) the aluminium foil insulated column toroid and two heated transfer lines for connectivity to the central Calidus™ transfer line oven.

The inlet and outlet of the BP1 column were threaded through the heated transfer legs included with the column module, to ensure there were no cold spots that could cause solute condensation during temperature programmed analysis.

6.2.8 RFF-GC × GC with custom column modules

A Calidus™ GC (Falcon) equipped with a S/SL inlet, a resistively heated column module and a FID was used for developing a GC × GC method capable of separating SAB

diesel. The S/SL inlet was connected to a BP1 column (12 m × 220 µm ID × 0.25 µm d_f, Trajan). The BP-1 column was connected to a Port #A of a three-port SilFlow PMD(1) (Trajan). Port #B of PMD(1) was connected to a DFS sample loop (1 m × 250 µm ID, Trajan), which was then connected to Port #E of a three-port PMD(2) (Trajan). Port #C of the four-port PMD was connected to the inlet a SolGelWAX column (4.4 m × 250 µm ID × 0.25 µm d_f, Trajan). Port #D of PMD(1) and Port #F of PMD(2) were connected to a three-way solenoid valve using two pieces of SS capillary (30 cm × 1.0 mm ID, Trajan). Port #G of PMD(2) was connected to a bleed capillary (DFS, 100 cm × 150 µm ID, Trajan). The outlet of the SolGelWAX column was connected to a FID module, as shown in Figure 87.

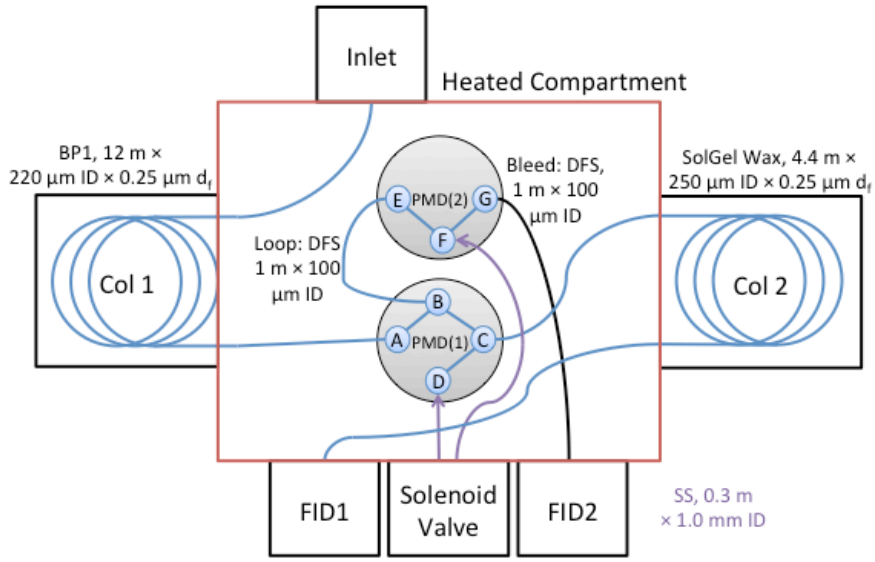

Figure 87 Schematic diagram of the RFF-GC × GC system developed using the Calidus™ GC platform and custom column modules. Notice that the number of additional unions between the columns, PMDs, inlet and FID modules has been reduced due to the addition of custom wound columns. This was achieve by allowing a 20 to 40 cm segment of custom wound column to protrude directly into the central heated compartment of the Calidus™ for connectivity with the inlet/PMDs/FID modules.

The FID was supplied with 13 mL min^{-1} of hydrogen and 130 mL min^{-1} air for flame operation. The transfer lines, PMD, S/SL inlet and FID were all maintained at 280 °C. The three-way solenoid valve (Lee Corporation) was connected to an auxiliary EPC (Parker) that was programmable using a microcontroller that interfaced with the EPC (Scielex).

The carrier gas was hydrogen; the BP1 column was operated at a flow rate of 0.6 mL min^{-1}, which required an initial inlet pressure of 19.83 PSI. The SolGelWax column was operated at a flow rate of 20 mL min^{-1}, requiring an initial pressure of 21.87 PSI. The initial ^{1}D and ^{2}D column temperatures were 40 °C (1 min), both columns were then ramped at 30 °C s^{-1} to 280 °C (1 min). The modulation period was 2.0 s and the injection period 110 ms. A 13-component test mix comprised of benzene, toluene, *n*-octane, 1-hexenol, *o*-xylene, *n*-decane, 1-octanol, naphthalene, 1-decanol, *n*-tetradecane, acenaphthene, fluorene, *n*-octadecane (Sigma Aldrich) was prepared (each component 100 mg kg^{-1} diluted in dichloromethane) and injected (1 µL) into the Calidus™ system for analysis. A sample of SAB diesel (Australian Antarctic Division) was analysed which was diluted to a concentration of 2250 mg kg^{-1} in dichloromethane prior to being injected (1 µL) at a split ratio of 100:1. Additionally a sample of tea tree oil distillate was obtained and diluted (1 % v/v in dichloromethane) and injected into the Calidus™ system at a split ratio of 60:1. FID data was collected with a sampling rate of 100 Hz, using Chrom Perfect software (Justice Laboratory Software, USA) on a laptop computer. Data files were exported in CDF format for processing and visualization in GC image software.

The SolGelWAX column (4.4 m × 250 µm ID × 0.25 µm d_f) was shortened to 2.5 m in length and replaced into the previously described setup with modified pressure set points to maintain the same flow rates through the first- and second-dimension columns. An additional BPX35 column (2.5 m × 250 µm ID × 0.25 µm d_f) was also

prepared and utilised in the system, which operated with matching flow set points to the SolGelWax (2.5 m × 250 µm ID × 0.25 µm d_f) for the analysis of a number of samples.

6.3 Results and Discussion

6.3.1 Integration of planar microfluidic devices for GC × GC modulation in the Calidus™ GC

The incorporation of PMDs for pulsed flow GC × GC modulation with the Calidus™ GC was carried out using a FFF-PMD that was commercialised by Agilent Technologies, based off the modulator reported by Seeley *et al.* [3,6]. The size and connection unions of the PMD are similar to the PMD Deans' switch described in Chapter 2, however the internal architecture includes a sample loop that is periodically filled with effluent from the ^{1}D column, and rapidly eluted using an auxiliary flow from an EPC. This FFF-PMD was installed within the Calidus™ GC's central transfer line oven to ensure that it was heated so that solutes could not condense within the device during its operation. Connections between the S/SL inlet, column modules, FFF-PMD, and detector were made with short sections of narrow bore DFS capillary to minimise the amount of dead volumes were introduced into the Calidus™ GC.

The Calidus™ GC was initially supplied with three column options, a non-polar MXT-1 column (3 m × 180 µm ID × 1.0 µm d_f) coated with 100% dimethylpolysiloxane, a low polarity MXT-5 column (3 m × 180 µm ID × 0.18 µm d_f) coated with 5% diphenyl- 95% dimethylpolysiloxane, and an MXT-1701 column (3 m × 250 µm ID × 0.1 µm d_f) coated with a 14 % cyanopropylphenyl- 76 % dimethylpolysiloxane stationary phase. The retention mechanism of the MXT-5 stationary phase is primarily based on dispersion interactions, with weak polarisation and basic hydrogen bonding mechanisms introduced by the 5% diphenyl polysiloxane component of the stationary phase polymer. The MXT-1 column has similar dispersive based retention mechanisms to the MXT-5 column, with further diminished polarisability and hydrogen bonding capabilities [10]. This column's internal diameter matched the MXT-5 column, however

its thick stationary phase coating was expected to diminish the separation performance due to the increased resistance to mass transfer imparted by the stationary phase coating [11]. The MXT-5 was initially selected as the first-dimension column due to its narrow internal diameter and modest stationary phase thickness, which was expected to yield the highest theoretical plate count (18,300, N_{max}) out of the columns available. Columns with narrow internal diameters (≤ 180 μm) are of great interest for portable GC applications, as they are capable of providing rapid separation while maintaining high plate counts, which facilitates high-resolution separation of complex samples [12].

Since the retention mechanisms of the MXT-1 and MXT-5 columns are very similar combining them into a GC × GC column set was unlikely to offer sufficient selectivity for a two-dimensional separation. Instead the MXT-1701 column was selected as the ^{2}D column, due to its high polarity stationary phase that facilitates dipole-dipole and hydrogen-bonding interactions with polar solutes, compared to the dispersion based retention mechanisms of the MXT-1 and MXT-5 columns [10]. The MXT-1701 column provides a theoretical plate count of approximately 13,200 (N_{max}), which should be sufficient for providing a useful second-dimension separation. The requirement of high second-dimension carrier gas flow rates ensures that solutes would not be retained for excessively long periods on the ^{2}D column, furthermore the thin stationary phase coating of the MXT-1701 column (0.1 μm d_f) should further minimise excessive retention.

Based on the performance experiments carried out in Chapter 2, it was clear that the optimal separation performance was obtained at low carrier gas flow rates (≤ 1.3 mL min^{-1} for the present 180 μm ID, MXT-5 column), since the contribution of longitudinal peak broadening was minimal for such a short column. Therefore, a low carrier gas flow rate of 0.25 mL min^{-1} was trialed in the first-dimension since this would maximise the separation obtained in this first separation, as well as generate peaks that were sufficiently wide for modulation purposes. The second-dimension column was operated

with a high carrier gas flow rate of 25 mL min^{-1} to ensure that the separation was rapid, and that the injection bandwidth from the modulator to the ^{2}D column was very narrow to maximise the separation capabilities of the column. The MXT-5 and MXT-1701 column configuration yielded the following separation (Figure 88), which was revealed to have minimal selectivity for the expected polar components of the petroleum sample that was separated.

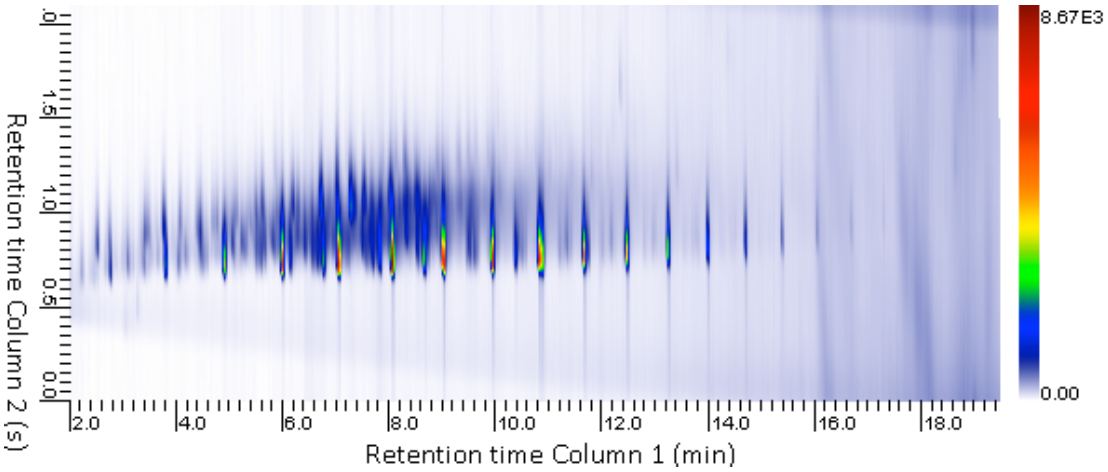

Figure 88 Two-dimensional chromatogram of a Special Antarctic Blend (SAB) diesel separation (2250 mg kg^{-1}, in dichloromethane). The temperature program for the ^{1}D and ^{2}D column was 60 °C (1 min) then ramped at 12 °C min^{-1} to 270 °C (1 min). Carrier gas flow rate: ^{1}D 0.25 mL min^{-1}; ^{2}D flow rate 25 mL min^{-1}. FFF GC× GC modulation, modulation period (P_m) 2.1 s, injection period (P_i) 100 ms.

The second-dimension peak widths were very broad (> 200 ms at half height), and tailing in peak symmetry, which was limiting the separation capabilities of the second dimension. In an effort to enhance the selectivity of the second-dimension column for the expected polar components of the SAB sample and better utilise the two-dimensional separation space, a temperature offset between the first- and second dimension columns was added to increase the retention factor of solutes within the ^{2}D

column, as shown in Figure 89, Figure 90 and Figure 91.

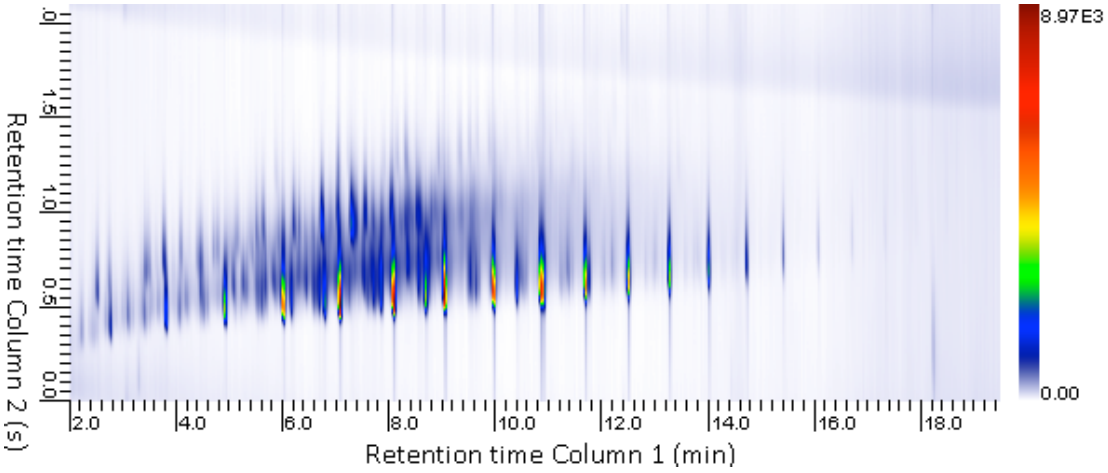

Figure 89 Two-dimensional chromatogram of a Special Antarctic Blend (SAB) diesel separation (2250 mg kg^{-1}, in dichloromethane). ^{2}D column temperature offset -10 °C relative to ^{1}D column, other analysis conditions as per Figure 88.

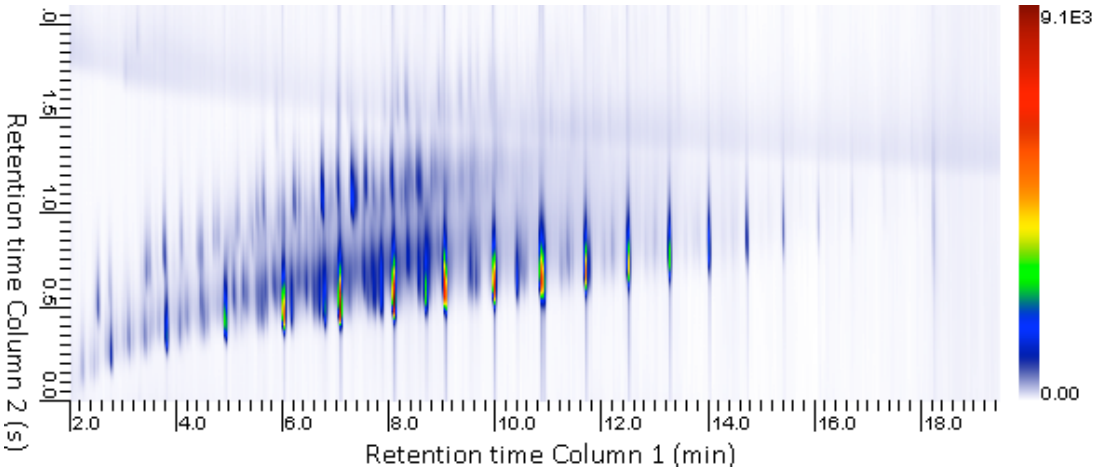

Figure 90 Two-dimensional chromatogram of a Special Antarctic Blend (SAB) diesel separation (2250 mg kg^{-1}, in dichloromethane). ^{2}D column temperature offset -20 °C relative to ^{1}D column, other analysis conditions as per Figure 88.

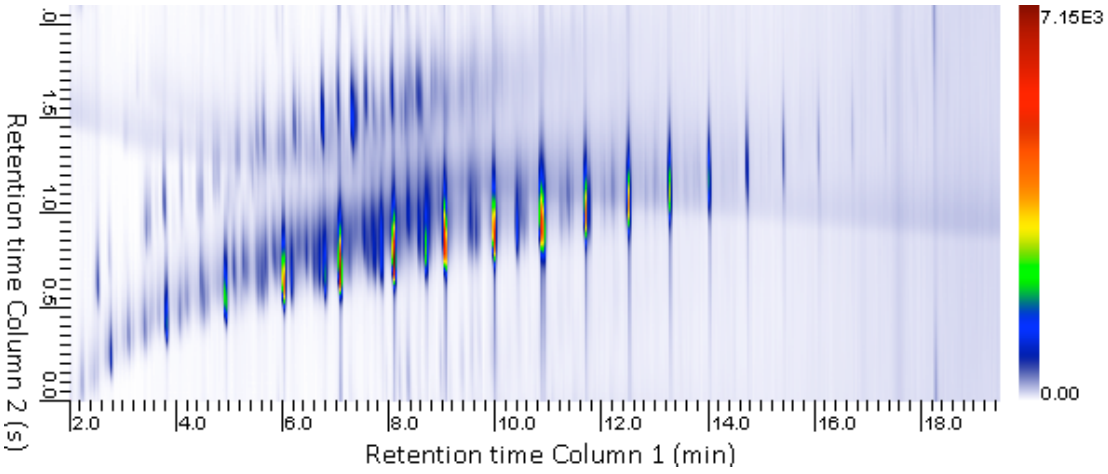

Figure 91 Two-dimensional chromatogram of a Special Antarctic Blend (SAB) diesel separation (2250 mg kg^{-1}, in dichloromethane). ^{2}D temperature offset -30 °C relative to ^{1}D column, other analysis conditions as per Figure 88.

Figure 88 to Figure 91 show that the addition of a temperature offset can serve to enhance the utilisation of the two-dimensional separation space, however the peak widths delivered by the Calidus™ system were substantially limiting the GC × GC separation performance. Components of the SAB sample were eluting in two diagonal series in the GC × GC chromatogram, with this effect being the most pronounced in the -30 °C ^{2}D temperature offset condition shown in Figure 91. This meant that the second-dimension column was retaining solutes based on dispersion interactions as a result of the temperature offset imposed between the ^{1}D and ^{2}D columns, therefore the retention mechanisms of each column were correlated with one each other [13,14]. The retention mechanism of the ^{1}D separation is a combination of that column's stationary phase selectivity and the temperature of analysis. The retention mechanism of the ^{2}D column should be uncorrelated with temperature, since this retention mechanism is a component of the first-dimension separation during temperature-programmed analysis. Any additional ^{2}D retention based on temperature will only contribute towards peak broadening of second-dimension peaks.

The second-dimension peak widths for a mixture of *n*-alkanes (*n*-C_8 to *n*-C_{20}) are reported in Table 16, these results quantitatively confirm that peaks were being substantially broadened either as a result of the modulation procedure, or as a result of the ^{2}D separation.

Table 16 Experimental second-dimension peak widths measured for a range of *n*-alkane compounds. Analysis conditions ^{1}D column MXT-5 (3 m × 180 µm ID × 0.18 µm d_f) with a flow rate of 0.25 mL min^{-1}, connected to an Agilent FFF-GC × GC PMD, ^{2}D column MXT-1701 (3 m × 250 µm ID × 0.1 µm d_f) at a flow rate of 25 mL min^{-1}. P_m is 2.8 s, P_i 200 ms. ^{1}D 0.25 mL min^{-1}, ^{2}D 25 mL min^{-1}. Initial analysis temperature 60 ° C (1 min), then ramped at a rate of 12 °C min^{-1} to 270 °C (1 min).

Compound	Retention time	Peak width (ms)	^{2}D peak symmetry
n-octane	1.43	160	2.89
n-nonane	1.9	150	3.03
n-decane	2.32	150	2.87
n-undecane	2.69	140	4.01
n-dodecane	3.1	140	3.1
n-tridecane	3.48	150	2.05
n-tetradecane	3.8	140	4.07
n-pentadecane	4.12	180	2.57
n-hexadecane	4.45	140	4.73
n-heptadecane	4.77	170	4.06
n-octadecane	5.05	200	3.37
n-nonadecane	5.37	220	2.68
n-eicosane	5.61	230	2.27

Higher molecular weight *n*-alkanes compounds were being broadened by up to 90 ms more than the less volatile alkanes confirming that the second-dimension was retaining solutes based on molecular weight, which is linked to the dispersion retention mechanism and solute boiling point (Table 16).

A variety of different modulation periods were tested to ascertain whether this parameter had a significant affect on the ^{2}D peak widths obtained using the FFF-GC × GC modulator. Ideally a modulator should provide narrow injection bandwidths to maximise the effectiveness of the second-dimension separation. The ^{2}D peak widths and symmetry factors for two compounds, *n*-decane and *n*-eicosane, are reported in Table 17 and compared with the theoretical injection bandwidths provided by the GC system. The theoretical injection bandwidths provided by a flow modulator can be estimated by dividing the modulation period by the ratio of carrier gas flow between the first- and second-dimension columns [4,15]. This theoretical injection bandwidth calculation provides a means of assessing the performance of a flow based GC × GC modulator.

Table 17 The effect of varying peak width and symmetry statistics for a range of different modulation periods. The carrier gas was hydrogen, See Table 16 for details on the GC analysis conditions.

P_m (s)	Injection bandwidth (ms)	Peak width half height (ms)		Symmetry factors	
		n-decane	*n*-eicosane	*n*-decane	*n*-eicosane
1.1	11	170	230	3.95	3.98
1.4	14	170	230	3.60	3.93
1.7	17	170	240	4.10	4.45
2.0	20	200	270	4.67	4.41
2.2	22	160	200	3.09	4.04
2.8	28	150	230	2.87	2.27
3.3	33	200	210	2.82	3.91

It was immediately apparent that, despite the narrow theoretical injection bandwidths afforded by the 1:100 column flow ratio, the measured peak widths were all an order of magnitude wider than anticipated. Although some peak broadening was anticipated as a result of the second-dimension column's retention mechanism, it appeared that the present system was not providing adequately narrow injection bandwidths to the ^{2}D column. The pulsed flow GC × GC device reported by Seeley *et al.*

was capable of post-separation peak widths of 65 ms at half height while operating with an auxiliary flow rate of 20 mL min^{-1}, which agreed well with the 75 ms peak widths predicted theoretically [3]. The current modulator was obtaining average peak widths of 200 ± 20 ms at half height, which were more than three times wider than the modulator developed by Seeley *et al.* that was operating at a lower flow ratio (1:20). Furthermore the ^{2}D peaks in the Calidus™ GC × GC system were tailing as reflected by the symmetry statistics in Table 17 (average symmetry values of 3.5 ± 0.5). Based on the data in Table 17, the current pulsed flow modulation procedure was responsible for 170 ms of additional peak broadening after subtracting the theoretical injection bandwidths.

The origin of these wide, tailing peaks was likely related to the installation and operating conditions of the FFF-PMD within the Calidus™ GC instrument. The components that could be responsible for the poor performance include the separation column, the FFF-PMD, the connectivity between the components of the instrument, or the FID used. Previously it was shown that the performance of the Calidus™ GC's FID matched the capabilities of a commercial bench top GC-FID instrument (Agilent 6850 GC) in Chapter 2, therefore it was unlikely that this was the source of the broad and tailing peaks. As previously highlighted in Chapter 5 the installation of a modulator within the Calidus™ GC's isothermally heated transfer line oven can have a significant impact on the effectiveness of modulator devices. Similarly, Chapter 5 showed that, at worst, the MXT-1701 column was responsible for approximately 90 ms of peak broadening, while being operated at a low carrier gas flow rate. Since the ^{2}D column was being operated at flow rates in excess of 20 times faster than the system reported in Chapter 5, any peak broadening should be proportionally reduced due to the lower column residence times of each solute. Moreover, previous research carried out by Seeley *et al.* also demonstrated that narrow peak widths of 65 ms were achievable using ^{2}D columns that are up to 5 m in length (250 μm ID) with mid- and high-polarity

stationary phase coatings (DB-210 and DB-Wax), while the present column was only 3 m in length (250 μm ID) and displaying wider peak widths [16,17].

To evaluate whether the MXT-5 column was the cause for the excessively broadened ^{2}D peaks generated by the Calidus™ GC × GC instrument, the elution temperatures for a series of *n*-alkanes were calculated and compared to the elution temperatures of these solutes separated using a longer conventional ^{1}D column. If a solute elutes at a lower temperature, its retention on the second dimension will be proportionately greater, and likely correlated with solute boiling point in addition to stationary phase selectivity, which is undesirable during GC × GC analysis. The elution temperatures of *n*-alkanes calculated for the Calidus™ GC × GC system were compared with a GC × GC separation carried out by the 6850 GC instrument (with single-stage thermal modulation) as shown in Table 18. The data presented in Table 18 revealed significant differences between the *n*-alkane elution temperature using the 25 m (250 μm ID) and 3 m (180 μm ID) column, where all solutes other than *n*-octane were eluted at progressively lower temperatures on the shorter column system relative to the longer column system. In the case of *n*-eicosane, a 103.9 °C reduction in the elution temperature was observed from the shorter MXT-5 column, which would have led to solutes having substantially greater ^{2}D retention factors and broadened ^{2}D peak widths.

There are a few strategies that can be used to increase elution temperatures and minimise excessive retention in the second-dimension column including: increasing the temperature programming rate, reducing the column flow rate, increasing the length of the first-dimension column, or using a more retentive stationary phase. Increasing the rate of temperature programming can enable higher temperatures to be obtained before solutes are eluted from the ^{1}D column.

Table 18 Elution temperatures for a homologous series of alkanes (*n*-C_8 to *n*-C_{20}) using a long (25 m) and short (3 m) 5 % diphenyl- 95 % dimethylpolysiloxane (equivalent phase) ^{1}D column. Analysis conditions: DB5-MS system (Agilent 6850 GC), carrier gas hydrogen 1.0 mL min^{-1}, initial temperature 40 ° C (60 s) then ramped at 5 °C min^{-1} to 320 °C (60 s). MXT-5 system (Calidus™ GC), carrier gas hydrogen 0.25 mL min^{-1}, initial temperature 60 ° C (60 s) then ramped at 12 °C min^{-1} to 270 °C (60 s).

Compound	DB5-MS, 25 m × 250 µm ID × 0.25 µm df		MXT-5, 3 m × 180 µm ID × 0.18 µm d_f		Difference in elution temperatures (°C)
	t_R (min)	Elution temperature (°C)	t_R (min)	Elution temperature (°C)	
n-octane	6.05	65.3	1.43	65.1	0.1
n-nonane	8.75	78.8	1.9	70.8	8.0
n-decane	11.80	94.0	2.32	75.8	18.2
n-undecane	14.85	109.3	2.69	80.2	29.0
n-dodecane	17.80	124.0	3.1	85.2	38.8
n-tridecane	20.60	138.0	3.48	89.7	48.2
n-tetradecane	23.30	151.5	3.8	93.6	57.9
n-pentadecane	25.80	164.0	4.12	97.4	66.6
n-hexadecane	28.25	176.3	4.45	101.4	74.9
n-heptadecane	30.55	187.8	4.77	105.2	82.5
n-octadecane	32.75	198.8	5.05	108.6	90.2
n-nonadecane	34.85	209.3	5.37	112.4	96.8
n-eicosane	36.85	219.3	5.61	115.3	103.9

Temperature programming scaling is commonly performed during method translation procedures [18], however this drastically reduces the separation space in the first-dimension due to the shorter experiment durations following such scaling. Reduction of the ^{1}D column flow rate can increase the elution temperatures of solutes, however since the ^{1}D flow rate was already very low (0.25 mL min^{-1}) this strategy would likely reduce the quality of the first dimension separation with minimal improvement in elution temperatures. A longer resistively heated column was not available at this time,

however a column with a thick film coating of MXT-1 stationary phase coated was available and tested as an alternative column to the former MXT-5 column, since thicker film columns provide additional retention compared to thinner film alternatives.

The MXT-1 column (3.0 m × 180 µm ID) was coated with a 1.0 µm thick coating of 100 % dimethylpolysiloxane polymer, compared to the thin 0.18 µm coating of the MXT-5 column. A faster temperature program (30 °C min^{-1}) was combined with the MXT-1 column to determine whether the GC × GC performance of the Calidus™ could be improved. A 13-component test mixture comprised of a variety of polar and non-polar solutes was injected into the Calidus™ GC with the MXT-1 ^{1}D column in place of the MXT-5, and the resulting two-dimensional chromatogram is shown in Figure 92.

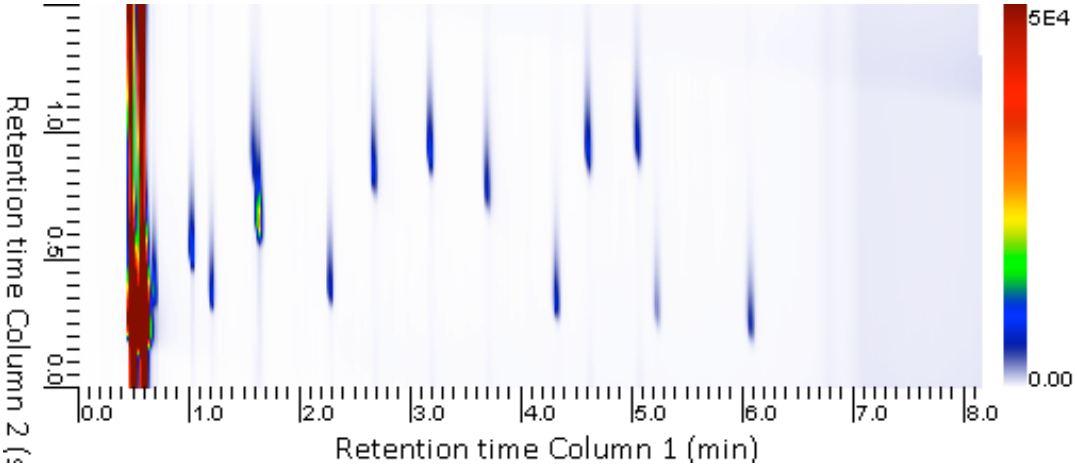

Figure 92 Two-dimensional GC × GC chromatogram of a 13-component test mixture. ^{1}D column MXT-1, 3 m × 180 µm ID × 1.0 µm d_f, ^{2}D column MXT-1701 3 m × 250 µm ID × 0.1 µm d_f. Carrier gas: hydrogen; flow rates: ^{1}D 0.6 mL min^{-1}, ^{2}D 20 mL min^{-1}. Initial ^{1}D column temperature 40 °C (1 min) then ramped at 30 °C min^{-1} to 280 °C (1 min); ^{2}D column trailing ^{1}D by -10 °C. P_m 1.5 s, P_i 110 ms.

The separation obtained using this system reveals improved utilisation of the two-dimensional separation (Figure 92) compared to the separations of SAB shown in Figure 91. However, peak tailing of all solutes was still evident in the chromatogram, with average symmetry values of 3.4 ± 0.4 (Table 19). The substitution of the MXT-1 column

for the MXT-5 column proved successful at increasing the elution temperatures of solutes, with *n*-octadecane eluting at a temperature of 190.8 ° C, which compares favourably with the elution temperature of *n*-octadecane (198.8 °C) on the longer column (25 m × 250 µm ID × 0.25 µm d_f) described in Table 18. This should ensure that solutes are not retained for excessively long periods on the ^{2}D column.

Table 19 Peak identities, retention times and other peak statistics for Figure 92.

Compound	^{1}D t_R (min)	^{2}D t_R (s)	^{2}D peak width (ms)	^{2}D Peak Symmetry	Elution temperature (° C)
benzene	0.68	0.28	150	3.73	40.0
toluene	1.00	1.92	160	3.20	40.0
n-octane	1.18	1.76	150	4.41	45.3
1-hexenol	1.58	0.78	170	3.22	57.3
o-xylene	1.60	2.05	170	2.80	58.0
n-decane	2.25	1.78	170	4.20	77.5
1-octanol	2.65	0.75	190	2.35	89.5
naphthalene	3.18	0.81	180	2.07	105.3
1-decanol	3.68	0.68	190	3.20	120.3
n-tetradecane	4.30	0.24	170	4.26	139.0
acenaphthene	4.60	0.82	190	3.17	148.0
fluorene	5.05	0.84	180	3.11	161.5
n-octadecane	6.03	1.66	180	4.09	190.8

The ^{2}D peak widths measured for the MXT-1 system were on average 50 ms narrower than those obtained using the previous MXT-5 column and analysis conditions, and the average peak widths were 173 ± 7 ms. Given that the flow ratio for this experimental setup was 1:33, the theoretical injection bandwidth should be approximately 45 ms which suggested that the ^{2}D column is unlikely to be the main source of peak broadening. This column set and analysis conditions were applied to the separation of SAB diesel (Figure 93) showing the limited GC × GC capabilities of the

present modulator, due to the wide peaks generated and substantial peak tailing that was reducing the peak capacity of the ^{2}D separation.

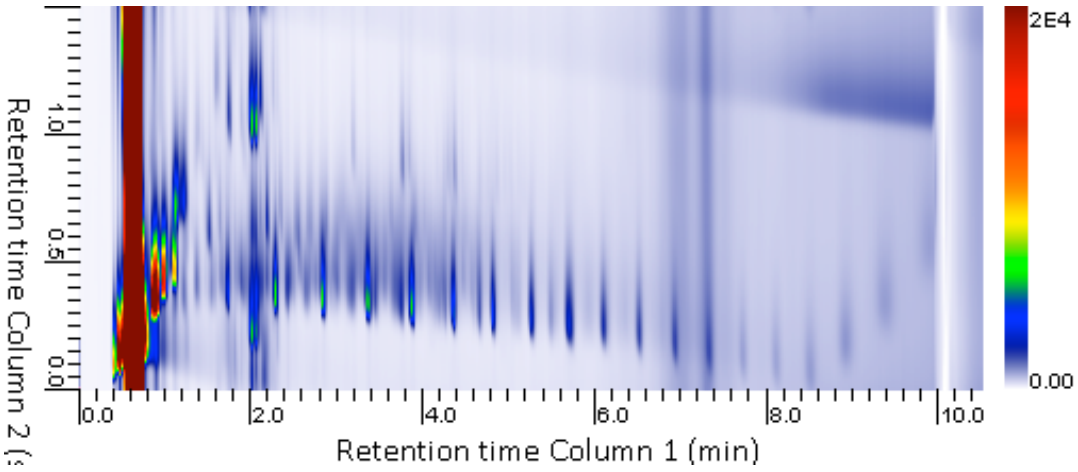

Figure 93 Two-dimensional GC × GC chromatogram of SAB Diesel (1000 mg L^{-1}, 1 µL injection, at 100:1 split ratio). ^{1}D column MXT-1, 3 m × 180 µm ID × 1.0 µm d_f, ^{2}D column MXT-1701 3 m × 250 µm ID × 0.1 µm d_f. Carrier gas hydrogen ^{1}D 0.5 mL min^{-1} ^{2}D 20 mL min^{-1}, temperature program ^{1}D 50 °C initial temperature (30 s) then ramped at 30 °C min^{-1} to 290 °C (120 s). ^{2}D temperature trails ^{1}D by -10 °C.

To determine whether the Calidus™ GC instrument configuration was the source of the poor GC × GC separation performance obtained thus far, a FFF-GC × GC system was constructed using an Agilent 6850 GC, with matched column phases and dimensions, as well as similar analysis conditions. Another test mixture comprised of a range of polar and non-polar compounds was separated using the system (Figure 94) and peak statistics were calculated for each analyte and presented in Table 20.

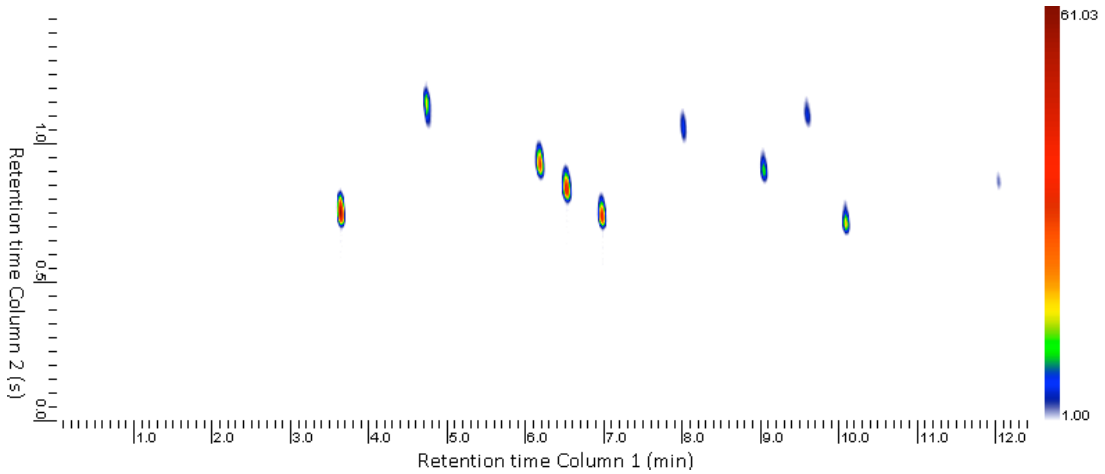

Figure 94 Two-dimensional GC × GC chromatogram of a 10-component test mixture, using the Agilent 6850 GC system. The compound identities, retention times, widths and symmetry values are tabulated in Table 20. ^{1}D column Rtx-1 3 m × 180 µm × 1 µm connected to a piece of DFS 0.7 m × 100 µm ID; Sample loop DFS 0.5 m × 250 µm ID; ^{2}D Rtx-1701 3 m × 250 µm × 0.1 µm df. Carrier gas hydrogen, ^{1}D flow rate 0.6 mL min^{-1}, ^{2}D 16 mL min^{-1}. Temperature programmed from 40 °C (1 min), then ramped at 10 ° C min^{-1} to 280 °C (5 min). FFF modulation, P_m 1.5 s, P_i 100 ms.

The average peak width at half height of all test mixture components in Figure 94 was 68 ± 6 ms (Table 20). The polar components of the test mixture were retained more strongly by the ^{2}D column, which caused additional band broadening (~72 ms) compared to non-polar solutes such as the *n*-alkane test compounds (~61 ms) inflating the peak width average somewhat. The ^{2}D peak symmetry of the selection of test compounds was relatively good with average peak symmetry values of 1.4 ± 0.2, indicating a small amount of tailing, however this performance was far better than similar peak widths and symmetry values obtained using the Calidus™ GC instrument.

Table 20 Summary of peak identities, retention times, peak widths and symmetry values for the separation shown in Figure 94.

Compound	^1t_R (min)	^2t_R (s)	^{2}D peak width (ms)	^{2}D symmetry
n-octane	3.63	0.76	70	1.53
1-hexanol	4.73	1.15	75	0.93
4-ethyltoluene	6.18	0.93	65	1.26
(+)-β-pinene	6.53	0.84	70	1.78
n-decane	6.98	0.74	60	1.56
1-octanol	8.00	1.06	80	1.21
1-bromooctane	9.03	0.91	60	1.46
naphthalene	9.58	1.11	80	1.16
n-dodecane	10.08	0.71	55	1.51
1-bromodecane	12.03	0.86	60	1.63

The peak widths obtained while using PMDs for FFF GC × GC modulation in a bench top 6850 GC were more than two times narrower (~68 ms) than the peak widths of matching solutes with matching columns and conditions (150 to 220 ms, Table 19). The peak widths of the PMD controlled FFF-GC × GC modulator was almost matching the theoretically calculated injection bandwidths (56 ms) that are predicted by the modulation period (1.5 s) and flow ratio (1:26). This experiment confirms that narrow peak widths and good peak symmetry can be achieved using a combination of short separation columns (^{1}D: MXT-1, 3 m × 180 µm ID, 1.0 µm d_f; ^{2}D MXT-1701, 3 m × 250 µm ID, 0.1 µm d_f) and FFF-GC × GC PMD hardware. An example of a separation of SAB diesel using the MXT-1 and MXT-1701 column is shown Figure 95, and this separation confirmed that the MXT-1701 phase was not suitable for promoting GC × GC separation of SAB diesel. The poor modulation and separation performance of the Calidus™ GC × GC system appeared to be caused by a component of Calidus™ GC connectivity or the resistively heated column modules being used thus far.

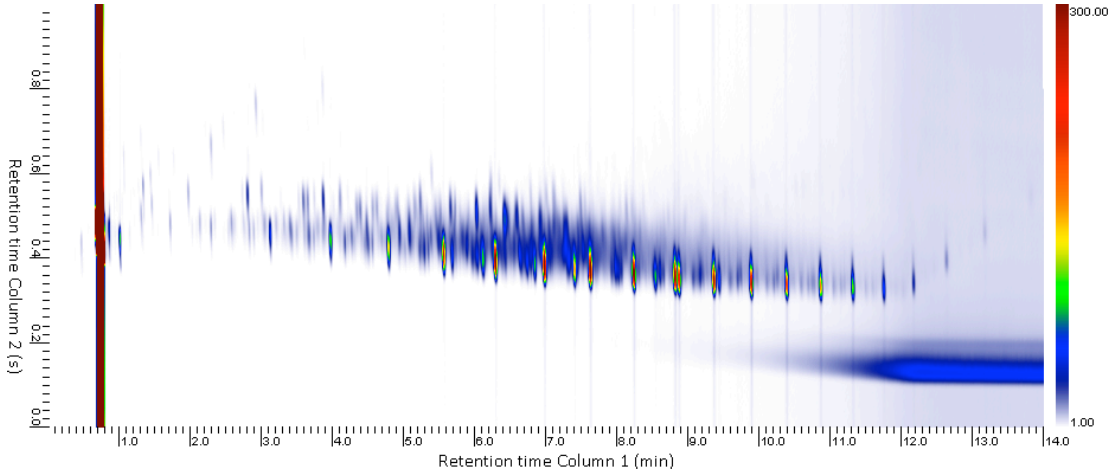

Figure 95 Two-dimensional GC × GC chromatogram of SAB diesel (2250 mg kg^{-1} in dichloromethane, 1 µL 100:1 split ratio). ^{1}D column Rtx-1 3 m × 180 µm × 1.0 µm d_f connected to a restrictor capillary, DFS 0.7 m × 100 µm ID; Sample loop DFS 0.5 m × 250 µm ID; ^{2}D Rtx-1701 3 m × 250 µm × 0.1 µm d_f. Carrier gas hydrogen, ^{1}D flow rate 0.6 mL min^{-1}, ^{2}D 20 mL min^{-1}. Temperature programmed from 40 °C (1 min), then ramped at 10 ° C min^{-1} to 280 °C (5 min). FFF-GC × GC modulation, P_m 1.0 s, P_i 100 ms.

An alternative RFF-PMD modulator was installed in the Calidus™ GC oven in an attempt to isolate whether the inability to obtain good ^{2}D performance was related to the FFF-PMD installation within the Calidus™ GC. The RFF-GC × GC system was constructed using two PMDs (a 3-port and 4-port PMD) similar to the RFF-GC × GC system reported by Griffith *et al.* [5]. A DFS capillary (1 m × 250 µm ID) was used as the sample loop installed between the ^{1}D and ^{2}D columns for modulation purposes. A MXT-1 column (3m × 180 µm ID × 1.0 µm d_f) was selected for the ^{1}D column once again, and combined with a new MXT-50 ^{2}D column (1 m × 180 µm ID × 0.18 µm d_f). The MXT-50 column phase was expected to provide superior selectivity for polar solutes containing delocalised π-bonds such as polyaromatic compounds that are common in petroleum based samples, and the length and internal diameter of the column were short to ensure a rapid separation was obtained. To gauge the utilisation of two-dimensional separation

space, the 13-component test mixture was injected and separated using the new RFF-GC × GC configuration (Figure 96).

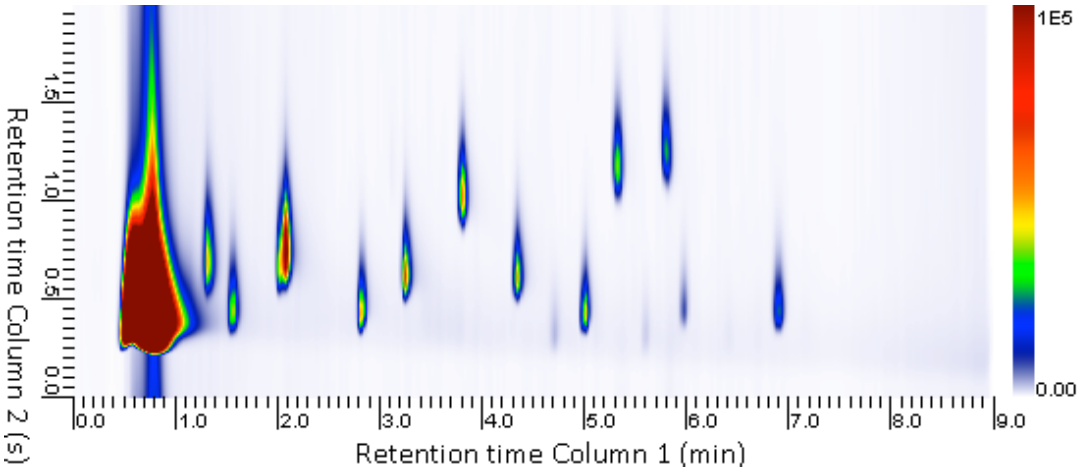

Figure 96 Two-dimensional GC × GC chromatogram of a 13-component test mixture. Columns: ^{1}D MXT-1, 3 m × 180 µm ID × 1.0 d_f, ^{2}D MXT-50, 1 m × 180 µm ID × 0.18 µm d_f. Carrier gas hydrogen ^{1}D 0.5 mL min^{-1} ^{2}D 20 mL min^{-1}, temperature program ^{1}D 40 °C initial temperature (30 s) then ramped at 30 °C min^{-1} to 280 °C. ^{2}D temperature program matches ^{1}D. Note that two components of the test mixture co-eluted at 2.0 min ^{1}D retention time.

The average peak widths for the test solutes in this separation were 230 ± 30 ms, indicating that the change to the RFF-GC × GC system worsened the peak width performance of the system, with similarly poor peak symmetry values of 3.6 ± 0.7 on average, despite the 1:40 flow ratio used in the system. The utilisation of the two-dimensional separation space was no better with the MXT-50 column, compared to the previous separations using the MXT-1701 column. An injection of SAB diesel confirmed that this short MXT-50 ^{2}D column was not providing useful selectivity for achieving two-dimensional separations; therefore it was abandoned as a ^{2}D column in favour of preparing customised resistively heated GC columns for the Calidus™ GC.

6.3.2 Custom GC × GC module construction and usage

Since the installation of two different PMD configurations was not able to improve the two-dimensional separation performance of the Calidus™ GC system, the resistively heated column modules were investigated as a potential means to improve the performance of the Calidus™ GC. Due to the limited availability of Calidus™ resistively heated columns and the prohibitive cost of purchasing additional units (~$3000 USD per column module) a means of preparing resistively heated GC columns in house was devised.

A column module containing a 3 m long, 180 µm ID column was disassembled to reveal a coil of SS capillary that was insulated with a glass fibre braid to prevent electrical shorting during the application of electrical current for resistive heating. The column was wound onto an aluminium ring that was reportedly incorporated in the design to facilitate heat distribution between each column loop [19]. The insulated SS capillary was removed from the module and the aluminium ring was discarded as discussed in Section 2.2.3. A BP1 column (100 % dimethylpolysiloxane stationary phase, 12 m × 220 µm ID × 0.25 µm d_f) was co-linearly wound with the SS capillary into a toroid shape with a 6 cm diameter. This toroid was then covered with a thin layer of aluminium foil, which served to hold the assembly together and form an insulated cohesive bundle, eliminating the need for the aluminium ring. The column toroid was then installed in the Calidus™ column module as shown in Figure 86. The inlet and outlet of the BP1 column were threaded through the heated transfer legs included with the column module, to ensure there were no cold spots that could cause solute condensation during temperature programmed analysis.

This column heating design was similar to the LTM resistively heated column modules developed by Mustacich and Richards [20]. The main difference between the column heating designs was the difference in heating elements, since Mustacich and

Richards used an insulated Nichrome wire element, rather than an insulated SS capillary for column heating. The LTM column heating strategy has been proven to be very effective and has been commercialised by a number of vendors. In the case of the Calidus™ GC, this modification improved the connectivity between the columns and other components, since all bulkhead unions could be bypassed and the column inlets/outlets could be directly connected to inlets, detectors and PMDs. This procedure offered greater flexibility in the selection of column phases and dimension, and an additional column was prepared containing a SolGel-WAX stationary phase (4.5 m × 250 µm ID × 0.25 µm d_f for use as a ^{2}D column. Each module included a long resistance temperature sensor that was installed in-line with the SS capillary bundle. This sensor provided feedback to the Calidus™ GC that was used to control the amount of power applied to the SS capillary column to achieve a given temperature-programming rate. The retention time repeatability for a series of *n*-alkanes was approximately 1.1 %, while using manual injection technique, indicating acceptable repeatability.

Before analysing the peak widths generated using the RFF-GC × GC modulator further, it was important to verify that the modulator was comprehensively transferring effluent from the ^{1}D column to the ^{2}D column. The reason for this concern was that since a bleed column was used, it was possible for ^{1}D column effluent to pass through the sampling loop if a long "fill" duration is used, or if the loop is not completely emptied during the injection phase of modulation. The easiest way to determine whether a RFF modulator is comprehensively transferring effluent to the second-dimension column is to monitor the bleed column outlet with a detector. Connection of the Calidus™ GC bleed column revealed that some effluent was not being injected onto the second dimension column (Figure 97). Given that the sample loop size was 1 m × 250 µm ID of DFS capillary, this segment of capillary would have an internal volume of 49 µL, which has a dead time of 3.7 s at a flow rate of 0.8 mL min^{-1}, it was impossible for the present loop to be overfilled while using modulation periods less that 3.7 s. Additionally the period

required to completely flush the contents of the RFF sample loop at the present ^{2}D column flow rate (23.8 mL min^{-1}) was 140 ms. However, due to the 2.5 s modulation period only 70% of the loop's volume was being used, an injection period of 100 ms should be sufficient to elute all of the contents. Injection periods between 30 to 220 ms were tested, in order to determine the duration that is required to completely transfer effluent from the loop to the ^{2}D column as shown in Figure 97.

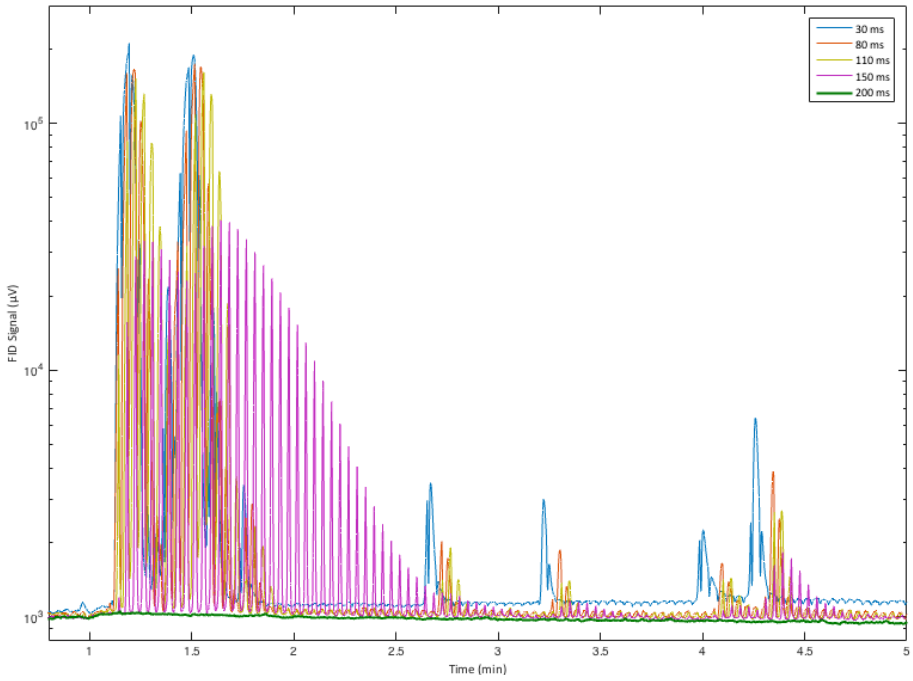

Figure 97 One-dimensional GC chromatogram overlays of the bleed channel FID for a range of injection periods (P_i = 30, 80, 110, 150 and 200 ms). Sample: 13-component test mixture (20 mg kg^{-1} each in dichloromethane) 1 µL injection at 100:1 split ratio. ^{1}D column BP1, 11 m × 220 µm ID × 0.25 µm d_f, ^{2}D column BPX35 2.5 m × 250 µm ID × 0.25 µm d_f. Carrier gas: hydrogen; flow rates ^{1}D 0.8 mL min^{-1}, ^{2}D 23 mL min^{-1}. ^{1}D temperature program 35 °C (1 min) then ramped at 12 °C min^{-1} to 295 °C (1 min), ^{2}D leads ^{1}D by +15 °C. RFF modulation, P_m 2.5 s.

Injection periods less than 100 ms should not be expected to prevent peaks from appearing on the bleed channel, and this was confirmed experimentally by the traces in Figure 97 for the 30 and 80 ms injection periods. Additionally the injection periods of

110 and 150 ms were allowing effluent to pass through the sample loop to the bleed channel, instead of being quantitatively transferred to the ^{2}D column. An injection period of 200 ms was required to ensure that no solute was vented to the bleed channel during modulation. The reason for the discrepancy between the theoretical (100 ms) and measured (200 ms) injection periods required to achieve quantitative transfer of effluent to the ^{2}D column was not clear. However it is important to ensure that all effluent is successfully modulated to maximise analytical sensitivity, therefore a 200 ms injection period was used for the subsequent experiments. It was remarkable that shorter injection periods could not be used to reduce injection bandwidths similar to the Deans' switch injection minimisation experiments that were conducted in Chapter 2, which suggests that a component down stream of the modulator is responsible for peak broadening.

The width of peaks obtained on the ^{2}D separation channel appeared to be uncorrelated with each injection period, with average peak widths at half height of 170 ± 20 ms for solutes that were weakly retained by the ^{2}D column. The peak intensity of solutes modulated with different injection periods were proportionally diminished as a result of the proportion of effluent vented to the bleed line. Injection periods of 200 ms or greater did not provide an increase in peak height as expected (Figure 98).

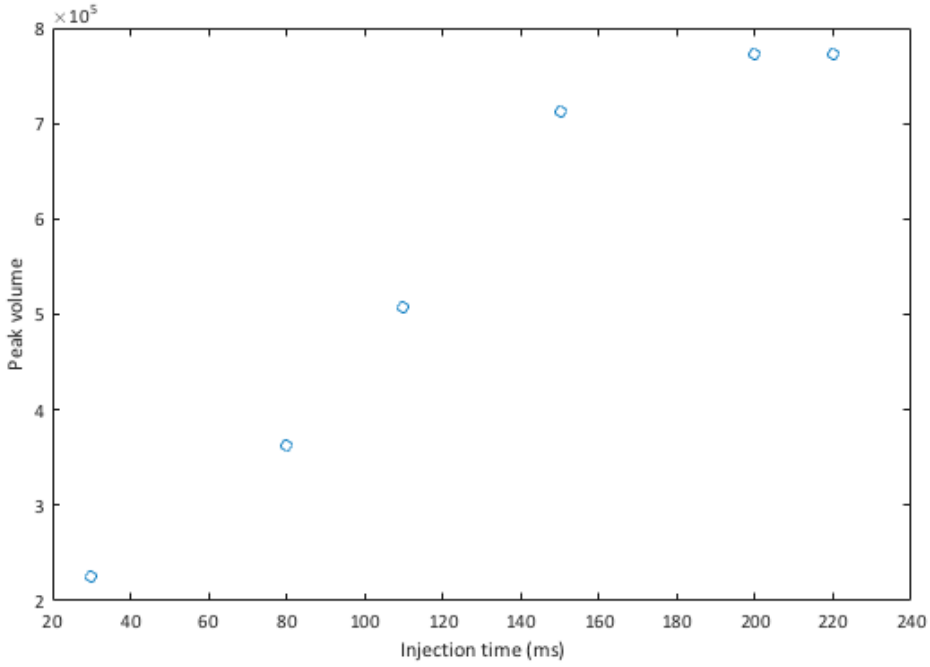

Figure 98 Injection time *vs.* peak volume for the solute *n*-decane using the RFF-GC × GC system described by Figure 97. Note that the peak intensities of each solute were measured using the analytical (^{2}D column) channel rather than the data collected on the bleed channel.

Following the optimisation of the injection period, the co-linear restively heated column set was assessed using the 13-component mixture to provide the separation shown in Figure 99. The peak widths of the non-polar *n*-alkanes in the test mixture had average peak widths at half height of 150 ± 15 ms which was three times as wide as the theoretically predicted ^{2}D peak widths of 50 ms. A number of the more polar compounds were experiencing substantial retention and wraparound on the ^{2}D column, which led to peaks as wide as 360 ms at half height. Peak symmetry statistics for the RFF-GC × GC modulation setup also indicated large amounts of peak tailing (Average values of 4.7 ± 0.6) suggesting that further optimisation was required.

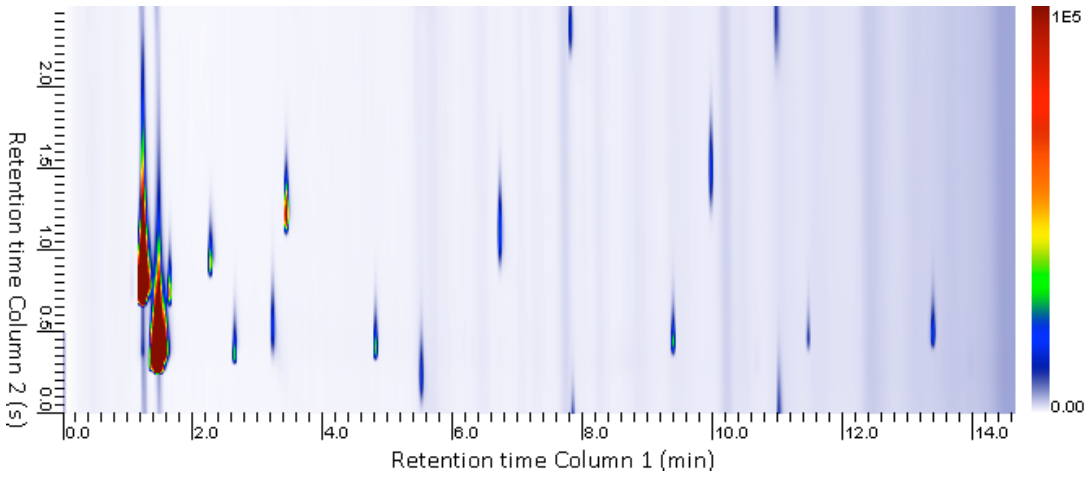

Figure 99 Two-dimensional GC × GC chromatogram of the 13-component test mixture, 20 mg kg^{-1} per compound in dichloromethane, 1 µL injection 100:1 split ratio. ^{1}D column BP1, 11 m × 220 µm ID × 0.25 µm d_f, ^{2}D column SolGel-WAX 4.4 m × 250 µm ID × 0.25 µm d_f. Carrier gas, hydrogen; flow rates: ^{1}D 0.6 mL min^{-1}, ^{2}D 30 mL min^{-1}. Initial column temperature 30 °C (60 s) then ramped at 30 °C min^{-1} to 260 °C (60 s), ^{2}D temperature leads ^{1}D by +10 °C. P_m 2.5 s, P_i 100 ms.

An injection of a diesel sample was performed to further evaluate the utilisation of two-dimensional separation space as shown in Figure 100. Similar to the 13-component test mixture shown in Figure 99, many solutes were wrapping around on the ^{2}D column, therefore the ^{2}D column characteristics needed further tuning to prevent excessive retention.

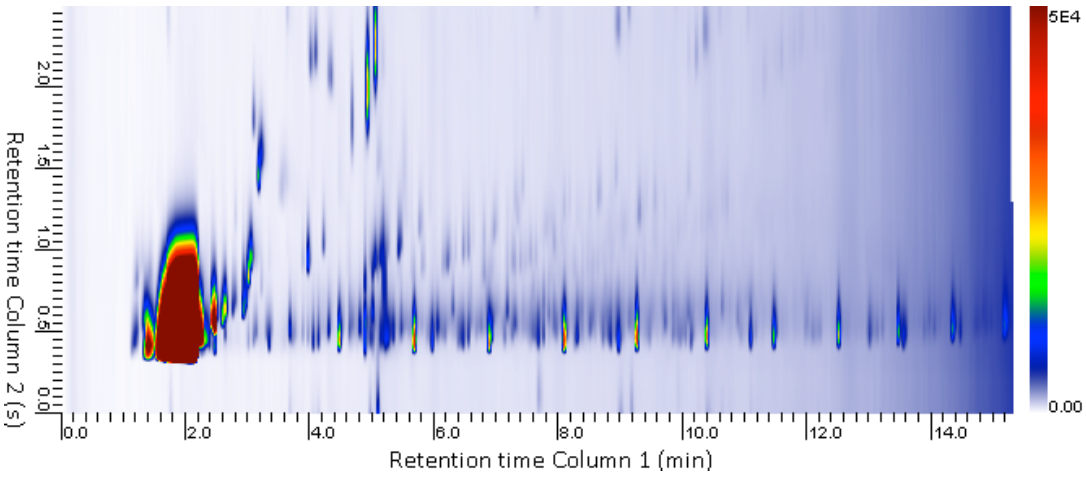

Figure 100 Two-dimensional GC × GC chromatogram of a wide cut diesel sample, 1000 mg kg^{-1} in dichloromethane, 1 µL injection 100:1 split ratio. ^{1}D column BP1, 11 m × 220 µm ID × 0.25 µm d_f, ^{2}D column SolGel-WAX 4.4 m × 250 µm ID × 0.25 µm d_f. Carrier gas, hydrogen; flow rates ^{1}D 0.6 mL min^{-1}, ^{2}D 30 mL min^{-1}. Initial column temperature 30 °C (60 s) then ramped at 30 °C min^{-1} to 260 °C (60 s), ^{2}D temperature leads ^{1}D by +10 °C. P_m 2.5 s, P_i 100 ms.

The SolGel-WAX column (4.5 m × 250 µm ID × 0.25 µm d_f) was shortened in length to 2.5 m in an attempt to reduce the incidence of wraparound, however two highly polar tri-aromatic species (fluorene, phenanthrene) were still being retained for durations greater than a single modulation period (2.5 s) as highlighted by Figure 101. Measurements of various peak statistics for the peaks in Figure 101 are given in Table 21. There was an average reduction in peak widths by 20 ms for non-polar solutes to 150 ± 20 ms after trimming the column, however polar solutes were still exhibiting wraparound on the ^{2}D column that led to excessive peak broadening. Peak symmetry values were somewhat improved with average values of 3.4 ± 1.5, however this tailing was still substantial compared to an ideal symmetry factor between a value of 1 and 1.2.

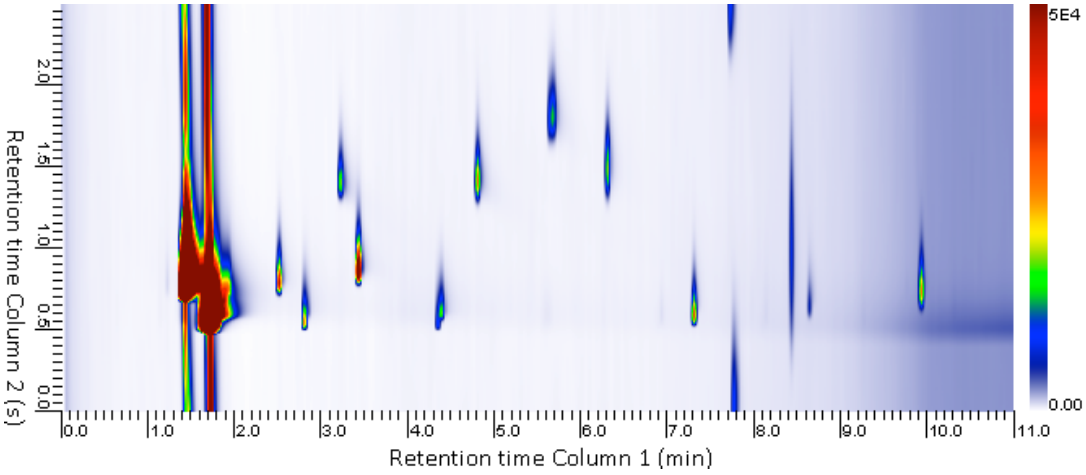

Figure 101 Two-dimensional GC × GC separation of a 13-component test mixture (20 mg kg^{-1} of each test compound in dichloromethane), 1 µL injection at 100:1 split ratio. ^{1}D column BP1, 11 m × 220 µm ID × 0.25 µm d_f, ^{2}D column SolGel-WAX 2.5 m × 250 µm ID × 0.25 µm d_f. Carrier gas, hydrogen; flow rates ^{1}D 0.5 mL min^{-1}, ^{2}D 20 mL min^{-1}. ^{1}D temperature program 30 °C (1 min) then ramped at 24 °C min^{-1} to 260 °C (1 min), ^{2}D leads ^{1}D by +10 °C. RFF modulation, P_m 2.5 s, P_i 110 ms.

Further trimming of the SolGel-WAX column would likely have reduced the wraparound of solutes further, however a less polar stationary phase was trialed instead of trimming the length of this column further. Another resistively heated column module was prepared using the procedure described above; this time a BPX35 column (2.5 m × 250 µm ID × 0.25 µm d_f) was chosen as the column. The BPX35 stationary phase has less selectivity for polar molecules *via* the hydrogen bonding and dipole-dipole interactions compared to the SolGel-WAX phase while still being significantly different to the BP1 column that was being used as the ^{1}D column [10,21].

Table 21 Peak statistics for a 13-component test mixture (20 mg kg^{-1} in dichloromethane, 1 µL injection at 100:1). Analysis conditions reported in Figure 101.

Compound	^{1}D t_R (min)	^{2}D t_R (sec)	^{2}D Peak width (ms)	^{2}D Symmetry
benzene	not separated from solvent			
toluene	2.50	0.79	140	2.7
n-octane	2.79	0.54	130	3.5
1-hexenol	3.21	1.40	180	3.7
o-xylene	3.42	0.86	140	5.8
n-decane	4.38	0.60	180	3.1
1-octanol	4.79	1.41	220	2.5
naphthalene	5.67	1.81	250	1.5
1-decanol	6.29	1.48	290	2.8
n-tetradecane	7.71	2.53	230	2.6
acenaphthene	7.29	0.59	140	4.8
fluorene	8.42	0.97	960	1.6
n-octadecane	9.92	0.74	210	2.8

The BPX35 ^{2}D column was then applied to the separation of the 13-component test mixture previously mentioned to yield the following separation (Figure 102). The peak widths and symmetries of the RFF-GC × GC platform appeared to be limited by its installation within the Calidus™ instrument. The BPX35 phase was combined with a +15 °C temperature offset between the ^{1}D and ^{2}D columns to ensure that solutes did not exhibit wraparound for the highly polar, tri-aromatic components included in the test mixture.

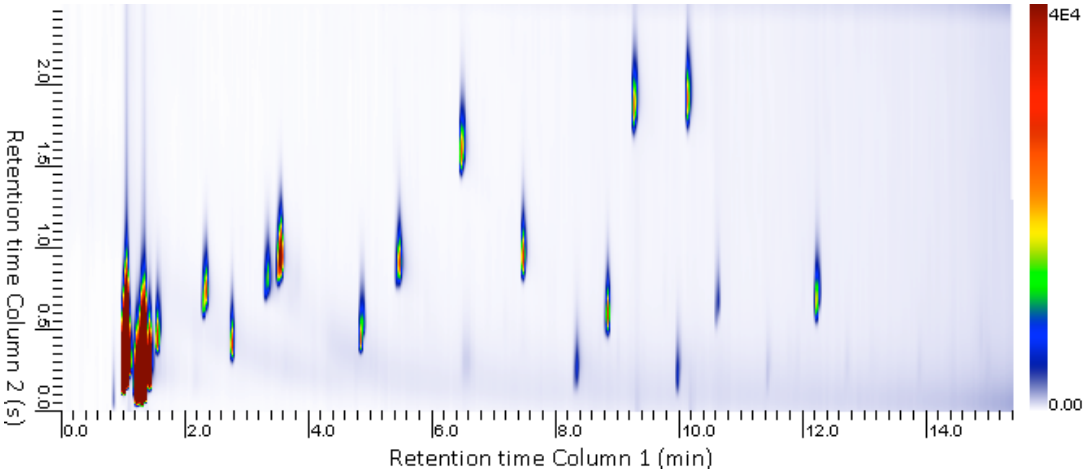

Figure 102 Two-dimensional GC × GC chromatogram of 13-component test mixture (20 mg kg^{-1} each in dichloromethane) 1 µL injection at 100:1 split ratio. ^{1}D column BP1, 11 m × 220 µm ID × 0.25 µm d_f, ^{2}D column BPX35 2.5 m × 250 µm ID × 0.25 µm d_f. Carrier gas, hydrogen; flow rates: ^{1}D 0.8 mL min^{-1}, ^{2}D 23 mL min^{-1}. ^{1}D temperature program 35 °C (1 min) then ramped at 18 °C min^{-1} to 295 °C (1 min), ^{2}D leads ^{1}D by +15 °C. RFF modulation, P_m 2.5 s, P_i 200 ms. Note that there were two unidentified contaminant peaks at 8.2 and 10.0 min.

There was a decent utilisation of the two-dimensional space for the test mixture, however the peaks generated with the BPX35 ^{2}D column were on average 210 ± 20 ms compared to the 150 ms than the peaks obtained using the SolGel-WAX column. Peak symmetry values were on the order of 4.5 ± 1.3 indicating that peak symmetry was still not ideal, with substantial tailing in the second-dimension as shown in Table 22.

Table 22 Peak statistics for each component of the GC × GC test mixture using the BPX35 column and analysis conditions reported in Figure 102.

Compound	^1D t_R (min)	^2D t_R (s)	Peak width (ms)	Peak Symmetry
benzene	1.54	0.44	170	6.6
toluene	2.29	3.24	240	2.6
n-octane	2.71	2.91	170	7.5
1-hexenol	3.33	0.82	240	4.2
o-xylene	3.54	0.95	190	2.6
n-decane	4.79	2.94	190	8.0
1-octanol	5.46	0.91	200	5.0
naphthalene	6.46	1.58	230	2.1
1-decanol	7.46	0.94	210	4.3
n-tetradecane	8.83	0.60	190	3.2
acenaphthene	9.25	1.86	260	2.1
fluorene	10.13	1.91	270	4.9
n-octadecane	12.21	0.68	230	5.1

This GC × GC column pair and analysis conditions were applied to the separation of a diesel sample as shown in Figure 103. The selectivity of the ^2D column was able to resolve aromatic and polyaromatic compounds from the aliphatic components of the diesel sample, which is desirable for their quantification that is otherwise complicated by multiple interferences in one-dimensional GC analysis.

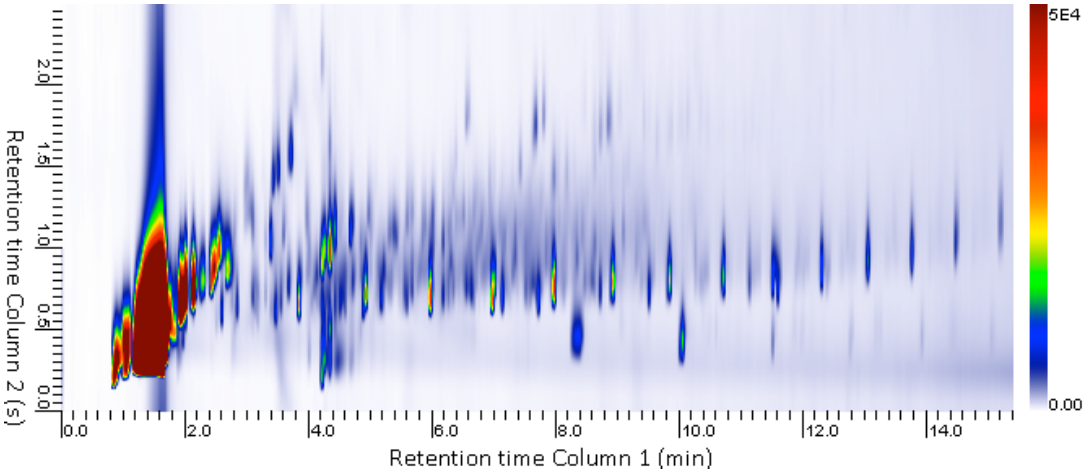

Figure 103 Two-dimensional GC × GC chromatogram of wide cut diesel sample (1000 mg kg^{-1} in dichloromethane), 1 µL injected at 100:1 split ratio. ^{1}D column BP1, 11 m × 220 µm ID × 0.25 µm d_f, ^{2}D column BPX35 2.5 m × 250 µm ID × 0.25 µm d_f. Carrier gas, hydrogen; flow rates ^{1}D 0.5 mL min^{-1}, ^{2}D 22 mL min^{-1}. ^{1}D and ^{2}D temperature programmed from 40 °C (1 min), then ramped at 18°C min^{-1} to 300 °C (1 min). P_m 2.5 s, P_i 200 ms.

The number of resolved compounds can be improved by reducing the temperature programming rate from 18 ° C min^{-1} to 9 °C min^{-1} at the cost of doubling the total run time (Figure 104). This also allows a longer modulation period (3.0 s compared to 2.5 s) to be used due to the proportional increase in ^{1}D peak widths.

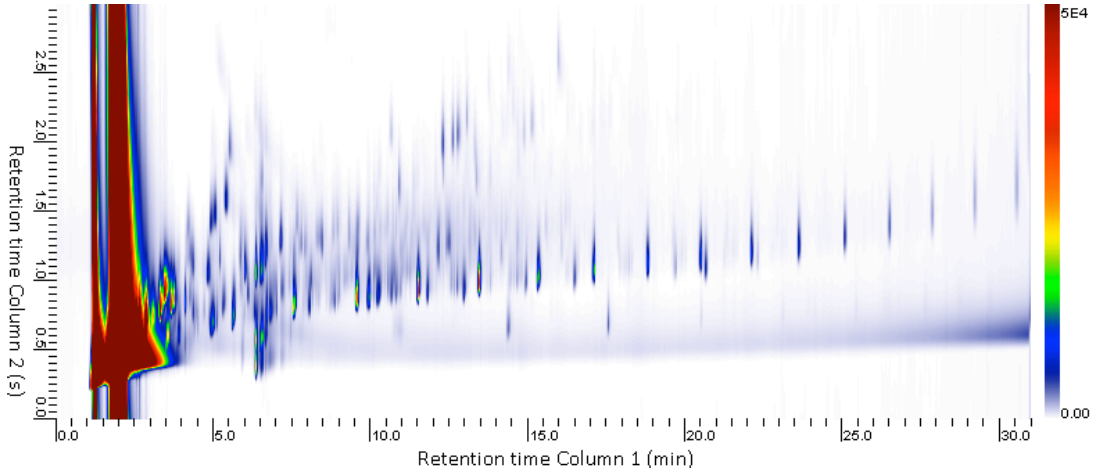

Figure 104 Two-dimensional GC × GC chromatogram of wide cut diesel (1000 mg kg^{-1}). ^{1}D column BP1, 11 m × 220 µm ID × 0.25 µm d_f, ^{2}D column BPX35 2.5 m × 250 µm ID × 0.25 µm d_f. Carrier gas, hydrogen; flow rates ^{1}D 0.5 mL min^{-1}, ^{2}D 22 mL min^{-1}. Temperature program ^{1}D 35 °C (60 s), then ramped at a rate of 9 °C min^{-1} to a 295 °C, ^{2}D leads the ^{1}D column in temperature by + 15 °C. RFF modulation P_m 3.0 s P_i 200 ms.

Slowing down the temperature-programming rate of the Calidus™ GC, did improve the quality of the GC × GC separation, and this resulted in a long analysis duration of 30 min, which was not ideal for a portable GC instrument. Nevertheless the system was capable of providing comprehensive two-dimensional GC for the analysis of petroleum-based samples.

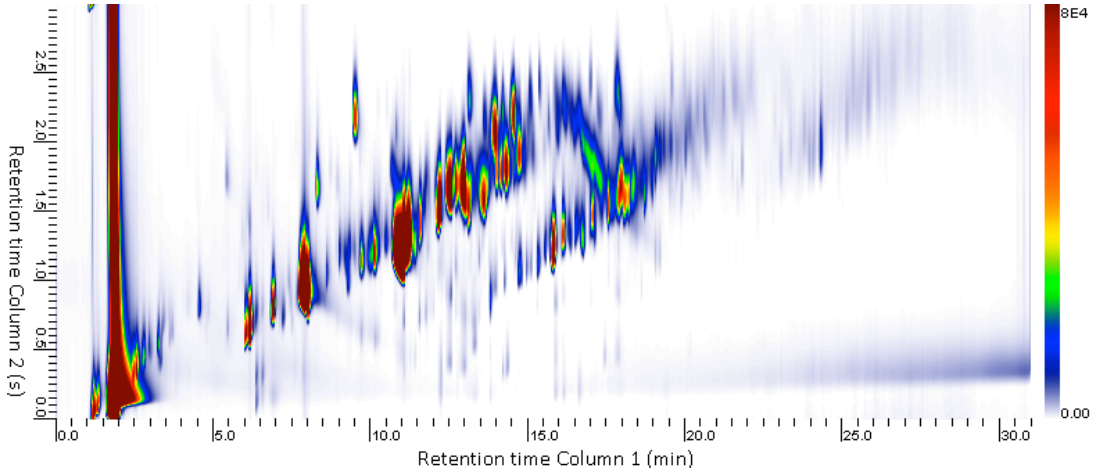

Figure 105 Two-dimensional GC × GC chromatogram of tea tree oil sample (1 % v/v in *n*-hexane) 1 µL injection at 60:1 split ratio. ^{1}D column BP1, 11 m × 220 µm ID × 0.25 µm d_f, ^{2}D column BPX35 2.5 m × 250 µm ID × 0.25 µm d_f. Carrier gas, hydrogen; flow rates ^{1}D 0.5 mL min^{-1}, ^{2}D 22 mL min^{-1}. ^{1}D and ^{2}D temperature programmed from 40 °C (60 s), then ramped at 18 °C min^{-1} to 300 °C (60 s). RFF modulation, P_m 3.0 s, P_i 200 ms.

A sample of tea tree oil distillate was also injected into the system using the same conditions as Figure 104, to determine whether a sample comprised of more polar, VOC and terpenoid compounds could be characterised effectively using the Calidus™ GC × GC instrument (Figure 105). The utilisation of the two-dimensional space for the tea tree oil sample was not optimal, with there being evidence for retention mechanism correlation between the ^{1}D and ^{2}D columns, as shown by the two diagonal series of compounds in the two-dimensional chromatogram (Figure 105). A different combination of columns would be required to better separate this essential oil, however further work on developing an ideal column set for this analysis was not performed at this time.

6.4 Conclusions

Pulsed-flow comprehensive GC × GC was incorporated into the Calidus™ GC using two different PMD configurations (FFF-GC × GC and RFF-GC × GC). Pulsed flow GC × GC required minimal additional hardware in the form of a PMD modulator, a three-way solenoid valve, an electronic pressure controller and a small microcontroller for valve actuation and control. These items were compact and easily incorporated into the Calidus™ GC instrument, while maintaining a robust, transportable system. This was in contrast to the single-stage thermal modulator explored in Chapter 5, which required an additional capacitive discharge power supply (5.6 kg) that needed to be transported along with the Calidus™ instrument. This makes pulsed flow GC × GC a more attractive option for portable analysis in future work.

Out of the two pulsed flow GC × GC configurations, FFF GC × GC modulation appears to be more attractive as an option, since its performance was just as good as the RFF GC × GC system while the additional bleed line was eliminated, thus preventing effluent from being eluted from the system without being injected to the second-dimension column. Both RFF and FFF-GC × GC (Chapter 6) delivered similar ^{2}D peak width performance to each other (~150 ms at half height), and both outperformed the single-stage thermal (Chapter 5) modulator when installed within the Calidus™ GC instrument. Unfortunately neither the FFF- nor RFF-PMD modulators performed as well as expected. Typical pulsed flow modulators deliver post-separation peak widths between 50 and 70 ms at half height, however installation of these devices in the Calidus™ GC increased the peak widths to between 150 and 220 ms depending on the exact configuration.

Optimisation of the columns, PMDs, temperatures, flow rates and capillary connectivity was unsuccessful at isolating the source of the wide peak widths generated by the Calidus™ GC. Construction of a pulsed flow GC × GC instrument using a conventional bench top instrument (Agilent 6850) with matching column dimensions,

phases and flow rates verified that peak widths of 50 to 70 ms at half height should be achievable using short columns in the first- and second-dimension. Unfortunately the performance of the 6850 GC could not emulated using the Calidus™ GC. Presently, the central oven cavity and connectivity between the components of the Calidus™ GC appears to be responsible for the poor ^{2}D peak widths and peak symmetry.

A method for preparing custom column modules using the resistively heated column modules provided with the Calidus™ instrument was developed. Standard polyimide-clad fused silica capillary columns were cut and co-linearly wound into a toroid shape with the SS capillary included with the Calidus™ column module. The toroid was then insulated using aluminium foil, which allowed both the SS capillary and the polyimide-clad fused silica capillary to be heated simultaneously. This procedure allowed any desired column to be incorporated into the Calidus™ GC and the process for preparing a custom column was relatively straightforward, requiring less than 30 min to complete. The use of a longer first-dimension column substantially improved the separation that could be obtained using the Calidus™ GC, while the option of different second-dimension columns allowed tuning of the second-dimension selectivity to maximise the separation performance of a GC × GC method.

6.5 References

[1] J.V. Seeley, N.J. Primeau, S.V. Bandurski, S.K. Seeley, J.D. McCurry, Microfluidic Deans Switch for Comprehensive Two-Dimensional Gas Chromatography, Anal. Chem. 79 (2007) 1840-1847.

[2] J.V. Seeley, Theoretical study of incomplete sampling of the first dimension in comprehensive two-dimensional chromatography, J. Chromatogr. A 962 (2002) 21-27.

[3] J.V. Seeley, N.J. Micyus, J.D. McCurry, S.K. Seeley, Comprehensive two-dimensional gas chromatography with a simple fluidic modulator, Am. Lab. 38 (2006) 24-26.

[4] P.A. Bueno, Jr., J.V. Seeley, Flow-switching device for comprehensive two-dimensional gas chromatography, J. Chromatogr. A 1027 (2004) 3-10.

[5] J.F. Griffith, W.L. Winniford, K. Sun, R. Edam, J.C. Luong, A reversed-flow differential flow modulator for comprehensive two-dimensional gas chromatography, J. Chromatogr. A 1226 (2012) 116-123.

[6] J.D. McCurry, J.V. Seeley, Single stage flow modulator for performing comprehensive chromatography, US20070193336A1 (2007) Agilent Technologies, Inc., USA .12 pp.

[7] B. Quimby, J. McCurry, W. Norman, Capillary Flow Technique for Gas Chromatography: Reinvigorating a Mature Analytical Discipline, LC-GC The Peak (2007) 7-10.

[8] J.D. McCurry, B.D. Quimby, Two-Dimensional Gas Chromatography Analysis of Components in Fuel and Fuel Additives Using a Simplified Heart-Cutting GC System, J. Chromatogr. Sci. 41 (2003) 524-527.

[9] J.V. Seeley, S.K. Seeley, Multidimensional Gas Chromatography: Fundamental Advances and New Applications, Anal. Chem. 85 (2013) 557-578.

[10] C.F. Poole, S.K. Poole, Separation characteristics of wall-coated open-tubular columns for gas chromatography, J. Chromatogr. A 1184 (2008) 254-280.

[11] L.M. Blumberg, Theory of fast capillary gas chromatography. Part 4. Column performance vs. liquid film thickness, J. High Resolut. Chromatogr. 22 (1999) 501-508.

[12] P.Q. Tranchida, L. Mondello, Current-day employment of the micro-bore open-tubular capillary column in the gas chromatography field, J. Chromatogr. A 1261 (2012) 23-36.

[13] C.J. Venkatramani, J. Xu, J.B. Phillips, Separation Orthogonality in Temperature-Programmed Comprehensive Two-Dimensional Gas Chromatography, Anal. Chem. 68 (1996) 1486-1492.

[14] J.B. Phillips, J. Beens, Comprehensive two-dimensional gas chromatography: a hyphenated method with strong coupling between the two dimensions, J. Chromatogr. A 856 (1999) 331-347.

[15] M. Poliak, M. Kochman, A. Amirav, Pulsed flow modulation comprehensive two-dimensional gas chromatography, J. Chromatogr. A 1186 (2008) 189-195.

[16] S.K. Seeley, S.V. Bandurski, R.G. Brown, J.D. McCurry, J.V. Seeley, A comprehensive two-dimensional gas chromatography method for analyzing extractable petroleum hydrocarbons in water and soil, J. Chromatogr. Sci. 45 (2007) 657-663.

[17] J.V. Seeley, S.K. Seeley, E.K. Libby, J.D. McCurry, Analysis of biodiesel/petroleum diesel blends with comprehensive two-dimensional gas chromatography, J. Chromatogr. Sci. 45 (2007) 650-656.

[18] M.S. Klee, L.M. Blumberg, Theoretical and practical aspects of fast gas chromatography and method translation, J. Chromatogr. Sci. 40 (2002) 234-247.

[19] N. Roques, J. Crandall, Fast micro gas chromatograph system, WO2010028398A2 (2010) Falcon Analytical Systems & Technology, USA, 50 pp.

[20] R.V. Mustacich, J.P. Richards, Electrically insulated gas chromatograph assembly, EP962767A1 (1999) RVM Scientific, Inc., USA, 20 pp.

[21] S.K. Poole, C.F. Poole, The orthogonal character of stationary phases for gas chromatography, J. Sep. Sci. 31 (2008) 1118-1123.

Chapter 7: Conclusions

Gas chromatography (GC) is one of the most useful techniques for the analysis of volatile and semi-volatile compounds due to its excellent separation capabilities for a wide variety of samples. Unfortunately the complexity of many samples is so great that the total separation with a single GC column in a timely fashion is unfeasible. A promising means for increasing the resolving power of many GC systems is to utilise MD separations to enhance their resolving power. MDGC is commonly achieved in either the heart-cut MDGC or comprehensive GC × GC analysis modes and each of these separation techniques allow an analyst to leverage the selectivity of two columns to enhance the amount of separation a GC instrument provides.

In this thesis MDGC and GC × GC was investigated as a means of enhancing the separation capabilities of a portable resistively heated GC instrument. The Calidus™ GC instrument was selected as a portable GC platform due to its small size (11.4 kg, with the dimensions 43 × 22 × 28 cm), and rugged construction. The resistively heated column modules were designed so that it was easy to swap column modules into the GC to meet a range of different analytical challenges. The instrument uses a low amount of power, while retaining fast temperature programming capabilities. A central temperature controlled compartment was included in the instrument to provides the opportunity to install a range of PMDs and other devices for the purposes of achieving MDGC and GC × GC analysis, as well as providing connectivity between instrument components.

Since portable GC instruments often operate under fast analysis conditions it was important to ensure that the injection procedure was adequately optimised, since the initial injection bandwidth has a dramatic effect on the separation capabilities of a fast GC system. Two different approaches were explored for reducing the initial injection bandwidths provided by the Calidus™ GC S/SL injector. In Chapter 2 a Deans' switch

PMD was installed between the Calidus™ S/SL injector and a separation column. This PMD was used for controlling the injection bandwidths introduced to a short separation column from the S/SL injector after the vaporisation of a sample. This method of injection bandwidth control was limited by the relatively slow switching speed of the solenoid valve and the large mass of compressible gas between the solenoid valve and the Deans' switch PMD. The narrowest injection bandwidth that could be delivered using this heart cutting configuration was 215 ms, while using S/SL injection at split ratio of 200:1 it was capable of providing injection bandwidths of 115 ms wide, without introducing any additional hardware.

While 100 ms switching times were not compatible with reducing the injection bandwidths being introduced to a GC column, this speed has previously been demonstrated to be more than fast enough to facilitate pneumatically controlled heart-cutting of peaks for MDGC applications. For this reason Deans' switching with PMDs was revisited in Chapter 4, where it was utilised for heart-cut MDGC analysis of trace levels of C_6 to C_8 aromatic compounds in Isoparaffins and styrene monomer. Two separations were developed that took advantage of a polar polyethylene glycol (VF-WAXms) column and highly polar ionic sorbent (CP-LOWOX) column for resolving aromatic compounds from interfering hydrocarbon species. The method developed has a low likelihood of false positive determinations since the additional separation column is able to resolve the target compounds of interest from interfering compounds. Low LODs of 0.8 and 2.7 mg kg^{-1} and LOQs between 2.4 and 9.4 mg kg^{-1} were obtained for each analyte of interest, while using low cost GC instrumentation. Low cost flame ionisation detection was found to provide sufficient sensitivity for this analysis after the interfering compounds were chromatographically resolved using the MDGC setup. This method served to alleviate the need for expensive mass spectrometry detection that is otherwise used to provide selective detection of aromatic species.

An alternative injection bandwidth minimisation strategy utilising a novel SS capillary trap was investigated in Chapter 3. The stationary phase of a polydimethylsiloxane (PDMS) coated SS capillary was chemically modified using a thermal-oxidative procedure that yielded a thermally stable stationary phase with substantial chemical and morphological differences compared to conventional PDMS stationary phase coatings. While the SS trap did not have sufficient retention for focusing volatile compounds for periods long enough to complete a GC injection (Chapter 3), the trap was found to be very promising when used as a single-stage GC × GC modulator (Chapter 5). The peak widths delivered by this resistively heated single-stage thermal modulator were as narrow as 65 ms, which is equal to or better than the performance provided by many commercial GC × GC instruments. Furthermore this modulator only requires electricity for its operations and is relatively compact, while commercial GC × GC instruments are very large and require liquid cryogen or refrigeration units to provide solute focusing for modulation. This GC × GC modulator was applied to the characterisation of petroleum spill samples obtained from Macquarie Island for the purpose of mapping the extent of petroleum contamination of soils, and was found to be effective for the quantitation and qualitative evaluation of such samples. Trace level quantitation of PHC with a method LOD of 11 mg kg^{-1} of soil and LOQ of 36 mg kg^{-1} of soil.

The single-stage thermal modulator was incorporated into the Calidus™ GC system and was successful in enabling GC × GC analysis, although the performance of the modulator was diminished by the installation of this device within the Calidus™ GC (Chapter 5). The selection of ^{2}D columns (1 to 3 m long) available was not ideal for the thermal modulator, due to the large dead volumes of these columns, which causes excessive peak broadening and solute wraparound in the during the second-dimension separation. As an alternative to thermal modulation, pulsed flow GC × GC modulation was explored as a means to achieve comprehensive GC × GC in the Calidus™ GC (Chapter

6). This method delivered a similar performance to the single-stage thermal modulator, and the limited selection of 2D columns was again problematic. To overcome the column limitations of the Calidus™ a method of preparing in-house resistively heated columns was devised to increase the separation capabilities of the instrument, and acceptable GC × GC performance was obtained.

In general the GC × GC and 1D separation performance of the Calidus™ GC was worse than the performance delivered by commercial bench top GC instruments. The connectivity between the various instrument components including the S/SL inlet, columns, detectors and other devices placed in the flow path limited the GC × GC and 1D-GC performance of the Calidus™ instrument. ^{2}D peak widths obtained while using the Calidus™ GC were routinely 100 to 150 ms wider (at half peak height) than ^{2}D peaks obtained using the Agilent 6850 GC with similar columns and conditions. Furthermore all of the peaks detected using the Calidus™ GC displayed tailing symmetry, which further diminished the two-dimensional performance of all separations. Despite a systematic evaluation and optimisation of various instrument components to minimise band broadening and peak tailing, the performance of the system was unable to match bench top GC instruments.

Future work

The Calidus™ GC instrument was not an ideal instrument for portable two-dimensional GC × GC or MDGC analysis in its current state. The large amounts of peak tailing and peak broadening that are evident indicate that significant re-engineering of the instrument connectivity is required before it can provide optimal performance. Selection of a more suitable portable GC platform for portable analysis would be ideal. Alternatively an in-house resistively heated GC × GC instrument column could be constructed using the excellent selection of flow controller hardware and low cost microcontrollers that are available.

Diaphragm valves present an interesting opportunity for controlling the injection bandwidths of GC systems to facilitate fast GC. Diaphragm valves have been demonstrated in the past to be very effective at providing rapid actuation speeds (< 10 ms), however their temperature stability is limited by the diaphragm materials used in their construction. The development of a PMD with an internal diaphragm valve that is robust and highly temperature stable across the GC temperature range would be very useful compared to the current thermally limited diaphragm valves. Such a valve would potentially be very useful in injection bandwidth minimisation, heart cutting and GC × GC.

The next step in developing the capabilities of the single-stage thermal modulator is to increase its solute loading capabilities for highly volatile solutes. Currently the trap is only able to modulate solutes less volatile than *n*-octane, which is problematic for many analyses. Increasing the length and thickness of the stationary phase coating should be investigated to increase the solute loading capabilities of the trap. Additionally, a more effective means of cooling the SS trap using multiple Peltier elements and improved heat conduits could improve the retention capabilities of the trap, while still retaining the

cryogen free and portable nature of the modulator. Investigation of the system in the dual-stage modulation configuration could also assist with reducing the incidence of solute breakthrough following a heating event. Finally the capacitive discharge power supply should be optimised to program the discharge voltage based on the temperature of the convection oven in which it is installed. In this way the peak temperatures of the trap can be reduced to maximise the lifespan of the trap stationary phase and SS capillary.

Following these modifications the GC × GC performance of the Calidus™ GC must be evaluated in a field application, to determine the robustness of the system. Presently all analysis was performed in a temperature controlled analytical laboratory, this environment does not reflect standard operating conditions for portable analysis systems. Further optimisation of the fast GC and GC × GC capabilities of the Calidus™ GC are required, to ensure that the analytical cycles of the portable instrument are more compatible with field based analysis (1 to 10 minutes).